The mechanical behaviour of elastomers when hollow microspheres are used as a particulate filler

Robert Shorter

School of Engineering and Material Science

Queen Mary

University of London

Mile End Road

London E1 4NS

March 2014

Thesis submitted for the award of the degree of

Doctor of Philosophy

I hereby declare that the work carried out and presented in this thesis for the degree of Doctor of Philosophy is original and my own.

Robert Shorter

Abstract

This study aims to understand the behaviour of a novel elastomer where hollow microspheres are used as a particulate filler. The behaviour of elastomers filled with rigid particles, is fairly well understood, where the stiffness increases as the amount of filler material is increased, alternatively, foamed elastomers which are usually produced with either closed cells or open cells, have been shown to become softer as the volume of the voids are increased. When traditional foam materials are compressed they exhibit non-linear behaviour in three distinct phases, the cell walls firstly bend, then they buckle and this is followed by densification.

To understand the overall physical behaviour of the material, tensile tests of the elastomer material were conducted using unfilled materials and filled with a range of the hollow sphere filler volume fractions. Compression tests were also conducted on small cylinders, again using unfilled and filled rubbers with a range of filler volume fractions. The physical tests showed that increasing the filler volume fraction increased the reinforcing effect at low strains with an associated increase in stiffness, but the material then became increasingly less stiff at higher strains. To understand the behaviour of the bulk material, the mechanical behaviour of single hollow spheres under strain were investigated, both as a standalone material and then also embedded in an elastomer.

To examine the mechanical behaviour of a single hollow plastic sphere a single microsphere was compressed using nano-indentation, the tests were then replicated at a larger scale using model table tennis balls. FEA software was used to model the behaviour of both types of hollow sphere, as well as a wide range of other spheres to better understand their buckling behaviour, to help predict the behaviour of microspheres with different ratios of wall thickness to diameters.

To examine the behaviour of hollow spheres in a rubber matrix, simple cylindrical unit cells were made with a single hollow plastic sphere embedded within them. These model cylinders were produced with a translucent elastomer containing a single table tennis ball. Their behaviour in compression and in tension and that of a single hollow plastic sphere embedded in an elastomer was also modelled using FEA software, the effects of debonding and buckling were determined for small and large

strains and were used to examine the more complex behaviour of the filled composite. A comparison between the measured behaviour and the various models indicates that the bulk behaviour of the microsphere filled elastomers is primarily determined by a progressive dewetting process of the rubber away from the microsphere in tension and by buckling phenomena of the hollow spheres in compression.

Acknowledgements

I would like thank my supervisor, Professor James Busfield for his guidance during my PhD studies. I would also like to thank my second supervisor Professor Alan Thomas and Professor Yoshihide Fukahori for their guidance throughout my studies.

I would like to thank the Defence Science and Technology Laboratory, particularly George Philpott, Jenni Henderson and Wendy Brooks for their support and for allowing me to take Special Leave to pursue my studies. I would also like to thank Dr John Smith from the Defence Science and Technology Laboratory for providing the subject for the project and some funding. I am also indebted to Dr John Smith and Dr Vince Coveney from the University of the West of England for the contributions that they made to a paper that we co-authored.

I would like to thank Queen Mary University of London and the Engineering and Physical Sciences Research Council for the scholarship that they offered me. I would like to thank the lecturing staff, particularly Dr Andy Bushby and Dr Ray Smith. I would also like to thank the support staff including John Caulfield, Vince Ford, Monsiha Philips and Chris Reynolds.

I would like to thank my fellow students from the Rubber Group at QMUL, Dr Ioannis Papadopoulos, Dr Hancheng Liang, Dr Vineet Jha, Dr Praveen Kumar, Dr Nutthanun (Mac) Suphadon, Dr Philip Gabriel, HG Lee, Dr Samuel Asare and Dr Kartpan Sakulkaew. I would like to thank my project students, Yi, Wei Wei, Anam and Suraeniya. I would also like to thank Dr Mohammed El-Habti, Dr Wei Tu, Dr Choothum Jeenjitkaew, Dr Keriakos Berketis and Dr Nattakan (Nancy) Soykeabkaew.

Finally I would also like to thank my friends Peter Clarkson, Timothy and Tracy Stodell and Emma Sajic and my parents June and David Shorter for their continued support.

List of Contents

List of Figures

List of Tables

List of Symbols

A	=	Area
α	=	Ogden constant, a real number
C_n	=	Constant used in Phenomenological Theories
E	=	Young's Modulus (or Modulus of Elasticity)
ε	=	True Strain
F, *f*	=	Force
G	=	Modulus of Rigidity (or Shear Modulus)
h	=	Wall thickness
I	=	Strain Invariant
Φ	=	Filler Volume Fraction
K	=	Bulk Modulus ("B" is sometimes used)
λ	=	Stretch Ratio, ("a" is sometimes used)
ν	=	Poisson's Ratio
η	=	Viscosity of an emulsion
η_O	=	Viscosity of an incompressible fluid
μ	=	Ogden constant
μ	=	Shear Modulus
R	=	Radius
σ	=	Stress
t or h	=	(Wall) thickness
T_g	=	Glass transition Temperature
T_β	=	Transition Temperature
τ	=	Shear Stress
U, u	=	Deformation
W	=	Strain Energy (Density) function, ("Φ" is sometimes used)
x	=	Deflection
γ	=	Shear Strain

Chapter 1 Introduction

1.1 The context of this study

The study reported in this thesis was conducted as part of a larger project for the Defence Science and Technology Laboratory (DSTL), which is a part of the Ministry of Defence. DSTL had a requirement to better understand the behaviour of a composite elastomer material where the elastomer is filled with thin walled hollow polymer spheres as a particulate filler. The physical behaviour of such materials is not well understood. This study aimed to better understand the mechanical behaviour of the filled material and that of the individual filler particles. Another aim was to develop a method to derive the properties of the filler from an analysis of the mechanical behaviour of the composite. This was made more complex by the small size of the individual filler particles.

1.2 General introduction

There are various reasons in general engineering practice to fill elastomers with fillers, including reducing the cost, changing the density, modifying thermal or electrical conductivity or to enhance processability. One of the most common uses is to enhance or reinforce a range of mechanical properties such as modulus, strength, tear or abrasion resistance. Some elastomers however are produced as foamed materials, this typically reduces the density as well as the modulus. This study examines a third type of elastomer material, a novel elastomer with hollow plastic microspheres as a filler material, the behaviour of which at least at the outset was relatively unknown.

The elasticity behaviour of elastomers filled with rigid particles, such as carbon black or silica, is very common in engineering practice and is fairly well understood, where the stiffness increases as the volume fraction of the filler is increased. Conversely it has been shown that elastomers produced as foamed materials become softer as the volume of the voids are increased. Foamed elastomers can be produced with either closed cells or open cells; the later being porous like a sponge. A significant amount of work has been conducted into the mechanical behaviour of foamed elastomers.

It has been shown that when elastic foam materials are compressed they exhibit non-linear behaviour in three distinct phases; an initial elastic cell wall bending, followed by cell wall buckling, which is finally followed by densification. However, the

alternative type of elastomer foam examined in this thesis includes a hollow thin walled elastic polymeric sphere which is used to create a novel closed cell material. This material has not been widely studied in the literature in the past.

1.3 The structure of this study

Elastomers in general are discussed in Chapter 2, as is their non-linear stress-strain behaviour, their incompressibility and their viscoelastic properties, also discussed are the statistical or kinetic theory of rubber elasticity together with other phenomenological theories that have been used to describe their real behaviour. The hydrodynamic theory of Einstein and the subsequent adaptation of Einstein's theory by Guth and Gold (1938) to understand how fillers might increase the modulus of an elastomer is discussed. The uses and behaviour of elastic foams are examined, with the work of Gibson and Ashby (1982) for example being examined to help understand the mechanical behaviour of cellular solids. Foamed elastomers have also been examined previously, typically using the approach first suggested by Gent and Thomas (1959, 1963). Hollow spheres are discussed, including their more common uses as a blowing agent and also as an engineering material and their elastic and buckling deformation behaviour as has been examined for example in the work of Pauchard and Rica (1998) and others. Finally Finite Element Analysis (FEA) techniques are discussed, to explain the methodology of creating unit cells to help model elastomers and in particular filled elastomers.

The various techniques used to characterise the materials used in this study are described in Chapter 3. This includes the methods used to characterise the microspheres and their material behaviour, including the composition and density of the material, in order to calculate individual dimensions of the spheres that are examined. Table tennis balls were used, as a larger scale model to help understand and measure the deformation found in the microspheres, as they have a similar ratio of wall thickness to diameter as the microspheres. It was therefore also necessary to characterise the mechanical behaviour of the table tennis ball material. The elastomer and the elastomer composites used in this study were also examined both in terms of their mechanical behaviour as well as their density.

Chapter 4 explores the physical behaviour of an elastomer with hollow microspheres as a particulate filler. This chapter conducts analysis on tensile tests of the

elastomer material both unfilled and filled with a range of filler volume fractions. Compression tests are also conducted on small cylinders, again using unfilled rubber and then filled with microspheres with a range of filler volume fractions.

Chapter 5 examines the mechanical behaviour of a single hollow rigid (as opposed to rubbery) plastic sphere. This includes the physical testing of a single microsphere in uniaxial compression and then by repeating these tests on a larger scale on a model table tennis ball. The table tennis ball was chosen from a wide range of possible model spheres as the ratio of wall thickness to diameter was very similar and the 'plastic' wall material was expected to behave in a similar manner.

In Chapter 6 a single sphere is modelled using FEA software to replicate the behaviour of the table tennis ball when compressed uniaxially. Once this was validated the model was used to replicate the behaviour of the tested microspheres and then predict that of other microspheres with a wide range of different ratios of wall thickness to sphere diameter.

The mechanical behaviour of a single hollow plastic sphere embedded in an elastomer is explored in Chapter 7. This is achieved using cylinders of a translucent elastomer material embedded with a single table tennis ball. The behaviour in tension and compression was observed for the effects of debonding and buckling of the hollow sphere.

In Chapter 8 the physical behaviour of a single hollow plastic sphere embedded in an elastomer is modelled using FEA software. The effects of debonding and buckling were determined for small and large strains and were used to explain the overall filled material behaviour.

A review of the work conducted for this study is presented Chapter 9. The study has produced some significant and interesting conclusions which are discussed, together with potential avenues for future work.

Chapter 2 Literature Review

2.1 Introduction

2.1.1 Aim

The main aim of this project is to understand the mechanical behaviour of elastomers when hollow microspheres are used as a particulate filler, therefore the behaviour of elastomer composite systems needs to be understood.

Elastomers are materials that can stretch, when subjected to a force, to a large extension and which return essentially to their original shape once the force is removed. They typically exhibit non-linear behaviour and are often filled with rigid particles such as carbon black, which increases the stiffness of the material as the volume fraction of carbon black filler is increased. Whereas foamed elastomers typically become softer as the volume fraction of the voids increases, this is the case for foamed elastomers that have either closed cells formed as individual voids, or open cells which make the material porous like as sponge. As foam materials are deformed the deformation is also non-linear and occurs in three phases; cell wall bending, cell wall buckling and then densification. These behaviours have been studied extensively in the past but the behaviour of a foamed elastomer that is produced using thin walled hollow polymer microspheres is still relatively unknown.

2.1.2 Introduction to elastomers and elastomer foams

There are many useful applications for elastomers, especially when manufactured as engineering components (Higgins, 1987) these include; tyres, seals, hoses, engine and gearbox mounts and belts.

Elastomers have the ability to be stretched reversibly to large extensions (Treloar, 1975). This unique property is used in many applications. Some components such as engine and gearbox mounts are also designed to provide damping, to lower the vibrations produced by the machinery during use. Bridge and earthquake bearings are rubber bearings which must withstand huge vertical compression with only modest displacements vertically but which can shear horizontally to allow the bridge components such as the deck to move due to thermal expansion. In these applications, it is necessary to have vibration damping at large shear strains. Fenders on ships and boats also provide large amounts energy absorption when the vessel makes contact with

another vessel and / or the harbour side or dock. Drive shafts in vehicles or other machinery often have flexible couplings that incorporate rubber components to dampen significant changes to the transmission during changes in driveshaft speed. Conveyor belts and drive belts are also often made from elastomers. Due to their electrical insulating properties elastomers are also used for cable coverings and other electrical components; they are also useful as a thermal insulator.

Elastomer foams are used for a variety of applications; the most common elastomer foam being polyurethane. Aerated silicone elastomer foam and latex foam which are produced from natural rubber are also common examples of other types of elastomer foam. Commercially available foams contain either closed or open cells, foams with closed cells contain voids which are separate, whereas open celled foams have interconnected voids. The most common uses are for cushions and other seating components, including domestic, industrial and automotive, carpet underlay, some anti-vibration mountings, as well as other industrial or medical devices.

2.2 Types of elastomer

2.2.1 Introduction

Polymers are often categorised as either natural or synthetic. Natural polymers are found in all living objects, both plants and animals, they include proteins, starch, lignin, cellulose, collagen, silk and natural rubber. Natural rubber (NR) for example is chemically cis-polyisoprene and is found in nature as a viscous-latex in the sap of certain plants.

Alternatively polymers can be synthesised from many different monomer units, the separate units are joined chemically end to end to form a long chain, with the polymer unit repeated thousands of times. The individual chains however are not joined together chemically. When all of the mers are identical the long-chain molecule is known as a homopolymer, if however the mers are of two different types, then a copolymer is produced, such as styrene-butadiene rubber. Terpolymers are made up of three types of mer, for example acrylonitrile-butadiene-styrene (ABS) (Busfield, 2003).

Elastomers are often cross-linked to form a macromolecular polymer network where the polymer chains are joined to each other at random intervals along their length by a suitable linkage. If there are many links or joints and they are close together the material becomes stiff, if there are fewer crosslinks then the material will be more

flexible. Elastomers are "vulcanised" or "cured" by adding crosslinking ingredients such as sulphur or peroxide, typically less than 3 % by volume. In elastomer formulations a mass fraction is often used whereby everything is rebased to the mass of the base polymer. In this case the amount of active crosslinking agent would be less than 2.5 parts of the ingredient per hundred parts of rubber (phr). Accelerators and other curatives are also added depending upon the type of crosslinking system that is being employed. Often the three dimensional network is produced by an elevated temperature vulcanising process where the material is heated to both activate the chemical processes and often to simultaneously reduce the polymer viscosity, typically 140 ºC to 180 ºC and it is then also compressed to a high pressure to both remove entrapped gases and to help the crosslinking process. Depending upon the cure chemistry different types of bonds can be formed. Often these are sulphur or carbon bridges covalently bonded between the polymer chains. This cross-linked network greatly controls the physical properties of the elastomer and can be changed by changing the mix composition prior to crosslinking as well as by varying the time and temperature of the vulcanisation process. Chemical accelerators are used to speed up the process to a matter of minutes, rather than potential cure times that can take hours if accelerators are not used. Vulcanisation increases the elasticity of the material, making it more "rubbery" and more elastic. If the elastomer is not vulcanised it will be sticky, have poor tensile strength and will retain at least some residual "permanent" deformation after the stress has been removed.

If a polymer is cooled sufficiently then the chains or parts of the molecules will not be able to move and the material is said to be "frozen". The temperature at which this transition to this 'glassy state' occurs is known as the glass transition temperature or T_g. As a result the operating temperature and its proximity to the glass transition temperature is possibly the most significant factor to affect the behaviour of an elastomer. When the polymer is cooled down and approaches the glass transition temperature, T_g, it changes into a more rigid brittle glasslike material, because the chains or parts of molecules within the material are constrained. Subsequent cooling to much lower temperatures results in the material becoming brittle and glassy. If the material is then warmed somewhat, it will reach a second transition, T_β, where only side groups of molecules are able to rotate. If warmed further the material will reach the glass-rubber transition, T_g, and larger segments are able to move. Whenever the temperature is increased above the T_g, the elastomer reverts to having a high strain capability (Powell,

1983). Another consequence of a rise in temperature for an elastomer is a large increase in volume due to thermal expansion.

Fillers also play an important part in controlling the properties of elastomer composites, some desirable properties such as increased hardness (which for elastomers is a crude measure of the modulus), abrasion resistance, tear strength and the possible redistribution of network stresses can be enhanced by the addition of carbon black and silica. Viscoelastic response and hysteresis losses are also enhanced by adding fillers. Some fillers including wax, paraffin and mineral oil greatly increase the heat dissipation characteristics of elastomers. Adding fillers and reinforcing agents can also be used to help reduce the cost of the elastomer (MARC, 1996).

The constitution of natural rubber as a hydrocarbon was established by Faraday in 1826 and was described chemically as $(C_5H_8)_n$. Natural rubber was originally derived from the latex sap which is tapped from the Hevea Brasiliensis tree and it is still most commonly obtained in this way (Treloar, 1975).

Other varieties of natural rubber include balta, guayule and gutta-percha, the latter of which was used in the manufacture of golf balls as early as 1860. Natural rubber has properties, including a high tensile strength, good wear resistance (particularly when carbon black is added) and good heat dissipation under cyclic loading, that make it preferable to synthetic rubbers for certain applications such as earthquake resistant mounts used in civil engineering applications (Higgins, 1987).

Synthetic polymers are generally synthesised from oil-based products and include materials like polyester, polyethylene and polypropylene. Synthetic rubber materials were initially produced in 1942, partly due to the Japanese invasion of Britain's Far East rubber plantations and partly because of the need for improved material properties (Higgins, 1987). The properties that were improved included resistance to oil, ozone, ultraviolet radiation and ageing. A wide range of synthetic rubbers including ones derived from chloroprene, isoprene, styrene-butadiene, butadiene, urethanes and nitrile are all used nowadays (Kalpakjian, 1995).

When most rubber components are exposed to sunlight for a long time they will become discoloured, brittle and show signs of crazing and stress cracking. These damaging ultraviolet radiation effects can be delayed by adding "stabilisers", including carbon black, or "masks" such as urethane-based paints. Ozone also has a damaging effect on exposed elastomer components, such as door and bonnet seals, as well as, but to a lesser extent, on gaskets, seals and elastomer boots (MARC, 1996).

Polymers, as with metals, are used on their own, but can also be "alloyed" with various ingredients to give the desired characteristics. Combinations of types of elastomer can also be utilised to provide the required characteristics for the particular application of a component. Pneumatic tyres, which make up over 50 % of all rubber use, are made using several different materials such as natural rubber (NR), styrene-butadiene rubber (SBR) and butadiene rubber (BR) in different regions and often blends are also used, but the treads are most commonly made from SBR (Busfield, 2003).

2.2.2 Types of elastomer

There are many elastomers available to the engineer, each elastomer has specific properties that make them suitable for a range of uses. Some of the most commonly used elastomers are described in this section (Busfield, 2003; Kalpakjian, 1995 and Higgins, 1987).

Natural rubber (NR) is also known as polyisoprene. It is sometimes the cheapest elastomer for a given application and is certainly widely developed, with a large variety of compounds available. Natural rubber is produced in an environmentally sustainable way. It is usually tapped from the Hevea Brasiliensis tree, without harming the tree. The tree sap or latex is obtained from a tree which throughout its life absorbs carbon dioxide, when the tree reaches the end of its useful life it can be made into furniture and it is then replaced by younger trees. Natural rubber as a material is both non-toxic and biodegradable. The raw natural rubber does however need further processing to provide it with desirable material properties. Uses of natural rubber include commercial vehicle tyres, seals, anti-vibration mountings, shock absorbers, dock fenders and components inside machines which do not contact oils (Powell, 1983).

Silicone Rubbers (SI) primarily contain oxygen and silicon along the polymer backbone as well as organic side groups, a comparison to natural rubber is shown in Figure 2.1. They are expensive compared to some elastomers but have a high temperature tolerance, typically between 200 °C (Higgins, 1987) and 315 °C (Kalpakjian, 1995). They also have a good tolerance for low temperatures. However, their strength and resistance to wear and oils and other organic liquids is only moderate. This can be increased by replacing some of the hydrogen atoms with fluorine, but this increases the cost further. Typical applications for silicone rubbers include; gaskets, seals, thermal insulation, high temperature electrical switches and electronic equipment. (Higgins, 1987).

Natural Rubber:

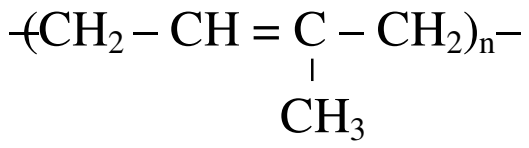

Silicone Rubber:

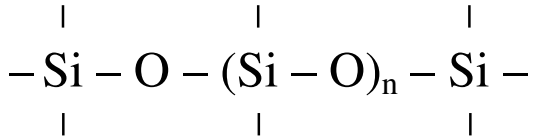

Figure 2.1: A comparison of the chemistry of natural rubber and silicone rubber.

Styrene-Butadiene rubber (SBR) is a synthetic elastomer that is processed in large quantities, it is widely used by tyre manufacturers for both commercial and passenger vehicles and by footwear manufacturers for shoes soles and heels (Powell, 1983).

Nitrile rubber (NBR) is also known as the Acrylonitrile-Butadiene copolymer, it is an elastomer developed with the aim of being oil resistant. NBR is ideal for resistance to petroleum based fluids and has the lowest cost for such applications, it is often used for oil seals, O-rings and seals against gases (Powell, 1983).

Hydrogenated Nitrile rubber (HNBR) has good physical properties, it is used for seals in vehicle engines, diaphragms resistant to heat and chemicals and applications within the oil exploration and oil production industries.

Chloroprene rubber (CR) is also known as polychloroprene, or by the trade name Neoprene. CR was one of the original elastomers developed to be oil resistant, therefore it has a good combination of properties at a low cost and is widely used where there are oils (but not fuels) such as machine mountings, automotive rubber boots and it is especially good for marine environments, including divers' wet suits (Higgins, 1987).

Ethylene-Propylene Diene Monomer (EPDM), ethylene propylene diene terpolymer and EPM, ethylene-propylene copolymer elastomers were developed originally in the 1950's for use in tyres, but became more widely used in many other versatile outdoor situations. They can be compared roughly to SBR, but have a better resistance to ozone, oxidation and atmospheric ageing generally. EPM has better weather resistance due to it being saturated, which means it cannot be cured using conventional cross-linking reactions. EPDM has been developed so that it can be cross-linked with conventional cure systems such as sulphur. EPDM has many uses including

car radiator hoses, sealing strips for car windows and general engineering applications which avoid oil, such as water seals in washing machines (Powell, 1983).

Butyl rubber is also known as isobutylene-isoprene copolymer and is used as liners for tubeless tyres and inner tubes due to its very low gas permeation properties (Powell, 1983).

Butadiene rubber also known as polybutadiene is commonly used for tyres, when blended with SBR and NR (Higgins, 1987).

2.2.3 Elastomer foams

A number of elastomer foams are used for a variety of applications, the most common is polyurethane foam, other elastomer foams include aerated silicone elastomer foam and latex foam, the latter is often produced from a natural rubber latex. There are methods for creating foams from a range of materials including polymers, metals and ceramics. Most commercially available foams have either closed or open cells. Man-made foams are produced on a large scale, predominantly for absorbing energy during impacts, such as for packaging, or for lightweight structures, such as in sandwich panels. The most common uses of polymer foams are for cushions and other seating components, including domestic, industrial and automotive seating, carpet underlay, some anti-vibration mountings, as well as other medical and industrial uses (Kalpakjian, 1995).

Most elastomer foams are not like the original elastomer materials that they are produced from, they have a much lower bulk modulus which clearly depends upon the void volume fraction and the strain level.

Elastomer foams can also be highly elastic which is often expressed as a material that is very resilient. The deformation of elastomer foams in compression is often explained as a process of the foam cell walls bending and buckling followed by a densification process (Gibson and Ashby, 1988), this is shown in Figure 2.2. If a tensile force is applied the cell walls can easily break which gives the material a worse tensile strength in comparison to its compressive strength, or when compared to an equivalent un-foamed material. The rate at which the strain is applied is also important in determining the response of the material.

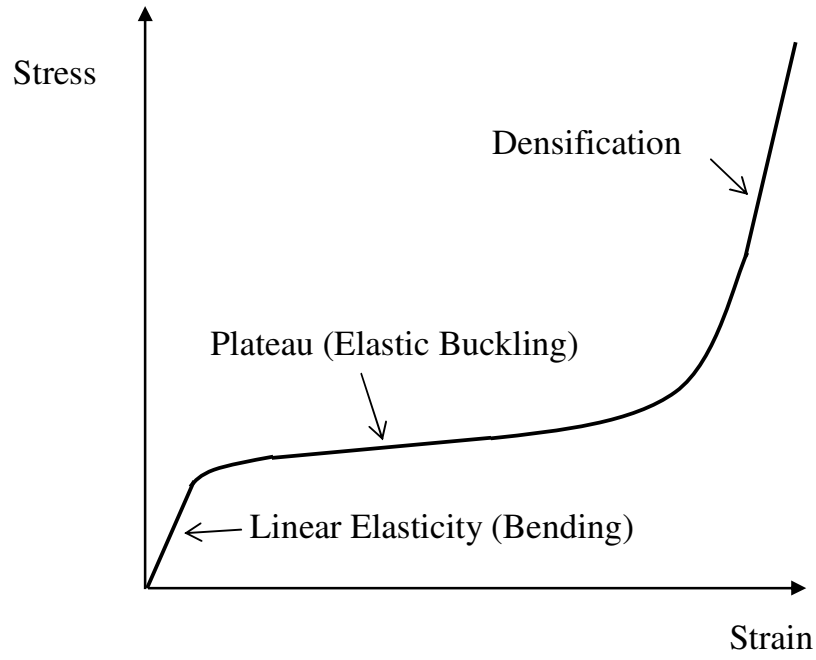

Figure 2.2: The compression behaviour of an Elastomer foam (Gibson and Ashby, 1988).

2.3 Mechanical behaviour of elastomers

2.3.1 Introduction

Elastomers are often made with a carbon backbone that consists of carbon atoms in the form of a long chain molecule. The angle of the bond between the atoms depends upon the elements found, but typically these bonds are free to rotate, which enables the long chain molecules to become coiled when the material is in an unstrained state and for the molecules to slide past each other when the material is stretched at a temperature above its glass transition temperature.

Elastomers are referred to as hyperelastic materials due to visibly large elastic deformations resulting from the application of relatively small applied loads. Loads that would for example deform a steel component of the same dimensions by an imperceptible amount. For elastomers the relationship between the force applied and the resulting deformation is only proportional in tension up to very small strains. As a result they are typically referred to exhibit non-linear behaviour. Materials that have linear elasticity characteristics obey Hooke's law up to a limit of proportionality when a load

is applied to them and they return to their original geometry once the load has been removed. Many materials are Hookean, for example steel, where a graph plotted of force against deflection would produce a straight line (Hearn, 1985).

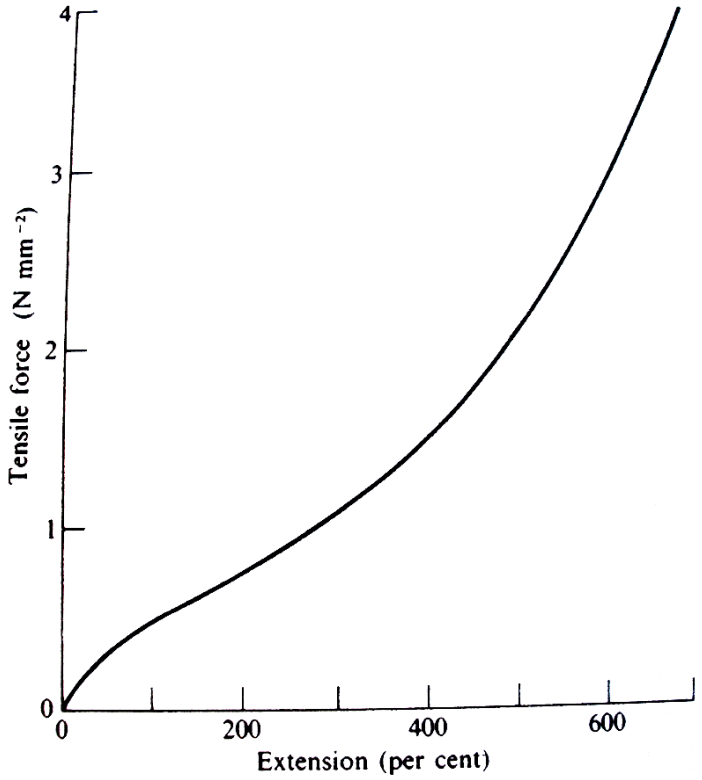

Figure 2.3: A typical force-extension curve for vulcanised rubber (Treloar, 1975).

A distinctive non-linear "S" shaped force against deformation curve, as shown in Figure 2.3 for a typical natural rubber, is obtained when a tensile force is applied to an elastomer test piece. The curve at small strains is initially linear and could remain linear up to a value of approximately 2 % dependent upon the detailed chemistry of the elastomer material. Above this limit of proportionality the Young's modulus of the material will vary (Treloar, 1975).

At much larger strains an upturn is observed in the stiffness, this is a result of the finite extensibility of the molecular network as the entanglements of the polymer molecules interfere with each other. For some elastomers the maximum extension can be in excess of 500 % strain (Treloar, 1975). The behaviour shown by the curve is also dependant upon temperature and other factors which will be mentioned in the following sections.

2.3.2 Viscoelasticity

Viscoelasticity is the term often used to describe elastomer materials, where they exhibit the behaviour of both an elastic solid and that of a viscous liquid.

If a force-displacement or stress-strain curve is produced from a tensile test of an elastomer material the results would be depend upon the rate of strain. If the load is then removed from the test piece, the material does not instantaneously recover to the initial undeformed shape. The material usually follows a different curve to the loading curve. So it is evident that the stress is not just proportional to strain, even within the elastic range. The stress-strain relationship is not only a function of the current load being applied, but also of the load history and it is also time-dependent and varies with time (Hall, 1968).

When an elastomer has a stress applied instantaneously there is a corresponding instantaneous elastic strain ε_O. If the stress is held constant, the strain continues to increase and this is referred to as the creep strain ε_c. When the stress is removed there is an instantaneous elastic recovery comparable in magnitude with the original instantaneous elastic strain ε_O. With time the residual strain will recover by an amount known as the creep recovery ε_r (Hall, 1968).

The creep effect for an elastomer is usually linear against the logarithmic value of time. If a tensile stress is applied for an extended period of time, the rate of creep will increase abruptly, due to the onset of oxidation effects over longer time periods. Different elastomers can show large differences in the amount that they creep. Typically harder elastomers creep more than softer ones and elastomers with more filler creep more than those with less filler (Hall, 1968)

Hysteresis is easily observed as the difference between the loading and unloading of the stress versus strain curves of an elastomer test piece, as shown in Figure 2.4. Roark (1989) defines mechanical hysteresis as; “The dissipation of energy as heat during a stress cycle, which is revealed graphically by failure of the descending and ascending branches of the stress-strain diagram to coincide”.

Because rubbers typically have low thermal conductivity, high temperatures can be reached in larger components when subjected to high-stress and / or high-frequency cyclic loading (MARC, 1996). The temperature increase can have a significant effect upon the stiffness of the material and at large strains or at high frequencies stress concentrations can cause hot spots.

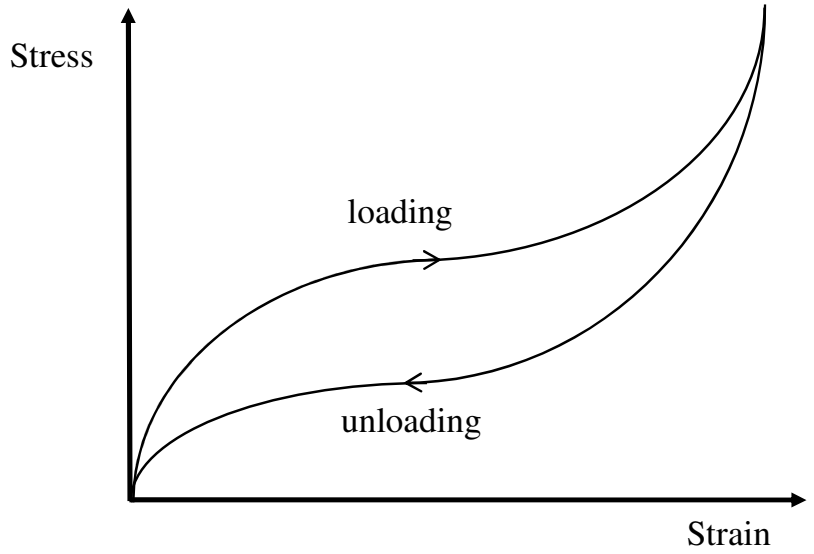

Figure 2.4: A schematic of the hysteresis curve for a typical elastomer, produced during the loading and unloading of an applied force.

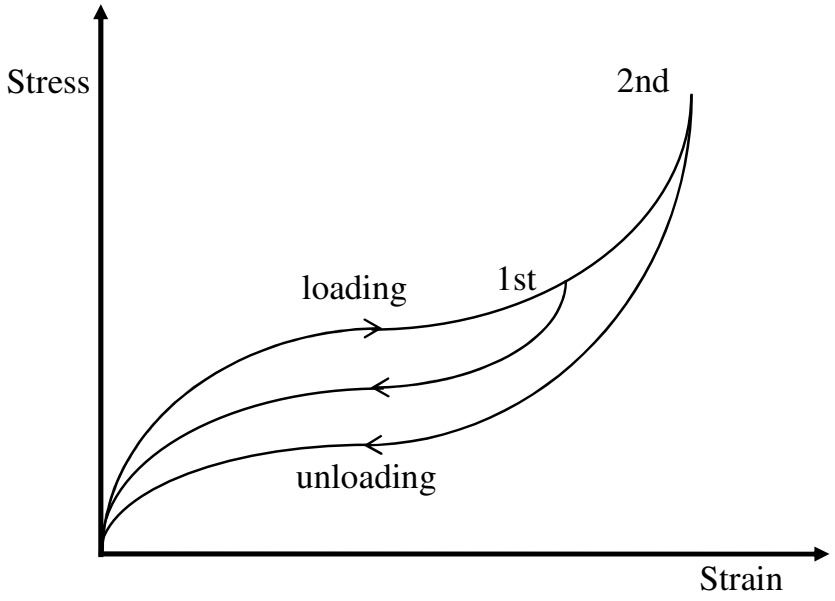

Figure 2.5: The Mullins effect for a typical elastomer, produced during repeated loading and unloading of an applied force.

Many elastomer components experience cyclic loading during their service life, such as engine mountings and suspension components in automobiles. This loading from cycle to cycle is often seen to reduce the modulus of the material.

The cyclic stress softening phenomenon was described first by Mullins and now bears his name. The Mullins effect, as shown in Figure 2.5, occurs when an elastomer has an initial load applied to it (MARC, 1996). The load causes the network structure to be modified and reformed due to the breaking of some of the cross-links between the polymer molecules. It is also proposed that in filled elastomer composite the polymer can slide around the filler surface and this combination of effects results in a lower stiffness and altered damping characteristics.

2.3.3 Mechanical behaviour of elastomers

The modulus of rigidity or shear modulus, G, is directly comparable to the modulus of elasticity for direct stress applications, where,

$$G = \frac{\tau}{\gamma} \tag{2.1}$$

and τ is the shear stress and γ is the shear strain.

The Bulk Modulus, B, is a ratio of stress and strain, but under hydrostatic pressure conditions with a pressure, σ, in all directions producing a corresponding volumetric strain,

$$B = \frac{\sigma}{\varepsilon_v} \tag{2.2}$$

At modest strains the bulk modulus and shear modulus are related to the Young's modulus or tensile modulus, E, and the Poisson's ratio, ν, by the following equations,

$$G = \frac{E}{2(1+\nu)} \tag{2.3}$$

and $$B = \frac{E}{3(1-2\nu)} \tag{2.4}$$

Elastomers have very low shear modulus and tensile modulus, but the bulk modulus is comparable to many other engineering materials. Therefore the Poisson's ratio is very close to 0.5 and the tensile modulus is almost exactly $3G$.

When an elastomer with a small cross sectional area is stretched perpendicularly, such as during a tensile test of a specially prepared test piece, large extensions result from relatively small forces. The extension to break for that the test piece can vary, but is usually somewhere between 100 to 1000 per cent of the original length. For practical

reasons the extension of the test piece is compared to its original length, it is given a corresponding ratio, λ the stretch ratio, where a λ of 5.5 is equivalent to an engineering strain of 450 %.

$$\begin{aligned} \lambda &= L / L_o \\ &= (L_o + x) / L_o \\ &= 1 + (x / L_o) \end{aligned} \tag{2.5}$$

L refers to the deformed length, L_o is the original length and x is the amount of deformation.

The true stress, σ (or Cauchy stress) is often a more appropriate value to use for the stresses in an elastomer material, rather than the engineering stress, due to the large deformations that occur when a force is applied to an elastomer component. The true stress within the component during a tensile test is calculated by dividing the resultant force for a given deformation by the cross sectional area of the material at that force and deformation, rather than the original cross sectional area.

$$\sigma = \frac{F}{A_d} \tag{2.6}$$

where A_d is the deformed cross sectional area.

The engineering strain ε is found by dividing the actual extension at a given point during the test by the original length. True strain is sometimes shown on a logarithmic scale for convenience, the logarithmic strain is found by taking a logarithm of the stretch ratio, at the corresponding stress.

$$\varepsilon = \ln\left(\frac{L}{L_o}\right) \tag{2.7}$$

Strain invariants are mathematical functions of the stretch ratios of a homogenous elastomer; a homogenous elastomer has elastic properties that are uniform throughout the material (Hall, 1968). The strain invariants are calculated from the stretch ratios that occur when an elastomer deforms. If forces occur in the three principal directions, x, y and z, there are three corresponding stretch ratios, λ_1, λ_2 and λ_3, these are shown in Figure 2.6. The three strain invariants I_1, I_2 and I_3 are then defined as follows,

$$I_1 = \lambda_1^2 + \lambda_2^2 + \lambda_3^2 \tag{2.8a}$$

$$I_2 = \lambda_1^2\lambda_2^2 + \lambda_2^2\lambda_3^2 + \lambda_3^2\lambda_1^2 \tag{2.8b}$$

$$I_3 = \lambda_1^2\lambda_2^2\lambda_3^2 \tag{2.8c}$$

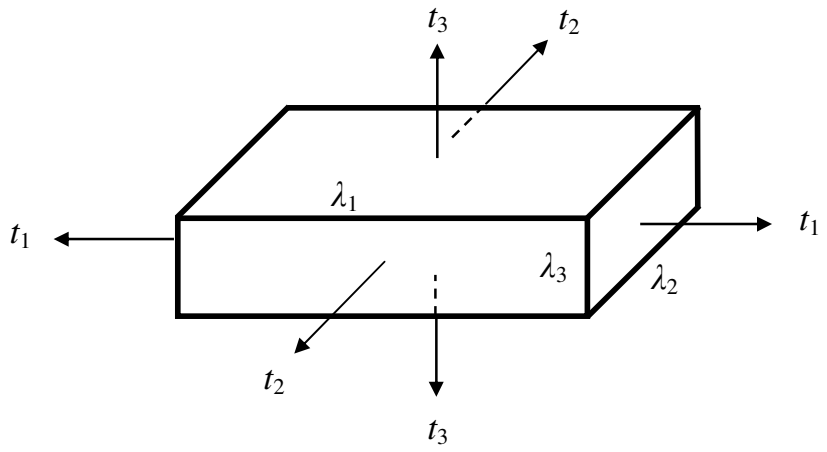

Figure: 2.6: The three stretch ratios resulting from a force in the three principal directions.

When Rivlin used a mathematical basis to develop his formula for a type of strain energy function for a pure homogeneous strain, he assumed that the material was isochoric (Rivlin, 1992). Isochoric materials are incompressible and isotropic when unstrained, isotropic means that the material has the same properties in all directions, particularly strength and elastic properties, such as the modulus of elasticity, the modulus of rigidity and Poisson's ratio (Roark, 1989). Elastomers are not truly incompressible, but are more accurately described as volume retaining, where there is no volume change when the material is subjected to a hydrostatic pressure. The strain in the material is not related to the hydrostatic pressure in the material and Poisson's ratio is almost 0.5 (typically 0.4995). As noted in the previously the bulk modulus is typically several orders of magnitude greater and when assuming approximately incompressible behaviour the third strain invariant is often assumed to be equal to 1.

where $I_3 = \lambda_1^2\lambda_2^2\lambda_3^2 = 1$ (2.9a)

so the remaining two strain invariants can be expressed as follows,

$$I_1 = \lambda_1^2 + \lambda_2^2 + \lambda_3^2 \quad (2.9b)$$

$$I_2 = 1/\lambda_1^2 + 1/\lambda_2^2 + 1/\lambda_3^2 \quad (2.9c)$$

2.4 Molecular theory

2.4.1 Molecular theory introduction

There are two types of theory commonly used to explain the molecular behaviour of elastomers, these are the statistical theory and the phenomenological theories. The statistical theory, sometimes referred to as the kinetic theory or neo-Hookean theory, is based on the entropy change when mechanical work is used to deform the material. The phenomenological theories use an approach which is based on finding appropriate equations to fit the measured mechanical behaviour of the material. Both types of theory develop a Strain Energy Function (SEF), sometimes referred to as a Stored Energy Function. The SEF relates the amount energy stored for a unit of volume at a specific strain (Ogden, 1972).

2.4.2 Statistical / kinetic theory

The statistical (or kinetic) theory was developed by Meyer et al (1932) as a way of understanding the behaviour of rubber elasticity that is based on a statistical concept of the long chain molecules within the material, where the thermal motion of the molecules is analogous to the kinetic theories of gases (Treloar, 1975).

In 1931 Haller investigated the effect of thermal fluctuations on the bond length and valence angles of paraffin chains and was the first to propose the notion of the long chain molecules coiling up. Karrer later applied this theory to muscle fibres, which are themselves long chain molecules and behave in a very similar way to soft lightly cross-linked elastomer materials, before Meyer and Ferri finally associated this with the behaviour of elastomers in 1935 (Treloar, 1975).

It was initially believed that, due to the thermal energy, vibrations occurred that were larger in a direction perpendicular to the long chain than in the direction of its length. Therefore, the lateral forces between the chains are weaker than the primary valence forces contained in them, so repulsive forces between each extended parallel chain pull both ends together, which is equivalent to a longitudinal tension. Therefore, when an elastomer test piece is loaded and stretched and the load is then removed, the test piece will contract until the internal molecules in the elastomer are in a statistically irregular arrangement and the molecules that interact with each other do not move away in any given direction (Treloar, 1975).

The development of the kinetic theory into a statistical theory was based on two separate assumptions. Firstly for a single long chain molecule related to its random geometry configuration, secondly it was extended to consider a network of long chain molecules such as with a cross-linked elastomer. According to Treloar (1975) the theory was developed further by Kuhn (1934, 1936) who found that the deformation of an elastomer can be based on statistics and probability, where the distance between the ends of the long chain molecule comply with a Gaussian probability distribution function which commonly occurs when investigating random events (Treloar, 1975), this is shown in Figure 2.7.

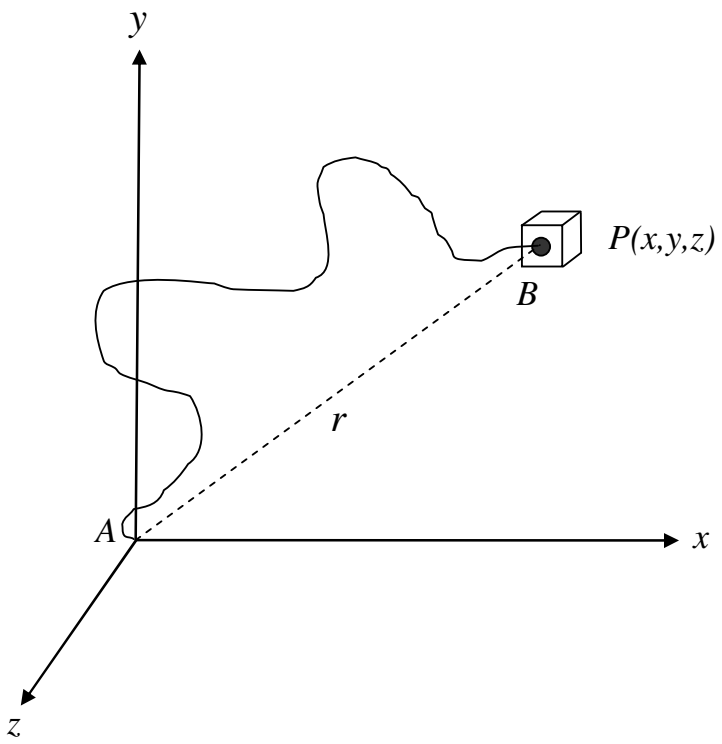

Figure 2.7: The statistically kinked long chain molecule (Treloar, 1975).

The statistical theory does not represent the entire physical phenomena exhibited by elastomers as, for example at higher strains when the material approaches a finite extensibility effect, the model does not show the observed increase in modulus. More recently phenomenological theories have been developed that are accurate over a wider strain range.

2.4.3 Phenomenological theories

The phenomenological theories disregard the molecular or structural forces that are developed to derive the statistical theory and instead use an approach that just aims to describe the physical phenomenon of rubber elasticity (Treloar, 1975). Several resulting theories have been developed, to explain the physical properties of an elastomer material at large elastic deformations.

The idea of calculating the elastically stored energy, or strain energy, W, to determine the mechanical properties of a perfectly elastic material in terms of the variation in strain was developed by Mooney (1940) and later added to by Rivlin (1948). The strain energy functions are divided into two types, those that use the three strain invariants I_1, I_2 and I_3 and those that use stretch ratios λ_1, λ_2 and λ_3.

The simplest strain energy function is the neo-Hookean model which obeys the rules of statistical mechanics and thermodynamics (Yeoh, 1990 and MARC, 1996) and is normally written as,

$$W = C_{10}\left(\lambda_1^2 + \lambda_2^2 + \lambda_3^2 - 3\right) \tag{2.10a}$$

or $$W = C_{10}\left(I_1 - 3\right) \tag{2.10b}$$

The neo-Hookean model is only really suitable for relatively modest tensile strains of up to 40 % or simple shear strains up to 90 % and for unfilled rubber materials (MARC, 1996). The C_{10} constant is derived from test data obtained from simple tests such as a tensile test of a dumbbell test piece and is equivalent to $G / 2$, where G is the shear modulus.

Mooney developed the Mooney formula as an expression for strain energy for the case of simple extension and uniaxial compression. It is not suitable for complex loading such as equibiaxial extension, which is analogous to uniaxial compression but compares well to uniaxial tensile test data. The Mooney formula for an incompressible solid in tension can be written as,

$$W = C_1\left(\lambda^2 + 2/\lambda - 3\right) + C_2\left(\lambda^2 + 2/\lambda - 3\right) \tag{2.11a}$$

or $$W = C_1(I_1 - 3) + C_2(I_2 - 3) \tag{2.11b}$$

The Mooney model is a special case of a more general approach that was developed by Rivlin (1948), it is suitable for strains of up to 100 %, although it cannot model the stiffening accurately above this. It is also unsuitable for predicting compression behaviour using data measured in tension. The Rivlin formula has been

used to examine large strains where it can be written as the sum of a series of terms (Treloar, 1975),

$$W = \sum_{ijk=0}^{\infty} C_{ijk} (I_1 - 3)^i (I_2 - 3)^j (I_3 - 1)^k \tag{2.12}$$

The formulas were developed to show deviations from the Gaussian theory by using the data from simple tensile tests. The work of Gumbrell (1953) on the behaviour of materials in relation to the Mooney function, as discussed by Ogden (1972), demonstrated that the constant C_1 is affected by the amount of cross-linking but almost completely independent of swelling, whereas for C_2 the reverse was true. Ogden (1982) also discusses the work of Mark (1975) which improved the previous work and which was examined by Treloar (1975). Mark showed that the Mooney formula is only suitable for predicting tension at small and moderate deformations, but if the deformations are large or a biaxial test is conducted, the formula deviates greatly from the experimental results. This is due to the C_2 term not successfully deducing the behaviour of the molecular structure; the formula agrees with the statistical theory but does not improve upon it.

In an attempt to model the non-Gaussian behaviour at higher extensions many people have expanded Rivlin's formula. Tschoegl (1971) adopted higher order terms which reportedly gave more accurate results for both unfilled and filled elastomers. A commonly used three term Mooney-Rivlin model is given as;

$$W = C_{10}(I_1 - 3) + C_{01}(I_2 - 3) + C_{11}(I_1 - 3)(I_2 - 3) \tag{2.13}$$

Higher order models can improve the fitting of the function with the experimental data, but predictions beyond the range of the collected data can be worse than when using simpler models.

The Yeoh (1990) model is simpler than many other phenomenological theories, as it only includes the first strain variant. Yeoh developed the model using the first three terms in $(I_1 - 3)$ of the Rivlin model. It therefore only requires data from a simple tensile test of a dumbbell test piece and is a versatile model as it can fit many types of deformation. Care still needs to be taken for small strains and small deformations. The Yeoh model assumes that the term for the second strain invariant $(I_2 - 3)$ can also be neglected. Most FEA software that can model rubber behaviour have implemented the Yeoh stored energy function which is written as,

$$W = C_{10}(I_1 - 3) + C_{20}(I_1 - 3)^2 + C_{30}(I_1 - 3)^3 \tag{2.14}$$

2.5 Physical behaviour of foams and foamed elastomers

2.5.1 Introduction

Foamed materials are primarily used to absorb energy from impact, to form a lightweight structure or to make comfortable soft human interface material. Many materials can be foamed, including polymers, metals, ceramics and glasses. Foamed materials generally have either closed cells where air, gases or liquids are trapped within each cell, or they have open cells and behave like a sponge, where the fluids can flow throughout the voids in the material. Examples of open-celled and closed-celled foams are shown in Figure 2.8 (Gibson and Ashby, 1988).

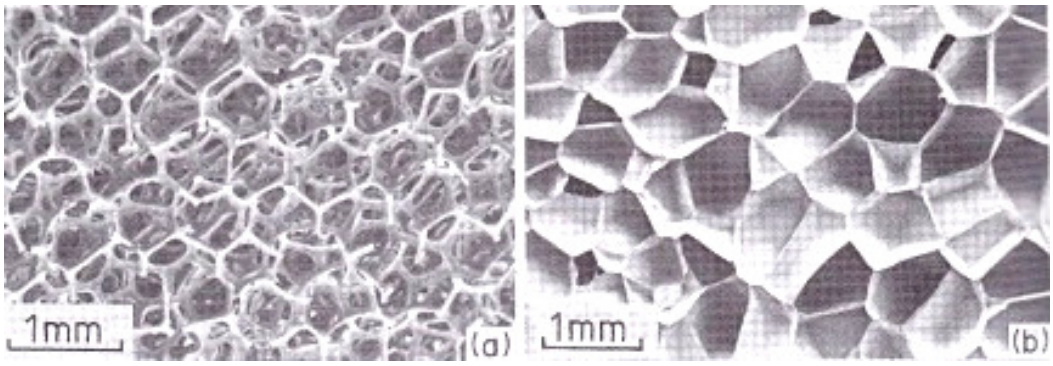

Open-celled Foam Closed-celled Foam

Figure 2.8: A comparison of the structure of open-celled and closed-celled foams (Gibson and Ashby, 1988).

Elastomer foams are produced in a number of ways from various elastomer materials, with polyurethane being the most commonly used elastomer foam. Other elastomer foams include latex foam, produced from natural rubber and aerated silicone elastomer foam. The most common uses are for seating components particularly cushions, other applications include carpet underlay, anti-vibration mountings, other industrial and medical devices (Higgins, 1987; MARC, 1990 and Kalpakjian, 1995).

The primary aim of this thesis is to examine the behaviour of a closed cell elastomer foam that has been produced by the addition of thin walled hollow plastic microspheres into a silicone elastomer to produce a closed cell elastomer foam.

2.5.2 Historical applications of foamed elastomers as submarine coatings

Elastomer coatings have been found to reduce the detection of submarines. The elastomer can be designed to direct enemy sonar away from the original source, as well

as diffusing echoes and the internal noise of the submarine. The former can be achieved because the acoustic impedance of the elastomer can be made to match that of the surrounding sea water, if the acoustic impedance of two materials is the same then at the boundary between them there is no reflection. To avoid detection the elastomer can also be made to convert longitudinal sound waves into shear waves, this can be achieved by using a thin elastomer film between two rigid surfaces or by adding inclusions to the elastomer such as small glass spheres or gas bubbles (Roland, 2004). Hence the interest and purpose of this thesis in understanding the behaviour of hollow plastic microspheres to create an elastomer foam.

During the Second World War research was conducted by German submarine designers, this resulted in an elastomer coating of approximately 4 mm in thickness being applied to the outer surface of the submarines that was designed to mask the vessel from sonar tracking devices (Baker, 1990). However, the coating was less effective at greater depth, a further problem was that it was difficult to apply successfully to the submarines surface and so it often became detached. Despite the problems it was the first anechoic covering for submarines, as it contained voids and air cavities which helped to reduce the reflection of the sonar.

During the Cold War an increasing amount of attention was paid to improving the stealth and to reduce the signatures of submarines especially acoustically for both active and passive sonar. Making a submarine quieter makes it harder to detect and also improves the sensitivity of its own sensors. Noise can also be reduced by improvements to machinery, engines and drive systems, as well as from hydrodynamic considerations.

During the 1970s Russian submarines were fitted with elastomer tiles that were several tens of millimetres thick and worked on the same anechoic principle as the early German coatings. It made the submarines more difficult to detect, although initially the tiles were not bonded effectively and they often detached, leaving gaps and reducing their effectiveness.

In 1988 the United States started to apply an anechoic coating to its submarines, it was at this point that the British Navy also adopted anechoic tiles. In the early tiles the voids in the material were of varying sizes, whereas modern tiles have voids that are more uniformly sized. The tiles usually are applied by either bonding them or casting them onto the submarine surface, in all cases the preparation of the bond surface is vitally important to prevent the material from detaching in service. In the past a spray coating of an elastomer onto the surface of the submarine was done to include voids and

this was applied in a number of layers of 2 mm in thickness. Spraying is no longer used and modern anechoic tile materials are more refined. Modern methods use a multilayered approach with anechoic properties used to absorb and dampen and further decoupling materials to reflect, as well as other materials to transmit sound from the submarines own sonar equipment (Baker, 1990). A modern Royal Navy submarine with anechoic tiles is shown in Figure 2.9.

Figure 2.9: A submarine showing the (elastomer) anechoic tiles fitted to the hull.

The recent development of anechoic tiles includes the incorporation of thin walled polymer microspheres as a filler material. A chosen uniformity of void size can more easily be achieved with microspheres of known diameters and the resilience of the microspheres means that they should return to their original shape once a load had been applied and then removed. It is worth noting that the tiles will experience many extreme changes in external pressure as the submarine dives and resurfaces frequently in use.

Akzo Nobel manufacture the types of microspheres, known under a trade name of Expancel, which are commonly incorporated in the tiles and for this reason they are examined in detail in this thesis. The Expancel product range has many industrial applications including being used as lightweight fillers and as blowing agents in ink, textiles and other materials. For the particular application studied here the cells are somewhat expanded, but they are used in this state as a filler in the acoustic damping tiles.

2.5.3 Physical behaviour of foams and foamed elastomers

The linear elasticity of a foam depends upon whether the foam contains open or closed cells. At low densities, foams with open cells deform principally by cell wall bending. This phenomenon has been examined by many researchers notably Gibson et al (1982) for two dimensional cellular materials and by Gibson and Ashby (1982) for three dimensional cellular materials, a comparison of the behaviour of different types of foam is shown in Figure 2.10. Lakes et al (1993) and others have also examined elastomeric cellular solids.

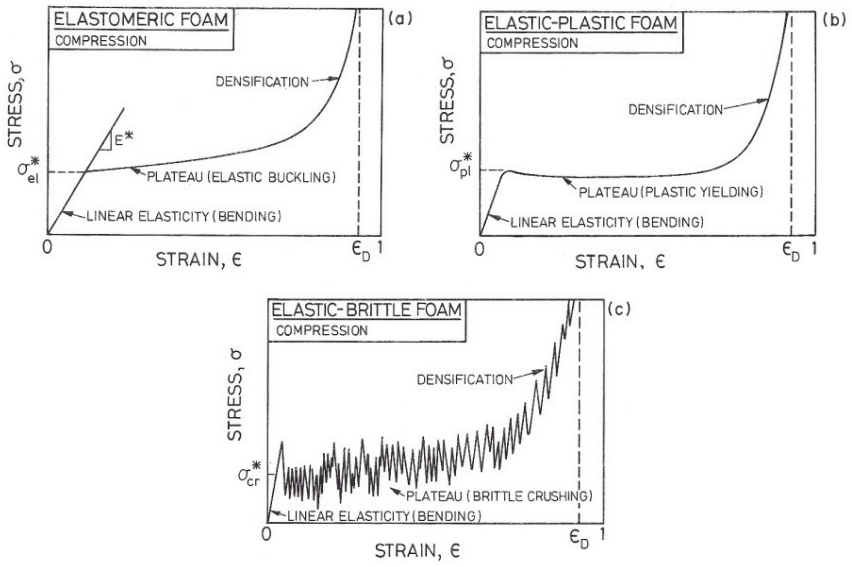

Figure 2.10: The typical behaviour of different foams when compressed (Gibson and Ashby, 1988).

As the relative density increases the extension or compression of the cell walls plays an increasingly significant role. If a foam with open cells contains a fluid, the fluid flow will contribute to the elastic moduli, especially if the fluid is highly viscous and the strain rate is high. If the foam has closed cells the cell edges bend and extend and contract, at the same time the cell faces, which are a membrane, stretch. The cell wall stiffness therefore contributes to the elastic moduli. Gent and Thomas (1959, 1963) and others have examined this phenomenon. If the cell walls do not rupture, then any fluid, usually air, contained within them will also contribute to the overall stiffness. When elastic foams are compressed they exhibit a non-linear elastic deformation that occurs in three distinct phases; cell wall bending, cell wall buckling and densification.

The graph in Figure 2.11 shows the relationship between the Young's modulus of a rubber foam, Y_F, to that of the solid rubber, Y, calculated from the measured density. The solid curve represents the theoretical relationship and the broken curve is a low density equivalent.

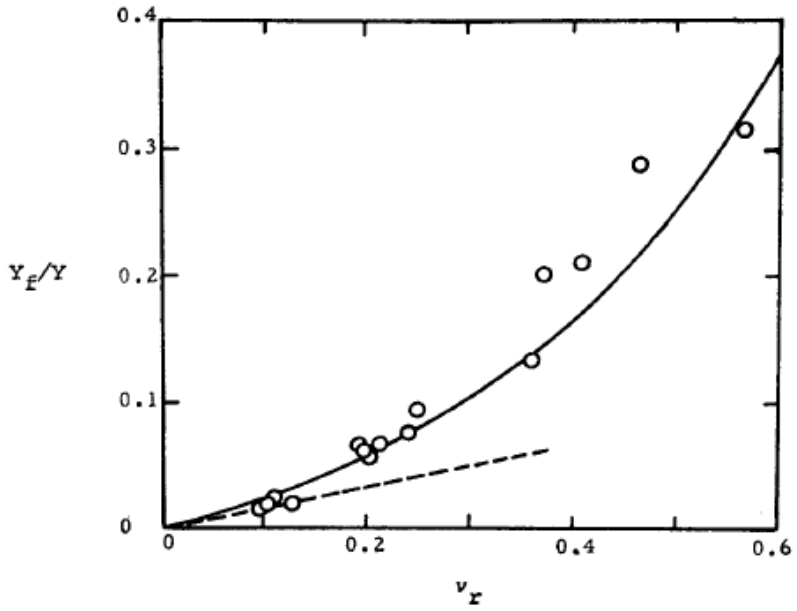

Figure 2.11: The relationship between the Young's modulus of an elastomer and its density (Gent and Thomas, 1963).

The work of Gent and Thomas (1959a) examined the behaviour of an unfilled latex elastomer, which is solid, compared to a range of foamed latex elastomers, with volume fractions ranging from just under 1 % voids to just over 56 % voids. It was evident that as the density of the elastomer decreased so too did the Young's modulus.

Gent and Thomas also found that foamed elastomers break at lower strains than the corresponding solid elastomer. For a foamed elastomer with an elastomer volume of only approximately 10 %, the tensile strength is also much lower when compared to the bulk material; it is about one hundredth of that of the bulk material. As the breaking load of the elastomer is reached during a tensile test the threads of material can be seen and heard to break. The tensile failure is due to flaws being present, the largest of which grow and the flaws become catastrophic at the breaking load (Gent and Thomas, 1959b). The tear strength can be calculated for a model consisting of many thin threads, using the energy criterion developed by Rivlin and Thomas (1963) for a solid elastomer.

The relationship between the tearing energy of an elastomer and its density is shown in Figure 2.12.

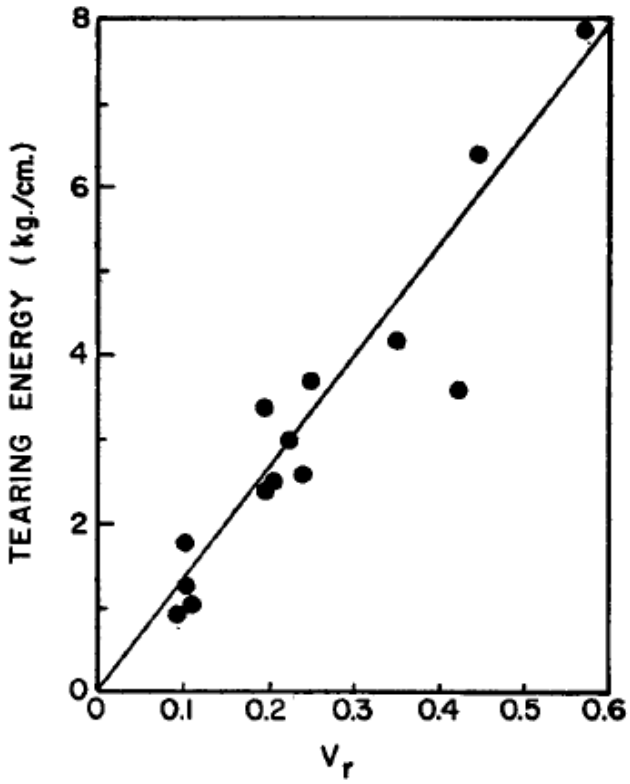

Figure 2.12: The relationship between the tearing energy, T_f, of an elastomer and its density, shown as the volume fraction of the rubber, v_r, (Gent and Thomas, 1963).

Christensen (1986) conducted additional work to derive effective elastic moduli for low density materials, as well as compressive strength for open and closed-cell isotropic materials. The work by Christensen examines the two main theories regarding materials with closed cells, firstly the theory that supports membrane deformation and secondly the theory that supports cell wall bending. Christensen proposes that the behaviour depends upon material type and the inherent differences between the geometries of the microstructures.

Christensen (1979) has also examined the effects of spherical inclusions on the effective moduli of a material. Where the particles are small and far apart, or dilute, the interaction between the particles is small and can be neglected. This is applicable to rigid particles in an incompressible matrix, such as for a carbon black filled elastomer

and is not necessarily applicable to a foamed elastomer, unless the filler material has some stiffness at low strains.

2.5.4 Hydrodynamic behaviour of filled elastomers

Einstein (1906, 1911) developed a viscosity law for rigid spherical particles embedded in a continuous liquid. Similar theories were later developed for suspended colloidal particles in either a liquid or a solid. The Einstein viscosity law was fundamental for the development of stiffness predictions in elastomer composites; it explains the change in viscosity when a rigid spherical particle is incorporated into an incompressible fluid, a filled elastomer is analogous to this situation. Einstein's viscosity law equation follows, where η is the viscosity of the emulsion, η_O is the viscosity of the incompressible fluid and Φ is the filler volume fraction.

$$\eta = \eta_O(1 + 2.5\phi) \tag{2.15}$$

Guth and Gold (1938) and later Guth (1945) proposed an equation for Young's modulus that was based on Einstein's viscosity law, but included an extra squared term to account for mutual disturbance at a higher concentration of particles.

$$E = E_O(1 + 2.5\phi + 14.1\phi^2) \tag{2.16}$$

E_O is the Young's modulus of the original unfilled elastomer and E is the Young's modulus of the filled elastomer. However, the formula is inadequate for reinforcing fillers particularly at high filler volume fractions as it uses the same assumptions as Einstein's equation. The assumptions are that all of the particles are well dispersed, there is no slip at the filler / rubber interface and the spheres are perfectly spherical. Therefore for practical purposes it is only suitable for small strains and for filler volume fractions of less than $\Phi = 0.2$ and where the particles do not agglomerate.

A further equation was proposed by Guth (1945) that included particles that were not perfectly spherical, this included a shape factor and was applicable to rod shaped and other particles.

2.6 Physical behaviour and uses of elastic hollow spheres

2.6.1 Introduction

The microspheres are a polymer shell containing a fluid, which if heated increases in pressure. As the temperature rises it causes a simultaneous softening of the thermoplastic shell, the microsphere expands to between thirty and fifty times its

original volume, depending on the type used. When the heat is removed the shell stiffens and the microsphere remains expanded.

Anechoic tiles such as those used on submarines are typically produced using a foamed elastomer material. Recent developments in the manufacture of anechoic tiles have seen the tiles incorporate microspheres that produce a closed cell foam, with the advantage that the size of the voids or pores can be regulated by using microspheres of a specified size. The microspheres are also resilient and will return to their original shape upon unloading after the repeated physical loading and unloading cycles due to changes in hydrostatic pressure that are experienced when a submarine changes depth. It is these two properties that make them a viable filler for the elastomer material for anechoic tiles.

2.6.2 Properties and uses of elastic hollow spheres

The microspheres used for this work were manufactured by Akzo Nobel and are known as Expancel, an image of some Expancel microspheres is shown in Figure 2.13. The Expancel microspheres are available with diameters between 6 μm and 40 μm unexpanded and 20 μm to 150 μm expanded. They have very low true densities of 25 kg/m^2 to 70 kg/m^2. The thin shell is made from a copolymer of three monomers; vinylidene chloride, acrylonitrile and methylmethacrylate and the blowing agent is either isobutene or isopentane. For many applications the unexpanded microspheres can be heated, usually between approximately 80 ºC and 200 ºC depending upon the type of microsphere used, this rise in temperature causes the unexpanded type of microsphere to expand further (Akzo Nobel, 2004).

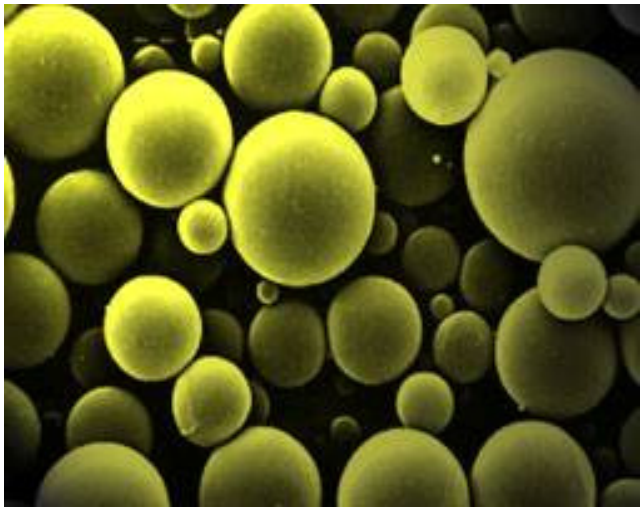

Figure 2.13: An image of the Expancel microspheres (Akzo Nobel).

Microspheres contain a fluid and as a result are highly resilient. The expanded microspheres are easily compressed and when the pressure is removed they regain their original shape and volume. This allows them to experience thousands of loading and unloading cycles without permanently collapsing or bursting.

Microspheres have a number of uses as a filler material including: as a blowing agent, a weight reducer and as a property improver. This produces a controlled foaming when conducted at low temperatures and produces a homogeneous cell structure with little cell collapsing.

Unexpanded microspheres are used as a blowing agent in printing inks to achieve a three-dimensional pattern on paper, wallpaper and textiles. They can also be added to sealants and underbody coatings where they have a low density and good thermo-mechanical properties. Thermoplastics can be foamed in a controlled and predictable way as the cell structure is completely closed and of a known size. Polyurethanes can be reaction injection moulded with microspheres added to compensate for moderate shrinkage.

Unexpanded microspheres can be added during the production of shoe soles, which gives low weight and a high elasticity. Adding 1 % by weight of microspheres to paper or board increases the volume by 20 %, significantly improving the stiffness and this can improve its printing properties. Microspheres are used as a single filler or with other fillers in polyester putties this reduces the density of the putty and lowers the porosity, they are also easier to sand and give a better finish than ordinary putties. They can be added to paint this reduces the weight and hence the transportation costs as well as improving the applicability and reducing splash when applied to a wall using rollers, due to the lower weight compared to standard paint.

By adding microspheres to thermosets such as a phenolic, glass, or a silica mixture the weight is reduced as are breakages, they are also easier to trim and drill. Expanded microspheres are added to polyurethanes in cast polymers, coating and sealings to reduce the density and improve shock, vibration and sound absorption. They are also used in cables with liquid petrolatum to fill the gaps between the conductors, this provides resistance to water penetration and can also increase the capacity of the cable and reduce the thickness of the insulation.

Adding microspheres to an expensive material might lower the overall cost of the product if the filler material is cheap compared to the matrix material and the lower weight also reduces transport and handling costs.

The microspheres used in this project are Expancel DE 551 40 d42 manufactured by Akzo Nobel and are dry expanded (DE) nominally 40 μm in diameter (40), they are dry and expanded with a density of 42 kg/m^2 ± 4 kg/m^2 (d42).

2.6.3 Physical behaviour of elastic hollow spheres

There are many situations where a sheet or plate, of a material, whether it is metal, plastic or rubber, can be in both tension and compression in two perpendicular directions at the same time, where the results are biaxial stresses in the material. When a thin walled container, such as a hollow sphere is subjected to internal pressure as in the case of a pressure vessel, or an external pressure as in the case of a submarine, it will experience similar phenomena.

When such a component is subjected to this type of loading, the predominant stresses are membrane stresses, which are constant through the component wall. But this is only true where the wall thickness is very small compared to the diameter, typically the ratio of wall thickness to diameter would be approximately 1:20. In this case any radial stresses produced can be assumed to be uniformly distributed through the thickness of the wall; they are also small compared to the meridional and circumferential stresses and so can be ignored, although this is only an approximation, in reality all three stresses will vary in magnitude through the wall thickness.

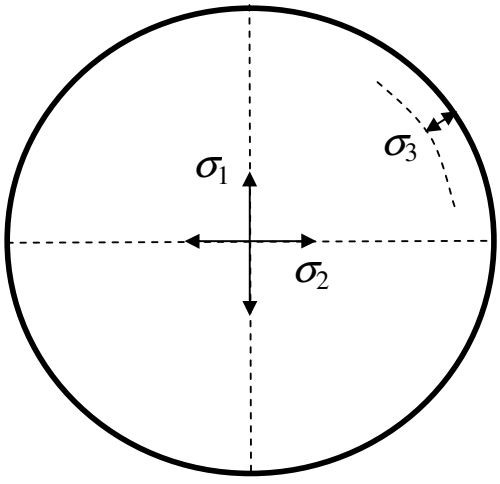

Figure 2.14: A spherical shell showing biaxial stresses.

If a globe is used as an analogy for a sphere the meridional forces occur vertically and the circumferential forces occur horizontally. The meridional membrane

stress σ_1 occurs parallel to the meridian, the circumferential membrane stress, or hoop stress σ_2 occurs along the circumference parallel to the equator as shown in Figure 2.14. The small radial stress σ_3 occurs through the thickness of the wall. Additional bending and / or shear stresses can also occur depending upon the external loading, such as concentrated loads, or where there are sudden changes in wall thickness, either thinner which causes a weak region or thicker where the wall can no longer be considered as a membrane and there is a large variation of σ_1 or σ_2 through the wall.

The behaviour of flat plates and spherical objects has been explained on numerous occasions most notably by Timoshenko and Goodier (1951) and Timoshenko (1968), much earlier analysis such as that for the buckling of an axially compressed elastic rod or column was published by Euler in 1757. However the buckling and folding phenomenon that occurs to hollow spheres under large deformations is less well understood.

When a hollow thin walled elastic sphere is compressed between two parallel rigid surfaces there is an initial flattening of the sphere where it is on contact with the rigid surfaces. Under further compression there is a snap through buckling of the flattened areas, finally at the more extreme compressions a number of ridges and folds are formed.

Pauchard and Rica (1998) studied the behaviour of elastic spherical shells, where they analysed the effect of two different separate compressive loads applied to table tennis balls. The first case was used a rigid plane to produce a flat contact between the sphere and the rigid plane and is of particular interest to this project. For the second case the load was applied locally as a point load.

The contact between two bodies at small strains can be examined according to the theory of Hertz, this approach was also explored by Pauchard and Rica. Hertzian theory states that where two elastic bodies are pressed against each other, elastic energy is stored in the volume where the elastic deformation occurs. Pauchard and Rica conducted a series of experiments with tennis balls and table tennis balls in static contact with a rigid plane and found a that a first order transition occurred as the compression was increased. This type of deformation is particularly useful for this project in order to understand how microspheres behave when compressed, either when they are tested singularly or embedded as a filler material in an elastomer matrix.

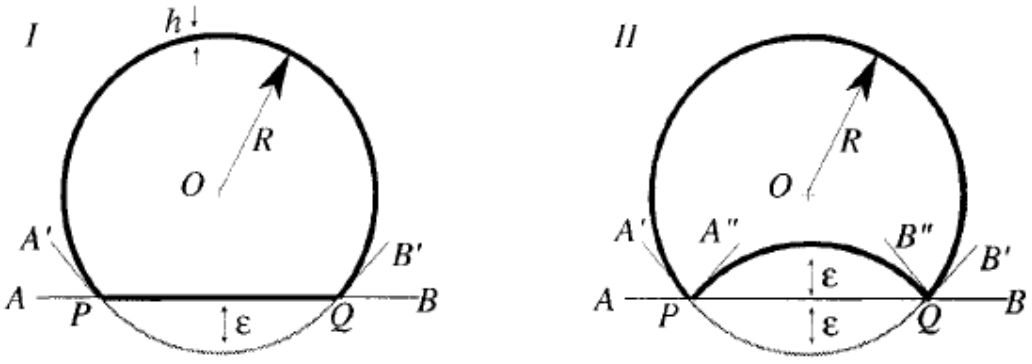

Figure 2.15: The flattening and snap through buckling of a sphere (Pauchard and Rica, 1998).

For their experiments Pauchard and Rica did not use a complete sphere, but a hemisphere that was compressed between two parallel rigid plates, where the circumference of the base of the hemisphere was fixed to one of the rigid plates in order to avoid non-symmetric deformations. When the plates were brought together two types of deformation were observed as shown in Figure 2.15. The sphere initially flattened against the rigid plate. Secondly a further deformation occurred in the form of a sudden snap through buckling of the flattened surface with the increase in compression and this resulted in an inverted curvature. The second deformation, the snap through buckling, was thought to occur at a deformation that was a little over twice the thickness of the sphere wall.

Pauchard et al. (1997) explored the Föppl-von Kármán theory and its application in an earlier paper. The Föppl-von Kármán theory for planar geometries has been applied to thick shells where the main deformation is larger than its radius of curvature.

Pauchard and Rica (1998) used the Föppl-von Kármán theory, along with observations of the second deformation to deduce the form of the energy for the axially symmetrically deformed shell, for both the initial and second buckling phenomena. The expressions produced by Pauchard and Rica qualitatively explained the observed features, although they included a set of unknown parameters that were thought to depend only upon the Poisson's ratio. This meant that the deformation required for the transition to an inverted curvature was not only proportional to the wall thickness, but was also dependent upon the Poisson's ratio.

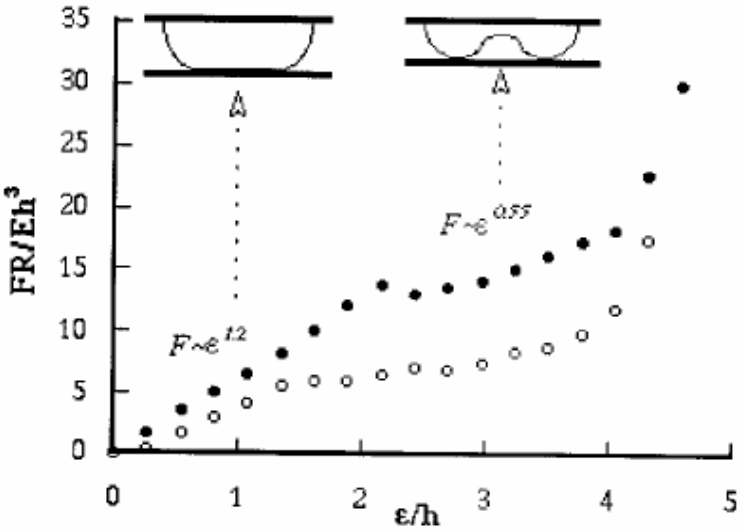

Figure 2.16: The force-deformation curve indicating the snap through point (Pauchard and Rica, 1998).

Pauchard and Rica also observed a corresponding change in slope and a kink at the point where the deformation process caused the sphere that is in contact with the rigid surface to change from a flat surface to an inverted surface; this indicated a change in the energy state and is shown in Figure 2.16.

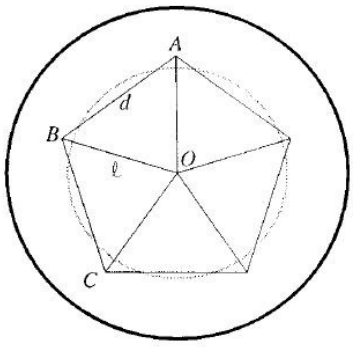

Figure 2.17: A typical pentagonal fold arrangement for a fully compressed sphere (Pauchard and Rica, 1998).

Pauchard and Rica found that additional compression, beyond the snap through buckling, to large deformations caused an inverted circular pattern to buckle further into a pattern of polygonal ridges and folds in an attempt to transition to a lower energy configuration, as shown in Figure 2.17 and Figure 2.18.

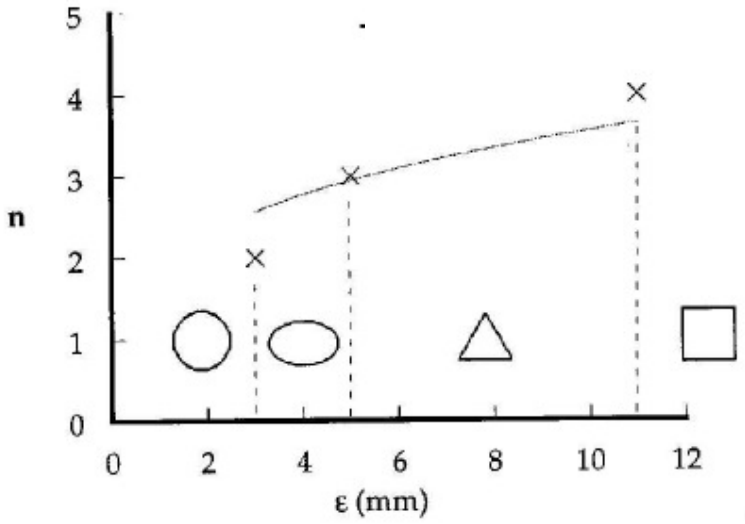

Figure 2.18: The possible change in number of folds with increasing deformation (Pauchard and Rica, 1998).

Updike and Kalnins (1970) also conducted an analysis of a hemispherical shell when crushed by a rigid wall, where the material such as a metal, was assumed to remain linearly elastic up to the point of buckling. They found that the shell cannot collapse without firstly a flat region forming in the area of contact with the rigid wall. For the hemispherical shell used in the experimental analysis the conjecture was that for larger values of the ratio of radius to wall thickness, buckling would occur prior to yielding, whereas the opposite would be true for smaller ratios. It was also proposed that partial yielding could occur immediately upon loading, the ratio of radius to wall thickness that this occurred at could be calculated by considering the stresses when flattening occurs without considering membrane effects. The membrane stress that occurred later would actually unload the inner surface and load the outer surface that is in contact.

They concluded that plastification of the material will alter the load deflection behaviour of the shell, but a purely elastic analysis can help with understanding the buckling of the shell.

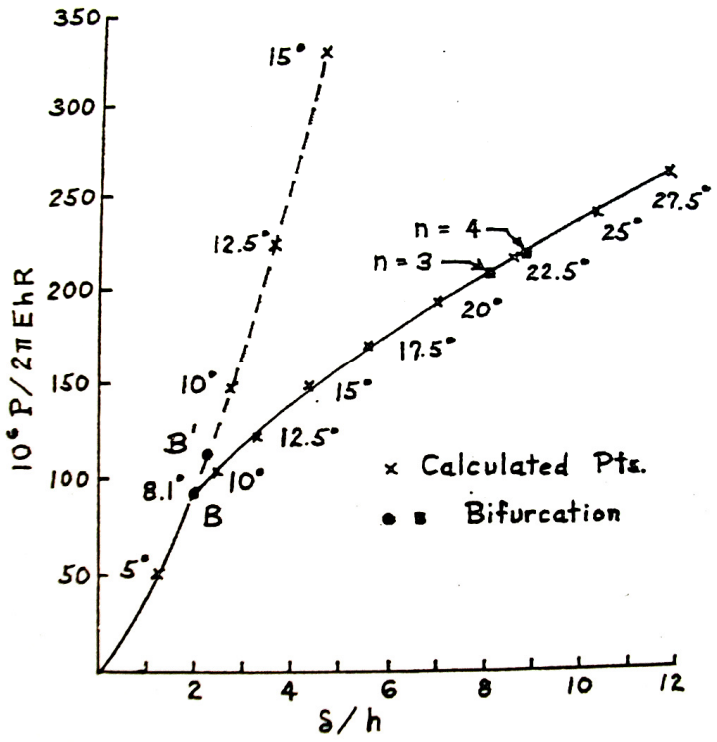

Figure 2.19: A theoretical curve for load versus displacement of a spherical shell (Updike and Kalnins, 1972).

Another paper by Updike and Kalnins (1972) continued the investigation to non-symmetric buckling and post buckling, beyond the previously observed flattening and formation of an inward dimple.

A load versus displacement curve, as shown in Figure 2.19, was produced using numerical methods, this indicated that for a hollow sphere with a radius to wall thickness ratio (*R/h*) of 100, the bifurcation point where the snap through buckling occurs is at a point where the displacement divided by the wall thickness is approximately equal to 2.

Crude experiments were conducted by pressing a Lucite plate against a deflated rubber ball with a diameter of 6 inches (152.4 mm) and a wall thickness that varied between 0.07 inches (1.778 mm) and 0.09 inches (2.286 mm). The plate was loaded at the corners by applying weights, so that the ball could be observed through the transparent plate which was kept approximately level throughout. The load was applied beyond the original dimple and a nonsymmetric shape with four lobes was produced, as

indicated in Figure 2.20. The curve of load versus displacement was similar to that of the numerical analysis up to the point of nonsymmetric buckling.

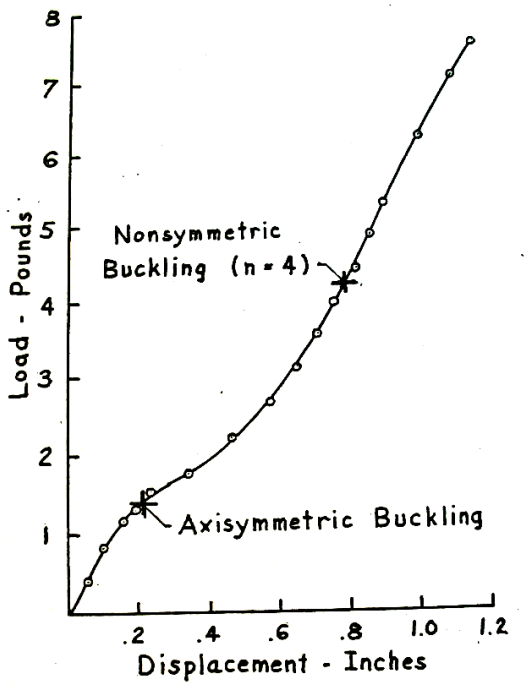

Figure 2.20: The load versus displacement for a plate pressed against a rubber shell (Updike and Kalnins, 1972).

Updike and Kalnins noted that the shell was stable at the onset of both axisymmetric and non-symmetric buckling, as a positive slope was produced throughout the loading curve. Therefore both bifurcation points were stable equilibrium points for the experimental results produced for a shell with a radius to wall thickness ratio of approximately 40.

Taber (1983) studied the compression of fluid filled spherical shells, when they were compressed by rigid indenters, using two theories; firstly a shell theory which included bending and stretching energy and secondly a membrane model that used stretching only. The rigid indenters had diameters ranging between 2.5 mm and 20 mm, which were considerably smaller than the diameter of the hollow filled spheres, approximately 50 mm. Despite these considerations there was a flattening effect on the sphere followed by the formation of a dimple, this was more prominent with the large diameter indenters, whereas the smaller indenter acted more akin to a point load. When the experimental observations were compared to the two models used, it was seen that as the deflection increased there was a transition from a predominant bending to a

predominant stretching. With a decrease in wall thickness or an increase in indenter diameter the region of bending decreased, bending effects dominated for thicker shells, whereas the membrane stress was higher in thinner shells even at small deflections. Taber concluded that the membrane theory was adequate for the large deflections of thinner shells, but for other loading conditions and geometries this may not be the case.

Cordingley et al. (2004) explored the deformations of elastic spheres at high strain rates, where they observed and modelled the impact of rubber tennis balls against a vertical rigid surface. The performance of the ball during impact was dominated by the behaviour of the ball material under the high strain rate conditions and depended upon the velocity and the ball dimensions. They used tennis balls that were both pressurised and further ones that were pressureless, they were also made of differing rubber compounds and were of different wall thickness. They found that the pressurised and pressureless balls behaved in a very similar manner. The tennis balls exhibited an inverted curvature under high deformations but, due to the nature of the sphere walls and the high speed of the tests, the buckling is of a different type than that which occurs with table tennis balls. The formation of polygonal ridges and folds is evident, but at larger deformations than observed by Pauchard et al.

Investigations by de Oliveira and Wierzbicki (1982) showed how to predict the crush resistance of rigid plastic shells of revolution by the loading of a metal hemispherical shell, a conical shell or a spherical cap with either a central point load, a rigid boss or by compression between two rigid plates.

Gupta et al (2007) observed the collapse behaviour of aluminium hemispherical and shallow spherical shells, at a range of thickness and radii, when subjected to impact loading by a drop hammer. They also observed the three main deformation characteristics, namely an initial flattening, inward dimpling and the formation of a number of lobes, for both static and dynamic loading. The hemispheres varied in size from a radius of 45 mm to 153 mm, with a range of wall thickness between 0.7 mm to 1.6 mm. The shallow spheres had a radius of 102 mm and 153 mm with a range of wall thickness between 0.7 mm and 1.2 mm (although the actual height of the specimen was lower than the actual radius of curvature). The experimental results were also examined numerically using LS-Dyna software, where the three deformation characteristics were modelled. It was found that the number of lobes varied between 5 and 7, depending upon the ratio of the shell radius and wall thickness, also dependent upon these

dimensions was the collapse load, where the shell was found to absorb more energy for the dynamic loading than the static loading.

Gupta et al. (1999) also compressed differing alloys of metallic spheres between rigid plates, the materials used were mild steel, galvanised steel and aluminium. It was noted that a rolling plastic hinge occurred in the shell where it was in contact with the rigid plate, this was observed after the snap through buckling had occurred and the deflected area increased in radius as the compression of the sphere increased. The spheres ranged from 40 mm in radius with a wall thickness of 1.9 mm to 127 mm in radius with a wall thickness of 0.9 mm, with a range of radii and wall thickness in between.

The behaviour of hollow metal spheres was examined by Lim et al. (2002) in the form of a bulk metal foam and as individual spheres of approximately 2 mm in diameter and with a wall thickness of 0.1 mm. The deformation was quasi-static compression between two rigid plates, variation in wall thickness between spheres and within an individual sphere made accurate assessment difficult. FE modelling using Abaqus software produced more uniform results although correlation with experiment showed that the predicted stiffness of the individual sphere was higher than in reality.

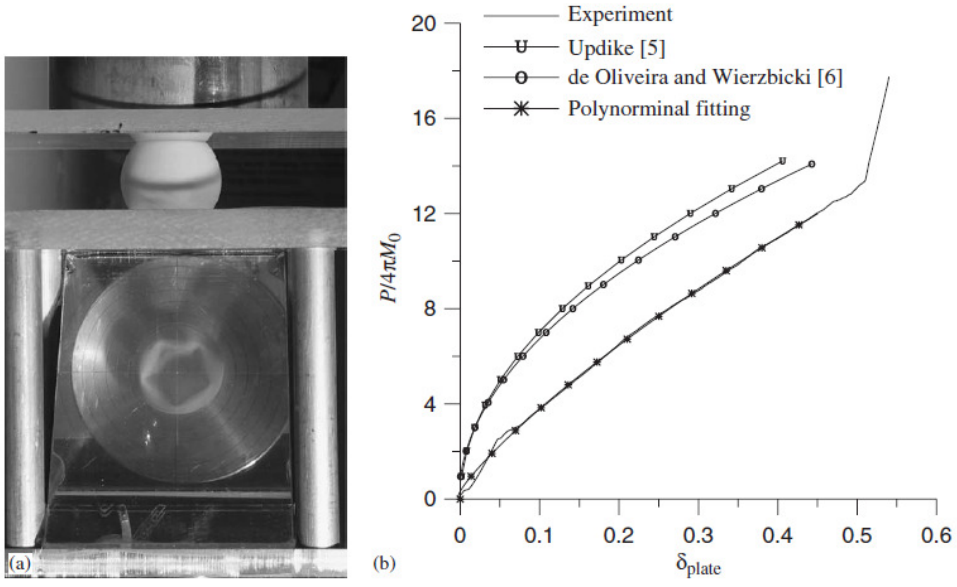

Fig. 8. Rigid plate compression: (a) the setup and the polynomial dimpling; (b) the normalized load-deformation curve.

Figure 2.21: Compression of a table tennis ball between rigid plates and resulting load-deformation curves (Ruan et al, 2005).

The crushing of table tennis balls was examined by Ruan et al. (2006) both individually and in a variety of arrays, much of the work investigated 1D and 2D configurations of a number of table tennis balls aligned in square and hexagonal arrays. Single spheres were compressed using a number of configurations including a point load, a rigid ball and a rigid plate. During compression of a single table tennis ball by a rigid plate dimpling was observed.

Ruan et al. (2006) noted that the theoretical models of Updike and Kalnins (1972) and de Oliveira and Wierzbicki (1982) where they overestimated the load carrying capacity of the shells and a 5 lobe polygonal dimpling occurring. When the upper and lower snap-through regions contacted each other Ruan et al. observed a large increase in force as can be seen in Figure 2.21

Light-weight metal matrix composites using ceramic microballoons were examined by He et al. (1995). The microballoons varied in size from ~ 20 μm to several mm. The foam behaviour was examined, as was the microballoons themselves, particularly the ratio of wall thickness to radius. The microballoon and matrix material were modelled as a unit cell using Abaqus software where the microballoon was assumed to exhibit elastic behaviour only. The stress distribution within the microballoon material was also examined for a range of wall thicknesses. Under compressive loads the maximum principal stress was located at the inner wall of the polar region of microballoons with thick walls, as the wall thickness was decreased principal stresses increased at the equatorial region, finally with a lower wall thickness the principal stresses at the equatorial region dominated.

Rachik et al. (2007) compressed a range of capsule membranes between two rigid plates to evaluate their mechanical properties. The classical laws used provided only an approximation for the thin shelled capsules, so Abaqus software was the only successful way to obtain the compression deformation of the thicker walled capsules. This was despite thicker walled models being more complicated than thinner walled models. It was especially difficult to model the contact between the rigid plates and the capsule. The capsule material was found to have a Young's modulus that increased non-linearly with wall thickness, resulting in capsules that were stiffer than expected.

Nanoparticle hollow spheres were deformed by Tamura et al. (2004) as shown in Figure 2.22. They deformed some fullerene-like hollow nanoparticle shells that were attached to a rigid surface; it was found that both continuous and discontinuous buckling due to large and small van der Waals forces occurred respectively. They also

noted that there was a formation of a polygonal structure due to bending and stretching energies of the elastic shell, however in the other experiments with elastic tubes, by Tamura et al. (2004), this was not observed.

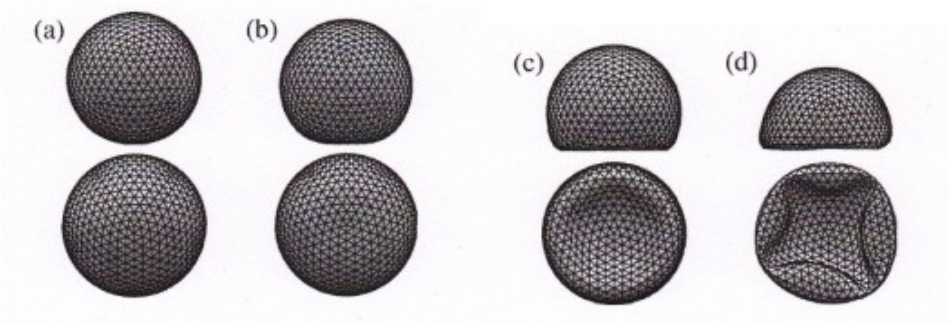

Figure 2.22: The deformation of a nanoparticle shell, showing side and bottom views (Tamura et al, 2004).

Kiser et al. (1999) investigated the mechanical response of a range of ceramic microballoon reinforced aluminium matrix composites, under both uniaxial compression and constrained die compression. The main variables for the study were the strength of the matrix and the ratio of wall thickness to radius of the microballoons. A range of diameter from 1 mm to 3.5 mm and wall thickness values ranging from 0.06 mm to 0.35 mm. The microballoons were not tested in isolation, but when the foam was crushed axially the deformation was similar to the theory of Ashby, that is the cell walls collapsed to produce localised deformation, followed by a densification process.

Finite Element modelling of carbon microballoons in uniaxial compression was conducted by Carlisle et al. (2007) using Ansys software. Boundary conditions were chosen to achieve axisymmetric behaviour with the compression being displacement controlled. Carbon microballoons were used to provide a range of radius to wall thickness ratios, the average diameter was approximately 25.5 μm with an average wall thickness of 1.67 μm. Two major flaws were detected in the microballoons, these were non-concentricity of the internal cavity and through-thickness holes, these flaws were modelled in a variety of locations to observe their effect on the behaviour of the microballoon under load. The thin regions did cause buckling despite the average wall thickness indicating that the microballoon should have been more resilient and although flexure would have been expected at similar loads, the through thickness holes had a dramatic effect as they acted as a stress raisers regardless of their location. The principal

stresses occurred on the inner wall directly under the contact region, this contradicts previous work where the maximum bending stress is expected to occur at the equator. Generally higher stresses were observed in thicker walled microballoons. The development of the flattened area of the sphere in contact with a rigid flat surface and the subsequent snap through buckling was described succinctly by Carlisle et al. as "it transitions from point through circular to annular".

Gregory et al. (1999) produced a mathematical solution to the problem of a hollow sphere when axially compressed by two point loads. A non-linear finite element formulation was developed by Maccarini et al. (2001). The work compared models of the collapse of a rubber (hollow) sphere, including that for a "racket ball" and a cylinder, with theoretical and experimental results, where the models used the proposed 3D shell elements and each node had five degrees of freedom. There was a good correlation between the proposed element and the theoretical results.

Zhu et al. (2002) examined a paradox for the buckling of thin cylindrical shells, where classical theory states that the buckling stress is directly proportional to the shell thickness, t, but empirical data shows that the buckling stress is related to the thickness as $t^{1.5}$. Previous work has also highlighted the possibility of a scatter in the buckling stress for a given ratio of radius to wall thickness; this is attributed to imperfections in the shell material. Zhu et al. attempted to explain the $t^{1.5}$ value by modelling thin walled open topped hollow cylinders in compression and comparing the results to empirical data. They found a clear relationship between wall thickness and buckling stress in compression, where the value of $t^{1.5}$ applied for shells that are loaded axially. But for shells that are loaded at an edge with a localised force the proposed $t^{1.5}$ relationship did not hold true, a "dimple" was seen to grow at a more-or-less constant force proportional to a value of $t^{2.5}$.

The work to date has mostly investigated the behaviour of spheres as a single unit, or in a matrix material, usually in compression between rigid surfaces. However, Fok and Allwright (2001) investigated the behaviour of a spherical shell when it is embedded in an elastic material and subjected to a hydrostatic pressure. They used an energy method and a Rayleigh-Ritz trial function to analyse the buckling of a spherical shell under these circumstances. Instability can occur in the shell wall when the pressure across the shell reaches a critical value. The work of Fok and Allwright ignored the effects of plasticity and imperfections and for simplicity were concerned with axisymmetric deformations and non-extensional buckling. Perfect bonding between the

shell and the matrix material was also assumed. Their work found that the surrounding material produced an increased critical load to achieve buckling of the spherical shell, although much less than when compared to a cylindrical shell. Also initial imperfections can reduce the buckling pressure required for buckling.

2.7 Finite Element Analysis (FEA) of elastomers

2.7.1 Introduction

There are a large number of engineering simulation programmes available. The Finite Element (FE) or Finite Element Analysis (FEA) technique is often incorporated into these programmes. The programmes such as Abaqus, Ansys and MSC MARC can be used to solve problems ranging from acoustics, soil mechanics and piezo-electrical analysis to thermal problems and heat transfer. The most popular application is for structural analysis, typically displacement and stress analysis, where components can be modelled in a large number of materials, including; metals, elastomers, plastics, composites, foams, rock, soil and concrete. It can be used to solve linear and non-linear problems. Abaqus version 6.5 and version 6.6 was used for the modelling presented in this thesis.

The FEA technique is based on the theory of virtual work. Stress analysis FEA uses this theory to obtain an approximate numerical solution to predict the response of a physical system or structure when it is subjected to external loads. The structure or component is represented with a geometry that is broken down into a number of smaller discrete segments, called elements, which are connected at points called nodes (Hearn, 1996), as shown in Figure 2.23. FEA solves thousands of simultaneous equations to determine various unknowns at the nodes; theses can include forces, displacements and / or rotations.

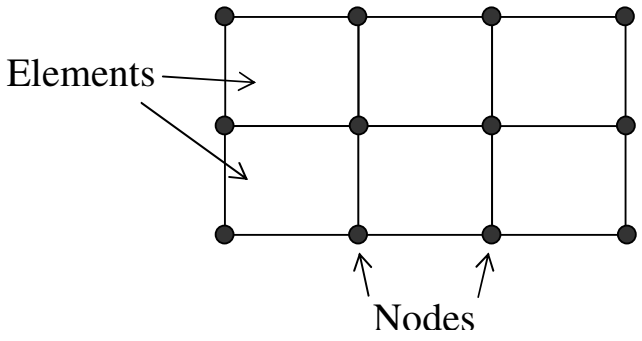

Figure 2.23: The element and node structure, with forces applied, as used in FEA (2 dimensional).

2.7.2 Theory

An engineering component can be represented in an FEA program using an initial geometry that is divided into a finite number of elements to form a mesh, with nodal points to join each element together. The mesh density and hence the number of elements and nodes can be varied to suit the given circumstances. For stress analysis the displacement of the nodes are vital for the relevant stress and strain to be calculated.

If a node is represented as a free body diagram the external force applied will be countered by an internal force, resulting from the stresses in the elements that are joined to the node. The external and internal forces must balance each other for the model to be in static equilibrium. For implicit methods as used in Abaqus Implicit, also referred to as Abaqus Standard, equilibrium equations are solved simultaneously using matrices to find the displacements. The stresses can then be calculated from the forces and the displacements. Abaqus Explicit uses a different method, which models stress wave propagation, where the force and displacement are calculated for each node in turn throughout the mesh for a series of time increments. This is based on the acceleration, velocity and concentrated force at each node and through each element, the strain is obtained by integrating the strain rate for a given time increment. The total strain is found by adding the initial strain plus the strain during the time increment. Once the strain has been calculated the stress can also be derived (Abaqus, 2004).

For the component geometry to deform a load must be applied to it. The two most common types of load used during FE stress analysis are point loads applied to a single node or a group of nodes and distributed loads which are applied to nodes at a surface. Other loads include edge loads, moments, body forces such as gravity and thermal loads, or a combination of two or more loading conditions

To prevent the geometry from moving in an unrealistic or undesirable manner boundary conditions must be applied to it. There are two types of boundary condition, those that fix nodes at a particular place, or zero displacements and those that allow a certain constrained amount of movement, or non-zero displacements. Depending on the model some nodes may be permitted to move in a certain direction, but not another, also the rotation about a node must be considered and prevented if this is required. The directions that a node can move are referred to by its degree of freedom (dof), these are shown in Figure 2.24 (Abaqus, 2004).

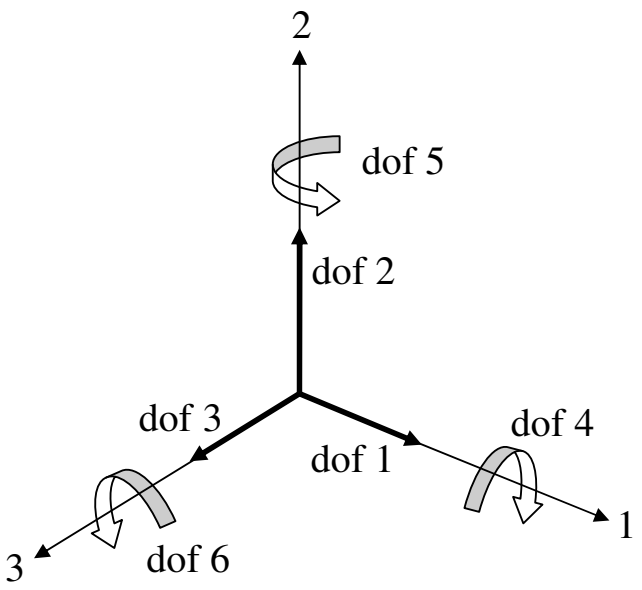

Figure 2.24: The axis and rotations that can be applied to a node.

2.7.3 Types of model

Where possible it is often more convenient to use a geometry that takes advantage of the lines of symmetry of a particular component, the production of the geometry and its mesh can invariably be simplified provided that care is taken when applying the boundary conditions and external forces or loads. The main advantage of a simplified geometry is a reduction in computational resources and time (Abaqus, 2004). A common example of a simplified geometry is that of a circular hole in the centre of a square plate subjected to a purely horizontal or purely vertical force, a quarter model can be used in this case where the lines of symmetry pass horizontally and vertically through the centre of the hole.

The geometry of components can often be represented as a two dimensional model, this often greatly reduces the complexity of the geometry and hence the ease with which it can be produced. Two common types of two dimensional models are plane strain models and plane stress models. Plane strain models effectively take a cross section through a component, but assume that the component is of infinite length, the elastomer seal between a car body and bonnet could be modelled in this way. A plane stress model could be used to examine a thin sheet of material under a load in the plane of the sheet.

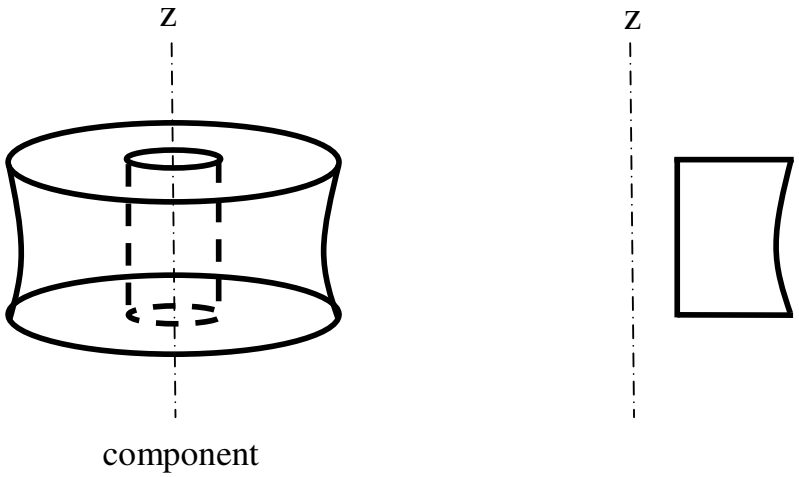

Figure 2.25: On the right is an example of an axisymmetric model of the three dimensional component shown on the left.

Axisymmetric models such as that shown in Figure 2.25 are often used where there is an axis of symmetry through a component, such as for an automotive elastomer boot on a drive shaft, where the axis of symmetry passes through the centre of the drive shaft (Shorter, 1998). This produces a complex model from a relatively simple geometry and is also computationally effective. Once again the boundary conditions and applied forces must be considered carefully. Axisymmetric models can be rotated through a range of degrees to produce a visual representation of the desired geometry.

Three dimensional models are often more complex to produce and usually require more computational resources compared to the previous types of model mentioned. It is however often easier to envisage how the boundary conditions and loads should be applied, as the model is more comparable to the component in service (Abaqus, 2004).

There are different types of element that are required for the different types of model configuration. The element library held within an FEA programme includes plane stress and plane strain, axisymmetric and three dimensional; there are others for other types of model, such as thermal and acoustic modelling. The elements that constitute the mesh of the geometry are divided into families, the most common of which are continuum elements which are solid elements, shell elements and beam elements; others include rigid, membrane and truss elements. The elements are identified by a series of letters and numbers, for example a simple plane strain or plane

stress element is denoted as CPE4 and CPS4 respectively, where "C" indicates a continuum element, "PE" represents plane strain and "PS" represents plane stress and the number indicates the number of nodes that the element contains, in this case four. CAX4 similarly denotes a Continuum Axisymmetrical element with four nodes. A common three dimensional element is the C3D8H, which is a Continuum, 3 Dimensional, 8 node, Hybrid element (Abaqus, 2004).

The element name indicates the geometry where they are most likely to be used; 8 node continuum elements are brick like and are used for three dimensional geometries, shell elements can be used for thin walled cylinders and beam and truss elements are often used in framework type structures.

Models often include rigid bodies as well as a finite element meshed component, the meshed component can be allowed to deform but a rigid body does not. Rigid bodies can be used to model very stiff components that are either fixed or moving. The body of a car and the bonnet can be represented by a pair of rigid bodies where an elastomer seal, represented by a finite element meshed geometry, comes into contact and is compressed between the two parts. In this case the load would be applied by the movement of the rigid body by a specified displacement (or with a specified force) toward the body of the car. The movement of a rigid body is usually controlled by a separate reference node, but if the rigid body is to be fixed in space the reference node is simply not allowed any degrees of freedom. Analytical rigid surfaces are a simple method of creating a simple rigid body, but for more complex situations a rigid body geometry may need to be created that is comprised of a series of rigid elements (Abaqus, 2004).

Contact is a boundary condition that can be considered as a restraint on a model that only applies when two or more components of the model are touching. Where the contact occurs friction behaviour can be included in the model, or it can be neglected and the contact considered frictionless. The two surfaces in contact must be specified as a master surface and a slave surface. The analytical rigid body, when used, is specified as the master surface and the deformable meshed geometry is the slave surface. The slave surface is usually the more finely meshed component of the model where two meshed geometries come into contact, or if the meshes are similar it is the softer material that is nominated as the slave surface. Caution is required when modelling contact as the model can behave in an unrealistic manner, this is because in certain circumstances the master surface can penetrate the slave surface as indicated in Figure

2.26, or nodes can fall behind an analytical rigid surface, although this can be prevented by extending the dimensions of the surface (Abaqus, 2004).

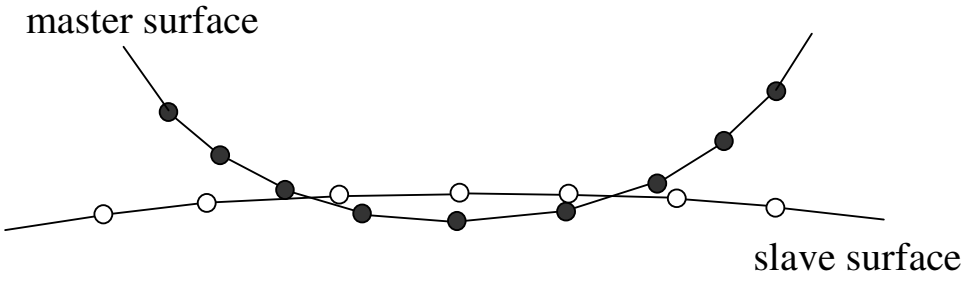

Figure 2.26: Contact between two surfaces showing the Master and Slave surfaces and possible through penetration.

Of the two solution methods, implicit and explicit, that can be used to execute a problem using FEA software the most common is the implicit method. The different methods are suited to different types of analysis, but for analyses where either type can be used, the most appropriate method is chosen based on computational efficiency. Implicit techniques are suitable for solving monotonic problems, explicit techniques are more suited to rapid elastic wave propagation analysis. Implicit methods can be problematic when solving problems that involve contact or instabilities such as buckling, however even if they can be solved by an implicit approach it might require an excessive number of iterations to solve each set of equations for each increment of the analysis.

Explicit methods were developed to solve problems that include high speed impacts and where inertia effects are important and contribute significantly to the results of the simulation. Explicit can be used to model quasi-static problems but the solution time is frequently accelerated as modelling quasi-static problems over long time scales requires a very large number of solution iterations to replicate an implicit static solution. However, when the problem is accelerated, the increasing inertial behaviour can affect the solution, therefore the solution should be executed in the shortest time possible but where the inertia remains inconsequential and does not have an adverse influence upon the results. The two methods of increasing the speed of the solution are by increasing the loading rate used in the model, or by mass scaling. Increasing the loading rate is not

always an option where the material is rate dependant, such as for elastomers. In this case a mass scaling method can be used (Abaqus, 2004).

2.7.4 FEA procedure

To produce a model in a finite analysis software programme requires a number of processes, which need to be conducted in a specific order.

Initially the type of model that is required must be considered, based upon the actual component that is to be analysed. The whole component may be represented with a two dimensional geometry or a three dimensional geometry. But it is more efficient to represent a section of the whole geometry, either a symmetrical portion as a two dimensional or three dimensional geometry, or as a plane stress, plane strain or axisymmetric model. Further consideration must also be made as to how the loads and boundary conditions will be applied.

The model geometry needs to be produced, this is usually drawn either using the FEA software or a separate Computer Aided Engineering (CAE) software package such as AutoCAD, or it can be imported from other design software. For the models created and represented in this thesis the CAE software I-DEAS 11 was used to create the geometries.

When the geometry has been completed a mesh needs to applied, the density of the mesh and type used depends on the shape and complexity of the geometry. As the geometry and mesh are created in a separate modelling package, I-DEAS 11, to the analysis software for this work, Abaqus, the nodes and elements definitions have to be grouped into sets to transfer the data.

The completed geometry, mesh and groups of elements and nodes are exported to Abaqus as a text file or “input deck”. This file can then be edited to include material properties, a chosen model where appropriate with accurately determined material constants, analytical rigid surfaces if required, contact criteria that may include friction and the boundary conditions and applied loads. Further commands are also added to provide steps for the model to follow; a first single step could be for initial contact if required, followed by other steps to proceed with the deformation of a meshed geometry. Commands are finally included to record results from the model in a report file, which can be extracted after the model has run.

The input file is then run using the Abaqus analysis software, if there are errors in the file then the analysis may be terminated and errors are reported in data files.

When the model has run successfully it can be viewed in the Abaqus viewer or Abaqus CAE software.

The Abaqus software can be used to visually represent initial and final deformations of the component as well as the deformation at specific stages of the analysis. The component can be represented accurately, for example an axisymmetric model can be shown in the software as a three dimensional representation, as well as being able to show various views of the model, for example from the side or from above. The various types of stresses, strains and deformations can be represented by contour plots shown on the model. Still images and movies can be produced showing the physical changes that occurred to the model, as would happen to the component in service.

Output data such as forces and deflections at various nodes and surfaces can be collected and sent to a report file for further analysis, such as force and deflection graphs.

In order to successfully model elastomer components using a FEA programme a suitable material model must be chosen and accurate material constants must be determined. The material constants are evaluated from the stress versus strain data for the particular elastomer, these are usually found by physically testing samples of the elastomer material, the most common and easiest test to perform is the uniaxial extension or tensile test on a dumbbell test piece. However, many elastomer components are of complex geometries and are subjected to complex loads when used in service, so it might be assumed that a correspondingly complex method of testing, or a number of different tests are required to replicate the in service behaviour. These complex testing methods, such as equibiaxial tension, uniaxial compression or planar shear are not always available and so are seldom used. If uniaxial testing alone is used the collected data can be implemented in the Mooney-Rivlin model, which is the most commonly used model and is available in most FEA software programmes.

The FEA software may also require a value for Poisson's ratio, in this case a value of just under 0.5, or more usually 0.49+ is used, as this assumes that the material is nearly incompressible. The value of 0.49+ helps the analytical process which is already complex and has to consider material non-linearity, large displacements and possibly difficult contact conditions let alone time dependent behaviour such as viscoelastic effects. Abaqus uses a default value for Poisson's Ratio of 0.475 for an explicit analysis, but the implicit analysis allows a value closer to true incompressibility

of 0.5. Elastomers are modelled as hyperelastic, which means that their behaviour is defined using a stored energy function. This means that they can be subjected to large strains beyond 100 %, so that when an elastomer component is analysed the mesh that makes up the geometry must allow for the large deformations that may occur.

The materials models available for elastomers in Abaqus include the neo-Hookean, Mooney-Rivlin and Yeoh models all of which have been described earlier.

2.8 Review Summary

Elastomers typically exhibit non-linear behaviour and are often filled with rigid particles such as carbon black, which increases the stiffness of the material as the volume fraction of carbon black filler is increased. For foamed elastomers the linear elasticity depends upon whether the foam contains open or closed cells. At low densities, foams with open cells deform principally by cell wall bending. This phenomenon has been examined by many researchers notably Gibson et al (1982) and by Gibson and Ashby (1982). Lakes et al (1993) and others have also examined elastomeric cellular solids. Gent and Thomas (1959, 1963) found that for elastomer foams the cell wall stiffness contributes to the elastic moduli and that that foamed elastomers break at lower strains than the corresponding solid elastomer (Gent and Thomas, 1959b). Einstein (1906, 1911) developed a viscosity law for rigid spherical particles embedded in a continuous liquid. Similar theories were later developed for suspended colloidal particles in either a liquid or a solid, such as the equations for Young's modulus proposed by Guth and Gold (1938) and later Guth (1945).

When a hollow thin walled elastic sphere is compressed between two parallel rigid surfaces there are three main deformation characteristics. There is an initial flattening of the sphere where it is in contact with the rigid surfaces, under further compression there is a snap through buckling of the flattened areas, finally at the more extreme compressions a number of ridges and folds are formed. Pauchard and Rica (1998) studied the behaviour of elastic spherical shells, they qualitatively explained the observed features, although they included a set of unknown parameters that were thought to depend only upon the Poisson's ratio. Pauchard and Rica also observed a corresponding change in slope and a kink at the point where the deformation process caused the sphere that is in contact with the rigid surface to change from a flat surface to an inverted surface. Additional compression, beyond the snap through buckling to large

deformations, caused an inverted circular pattern to then form a pattern of polygonal ridges and folds. Updike and Kalnins (1970) conducted an analysis of a hemispherical shell, their conjecture was that for larger values of the ratio of radius to wall thickness, buckling would occur prior to yielding, whereas the opposite would be true for smaller ratios. Updike and Kalnins (1972) later proposed that for a hollow sphere with a radius to wall thickness ratio (*R/h*) of 100, the bifurcation point where the snap through buckling occurs is at a point where the displacement divided by the wall thickness is approximately equal to 2. Cordingley et al. (2004) explored the deformations of elastic spheres at high strain rates. They used tennis balls that were both pressurised and further ones that were pressureless, they found that the pressurised and pressureless balls behaved in a very similar manner. The formation of polygonal ridges and folds is evident, but at larger deformations than observed by Pauchard and Rica (1998). Investigations by de Oliveira and Wierzbicki (1982) showed how to predict the crush resistance of rigid plastic shells of a metal hemispherical shell, a conical shell or a spherical cap with either a central point load, a rigid boss or by compression between two rigid plates. Gupta et al (2007) observed the collapse behaviour of aluminium hemi spherical and shallow spherical shells, at a range of thickness and radii, they also observed the three main deformation characteristics and that after the snap through buckling a rolling plastic hinge occurred in the shell where it was in contact with the rigid plate. Ruan et al. (2006) crushed table tennis balls, they observed a large increase in force when the upper and lower snap-through regions contacted each other. Nanoparticle hollow spheres were deformed by Tamura et al. (2004), they noted the formation of a polygonal structure due to bending and stretching energies of the elastic shell. Most work to date has investigated the behaviour of spheres as a single unit, usually in compression between rigid surfaces. Fok and Allwright (2001) investigated the behaviour of a spherical shell when it is embedded in an elastic material and subjected to a hydrostatic pressure. Their work found that the surrounding material increased the critical load and the buckling.

The main aim of this project is to understand the mechanical behaviour of a novel elastomer where hollow microspheres are used as particulate filler. Elastomer foams are relatively well understood, as is the behaviour of hollow plastic spheres, although for this study there are aspects of the latter in particular that need to be better understood in order for the behaviour of the filled elastomer to be examined.

Chapter 3 Characterisation of materials used for this study

3.1 Introduction

The primary aim of this study is to examine the mechanical behaviour of elastomers filled with hollow microspheres to create a closed cell elastomer foam. A secondary aim is to understand how the microspheres behave both independently of the elastomer as well as in an elastomer matrix in a clearly identifiable unit cell. This behaviour will help to elucidate the behaviour of the elastomer foam material.

There are a number of uncertainties regarding the dimensions of the microspheres. The range of dimensions, for example, as given by the distribution of diameters, was measured using a Malvern Mastersizer that produces an external particle diameter distribution from a large sample. The range of typical wall thickness values also has to be determined. The material composition of the microspheres must also be examined, together with the density of the various materials tested.

Table tennis balls have been used as easy to visualise models for the behaviour of a single hollow sphere due to the difficulties of handling spheres with as small a set of dimensions as the microspheres. To understand the behaviour of these model table tennis balls it is therefore necessary to also measure their material properties. Mechanical properties such as the Young's modulus were found using traditional screw driven mechanical testing machines and also by using a Dynamic Thermal Mechanical Analysis (DTMA).

The elastomer used during this study was characterised carefully. The mechanical properties of modulus and strength were carefully measured using various tensile tests and its density was measured using specific density measuring equipment. These properties have been found for both the unfilled elastomer and for sphere filled elastomer composites.

The various material properties have in turn been used in the FEA modelling described in the following chapters. This chapter explains the process and methods used in order to understand the various properties and characteristics of the materials involved.

3.2 Microsphere characterisation

3.2.1 Introduction

The microspheres used for this work were supplied by the project sponsor as manufactured by Akzo Nobel. Their trade name is Expancel and the specific product number used was 'Expancel DE 551 40 d42', according to Akzo Nobel (2010) they have the following properties; the microspheres are dry expanded (DE) nominally 40 μm in diameter (40) with a true density of 42 kg/m^2 ± 4 kg/m^2 (d42). Other Expancel microspheres are available between 6 μm and 40 μm in diameter unexpanded and 20 μm to 150 μm expanded.

Akzo Nobel state that the microsphere shell is made from a copolymer of three monomers and that the blowing agent used is either isobutene or isopentane. The range of wall thickness values used for the shell material is not defined by the manufacturer.

This section describes the methods used to obtain;

- a verification of the composition of the shell material,
- the true size distribution of the samples provided,
- the density of the shell material in isolation,
- the calculated wall thickness of the microspheres.

3.2.2 Composition, using Thermo-Gravimetric Analysis (TGA)

The manufacturer's literature states that the Expancel microsphere shells are made from a co-polymer of three monomers, these are; vinylidene chloride, acrylonitrile and methylmethacrylate.

Thermo-Gravimetric Analysis (TGA) was used to confirm the types of monomer contained within the co-polymer and the relative amount of each monomer. The type of each monomer is determined by seeing when the various component monomers are evolved with an increase in temperature and the amount of each monomer is indicated as a percentage of the total mass of the sample that is evolved. The process relies on different constituent materials evolving at different temperatures, which should mean they are easily identified providing that the temperature is increased at a rate that is slow enough.

For this study a TGA machine manufactured by TA Instruments was used. Part of the sample was placed in a weighing pan which was in turn placed on a hook in a chamber in the TGA machine. The machine operated automatically once the initial test

parameters had been input. The temperature gradually increased within the chamber whilst nitrogen gas was passed over the sample. The temperature was set to increase at a constant 10 ºC per minute, from an initial temperature of 30 ºC to a maximum of 600 ºC. The microsphere material was evolved as the temperature of the chamber increased, with the different co-polymers evolving at different stages as the temperature increased. During this process the mass of the material was monitored by the machine. The machine records both the actual mass as a percentage of the original mass and the rate of loss of the mass in mg per minute. The data was collected automatically and graphical results were produced.

The following two graphs were produced by the software that operates the TGA machine.

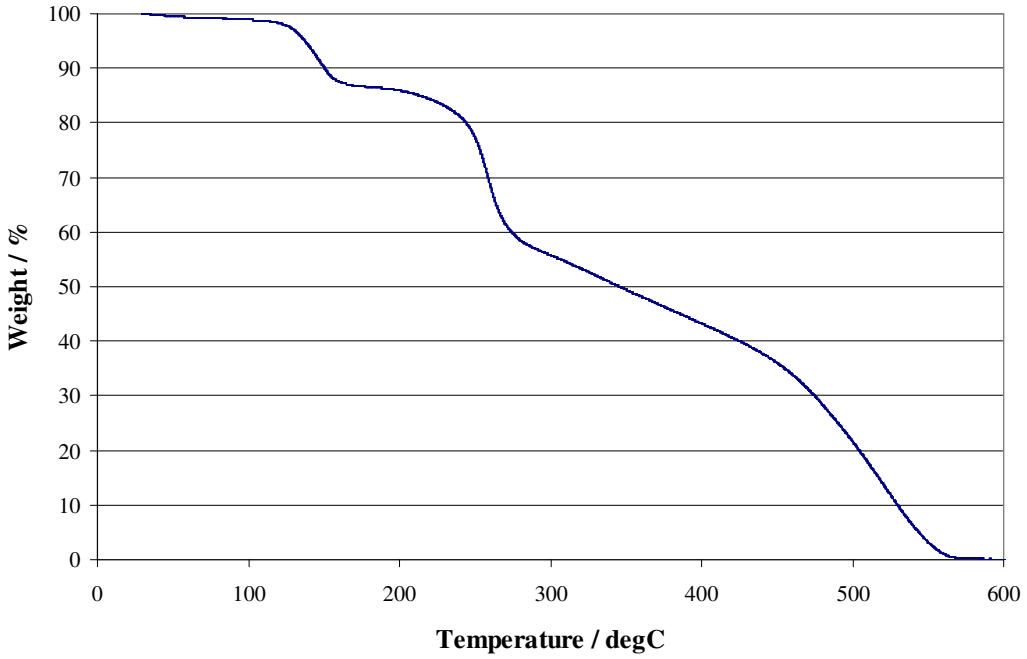

Figure 3.1: TGA, loss of sample mass with temperature increase.

The first graph, Figure 3.1, shows the mass lost as the temperature was increased from 30 ºC to 600 ºC where the mass lost is expressed as a percentage of the original mass that was placed in the pan of the chamber of the TGA machine.

The following graph, Figure 3.2, more clearly shows the three distinct drops in mass, these correspond to each constituent of the co-polymer as it is evolved, where the temperature that each peak occurs corresponds to a particular constituent material.

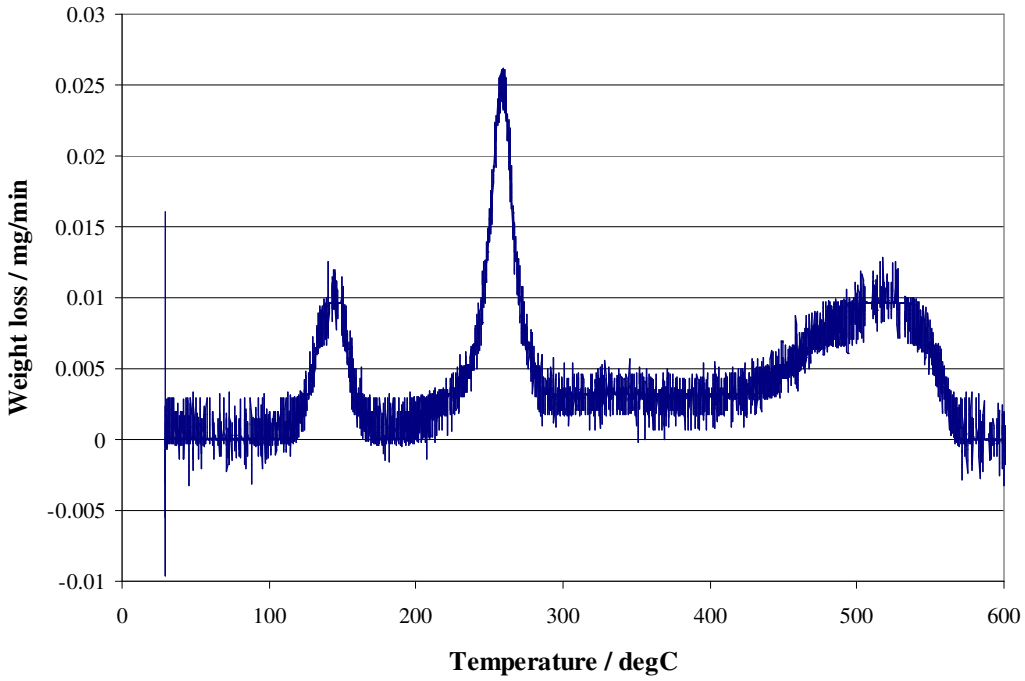

Figure 3.2: TGA, mass lost, relating to the three constituent materials.

Material	Percentage, %	Material Type
1	13.4	Methylmethacrylate
2	38.2	Vinylidene Chloride
3	48.3	Acrylonitrile

Table 3.1: Constituent parts of the microspheres.

The TGA machine also produces raw data that allows the percentage and types of material to be calculated. The constituent parts of the co-polymer were identified and are shown in Table 3.1. The monomers relate to the temperatures that they evolve. The results agree with the manufacturer, Akzo Nobel (2004), which states that the shell material is a thermoplastic copolymer. According to a safety data sheet it also contained Acrylonitrile and Vinylidene chloride although the exact composition was not known (Canada Colors and Chemicals Limited, 1992).

3.2.3 Diameter size distribution

The Expancel microspheres used during this work were nominally 40 μm in diameter. The manufacturer Akzo Nobel (2004) specifies the range of diameters for

each type of microsphere. For the microspheres used in this study the specified diameters ranged from 30 μm to 50 μm.

By placing a sample of the microspheres on a microscope slide and observing them using an optical microscope it was evident that there was a larger variation in diameter than that indicated by the manufacturer. Upon mixing a sample of the microspheres into some silicone elastomer, the large variation in the microsphere diameter was also observed

To determine the distribution of the microsphere dimensions an analysis was conducted to determine the particle size distribution of the microspheres. The machine used to perform the analysis was a Malvern Mastersizer. The Malvern Mastersizer is a particle sizing machine that is able to measure particles from submicron to a millimetre in size, the sample can be provide as either a wet or dry composition, for sample sizes of very small quantities of only a few milligrams.

Before an analysis is started the refractive index of the sample material must be estimated. The refractive index for Polymethylmethacrylate and Polystyrene Acrylonitrile was obtained from the data sheets that accompany the machine, the values for a Vinylidene Chloride monomer and Polyvinylidene Chloride (crystalline) were obtained from Dow Plastics (2000). The shell material is made from a mixture of Vinylidene Chloride, Acrylonitrile and Methylmethacrylate according to the manufacturer's literature and was supplied by the TGA analysis. The following refractive indexes were used to obtain an average value:

- Polymethylmethacrylate 1.4760
- Polystyrene Acrylonitrile 1.56-1.57
- Vinylidene Chloride monomer 1.43
- Polyvinylidene Chloride (crystalline) 1.63

An approximate average of 1.5 was used during the analysis.

The Malvern Mastersizer operates in the following manner:

- A sample is poured into a bowl of distilled water attached to the side of the machine.
- The water is then pumped through the machine, including a chamber within the machine which has clear lenses on each side.

- A laser beam is passed along a tunnel and through the lenses, where the particles contained in the water diffract the light. The amount of diffraction is observed at sensors further along the tunnel.
- The locations of the sensors that are hit by the diffracted laser beam indicate the sizes of the particles and the intensity of the signal at each sensor allows a measure of the percentage of spheres of each size to be determined

For this analysis a sample of 0.25 grams of microspheres was weighed and poured into the bowl on the Mastersizer machine. The initial dispersion was poor when this initial sample was tested.

Adding a few drops of the detergent Teepol created an adequate dispersion to a second sample of 0.247 grams of microspheres. The Teepol helped to stop the particles sticking to each other and agglomerating. The second more dispersed sample had approximately 25 % volume fraction of particles compared to the water and Teepol to provide a more reliable analysis, this dispersion was ideal and less than the manufacturers recommended maximum of 30 %.

Test	**Diameter, μm**		
	d (10 %)	**d (50 %)**	**d (90 %)**
1	21.264	32.245	49.320
2	20.752	31.392	47.977
3	20.372	30.753	46.717
Average	20.783	31.454	48.032

Table 3.2: Malvern Mastersizer results for Expancel Microspheres.

The machine automatically analysed the data and produced tables and a series of graphs that showed the size distribution of the microspheres. Each analysis conducts three tests and then calculates average values for the percentiles, as shown in Table 3.2, with the diameters of the microspheres indicated in μm, a percentile value is shown in brackets where the 50^{th} percentile value represents the median of the distribution as shown in Figure 3.3.

The average value for 50^{th} percentile of the diameter of the microspheres was 31.5 μm, with a 10^{th} percentile value of 20.8 μm and a 90^{th} percentile value of 48.0 μm. This 50^{th} percentile diameter is lower than the manufacturer's stated average value of 40 μm and the bottom decile value was much smaller than the manufacturers' minimum

of 30 µm but the top decile size from the analysis was close to the manufacturer's maximum of 50 µm. The machine automatically calculated the dispersion profile shown in Figure 3.3.

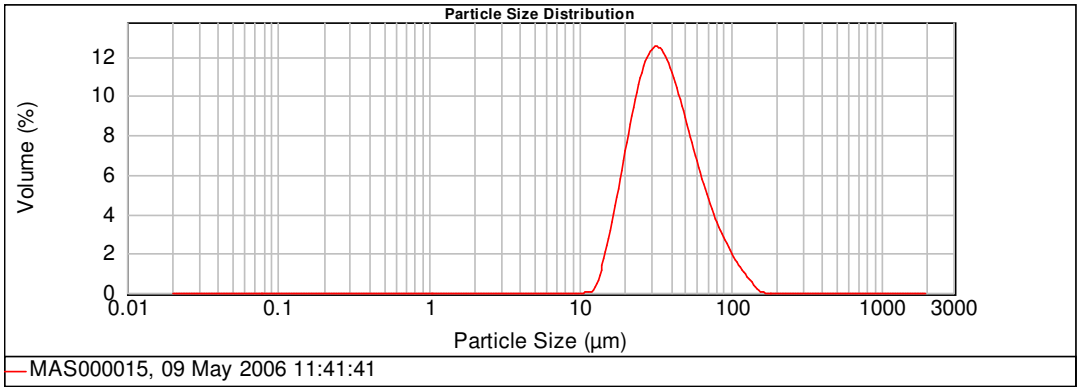

Figure 3.3: Size distribution measured by the Malvern Mastersizer for Expancel Microspheres.

3.2.4 Density

The relative density of a material is simply the ratio of the mass of the material divided by the volume of the material, but for some materials it is a difficult measure. The basic formula is given by $\rho = m / v$, with the SI units of kg/m^3.

Usually the easiest way to measure the density of an object is to relate the mass of the object using the Archimedes principle. The principle states that when a solid body is immersed in a fluid it will experience an upward thrust equivalent to the mass of the fluid that is displaced. Weighing in air and in water (or a liquid of a known density) allows the density to be derived. This method is suitable for larger specimen sizes, such as the silicone elastomer samples described later. But the method is not suitable for small or light specimens, such as the microspheres.

Pycnometry uses a similar method to the Archimedes principle, it is often used to measure the density of liquids. Typically a pycnometer or specific gravity bottle resembles a laboratory flask, made of glass with a stopper that has a capillary tube to allow air to escape. The flask is usually weighed empty, then full of water and finally full of the liquid to be measured. The density of a powder can also be measured using this method.

The third common method of obtaining the density of a solid is to use a gas pycnometer, this compares changes in pressure in a closed volume or chamber. Firstly a reference object is placed in the chamber, usually a steel sphere or similar object of a

known volume, this calibrates the chamber. The pressure is then compared to that when the sample is in the chamber, the change in pressure represents the volume, so if the mass of the sample is known, the density can be calculated.

Advantages of gas pycnometry are that very small samples can be measured including powders and porous materials, however, the disadvantages are that the samples must by dry and must not have closed pores, the later would not provide the true volume or density of the material.

Gas pycnometry was the chosen method to measure the density of the microsphere material, so the sample had to be made into a solid test sample. This was achieved by dissolving some of the microspheres in Acetone in a small glass dish and then allowing the Acetone to evaporate off. This method produced a thin solid film of the microsphere material.

Figure 3.4: The Micromeritics AccuPyc 1330 Gas Pycnometer.

The gas pycnometer used is shown in Figure 3.4. It was a Micrometrics AccuPync 1130 which uses Helium as a gas. The machine was calibrated using the small steel cylinder provided. The smallest sample that could fit in the chamber is 1 cm^3. The microsphere sample was easily small enough and when placed in the chamber was found to have a mass of 0.0296 grams. The sample was purged ten times and an average volume was calculated, the test was then repeated with another ten purges, this was to ensure that any moisture was removed in the first test and the average of the

second test should provide a more accurate result. The temperature in the chamber was 25.5 °C. The average density from the first test was 1.5542 g/cm^3, this was thought to be high when the three constituent monomer materials of the microsphere shell were considered, it was also noted that the density was dropping throughout the test, probably due to excess moisture being purged. The density from the second test was considered to yield a more credible result as the density was almost constant throughout the test and was found to be an average of 1.28 g/cm^3.

3.2.5 Wall thickness

The diameter of an individual microsphere, to back up the average measurement of 31.454 μm produced by the Malvern Mastersizer, can also easily be calculated using the scale bar on images captured from a microscope with a camera attached, as shown in Figure 3.5.

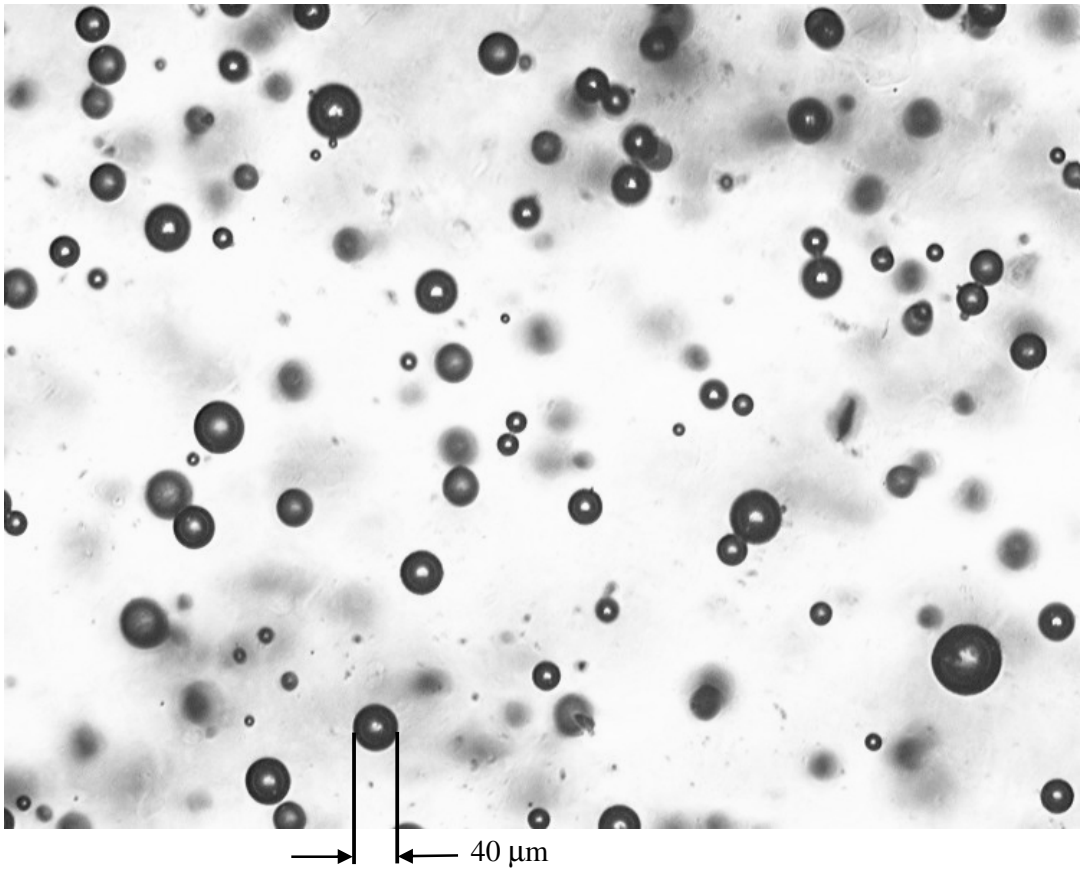

Figure 3.5: Expancel microspheres embedded as a filler in a silicone elastomer.

However, measuring the wall thickness for a given hollow microsphere is much more difficult due to the small scale of the microspheres. However the typical wall

thickness values are of paramount importance in this work as any buckling behaviour of the spheres under strain will be very dependent on this parameter. It is the most important geometric unknown in both the FEA modelling of a single sphere and when trying to understand the behaviour of the hollow sphere filled micro-composites.

To observe the true wall thickness of a microsphere, two criteria had to be met, firstly the microscope would need to be more powerful than the optical microscope used to capture the image in Figure 3.5 and secondly samples of single microspheres of a known diameter would need to be cut or broken to reveal a clean edge in order for the wall thickness to be measured.

Electron microscopes can resolve far greater detail than optical microscopes. However, bombarding an object with electrons can damage it, so a small amount of sample preparation is required which may alter the features that are to be investigated.

A Scanning Electron Microscope (SEM) was used to observe the microspheres and to measure the thickness of the shell walls. SEMs form a three dimensional image of a samples surface with an excellent depth of field allowing all regions of a complex topography to be in focus. A focused electron beam is scanned across the surface of a sample, the scattered electrons and secondary electrons that are ejected from the sample surface are then collected and counted. This process builds up an image pixel by pixel. The SEM can produce images with greater than 100,000 times magnification, this with the large depth of field results in images with very high detail.

An initial attempt to freeze fracture some microspheres was conducted by immersing a small number of them in liquid nitrogen. The aim being then to crush some of them using a pestle and mortar, but this proved unsuccessful due to the boiling action of the liquid nitrogen, keeping the very light microspheres near to the top of the boiling liquid.

Due to the difficulty of breaking individual microspheres a square sample, approximately 10 mm by 10 mm, of the silicone elastomer that was filled with approximately 10 % volume fraction of microspheres was placed in liquid nitrogen and this was broken in half. The two parts were then mounted on a steel plinth using carbon cement, as the silicone elastomer was non-conductive, as shown in Figure 3.6. The top surfaces of the samples were then coated with gold using an Agar Auto Sputter Coater. The prepared sample was then placed into and observed by the Oxford Instruments SEM, FEI Inspect F and a number of features were examined and images were captured.

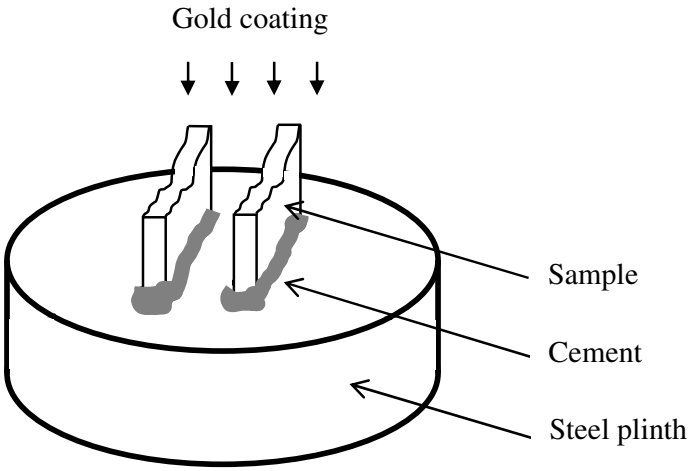

Figure 3.6: The samples as analysed by the SEM.

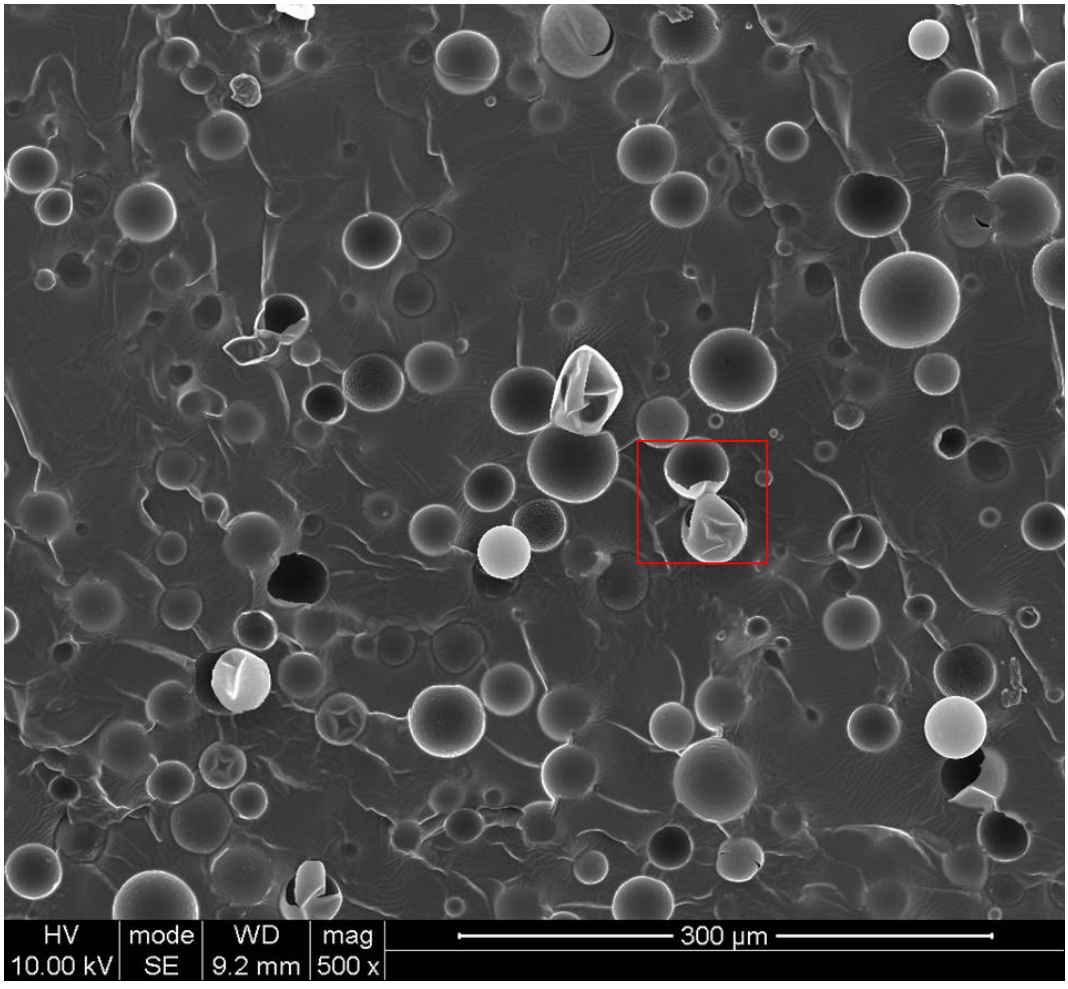

Figure 3.7: SEM image of microspheres in Silicone elastomer.

Two images of the freeze fractured microspheres in the silicone elastomer are shown in the following two figures, Figure 3.7 and 3.8. Figure 3.7 shows a number of microspheres, some of which are broken. Figure 3.8 shows two single microspheres in detail as highlighted by the red square in Figure 3.7. The wall thickness can be seen and measured although the precise wall thickness was still difficult to measure due to the uncertainty of viewing a perpendicular section of wall rather than at a slight angle. Figure 3.8 shows a fractured microsphere with a diameter of approximately 38 μm, the wall thickness is approximately 0.35 μm.

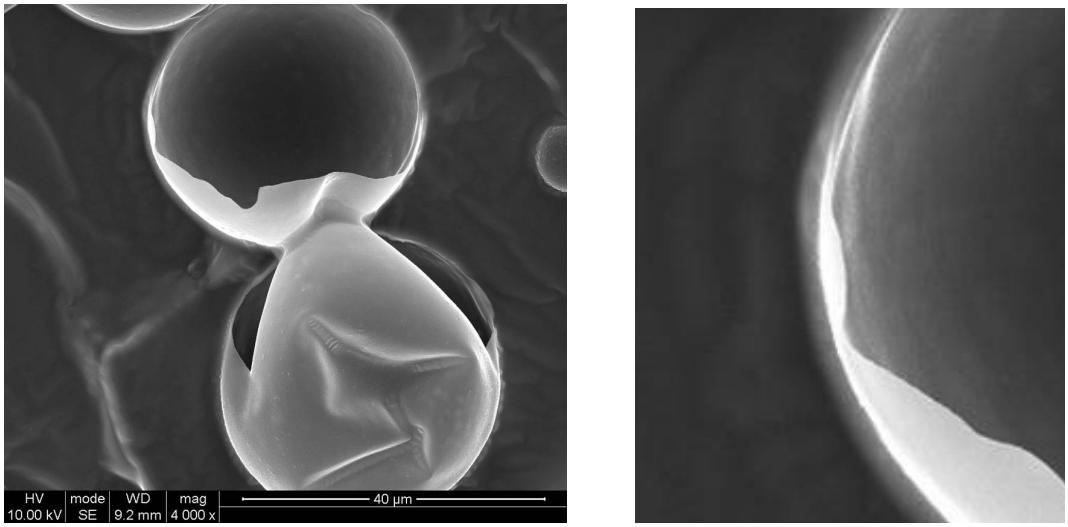

Figure 3.8: SEM image wall thickness of microspheres in Silicone elastomer with detail.

3.3 Table tennis ball material characterisation

3.3.1 Introduction

The physical properties of the table tennis ball material needed to be measured for three reasons: to interpret the behavior of the table tennis ball embedded in silicone elastomers, to ensure that their properties relate sensibly to the microspheres and to provide the correct properties to be input into the Abaqus FEA modeling.

The material from which table tennis balls are traditionally manufactured is celluloid according to Stiga, the manufacturer of the table tennis balls used in this study. The raw cellulose is traditionally obtained from cotton linters, these are fibres which are too short for spinning into yarn, but cellulose is found in many types of plant life. Nitrocellulose and camphor are then combined to create celluloid which is made to be rigid, strong and tough by adding stabilizers and other agents, but cellulose materials generally weather poorly and are affected by heat and chemicals. Cellulose nitrate is

also used to make lacquers, artificial leather cloth and thin sheets. Cellulose acetate is used to make 'plastic' items such as pens and pencils, it was also a traditional material for radio cabinets and photographic film (Higgins, 1987) and was historically sandwiched between two sheets of glass to make safety glass (Kalpakjian, 1995).

Young's modulus is the ratio of the stress divided by the strain in the elastic region of deformation. The Young's modulus is traditionally found by performing mechanical tensile tests upon samples of material. Linear elastic materials obey Hooke's law, when there is a linear relationship between the stress divided by the strain. Two methods were used to measure the Young's Modulus, E, of the table tennis ball material, both a traditional mechanical tensile testing approach as well as a Dynamic Thermal Mechanical Analysis (DTMA) approach. These measured values were compared with literature values such as the CES materials selection database where the Young's modulus for Cellulose Acetate, moulding not sheet, was 1.65 GPa to 1.74 GPa (Cambridge Engineering Selector Software, 2013). The Poisson's ratio for cellulose was found from various data tables of material properties, a value of 0.3 was used as quoted by Nakamura et al (2003).

3.3.2 Mechanical tensile testing

The brand of the table tennis balls used for this study were 'Master', designed by Stiga in Sweden and manufactured in China. To understand the behaviour of the table tennis ball material and to ensure that accurate material properties were used in the FEA models of the table tennis balls a number of tensile tests were conducted.

The initial batch of tensile tests was conducted using rectangular strips of material cut from the shell of the table tennis balls. The strips were approximately 50 mm in length, by 6 mm wide. The strips were not entirely flat due to the curvature of the table tennis ball and so they were gently flattened using a hot press set to 100 °C, this proved difficult and a more effective process used a domestic iron with the test piece placed in the fold of a piece of paper. It was assumed that by using a sufficiently low temperature the structure of the material and hence its properties were not significantly altered, the results for non-flattened test pieces were compared and produced very similar results.

The table tennis balls are manufactured from two halves, they have an equator where the two halves are joined together. To investigate if the manufacturing process had an effect on the material the test pieces were produced avoiding the join region in

two directions, parallel to the equator and perpendicular to the equator, this was to ensure that the material was isotropic, having the same strength and elastic properties in all directions. Two strips were cut from each table tennis ball, one in each direction, each test batch consisted of six table tennis balls.

The first set of test pieces were tested using an Instron 5584 fitted with a 1 kN load cell, the force was recorded, as was the crosshead displacement data from which the strain was then calculated. Another batch of tests on rectangular test pieces was conducted using an Instron 5564 machine fitted with a digital camera. The camera recorded the displacement of two dots that had been draw onto the surface of the test piece to represent the gauge length. Data was collected on a personal computer and analysed to find the elastic and yield behaviour from the stress and strain behaviour.

A further series of dumbbell test pieces were cut from the shells of table tennis balls using a small dumbbell cutter, as shown in Figure 3.9, using the hydraulic press, as shown in Figure 3.10. The thin gauge length section of these test pieces suffered from a less obvious curvature than the previous rectangular test pieces. The dumbbell test pieces had a total length of 70 mm and a total width of 12 mm. The gauge length was 3 mm wide and the dots to represent the gauge length were central to the gauge length area and were 20 mm apart.

Figure 3.9: Small dumbbell cutter.

Figure 3.10: Hydraulic Press, used to cut dumbbell test pieces.

The small dumbbell test pieces that were cut from the shell of the table tennis balls were tested on an Instron 5880 machine, as shown in Figure 3.11. The Instron machine used a video camera to follow marks made at the initial gauge separation for the test pieces. The marks were drawn onto the test pieces using a black ink pen. This method of recording the displacement was much more accurate than simply recording the crosshead displacement. The dumbbell test pieces should also be more accurate than simple strips of material as any deformation, such as necking or stretching, should occur only to the narrow gauge length part of the dumbbell, also if a test piece were to slip in the grips of the machine the effect on the recorded displacement would be smaller.

The data chosen to calculate the table tennis ball material properties is shown in Figure 3.12. This was the best representative test as it provided the most accurate results based upon the dumbbell test piece being used and the video camera obtaining the displacement, this result was selected from the batch of five test pieces as the 'average' test of those conducted, neglecting the most outlying results.

Figure 3.11: An Instron 5880 machine, as used to test the table tennis ball material.

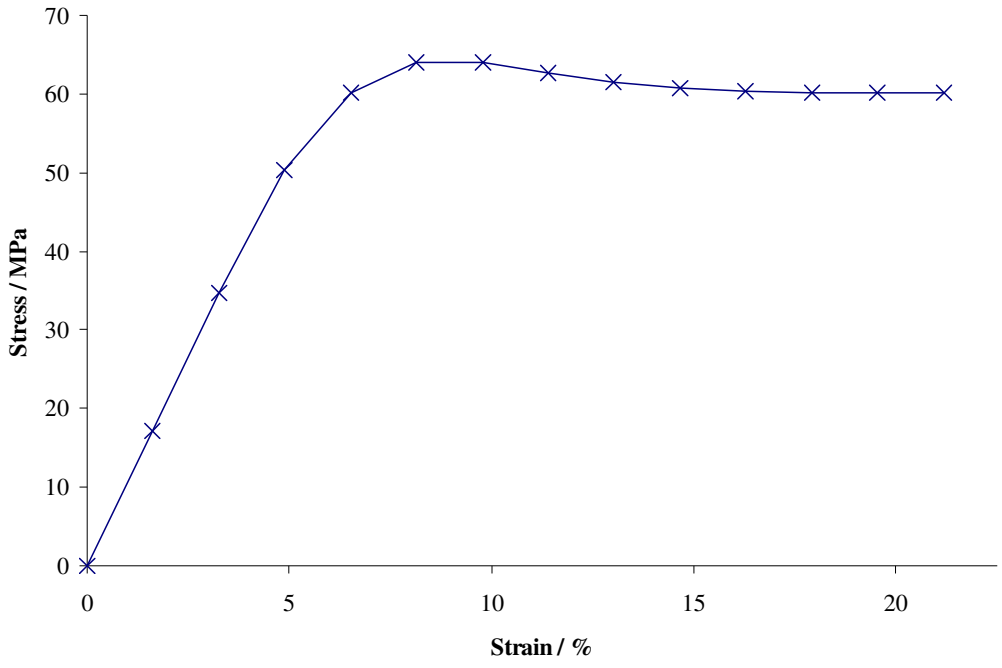

Figure 3.12: The tensile test results from the table tennis ball material, used to calculate the material properties.

The results were extrapolated to zero force to remove the initial lead-in, this was achieved by extrapolating the straight portion of the curve from the point at approximately 35 MPa through the point at approximately 18 MPa and onwards to zero Stress, where this point crossed the x axis was deemed to be zero strain. The lead-in was probably caused by the straightening out of the small amount of residual curvature of the test piece; this was a visible effect during the initial stages of each test and could be compared to the curve as it was being plotted on the monitor that accompanied the Instron machine. The results were then plotted as engineering stress versus engineering strain, shown in Figure 3.12.

The slope of the graph shown in Figure 3.12 was used to calculate the elastic behaviour of the material, the Young's modulus as 2200 MPa; however this value appeared slightly higher than that suggested by the available literature, such as the CES materials selection database. The yield behaviour was calculated based on the peak of the slope where the yield point was taken as 50 MPa, with the ultimate tensile strength given as 64 MPa.

3.3.3 Dynamic Thermal Mechanical Analysis (DTMA)

Dynamic Thermal Mechanical Analysis (DTMA) otherwise known as Dynamic Mechanical Analysis (DMA) or Dynamic Thermo-Mechanical Analysis (DTMA) is a technique that allows a materials behaviour to be characterised.

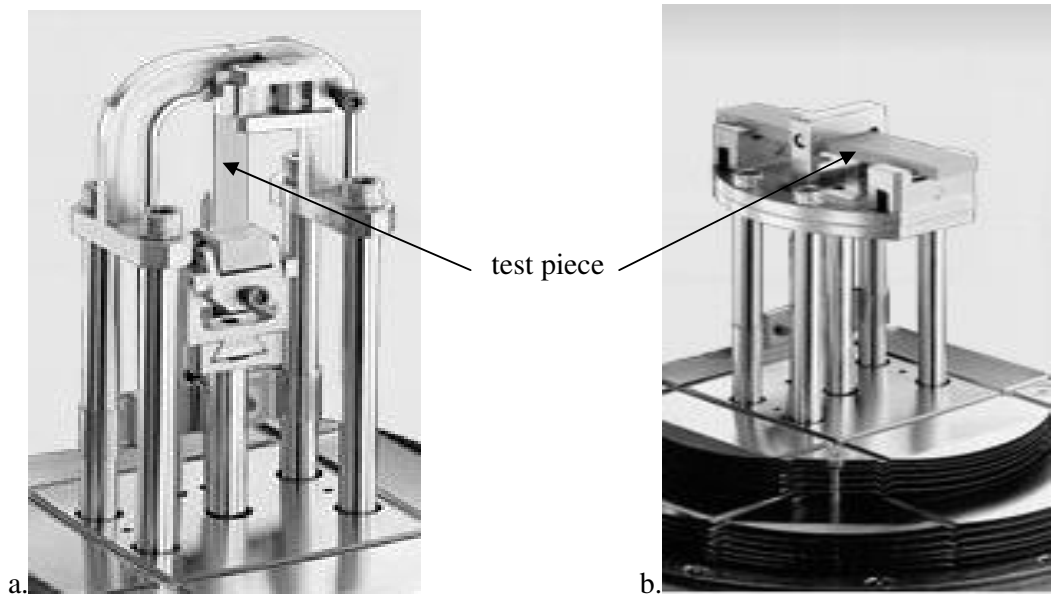

Figure 3.13: The DTMA test arrangement for a tensile test (a) and a three point bend test (b).

DTMA is primarily used to examine the viscoelastic nature of polymers. In this work a forced oscillation was used where a force is repeatedly applied to a sample and the resulting displacements are measured.

The two most common methods of applying the force to a sample are as a tensile test, this arrangement is shown in Figure 3.13 (a), or as a three point bend test as shown in Figure 3.13 (b). The oscillation is caused by the central post being raised and lowered during the test and applying a force to the clamped specimen.

From the test the Young's modulus can be calculated. The damping properties can also be determined by measuring the time lag of the sample during oscillation, due to energy dissipation. The temperature during the test can also be changed, to allow the glass transition temperature, T_g, of the material to be determined.

This study used a TI Instruments DTMA Q800 to obtain the Young's modulus of the table tennis ball material as shown in Figure 3.14, where the closed test chamber can be seen on the left hand side of the machine and the control panel on the right.

Figure 3.14: The TI Instruments DTMA Q800 machine used during this study.

Smaller rectangular test pieces were cut from the table tennis balls in an identical manner to that previously mentioned. The curvature of the test pieces were again carefully flattened using the domestic iron as before, a low heat was use so as not to affect the morphology of the material, although the temperatures used during the

experiment may have had some effect. The test pieces were approximately 25 mm long and 3 mm wide.

Both the three point bend and the tensile test methods were used and the results compared. Each test arrangement is prepared and then placed into the enclosed test chamber of the machine. During both experiments the sample was in a pure nitrogen atmosphere to avoid complications caused by oxidative degradation and the temperature was increased at a controlled rate of 5 °C per minute from 30 ºC to 150 ºC.

When an oscillating force is applied to a material that is not perfectly elastic the resulting strain during deformation lags behind the stress by a small amount. During cycling the elastic in-phase response and the viscous out-of-phase response can be represented as the storage modulus, *E*', and loss modulus, *E*'', respectively. The overall modulus is referred to as the complex modulus, *E*.

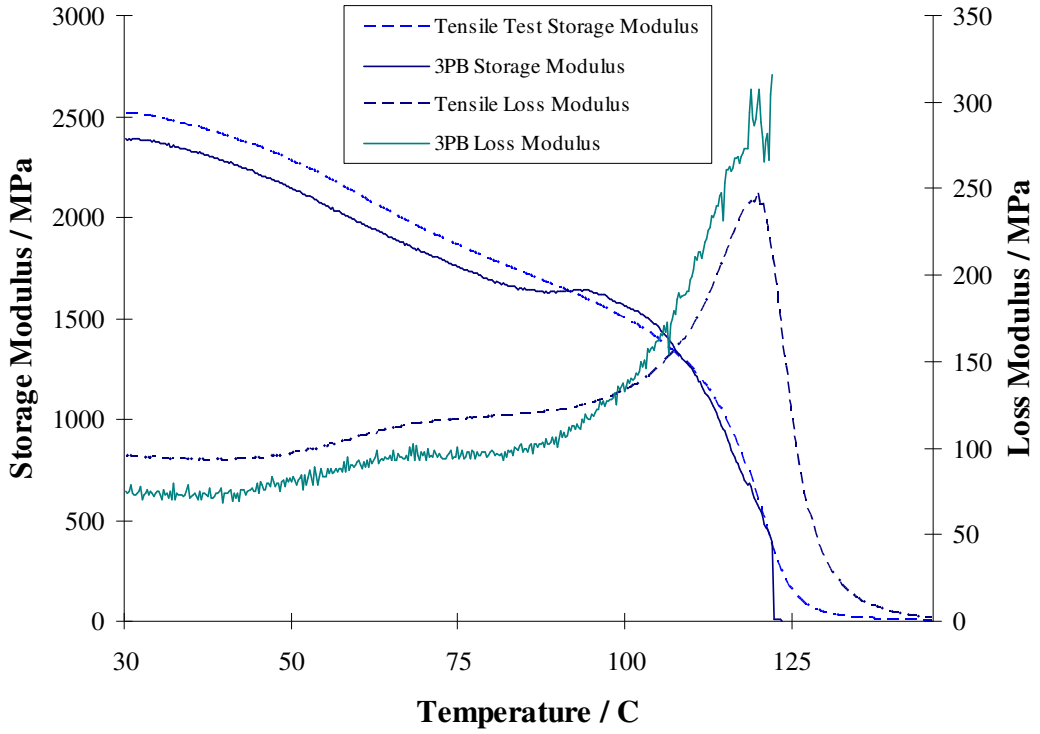

Figure 3.15: The DTMA results for the tensile test and three point bend (3PB) test of the material extracted from the table tennis ball.

During the tests conducted, a small oscillatory force was applied and the resulting stress and strain was measured, from this the storage modulus and loss

modulus were obtained over the range of temperatures, the graphs from the data collected by the DTMA machine software are shown in Figure 3.15. This shows results for the tensile test and the three point bend test (3PB) for both the storage modulus and the loss modulus.

The results obtained from the tensile test and the three point bend test are very similar, the small differences could be due to inaccuracies in the precise test piece geometry or the test pieces not being completely flat. The tensile test is a less complex test method, the test piece is more easily clamped and less likely to slip in the grips and the test piece shape is less likely to affect the test behaviour, therefore these values were favoured as representing the table tennis ball material.

A value of approximately 2200 MPa was determined for the Young's modulus from the mechanical tensile tests. The DTMA results were slightly higher, as the value of 2200 MPa was closer to the theoretical value, such as that from the CES materials selection database, it was chosen for use in the Abaqus FEA models.

3.3.4 Composition, using Thermo Gravimetric Analysis (TGA)

Stiga, the manufacturer of the majority of the table tennis balls used in this study, states that the material that the table tennis balls are made from is celluloid. The table tennis ball shell material was tested to confirm this, using Thermo-Gravimetric Analysis, in a similar way to the microsphere shell material described earlier in this chapter.

A piece of table tennis ball shell material was placed in the weighing pan of the TGA machine, this was then in turn placed on a hook in a chamber in the machine, the sample was approximately 8.1 mg. The test chamber was purged with nitrogen and gradually the temperature was increased by 10 ºC per minute. The initial temperature was 30 ºC, but this time the maximum was set at 980 ºC. As the table tennis ball material evolved the mass of the sample was monitored. The machine reports the mass as a percentage of the original.

The graph, Figure 3.16, shows the mass lost as the temperature was increased from 30 ºC to 980 ºC. It can be seen that the majority of the sample started to evolve at approximately 180 ºC, this temperature is appropriate for celluloid, the residual mass at a higher temperature being carbon and approximately 15 % carbon remained in the pan of the TGA machine when the experiment was completed.

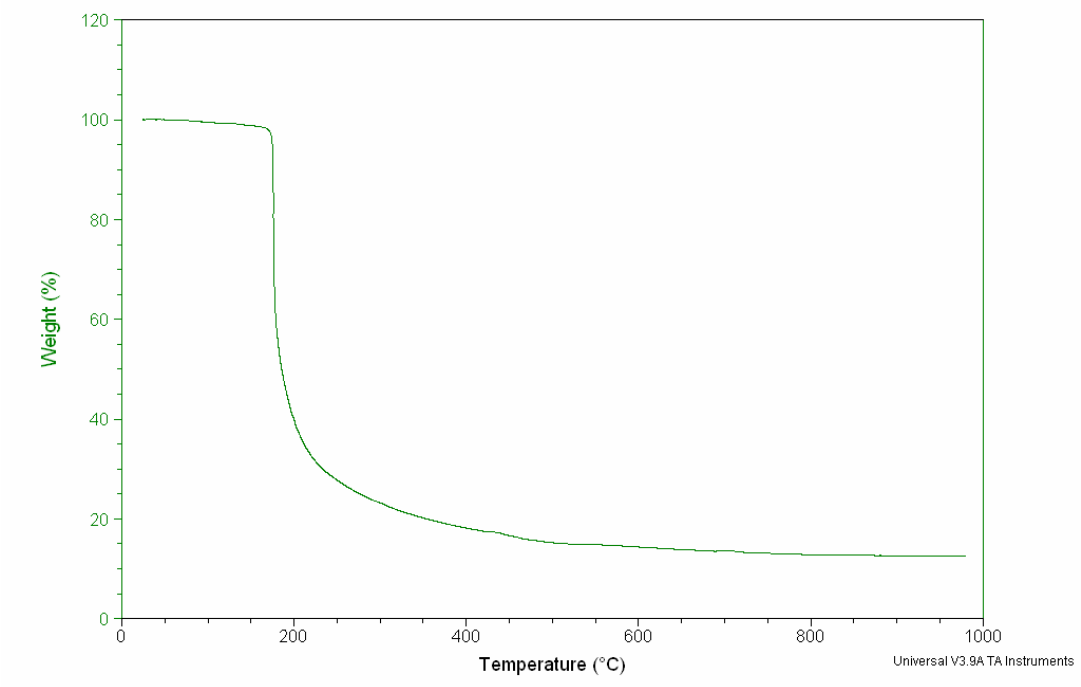

Figure 3.16: The TGA results for the table tennis ball material.

3.4 Elastomer Characterisation

3.4.1 Introduction

The elastomer used throughout this study was a silicone elastomer produced by Ambersil, it is referred to by the manufacturer as a two-part Translucent Moulding Rubber, called RTV 282, where RTV means it is a Room Temperature Vulcanising elastomer. This particular elastomer was specifically chosen to be room temperature curing and to ensure that the microspheres could be mixed into the elastomer without damaging them either mechanically during mixing or by the heating during a cure process. That is because the traditional method of mixing a filler into a high viscosity rubber using a two roll mill would have produced shearing effects that would have damaged the microspheres. Also microspheres are significantly altered by thermal effects, as they are set to dramatically expand at a temperature of between 80 ºC and 100 ºC depending upon the specific type used, therefore the normal temperatures required to achieve vulcanisation, typically greater than 100 ºC would be too high.

The elastomer was also transparent which allowed the microspheres to be observed when used as the filler material or to observe a single filler particle or a table tennis ball as a representative single filler. A transparent polyurethane rubber was also

evaluated, but was avoided on safety grounds as the isocyanates given off during sample preparation were much more dangerous.

3.4.2 Silicone elastomer manufacture

The elastomer is produced as a two part system, consisting of two liquids, where one part is the un-cured elastomer and the other part is the accelerator or catalyst. When the two parts are mixed together the elastomer material vulcanises at room temperature, typically over a period of twenty-four hours. The silicone elastomer was manufactured in a series of batches, initially as sheets of unfilled material and then with various filler volume fractions of microspheres. Further samples were made using cylindrical moulds, a large one that could include a single table tennis ball and smaller moulds to produce a batch of small cylinders that could include differing volume fractions of the microspheres as a filler material. The mixing process was similar for all types of moulding.

The Silicone elastomer is mixed in a ratio of 19:1 (95 % to 5 %) of the A and B parts, the A part is a thick translucent viscous treacle-like liquid, while the B part is a clear water-like liquid. The parts are mixed by mass, where 100 g of material would consist of 95 g of part A and 5 g of part B. The mixed rubber density is approximately 1.05 g/cm^3, according to the Technical Data sheet supplied by the manufacturer Ambersil (2003). When mixing the two parts for an unfilled sheet of material, the parts are each poured into small plastic or glass containers which have been weighed empty and the balance zeroed. The two parts are then weighed as they are poured in turn into each container until the required amounts are reached. To mix the material the B part is slowly added to the A part a few drops at a time, whilst stirring continuously. The stirring must be gentle to try to avoid the entrapment of too many air bubbles into the material, although some are inevitable. The material must be stirred thoroughly to ensure it is homogenous. The mixed elastomer has a pot life of approximately one hour, this is the time allowed to fill the mould and work the elastomer before it begins to cure and stiffen.

A steel mould was used to produce flat elastomer sheets approximately 1.5 mm in thickness and 180 mm by 180 mm. The poured material was kept in the mould for twenty-four hours; the mould was kept level to ensure as uniform a sheet thickness as possible by the use of a spirit level and thin pieces of metal plate placed under the corners of the mould. The mould was covered to keep dust and debris off of the curing

elastomer, but an air gap allowed the material to "breathe" and to cure completely. Any air bubbles that may have been incorporated during the mixing and pouring processes rose to the surface and were completely eliminated from the material within two hours of it being poured.

To obtain the correct filler volume fractions for a range of microsphere filled samples the mass of a particular volume fraction needed to be calculated, this methodology required knowledge of the mass of a single sphere and its volume.

Kepler's conjecture of 1611 examined the packing of solid spheres into a given volume. He examined the problem, of finding the most efficient way to pack spheres together and the true volume that they occupied neglecting the air gaps, by considering stacks of cannon balls for the battlefields and ships of the day, but the problem was also relevant to other packed spheres such as oranges at a market stall. The Kepler Conjecture proposes that "No packing of balls of the same radius in three dimensions has density greater than face-centered cubic packing", there are other methods that provide the same density, the most common alternative being hexagonal close packing, Hales (2000). For these methods, the volume occupied by the spheres was found to be slightly less than 75 %, the remaining amount a little over 25 %, being air.

The approximate volume occupied by the spheres can be found using the following formula;

$$Volume = \frac{\pi}{\sqrt{18}} \approx 74\%$$

This ratio was used in the following calculations to arrive at a 2.5 % volume of microspheres for the required amount of filled elastomer material. It does however assume perfect packing and that all of the microspheres are of uniform shape and size.

The calculation for 2.5 % volume fraction of microspheres was conducted as follows;

Elastomer volume for mould = 180 x 180 x 1.5 mm^3 = 48,600 mm^3 = 4.86 x 10^{-5} m^3
Therefore, 2.5 % of this volume for the microspheres = 1.125 x 10^{-6} m^3
Akzo Nobel provides the density and size of the microspheres as follows:
Microsphere Density = 42 kg/ m^3
including air, assuming that the average diameter for a single sphere = 40 x 10^{-6} m

Mass of single sphere:

No. of spheres assuming uniform size per $m^3 = 1.5625 \times 10^{13}$

from $1 / (40 \times 10^{-6}) \times 1^3$

The volume is the same however packed (Kepler)

The volume and quantity is the same for air and rubber

Mass of single sphere = $kg/m^3 / m^3$

$= 42 / 1.5625 \times 10^{13}$

$= 2.688 \times 10^{-12}$ kg

Vol. of single sphere $= \pi d^3/6$

$= \pi \times (40 \times 10^{-6})^3 / 6$

$= 3.3510 \times 10^{-14}$ m^3

No. of Spheres = 2.5 % Vol. / Vol. of single sphere = $(1.125 \times 10^{-6}) / (3.3510 \times 10^{-14})$

= 36,257,833 (Expancel state 700,000,000 in a Tennis Ball)

Mass of Spheres = No. of spheres x Mass of single sphere

$= 36,257,833 \times (2.688 \times 10^{-12})$

$= 9.7461 \times 10^{-5}$ kg

= 0.09746 g

The 2.5 % volume fraction of microspheres was used initially, this was then scaled to produce volume fractions of 5 %, 10 %, 20 %, 30 % and 40 % with the mass of the rubber reduced accordingly.

The actual amounts mixed for a filler volume fraction of 2.5 % were as follows:

Rubber Total	=	47.385g
Pt A	=	45.016g
Pt B	=	2.369g
Microspheres	=	0.098g

The part A and part B were measured as for the unfilled material vary carefully to this amount. The microspheres were also measured in an identical manner and added once the two liquid parts were fully mixed. The microspheres were thoroughly mixed into the elastomer liquid to ensure that they were well dispersed. The mixture was then poured into the mould and cured in the same way as the unfilled material.

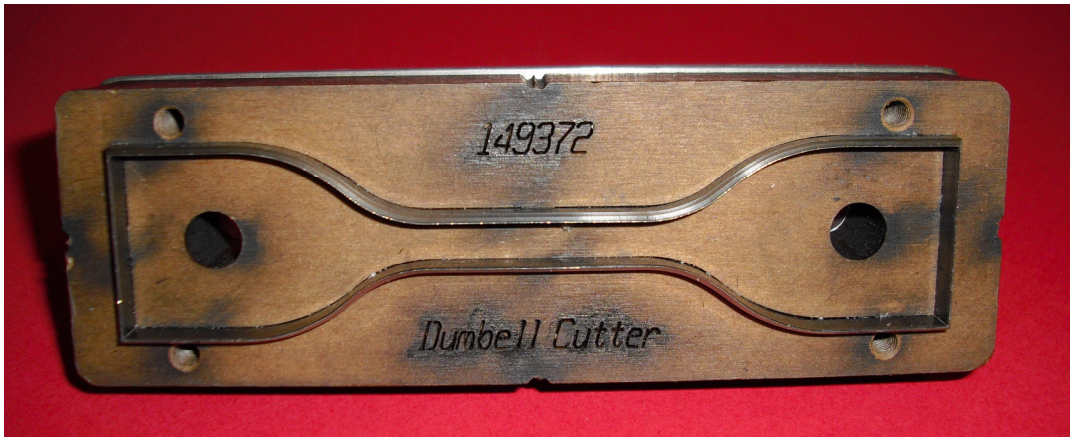

Figure 3.17: Large dumbbell cutter.

Once the material, whether unfilled or filled, had cured, it was removed from the mould as a complete sheet by peeling it gently from one edge. Care was taken not to apply too large a strain to the material as this pre-strain could affect the physical test results. The sheet was then cut into a number of dumbbell test pieces for tensile testing. The cutting was achieved using a shaped steel cutter as shown in Figure 3.17 using the hydraulic press as shown previously in Figure 3.10. The rubber sheet was placed on a cutting mat to prevent damage to the sharp edge of the cutter. The test pieces were measured for thickness by placing them on a flat surface and using a dial gauge. Measurements were taken at five positions along the gauge region of the test piece and a mean value calculated. The test pieces were then used to determine the Young's modulus and other mechanical properties.

3.4.3 Tensile testing of dumbbell test pieces

The unfilled and filled dumbbell test pieces were tested at different times using a variety of Instron screw driven test machines including the Instron 5564, the Instron 5566, the Instron 5567 and the Instron 5588. Instron type machines are available with two common methods to move the crosshead and hence the grips, they are either servo-hydraulic or screw driven. Servo-hydraulic machines are most suitable for cyclic testing; the screw driven machines are most suitable for single cycle compression and tension testing.

Typically each machine was fitted with a 1 kN load cell, which can measure loads up to 1 kN in tension or compression. Some of the machines were fitted with a camera or optical sensors; these were used to follow dots that could map the

displacement of the surface of the test pieces. Dots were drawn using a black marker pen, approximately 20 mm apart. Knurled sprung grips were used to grip both ends of the test pieces; these are specifically for use with soft materials such as elastomers, their cam design also ensures that they grip tighter as the tension increases. Occasionally knurled grips were used where the jaws were tightened onto the test piece, these require the material to be gripped tightly enough to prevent slipping, but not so tight that the material tears in the grip. The camera or optical device was calibrated and the gauge length measured for each test piece, this is measured as the distance between the central points of the two dots placed on the gauge length of the test piece.

The crosshead speed was set to move at 5 mm/min for each test, as the crosshead moved up the camera or optical sensors measured the distance between the dots on the test pieces to obtain the strain data. The force was measured by the load cell. In each case the data was collected on a personal computer connected via a data link to the Instron machine. The data was analysed using Microsoft Excel.

An example test result is shown in Figure 3.18, the results of the tensile test were used to obtain the modulus from the slope of the graph up to a strain of 10 %. The neo-Hookean and Yeoh material values used in the finite element models were also derived using this stress / strain data.

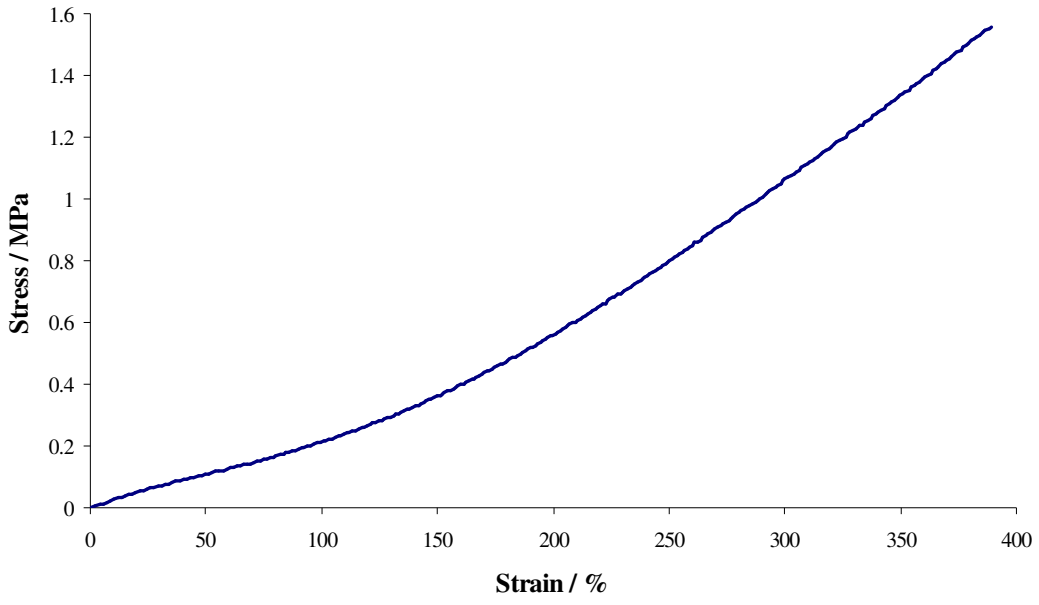

Figure 3.18: Uniaxial tensile test result for unfilled silicone elastomer.

3.4.4 Density measurement

Often the easiest way to measure the density of an object is to use the Archimedes principle. Archimedes found that when a solid body is immersed in a fluid it will displace an amount of fluid that is the same mass as the solid body itself. A more accurate result can be found by weighing the body in air and in water or an alternative fluid of a known density, such as ethanol. This method is suitable for larger specimen sizes, such as the silicone elastomer samples mentioned in this chapter. But the method is not suited to small specimen sizes, such as the microsphere material.

For this study a series of unfilled and filled elastomer samples were cut from the flat sheets as used for the tensile tests. The samples were cut into squares with each side approximately 10 mm and the thickness was approximately 1.5 mm. The samples were initially weighed in air on the balance before being immersed in the water and weighed again with care being taken to ensure no air was trapped on the surface. Distilled water was used, the temperature of the water was maintained at 25 °C throughout. The weight of the unfilled and filled elastomer samples in air and in water are shown in Table 3.3.

The apparatus used to measure samples of the silicone elastomer, both unfilled and filled with microspheres, is shown in Figure 3.19.

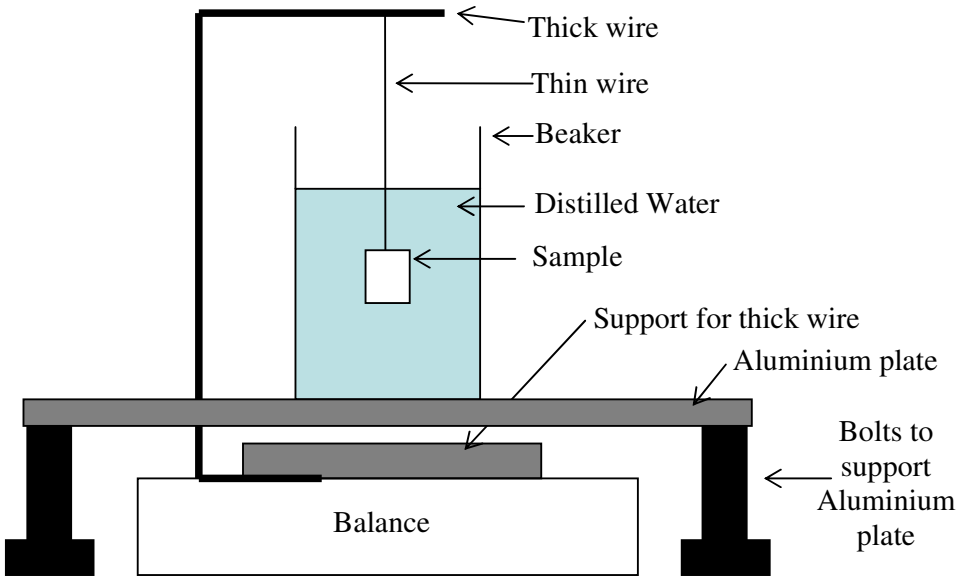

Figure 3.19: A diagram of the density measurement equipment used during this study.

The following formula was used to calculate the density of the samples.

$$\rho = \frac{A}{A-B}(\rho_O - \rho_L) + \rho_L$$

Where; A is the weight of the sample in air in grams, B is the weight of the sample in the fluid also in grams, ρ_O is the density of the liquid, ρ_L is the density of air and ρ is the density of the sample in g/cm^3. Samples were measured with no filler and with filler volume fractions of 10 %, 20 %, 30 % and 40 %, these filler volume fractions were based on calculations as shown previously in this chapter.

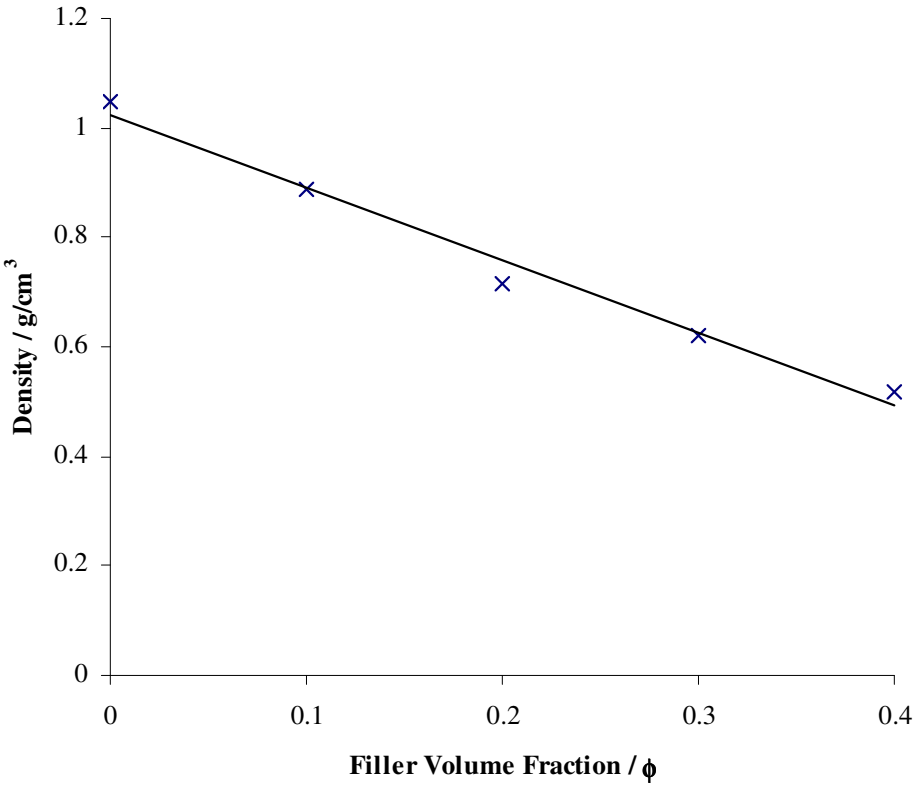

Figure 3.20: Density results for elastomer samples tested.

The "true" or experimental filler volume fractions of the samples were also calculated from the obtained density values, using the formula from the previous page, the results are shown in the following table, Table 3.3.

Air bubbles and any inherent buoyancy of the thin wire that is immersed into the water may affect the results and make the mass and hence densities have some significant experimental uncertainty, the difference between the experimental results

obtained for the microsphere diameter and those quoted by the manufacturer would also have an effect.

Anticipated filler volume fraction assuming uniform particle size and perfect packing, %	**Weight of sample in air, g**	**Weight of sample in water, g**	**Measured density, g/cm^3**	**Deduced experimental filler volume fraction, %**
0	0.433	0.022	1.049	0
10	0.422	-0.052	0.8871	15.45
20	0.291	-0.116	0.7142	31.93
30	0.407	-0.246	0.6217	40.74
40	0.319	-0.296	0.5175	50.68

Table 3.3: Filler volume fractions, originally calculated compared to those calculated from the density experiments.

3.5 The material properties used for FEA modelling

The material properties obtained during the testing described in this chapter were used in the FEA modelling of the table tennis balls and the microspheres, the properties used are shown in the following table, Table 3.4.

Material	**Material Property**	**Value**	**Units**
Table Tennis Ball / Microsphere	Young's modulus	2200	MPa
	Poisson's ratio	0.3	
	(Plastic) Yield Point	50	MPa
	Ultimate Tensile Strength	60	MPa
	Density	1.3	g / cm^3
Silicone Elastomer	Density	1.05	g / cm^3
	Yeoh model value for C_{10}	0.056	
	Yeoh model value for C_{20}	0.0054	
	Yeoh model value for C_{30}	0.0000003	
Note: The value for Poisson's ratio was obtained from Nakamura et al (2004).			

Table 3.4: Material properties determined for use in this study.

Chapter 4 The physical behaviour of an elastomer with hollow microspheres as a particulate filler

4.1 Introduction

The experiments in this chapter were conducted to enable an understanding of the physical behaviour of an elastomer when a hollow microsphere is used as a filler material. This was achieved by performing tensile experiments using dumbbell test pieces cut from thin sheets of filled composite materials and compression tests on small cylindrical test pieces, these were unfilled and for a range of filler volume fractions in each case.

By adding microspheres to an elastomer a novel foam material was created. Foams usually have either open cells or closed cells, open celled foams are similar to a sponge where air or liquid can move freely through the material, closed cell foams have separate cells where the air or a liquid is trapped within each cell and the cell itself is simply a void within the material. Foams created using microspheres have individual cells where each cell has its own structure provided by the hollow plastic shell of the microsphere.

The theoretical behaviour of open and closed cell foams is discussed in detail in Chapter 2, where there is a process of bending, buckling and densification. Gibson and Ashby (1988) have looked at many cellular materials and have described this behaviour in depth. Gent and Thomas (1959, 1959b and 1963) have also looked in particular at the behaviour of traditional elastomer foams. However, the behaviour of a novel hybrid foam created using hollow microspheres was, until now, unknown.

4.2 Tensile tests using dumbbell test pieces

4.2.1 Introduction

A uniaxial tensile test using a dumbbell test piece is the standard method used to obtain the material properties and characteristics of an elastomer material. The theoretical behaviour of an elastomer has been discussed in Chapter 2, where an “S” shaped curve typically results from a tensile test. The production of the elastomer

material, both unfilled and filled has been explained in Chapter 3, as has the subsequent manufacture of the dumbbell test pieces. The method of conducting the tensile tests has also been explained in Chapter 3.

4.2.2 Elastomer and test piece manufacture and testing

The translucent silicone elastomer used for the dumbbell test pieces was used throughout this study. The manufacturing method was also virtually identical throughout, although a vacuum machine was used to remove trapped air bubbles, before the mixed elastomer was poured into the moulds of the deeper small and large cylinder test pieces. For the dumbbell test pieces the relatively thin sheets, approximately 1.5 mm thick, facilitated any air bubbles created during the mixing process to rise to the surface and escape from the liquid material before it set.

Figure 4.1: A photograph of a typical silicone elastomer sheet from which the dumbbell test pieces were cut.

The dumbbell test pieces were made in batches of five or six test pieces. As well as unfilled test pieces, hollow sphere filled test pieces were also made for a range of filler volume fractions, typically two separate batches were made for each of the filler

volume fractions and the unfilled material. Figure 4.1 shows a sheet of the silicone elastomer filled with microspheres and cut using a dumbbell cutter to produce the test pieces.

The batches of unfilled and filled dumbbell test pieces were tested at different times using a variety of Instron screw driven test machines. Typically the machine was fitted with a 1kN load cell, some of the machines were fitted with a camera or optical sensors which monitored strain by following dots drawn on the test piece surface. The most reliable method was to draw dots to represent the gauge length on the test piece in the narrowed mid section away from the gripped ends using a black marker pen. An initial technique used small black adhesive dots applied to the surface, unfortunately as the sample was stretched these slipped and moved unpredictably. Knurled grips, either screw tightened or sprung, were used to grip both ends of the test pieces. The crosshead speed was set to move at 5 mm/min for all of the tests.

4.2.3 Results from the unfilled elastomer tensile tests

The elastomer was tested initially as the standard material without fillers and later with the microspheres as a filler for a range of filler volume fractions.

The first batch of tests was conducted using the movement of the crosshead of the Instron machine to provide the displacement and from this the strain values were calculated. The engineering stress and engineering strain results from these tests provided a large dispersion between the results as can be seen in Figure 4.2.

Another batch of the unfilled material was manufactured and tested using the same test procedure but using an Instron machine with a video camera fitted to follow the gauge length marked on the test pieces. Careful calibration of the camera was essential, but the non-contact method using the machines fitted with a camera, or other optical sensor, provided much more reproducible results than relying on a value of strain calculated from the measurement of the displacement of the machine crosshead.

Typical engineering stress and engineering strain results can be seen in Figure 4.3, where there is a much closer grouping of curves.

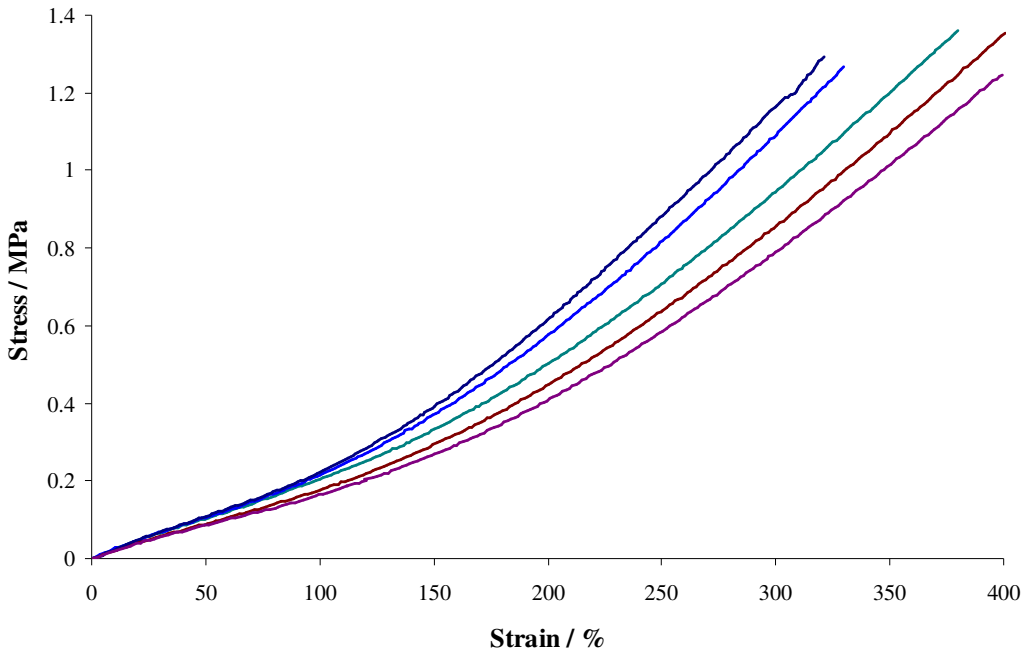

Figure 4.2: A graph showing initial tensile test results for unfilled silicone elastomer dumbbell test pieces.

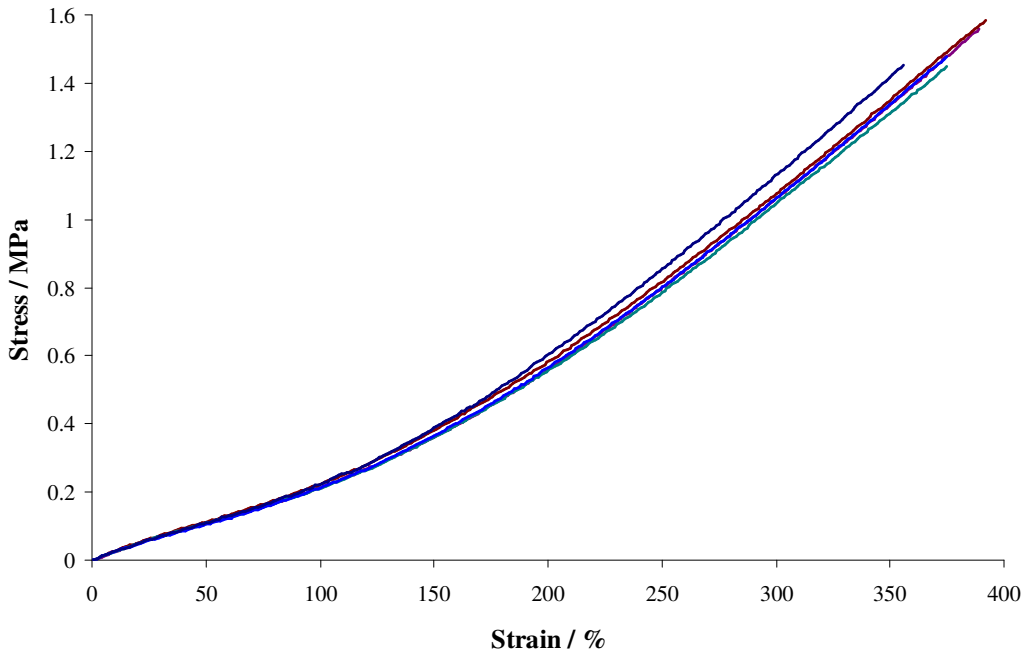

Figure 4.3: A graph showing the follow up test for the unfilled silicone elastomer dumbbell test pieces using strain mapping on the surface of the test sample.

Another factor that affected the accuracy of the tensile test results was the type of grips used. Knurled sprung grips are specifically designed for use with soft materials such as elastomers, where their cam design ensures that they grip tighter as the tension increases. However, this type of grip can sometimes not grip sufficiently tightly enough, causing the test piece to slip slightly in the grip during the test, this affected the displacement values during the test and hence the strain values. It was usually very easy to see from a series of tests if an individual test had slipped during testing.

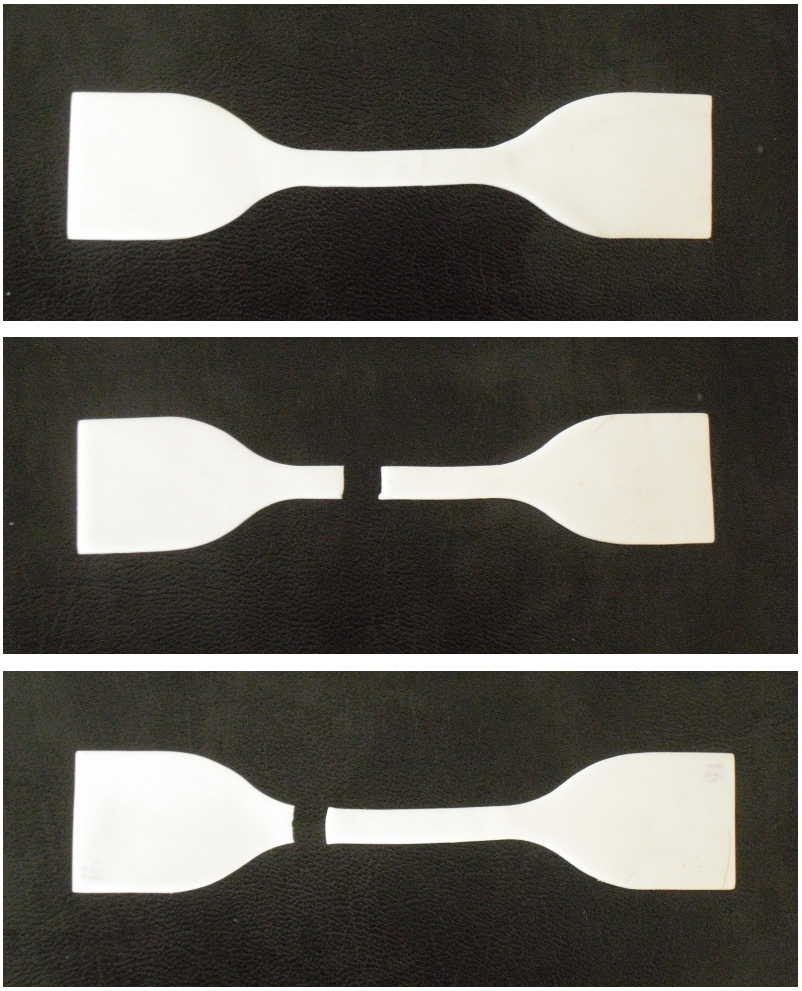

Figure 4.4: A photograph of a typical dumbbell test piece and a pair of dumbbell test pieces after testing.

Grips that were manually tightened could be tightened sufficiently to prevent the test piece from slipping from the grip during the test, but over tightening produced stress raisers near to the grip which sometimes caused the test piece to fail at the grip

rather than within the gauge length. Figure 4.4 shows typical dumbbell test pieces used during the tensile tests.

The test pieces in the figure all contain a microsphere filler volume fraction of 20 %. The upper photograph shows a test piece prior to testing. The lower two photographs show a conventional test piece failure within the gauge length and a failure that occurred towards the end of the gauge length. Most failures occurred within the gauge length; rarely did they occur at the wider neck region of the test piece or at the grips.

4.2.4 Results from the filled elastomer tensile tests

By testing the elastomer material filled with microspheres and comparing it to the unfilled material, it was hoped that the behaviour of the elastomer and any effect of the filler would be understood. It might be anticipated that the effect of introducing the hollow filler material might be to increase the stiffness with an increase in the filler material, due to the additional stiffness provided by the rigid shell of the hollow plastic filler similar to the increase in stiffness observed using traditional solid fillers such as carbon black. Alternatively, the stiffness might decrease as for an elastomer foam material with an increasing amount of voids.

Following the tensile tests on the unfilled elastomer, tests were conducted on the filled elastomer for a range of microsphere filler volume fractions, these were; 2.5 %, 5 %, 10 %, 20 %, 30 % and 40 %.

The tests conducted with a 2.5 % filler volume fraction of microspheres produced a set of curves that were very close to the unfilled material when analysed. There was also a slight dispersion between the curves which aligned some of the test results for the filled material closely to the results of the unfilled material. Therefore, it was not possible to differentiate between some of the results, so there could be little confidence in identifying an effect of the microspheres as a filler at such a low volume fraction. The following graphs compare the unfilled elastomer with a range of filler volume fractions, starting with 5 %. All of the graphs show the middle curve from each batch of tests for each filler volume fraction, each batch of tests was conducted using five or six test pieces. The unfilled material produced a characteristic elastomer “S” shaped curve but the filled material produced a more linear curve with a less pronounced “S” shape.

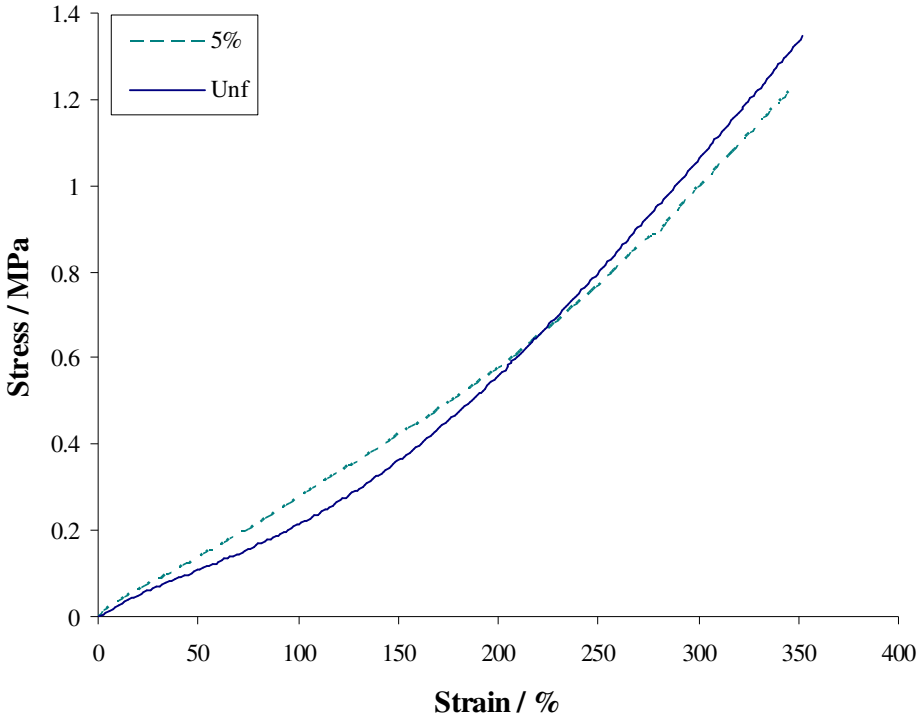

Figure 4.5: A graph showing tensile test results for the silicone elastomer, unfilled and with 5 % filler volume fraction of microspheres.

The elastomer was then tested with a microsphere filler volume fraction of 10 %, there appeared to be a trend developing, which was later confirmed by completing further tests with a filler volume fraction of 20 % microspheres and comparing the engineering stress and engineering strain results.

At lower strains the microspheres were acting as a traditional filler material, such as carbon black, reinforcing and stiffening the elastomer. However, at higher strains the microspheres were acting as voids in a foamed elastomer causing the material to become softer.

Figure 4.6 includes material with 10 %, 20 %, 30 % and 40 % filler volume fractions of microspheres compared to the unfilled material. The trend continued to be observed for filler volume fractions of 30 % and 40 % particularly at lower strains as can be seen in the graph. However, for higher strains, beyond a strain of 150 %, the material with a filler volume fraction of 30 % microspheres was no softer than the material with 20 % filler volume fraction of microspheres, this was observed for all test pieces with a filler volume fraction of 30 %.

The material with 40 % filler volume fraction was greatly weakened in tension by the filler and typically reached a maximum strain of only 150 % before the test pieces broke.

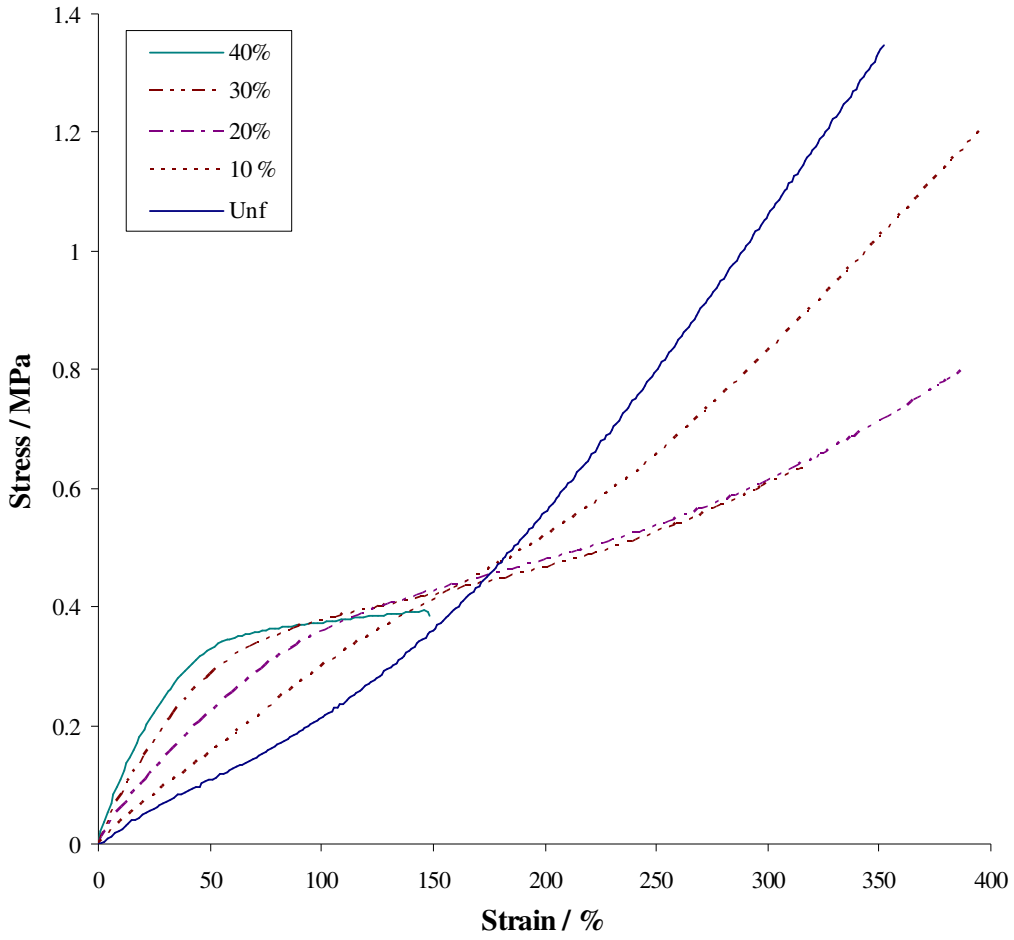

Figure 4.6: A graph showing tensile test results for the silicone elastomer, unfilled and with 10 %, 20 %, 30 % and 40 % filler volume fractions of microspheres.

The behaviour can be explained where the microspheres acted as rigid fillers at lower strains which stiffened the material, but due to the process of the microsphere cell walls bending and buckling the reinforcing effect of the filler diminished with strain. Similar behaviour has been described by Ashby and Gibson, although not for an elastomer with as novel a filler as this. They noted that for a conventional foam material during compression there were three distinct areas of behaviour; cell wall bending, cell wall buckling and densification as described earlier in Chapter 2.

At higher strains the microspheres continued to deform and no longer acted as reinforcement, as the densification process continued the elastomer material behaved more like traditional rubber foam.

The trend agrees with the work of Gent and Thomas (1959a) who observed the behaviour of elastomers filled with carbon black which became stiffer as the filler volume fraction of the filler material was increased and foamed elastomers which became softer as the volume of the voids increased. This behaviour has also been covered in detail in Chapter 2.

4.3 Compression tests using small cylinder test pieces

4.3.1 Introduction

The tensile experiments using dumbbell test pieces provided a good understanding of the physical behaviour of an elastomer when a hollow microsphere was used as a filler material. Following the tensile experiments a series of experiments in uniaxial compression were conducted on small cylindrical test pieces, again these were unfilled and for a range of filler volume fractions. These experiments were conducted with the aim that they may add to the understanding of the effect of the microsphere filler on the behaviour of the elastomer material.

4.3.2 Elastomer and test piece manufacture and testing

The silicone elastomer was manufactured for the small cylinder test pieces in an identical manner to the material for the tensile test pieces. The test pieces were made in batches of five, each test piece was approximately 29.5 mm in diameter, the heights of the initial test piece varied between 15 mm and 20 mm, later test pieces were all 15 mm tall.

The unfilled elastomer for the first batch of test pieces was not placed in the vacuum machine and once it had cured there were still a large number of bubbles trapped within each test piece. The depth of the test piece and the relatively small surface area had not allowed the bubbles to reach the surface and escape from the material as for the thin sheets produced for the tensile test pieces. The mixed material for each of the subsequent batches was placed in the vacuum machine to remove the bubbles that were inevitably incorporated during the mixing process.

The elastomer for the small cylinder test pieces was poured into moulds made from 35 mm film cases. The cases had a circular hole cut in the bottom to allow the cylinder to be pushed out of the mould once it had cured. A circular piece of plastic, a disk, was placed in the mould to act as the bottom surface. Figure 4.7 shows a schematic of the early mould design.

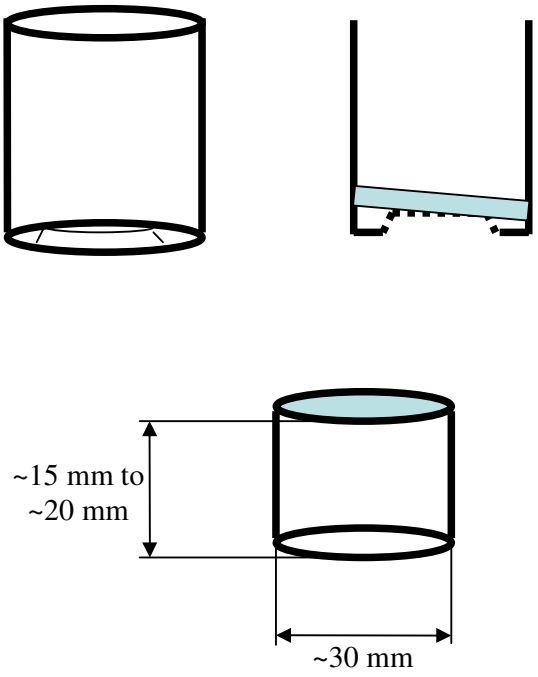

Figure 4.7: A schematic of the original mould and the test piece that it produced.

There were a number of limitations with the initial design. The bottom surface of the original case was not flat, there was a central circular raised area inside the bottom surface, therefore the disk did not always sit horizontally within the mould and when the test piece was removed from the mould it sometimes had a sloping bottom surface. The side of the mould also tended to attract the liquid silicone and when it had cured there was a raised meniscus around the top edge of the test piece. The test pieces were also difficult to remove from the mould as the disk was of thin plastic and was not rigid enough for a large force to be applied through the circular hole in the bottom of the mould. The test pieces were also of different heights, the mould was approximately 46 mm from the rim to the plastic disk when fitted, the aim was to fill the moulds by a similar amount, but this was not easy and once cured the test pieces varied between approximately 15 mm and 20 mm.

Following the initial unsatisfactory results with the initial moulds a number of modifications were made. Figure 4.8 shows a schematic of the modified mould and the test piece that it produced. The bottom surface had a larger hole cut so that the previously raised inner bottom surface was completely removed to leave the bottom surface completely flat. A set of thicker Polytetrafluoroethylene (PTFE) disks, 4 mm thick, were manufactured by the QMUL workshops to a specification provided by the author, these allowed more force to be applied to them and aided with the removal of the cured test pieces.

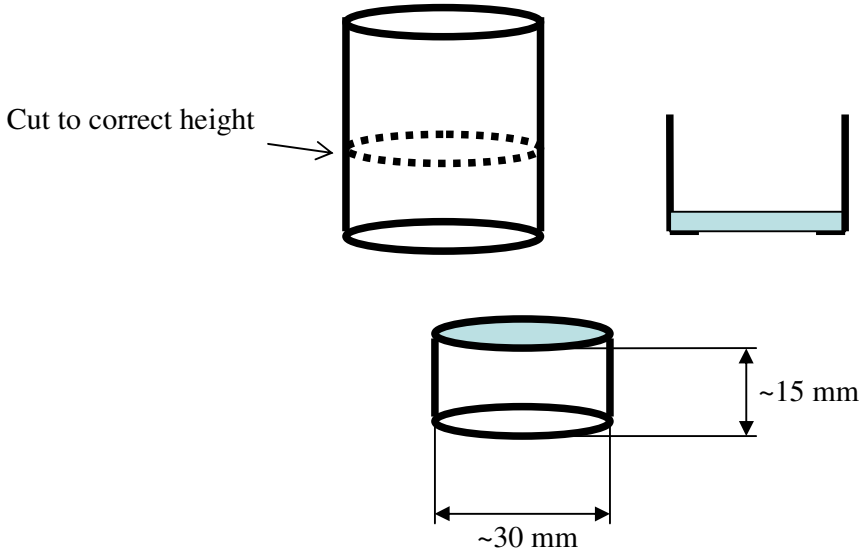

Figure 4.8: A schematic of the modified mould and the test piece that it produced.

The film cases were cut to a height that allowed for the disk to be inserted leaving a height of 15 mm height to the rim. This allowed each mould to be filled completely to the top and resulted in test pieces of the same height and it also avoided the formation of a meniscus. The modifications ensured that all of the test pieces were of a uniform height and had flat top and bottom surfaces.

Figure 4.9 shows various photographs of the 35 mm film cases and their conversion into moulds for the small cylinder test pieces. Photograph “a” is of the unmodified film case. The raised internal bottom surface can be seen.

a.

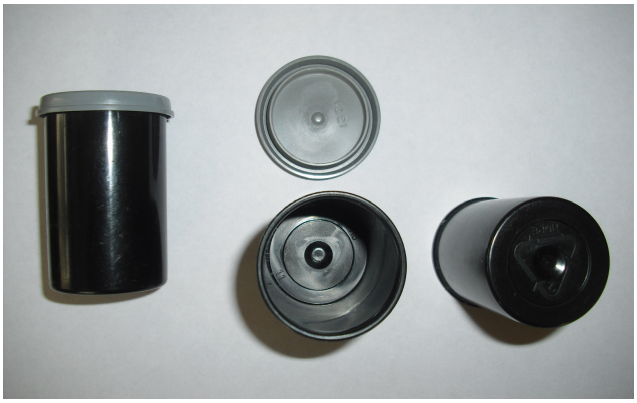

b.

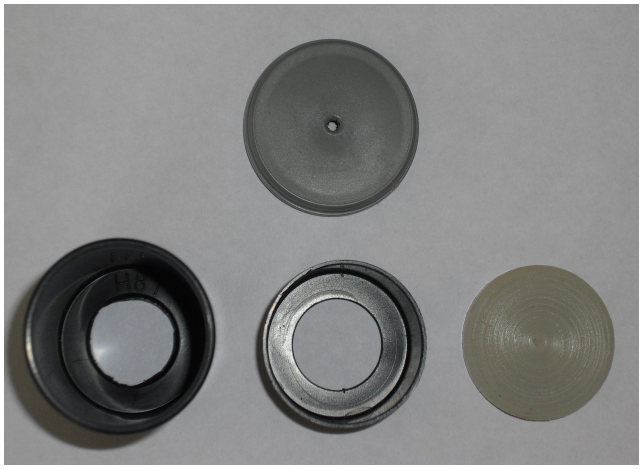

c.

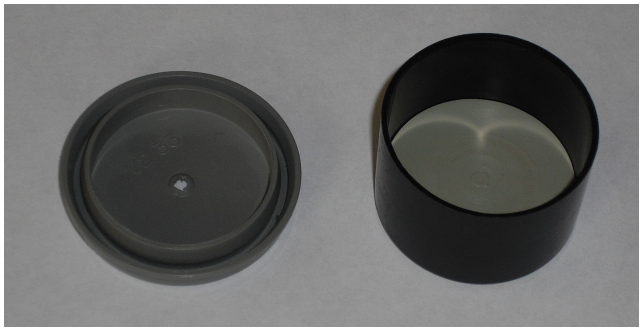

Figure 4.9: A photograph showing an original film case (a) and one adapted for use as the initial and final mould (b) and the final mould assembled (c).

Photograph "b" shows a hole in the lid of a film case, this was to allow air to enter the mould, but dust to be kept out during the curing process. The left side image shows the initial mould where a circular section had been cut from the bottom surface to enable the cured test piece to be pushed out, but the bottom surface is not completely flat. This has been remedied in the central image, where more of the bottom surface has been cut out, this was possible due to the extra rigidity provided by the thick disks, one of which is shown on the right. The thicker disk also made the removal of the test piece

easier once it was fully cured. The central image also shows the reduction in height of the mould compared to the image on the left.

Photograph "c" shows an example of the final mould with the disk inserted. The distance from the rim of the mould to the surface of the disk is exactly 15 mm. The moulds were filled to the very top and the lids were placed gently on top to protect the elastomer whilst it cured.

a. 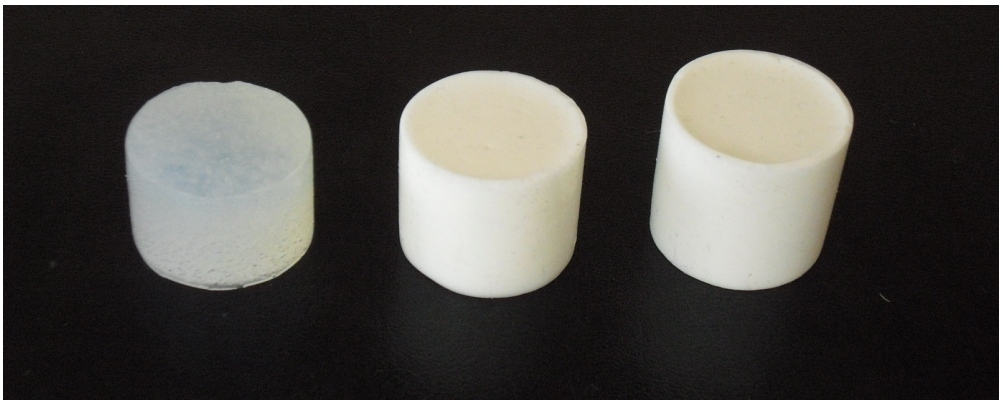

b. 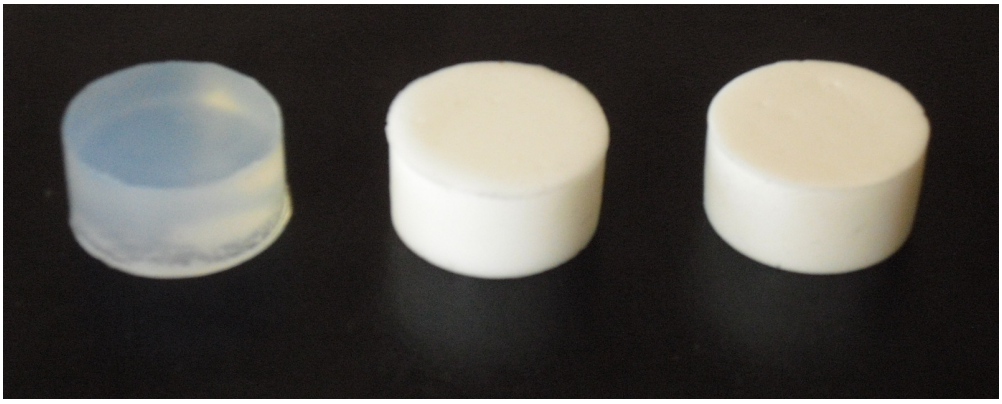

Figure 4.10: A photograph of early test pieces (a) and a later smaller ones (b).

Figure 4.10 shows, in photograph "a", examples of test pieces made using the original moulds and in the photograph "b" examples of test pieces made using the later moulds.

The test pieces in photograph "a" can clearly be seen to vary in height, ranging between 15 mm and 20 mm. The unfilled test piece on the left is from the first batch produced and can be seen to contain a large number of air bubbles. The edge meniscus can also be seen on the two filled test pieces, some of this still remains despite being trimmed off. The photograph "b" shows later test pieces, all of a uniform height of 15 mm and with perfectly flat surfaces, top and bottom. The unfilled test piece, again on the left, can be seen to contain very few air bubbles. These uniform test pieces with a

height to width ratio of approximately 1:2, produced much more comparable results than the previous test pieces with a range of heights.

The tests of the small microsphere filled cylindrical test pieces were all conducted using a screw driven Instron 5584 mechanical testing machine with the crosshead displacement set to move downward at a rate of 5 mm/min. A 1 kN load cell was fitted to the crosshead, initial tests were conducted up to a maximum of 500 N. Later tests were conducted with the maximum force permitted set to a value of 950 N to ensure that the test would stop and the load cell would not be used above its rating of 1 kN.

The Instron machine had a small flat steel plate placed directly below the axis of the load cell to provide a flat stable surface for the test piece to be placed. The steel plate was also of sufficient mass to remain perfectly in place during the test. A similar smaller plate was placed upon the top surface of the test piece to create a sandwich, with the test piece between two flat rigid steel plates.

The crosshead of the Instron machine was fitted with a ball and socket adapter which had a flat bottom, the flat bottom was able to sit perfectly flatly on the upper surface of the top steel plate due to the nature of the ball and socket joint. This ensured that the system was not misaligned and the force applied by the descending crosshead would be more reliable than if a completely rigid system was used.

Before each test was initiated the crosshead was lowered manually until it touched the top test piece with a negligible contact force of a few tenths of a Newton being indicated. The tests were conducted in batches of five test pieces. The small microsphere filled cylindrical test pieces were tested in the same manner as used to measure the behaviour of samples containing a large single sphere described later.

4.3.3 Results from the unfilled elastomer compression tests

The initial tests were conducted using unfilled elastomer cylinders, the test pieces were not uniform in height and when compared as a force displacement graph as shown in Figure 4.11, there is a clear discrepancy between the curves for the variety of heights. The initial tests were conducted to a maximum force of 500 N, as it was not known how the test pieces would behave.

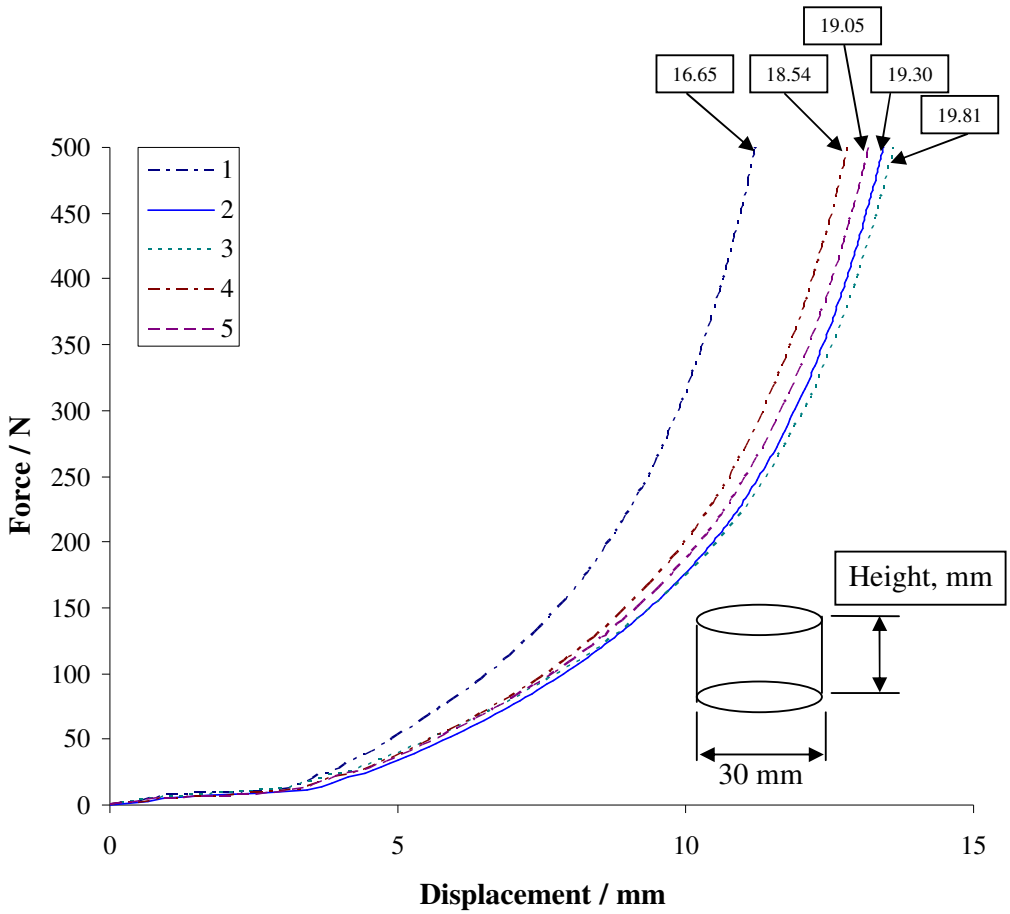

Figure 4.11: A graph showing initial compression test results for the small unfilled silicone elastomer cylinders.

As might be expected for cylindrical test pieces of an identical diameter, the smaller test pieces are stiffer compared to the taller test pieces. The height of the test pieces produced a sequential set of curves where the stiffness decreased as the height increased. It is also evident that the test piece that was substantially smaller, 16.65 mm tall, produced a curve that was much stiffer than the other four test pieces that were more comparable in height, 18.54 mm to 19.81 mm, which produced a tighter sequence of curves.

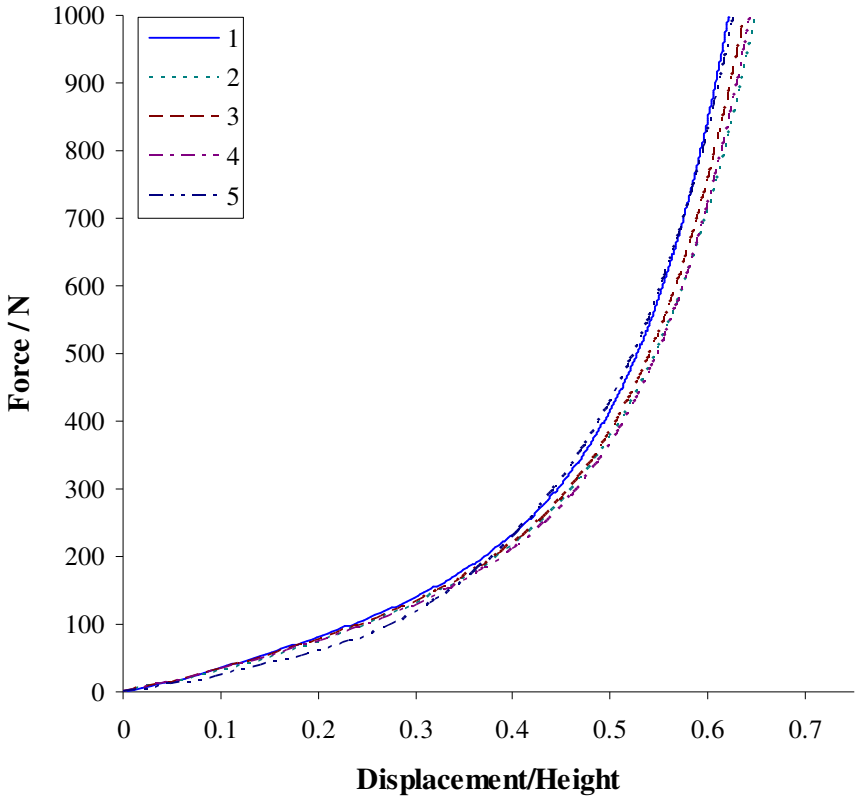

Figure 4.12: A graph showing normalised compression test results for the small unfilled silicone elastomer cylinders.

Figure 4.12 shows a set of curves for a second batch of five test pieces again of varying cylinder height. These tests were conducted up to a value just below the maximum value of 1 kN for which the load cell was rated. Here the height factor has been eliminated by dividing the displacement by the height for each test, to produce a "normalised" set of curves. These curves are much more comparable and this method was adopted to compare the filled and unfilled test pieces. The values have also been "zeroed" to reduce any errors in the values that the experimental set up may have introduced during the initial displacement.

The tightly grouped curves provided confidence that when comparing a series of curves for the unfilled and filled elastomer cylinders the differences would be real and not a manifestation of the experimental set up, the test piece geometry or from the manner that the data was presented.

4.3.4 Results from the filled elastomer compression tests

Results taken from three batches of tests for elastomer cylinders that were unfilled and those that had a 10 % and a 20 % filler volume fraction are shown in Figure 4.13.

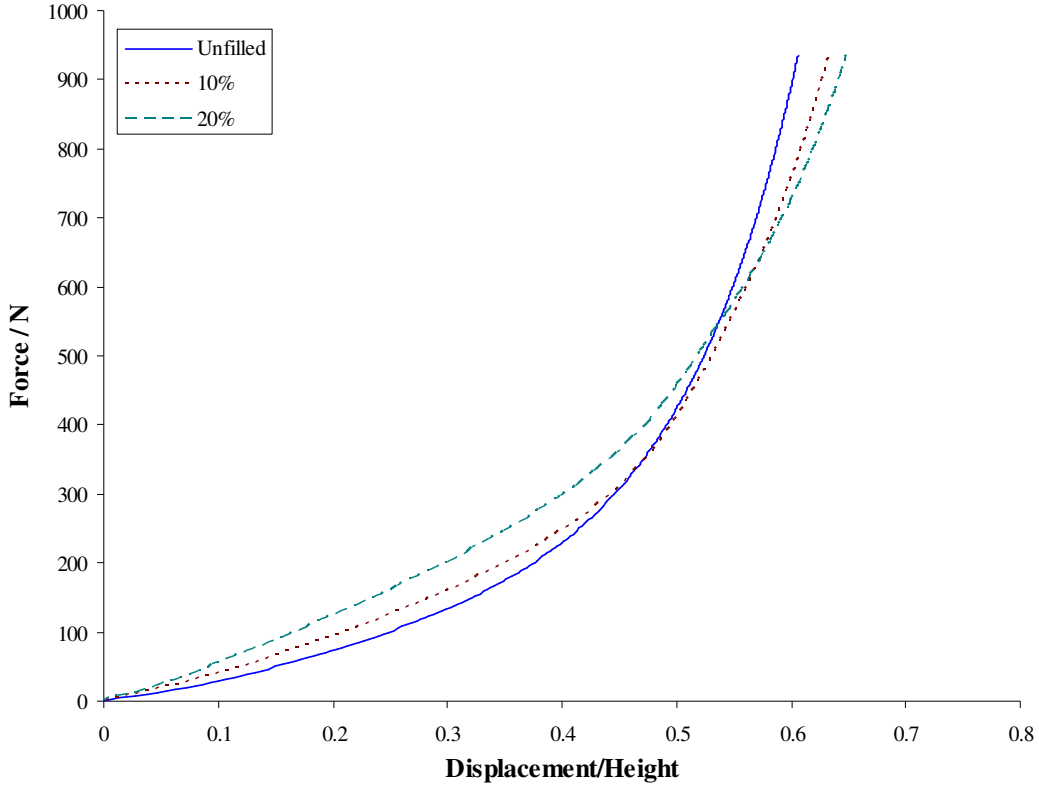

Figure 4.13: A graph showing normalised compression test results for the small silicone elastomer cylinders, unfilled and with 10 % and 20 % filler volume fraction.

The test pieces were of the later type which had flatter top and bottom surfaces and no meniscus, ensuring that the cylinder height was uniform. There was still a small discrepancy in the results for each batch which was again removed by normalising the results by dividing the height by the displacement.

The results for the smaller cylinders in compression produced an identical pattern to the dumbbell tensile test results. The increase in filler volume fraction produces an increase in the stiffness at lower displacements due to their enhanced initial stiffening effect. However, at larger displacements, once the spherical hollow fillers have buckled, the stiffening effect is reduced and the larger filler volume with the larger number of inherent voids causes the material to become softer and behave in the manner of a normal foamed elastomer.

4.3.5 Behaviour of the filled elastomer

The overall behaviour of an elastomer filled with microspheres has been determined. Two phenomena have been discovered, the microspheres have been shown to increase the stiffness of the elastomer at low strains, this is true for cases of both tension and compression. However, at higher strains the elastomer becomes softer with an increasing volume of microspheres.

The stiffening phenomena is due to the initial stiffness of the microsphere shell but the cause of the softening behaviour is likely to be due to subsequent dewetting between the microsphere and the elastomer, or by buckling of the microsphere shell, or a combination of the two effects, the cause of the softening behaviour is investigated in detail in the following chapters.

Chapter 5 The mechanical behaviour of the hollow plastic sphere

5.1 Introduction

The mechanical behaviour of the hollow plastic sphere has been investigated. The investigation included physical tests of microspheres under uniaxial compression, this was then repeated at a larger scale by examining the behaviour of a table tennis ball. A number of other types of hollow sphere were also tested to observe their behaviour for comparison.

Chapter 6 describes the use of FEA software to simulate the behaviour of hollow spheres under uniaxial compression. The models used included those of table tennis balls and also of the microspheres with a range of ratios of wall thickness to diameter. Finally a method was developed where the wall thickness of a hollow sphere and the modulus of its constituent material could be derived from a simple uniaxial compression test.

5.2 Physical Testing

5.2.1 Introduction

Testing the behaviour of single microspheres is an understandably difficult task due to their small size. The samples tested ranged from 20 μm to 50 μm in diameter, a microsphere with a diameter of 40 μm was expected to have a wall thickness of 0.4 μm based upon information available from the manufacturer. A nanoindentation testing facility at QMUL was used for this study.

Due to the small scale of the microspheres, a physical model was deemed useful in order to more easily observe their behaviour, an appropriate model being a table tennis ball. They are made from a material of comparable modulus and strength to the microspheres and although they are made from celluloid rather than the plastic polymer mixture of acrylonitrile, vinylidene chloride and methylmethacrylate, they also have a diameter to wall thickness ratio similar to the microspheres and they are easy and cheap to source. The table tennis ball has a diameter of 40 mm and a wall thickness of 0.4 mm.

Standard Instron test machines were used to conduct the compression testing of the table tennis balls and the other balls that were used. The theoretical behaviour of

thin-walled hollow plastic spheres is described in Chapter 2, the testing methods used to obtain the material properties of the microspheres and the table tennis balls are described in Chapter 3.

The tests in this chapter aim to provide an understanding of the physical behaviour of the microspheres and hollow spheres in general. By obtaining the compression characteristics of microspheres and table tennis balls and knowing the material properties, a series of FEA models could be developed for a range of sphere diameters and wall thicknesses.

From these models a master curve could then be developed that would enable the wall thickness to be evaluated from the stiffness and buckling behaviour for any sized hollow sphere simply by conducting a simple compression test.

5.2.2 Microsphere compression testing procedure

The single microspheres were tested in compression. To prepare a sample of the microspheres for testing a small specimen spoon was used to place a number onto the surface of a microscope slide, these were then dispersed using a drop of pure de-ionised water, which then evaporated. The microscope slide was then attached to a small plinth that fits into the nanoindentation machine. The slide was attached using some dental wax, which was melted on a hot plate at approximately 40 °C and allowed to cool and set.

The nanoindentation machine was zeroed prior to use. The zeroing process was achieved by using a small piece of aluminium attached to a separate plinth. An indenter with a point was used to create a small mark on the surface of the aluminium. This indentation was then located by using the integrated video microscope, this location and its corresponding X and Y coordinates were then set as the reference point.

Once the machine had been zeroed the plinth containing the prepared sample of microspheres was then placed into the indentation enclosure. A single microsphere was located using the X and Y coordinates and the video microscope display. The first microsphere chosen was approximately 40.48 μm in diameter, this was a sensible representative size based on the typical size range measured in Chapter 3.

It was important that the chosen microsphere was also isolated from other microspheres so that only a single microsphere was compressed, if other microspheres were too close these could be compressed at the same time and this would consequently affect the results.

The microsphere was located and the indenter was placed with a small clearance of approximately 60 μm to 70 μm above it. The machine was then left for thirty minutes to equilibrate. The indenter used had a smooth circular ruby tip with a diameter of approximately 1 mm. This diameter compared to the 40 μm diameter of the microsphere meant that the indenter surface was effectively flat. Initially the indenter tip was moved in the –Z direction until the resulting force was 10 μN. This force deformed the microsphere by a small amount, the indenter tip was then raised until the force was eroded.

A number of compression tests were conducted on the chosen microsphere using a load control setup. The machine was configured to dwell for thirty seconds once the specific force had been reached, the indenter was then raised to the original start position and a dwell time of thirty seconds was included to allow the microsphere to fully recover, although according to the manufacturer's literature the microspheres are elastic and might be expected to recover instantaneously (Akzo Nobel, 2004). The loading sequence adopted was; 0.1 mN, 0.25 mN, 0.4 mN, 0.5 mN and 0.75 mN.

The final force of 0.75 mN was chosen during the experiment to achieve a required deformation of 20 μm which is approximately 50 % of the original diameter. A computer was used to collect the results, the depth of indentation and the applied force were recorded throughout the various loading sequences. The data files were processed using Microsoft Excel.

Ten further tests were conducted to characterise a range of different microspheres. The procedure was repeated but each microsphere was compressed once only. The original diameters tested were as follows; 16.9 μm, 22.2 μm, 28.3 μm, 29.0 μm, 38.3 μm, 38.4 μm, 41.3 μm , 48.4 μm, 50.1 μm and 51.2 μm.

5.2.3 Microsphere compression testing results

The first microsphere with a diameter of 40.48 μm was compressed in five loading cycles. After each test the microsphere was allowed to recover. The maximum force data in each cycle is shown if Table 5.1.

Nominal Force Applied (mN)	**Actual Force Measured (mN)**	**Displacement (µm)**
0.1	0.09665	2.772
0.25	0.2468	10.239
0.4	0.39596	14.386
0.5	0.49735	17.076
0.75	0.74802	20.507

Table 5.1: Results of 40.48 µm diameter single microsphere compression tests.

Figure 5.1 shows the second cycle loading, for test 2, the curve is initially smooth until it reaches approximately 2 µm where it exhibits a point of instability.

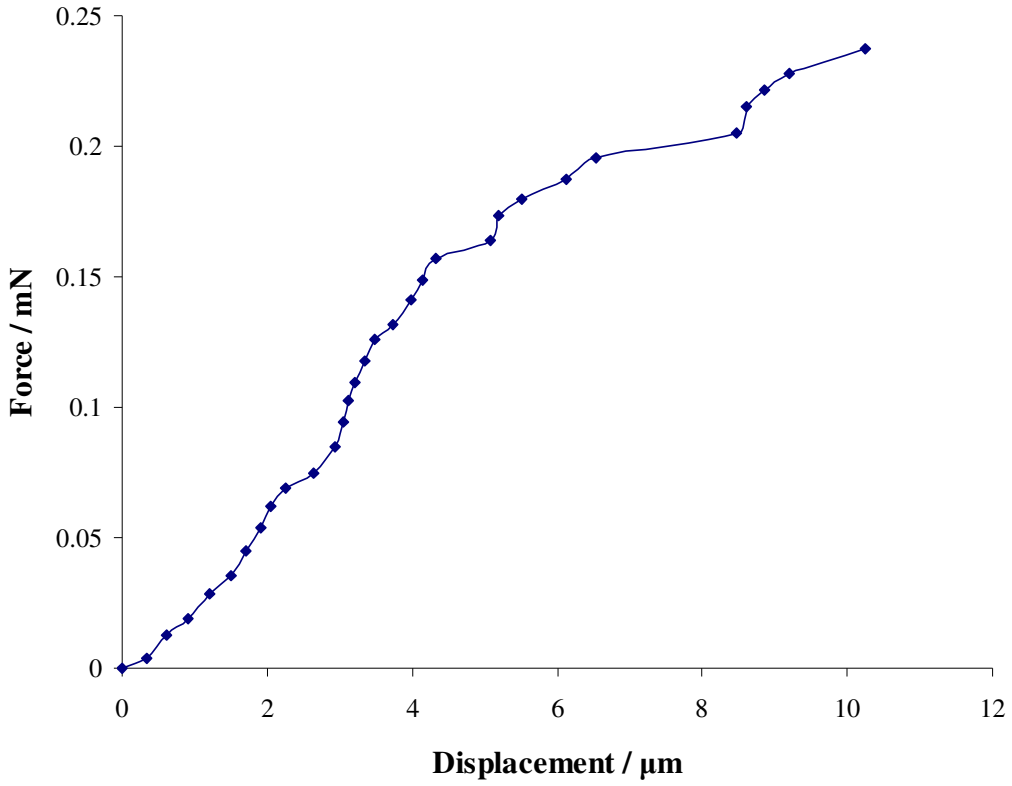

Figure 5.1: An example curve from the initial tests of a single microsphere.

Figure 5.2 shows all five of the initial loading and unloading cycles on the single microsphere. Each loading cycle does not follow the previous loading cycle indicating some yielding in the post buckled state. Therefore it can be deduced that the

microspheres exhibit hysteresis and / or plastic yielding behaviour. In the fifth cycle a force of 0.75 mN was attained, however, the full travel of the machine was reached. This produces a vertical line at this deformation. True maximum displacement was therefore approximately 50 % of the original diameter of the microsphere.

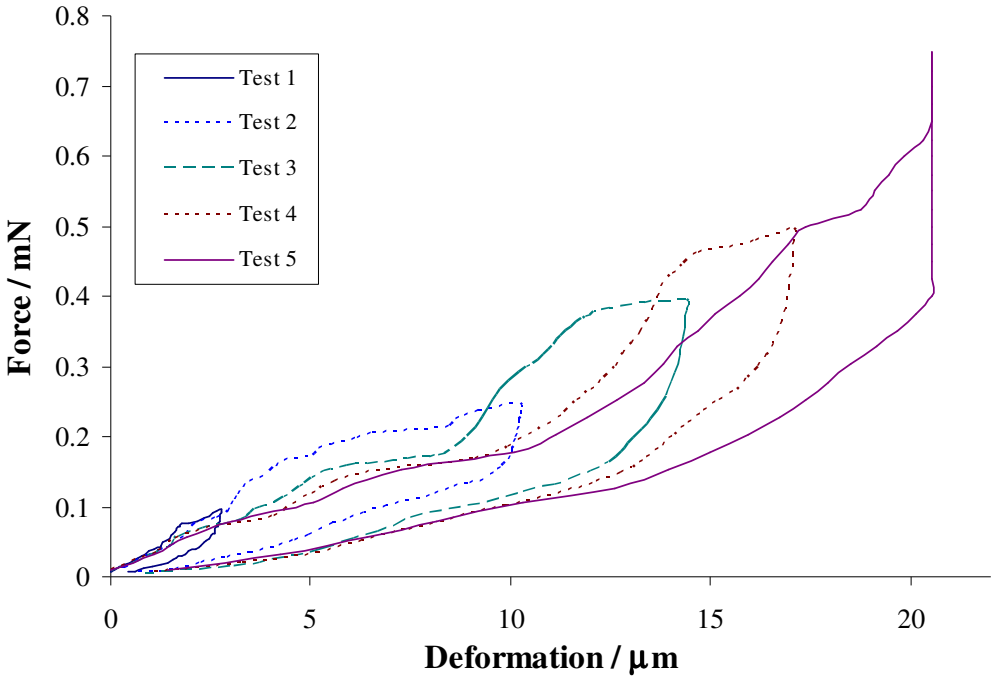

Figure 5.2: The first five loading cycles showing the inelastic nature of the test.

The results for the further two batches of microspheres produced similar results. In these tests each microsphere was compressed only once. Some of the tests produced strange anomalies in the curves. The anomalies were probably due to the indenter tip inadvertently coming into contact with a neighbouring microsphere.

A sample of reliable curves is shown in Figure 5.3, where the legend represents the approximate diameters of the microspheres in µm. The curves produced are similar in form to the original curves produced for the single microsphere, but there are inevitable differences due to the different sizes of the microspheres used, the tests also show variations due to the difficulty of determining an initial zero deformation.

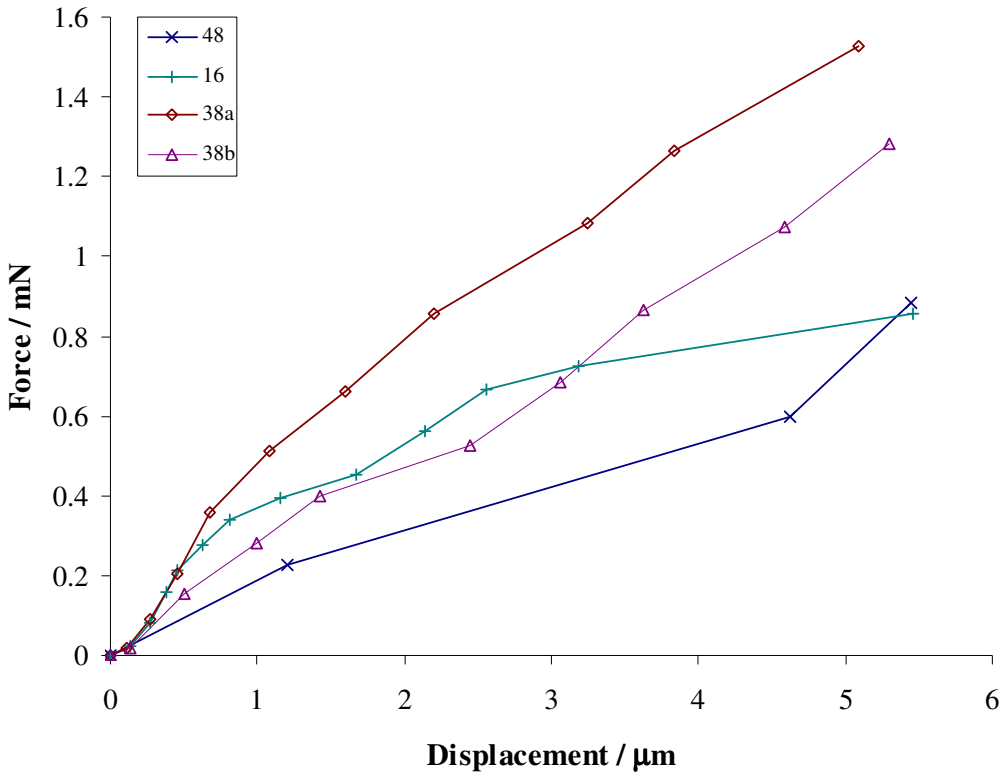

Figure 5.3: A sample of curves from the two batches of microsphere compression tests.

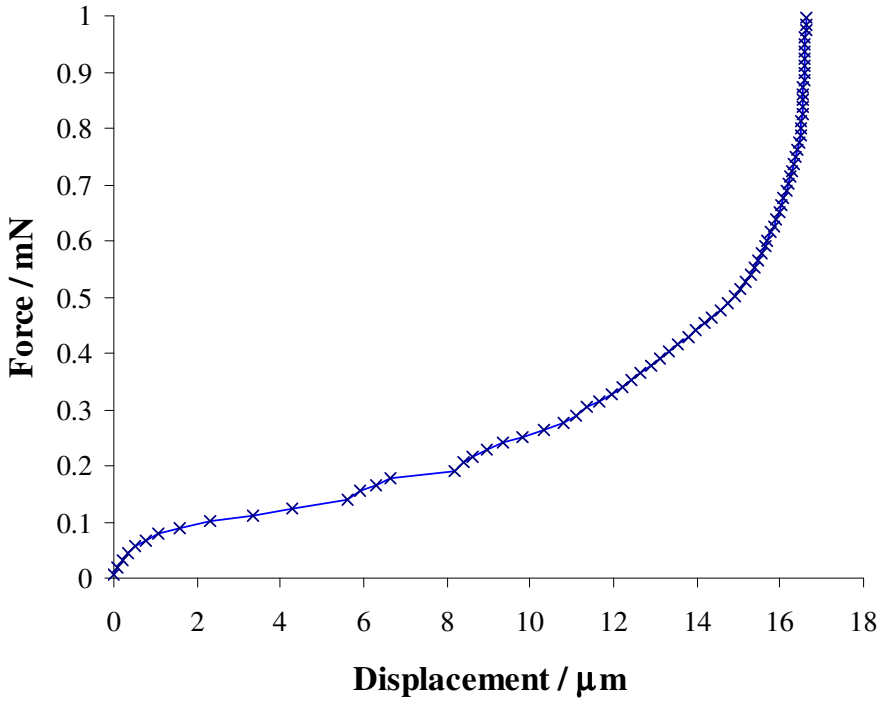

Figure 5.4: A microsphere compression test where the indenter appears to have contacted a second microsphere.

Figure 5.4 shows an example of a curve for a microsphere with a diameter of 28.3 μm, when the deformation of the microsphere reaches approximately 17 μm the force increases rapidly, this is due to the indenter tip coming into contact with a nearby microsphere.

5.2.4 Table tennis ball compression testing procedure

The methods used to obtain the material properties of the table tennis ball and the properties obtained are described in Chapter 3. This section describes the compression tests conducted to observe the physical behaviour of the table tennis ball when compressed uniaxially between two flat surfaces.

A series of compression tests were conducted using table tennis balls manufactured by Stiga, the table tennis balls were sourced in boxes of six, so typically five or six tests were conducted each time. The table tennis balls were measured prior to each test and all were found to be not less than 40 mm and not more than 40.2 mm in diameter.

The International Table Tennis Federation (ITTF) states that;

- 'The ball shall be spherical, with a diameter of 40mm'.
- 'The ball shall weigh 2.7g'.
- 'The ball shall be made of celluloid or similar plastics material and shall be white or orange and matt'.

The compression tests were conducted using an Instron 5584 machine, the crosshead on the machine was screw driven. For each of the tests the table tennis ball was placed on a flat smooth mild steel plate that was approximately 10 mm in thickness. Table tennis balls are manufactured in two halves with a welded seam joining the two parts. The balls were placed so that the seam was horizontal, if the seam was placed vertically it would have had a stiffening effect, with the seam being horizontal the effect is minimised.

A 1 kN load cell was fitted to the crosshead to measure the force. The displacement was measured by the movement of the crosshead. An attachment with a flat surface was fitted to the crosshead load cell to compress the table tennis ball. A test method was established to compress at a continuous rate of 5 mm/min. A schematic of the experimental set-up is shown in Figure 5.5.

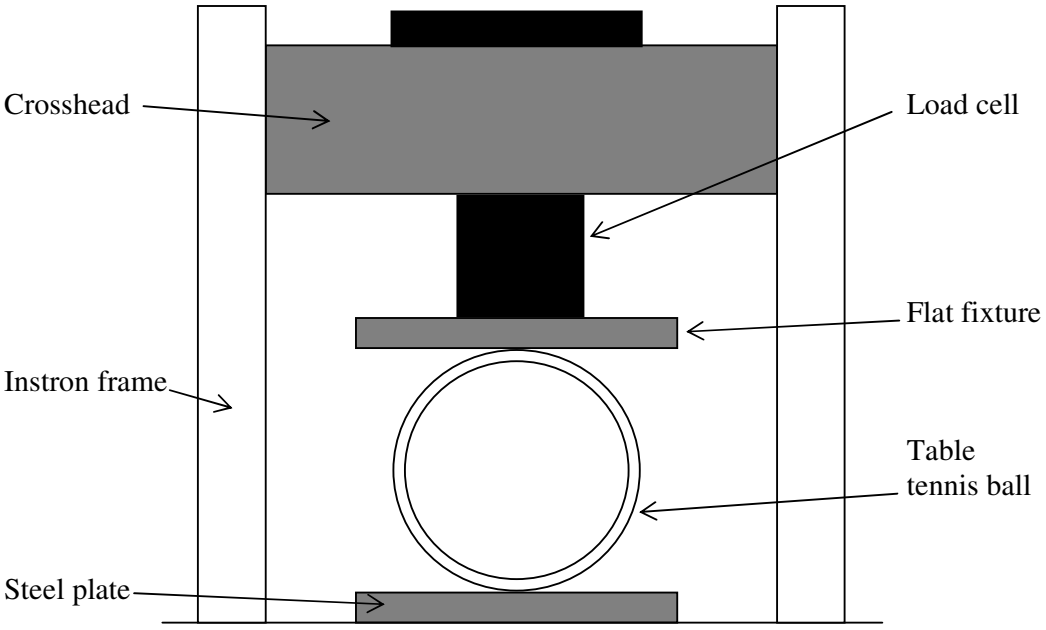

Figure 5.5: A schematic of the experimental set-up used during the table tennis ball compression tests.

An initial test was conducted to a compression of 35 mm, this approached the maximum force limit for the load cell. Subsequent tests were conducted to a maximum displacement of 30 mm. Table tennis balls have a diameter of approximately 40 mm, so the compression by 30 mm is equivalent to a compression of approximately 75 %.

Tests were conducted to see if the air trapped within the table tennis ball made a contribution to the compression stiffness. A small pin hole in the wall of the ball was introduced. The hole was made at a position where it was thought to not have a significant effect on the stiffness of the ball, the hole was therefore made at the bottom of the ball with the seam of the ball held horizontally. Further tests were also conducted with holes positioned halfway between the seam of the ball and the pole, to verify the effect of the position of the hole.

Further tests were also conducted to investigate whether the seam had a reinforcing effect if placed vertically. Table tennis balls manufactured by Dunlop and Donic were also tested and compared to those manufactured by Stiga. Data from each test was collected on the computer attached to the Instron machine with the data imported into Microsoft Excel for analysis.

5.2.5 Table tennis ball compression testing results

Compression tests were conducted to understand the deformation and buckling of table tennis balls and therefore the buckling behaviour that may be exhibited by microspheres and other hollow spheres with similar ratios of thickness to diameter and also with similar mechanical properties.

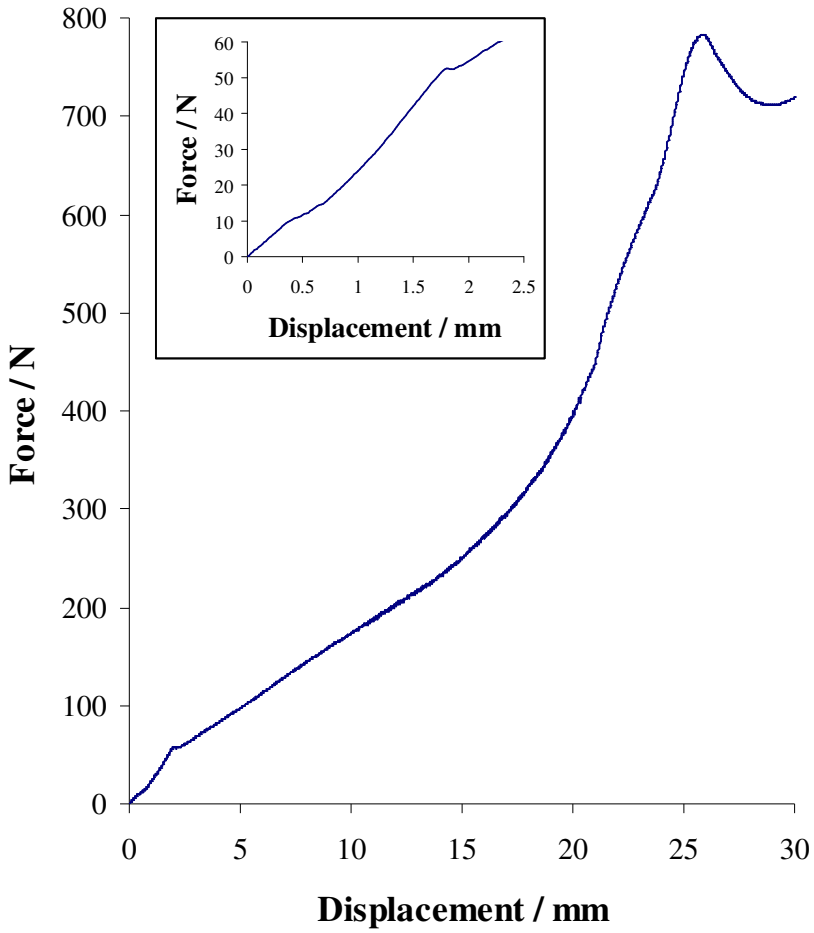

Figure 5.6: A typical curve produced during a table tennis ball compression test.

Force versus displacement graphs were produced using the measured data. Figure 5.6 shows a typical force versus deflection curve produced during a table tennis ball compression test. It can be seen that a small kink occurs in the curve at an approximate displacement of 0.5 mm, as highlighted in the inset graph of the detail at small displacements. Careful observation shows that this is the point where the top and bottom surfaces of the table tennis ball are forced flat by the downward movement of the top rigid plate. A second kink occurs at an approximate displacement of 2 mm, this

is due to the snap-through buckling of the top and bottom surface of the table tennis ball where the flat surfaces invert to produce a bowl profile. This snap-through buckling was anticipated from the preview work by Updike and Kalnins (1972). These two buckling phenomena are also identified by FEA modelling, as shown in Figure 6.4 of an implicit model for the initial compression curve of a table tennis ball, which corresponds to the inset graph in Figure 5.6.

The graph shows an increase in stiffness at a displacement of approximately 20 mm, this is due to self contact of the inverted profiles of the top and bottom surface where they meet inside the table tennis ball. The fluctuations in the curve beyond 25 mm are due to the buckling and folding phenomena that occur as the table tennis ball is crushed at the largest displacement.

Figure 5.7 shows the reproducibility of the table tennis ball compression tests, the initial part of the curve is very similar, but beyond 25 mm there is a difference in the final buckling and hence the folds that are produced on the top and bottom surfaces of the table tennis ball. The folding patterns were similar to those predicted by Pauchard and Rica (1998) and modelled by Cordingley et al (2004).

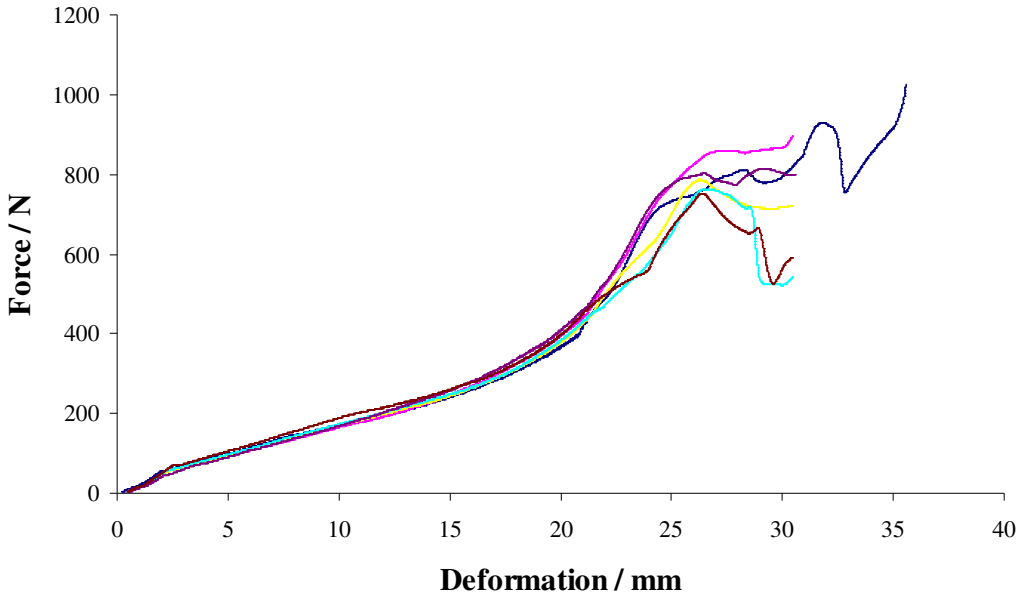

Figure 5.7: Six different table tennis ball compression tests showing similar behaviour.

The experiments conducted for this study produced two type of pattern for table tennis balls, either a four sided square or a five sided polygonal folding pattern. There was no obvious indication as to which pattern would develop during each test. The

distribution appeared random with some table tennis balls having two four sided patterns, others two five sided patterns, whilst others had one of each pattern.

Figure 5.8 shows a range of table tennis balls exhibiting the variety of patterns. It was difficult to observe a change in the number of folds during the tests as the table tennis ball was only visible from the side and not from above or below. The table tennis balls only ever showed four or five fold patterns.

Top

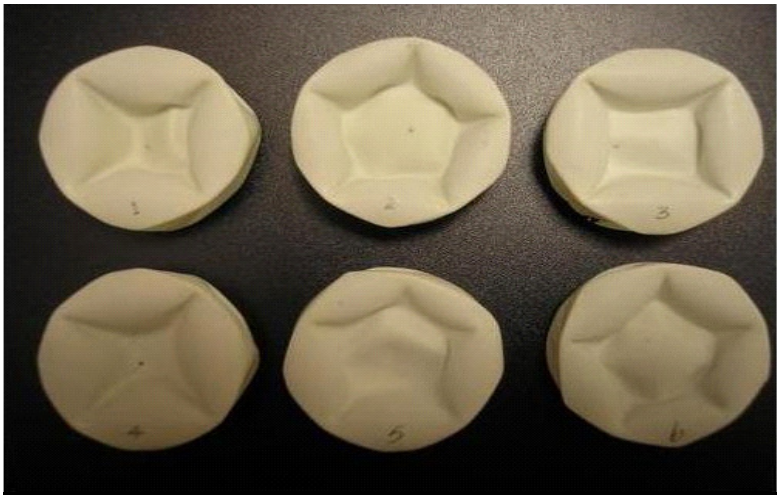

Bottom

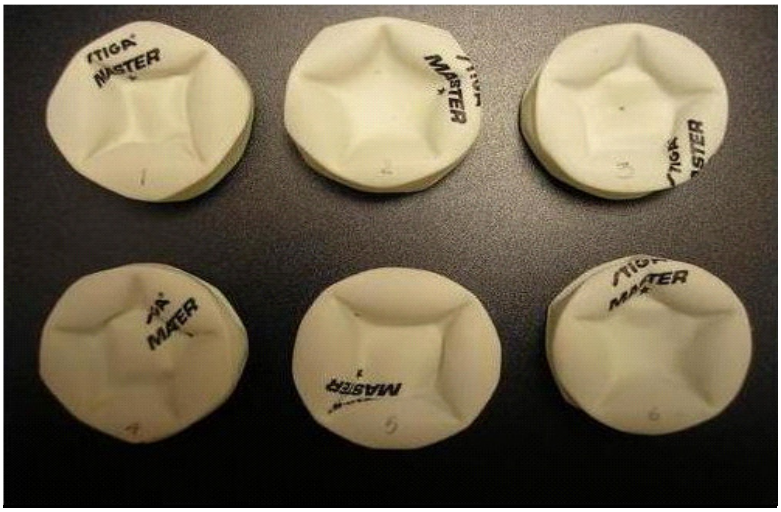

(1). 4 folds on top, 4 folds on the bottom

(2). 5 folds on top, 5 folds on the bottom

(3). 4 folds on top, 5 folds on the bottom

(4). 4 folds on top, 5 folds on the bottom

(5). 5 folds on top, 4 folds on the bottom

(6). 5 folds on top, 5 folds on the bottom

Figure 5.8: A sample of table tennis balls after compression testing, showing a range of fold patterns.

Further table tennis balls were tested, with a small hole introduced through the thickness of their wall to allow any air inside to escape during the compression. For four of the tests the holes were positioned at the bottom of the ball, with the seam placed horizontally. The other two balls had a hole at a position half way between the horizontal seam and the bottom of the ball. The location of the hole did not affect the initial behaviour as shown in Figure 5.9. However the table tennis balls with holes were less stiff as the deformation increased above 10 mm. The table tennis balls without holes also produced a smooth curve, but the table tennis balls with holes produced a shallower, flatter curve up to this clear instability point. Beyond a deformation of approximately 20 mm the stiffness increased as expected, the eventual buckling and folding process was not affected by the table tennis balls having holes, they behaved in a near identical manner to the table tennis balls without holes.

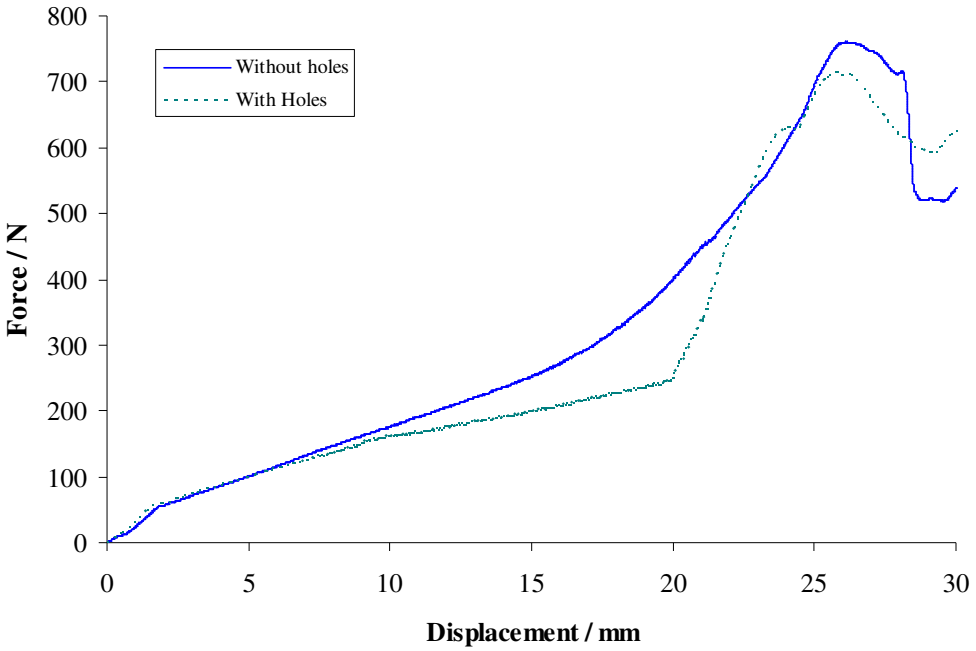

Figure 5.9: Comparison of table tennis ball compression tests, with and without holes in the shell.

Twelve more tests were conducted to examine if the orientation of the seam, that is formed where the two halves of the table tennis ball are welded together during the manufacturing process, has any effect during the tests. The compression tests were performed exactly as before, but with the seam vertical each time. The results are shown in Figure 5.10, where a sample of the tests with the seam vertical is compared to a

sample of the tests where the seam is in the "normal" horizontal position. It can be seen that the vertical orientation of the seam has a small stiffening effect at small displacements and appears to affect the snap through buckling point slightly. There is also an increased stiffening effect when internal self contact occurs at a displacement of approximately 20 mm, but there is little significant difference for most of the curve.

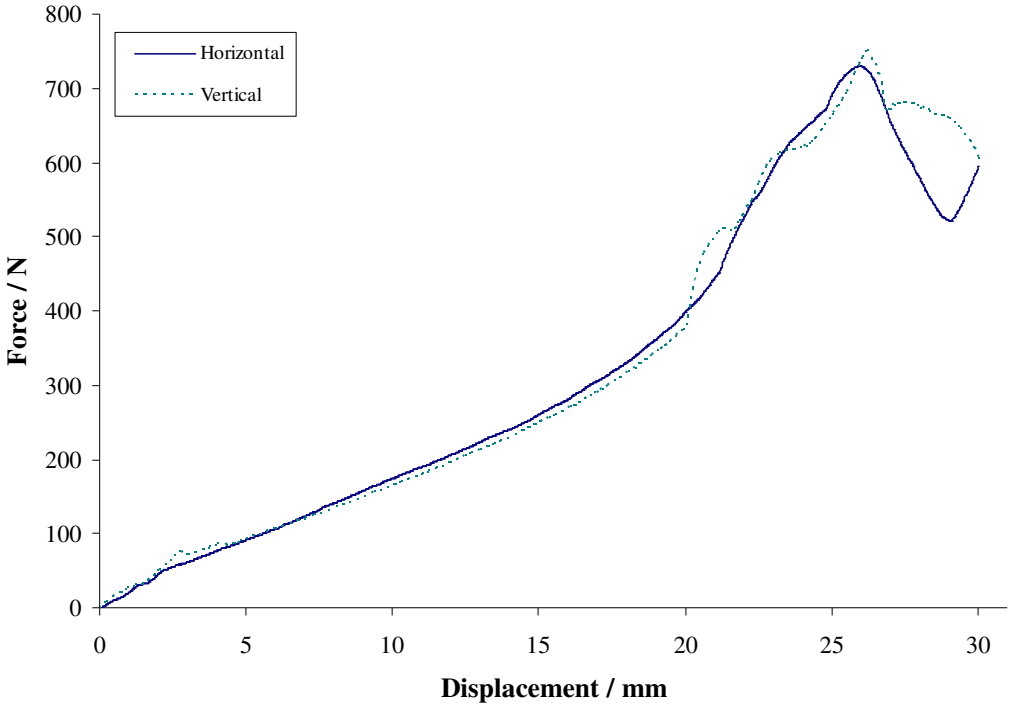

Figure 5.10: Comparison of table tennis ball compression tests, with the seam tested both vertically and horizontally.

5.2.6 Compression tests of other types of ball as a comparison

5.2.6.1 The squash ball

Compression tests on squash balls were conducted using the same test configuration and procedure as for the compression tests of the table tennis balls. The tests were conducted until the limit of the 1 kN load cell was reached, this produced deflections of approximately 32 mm.

The World Squash Federation (WSF) specifications for the standard yellow dot squash ball as used in this study state that the squash ball diameter must be 40.0 mm, + or – 0.5 mm. The weight must be 24.0 g, + or – 1.0g and the initial stiffness 3.2 N/mm, + or – 0.4 N/mm, at 23 °C. The Dunlop Sport yellow dot squash balls used in this study all had a diameter of approximately 40 mm. The wall thickness of the squash

balls was 4 mm. Squash balls are manufactured from an elastomer material, typically natural rubber with some natural and synthetic ingredients added.

Several squash balls were tested, two were standard squash balls and two had holes in their wall to see if the air trapped within the ball made a contribution to the stiffness during compression. The results from the tests are shown in Figure 5.11, where it can be seen that the curves for the balls without a hole and the balls with a hole, produced almost identical results with the air within the balls having a negligible effect on their stiffness.

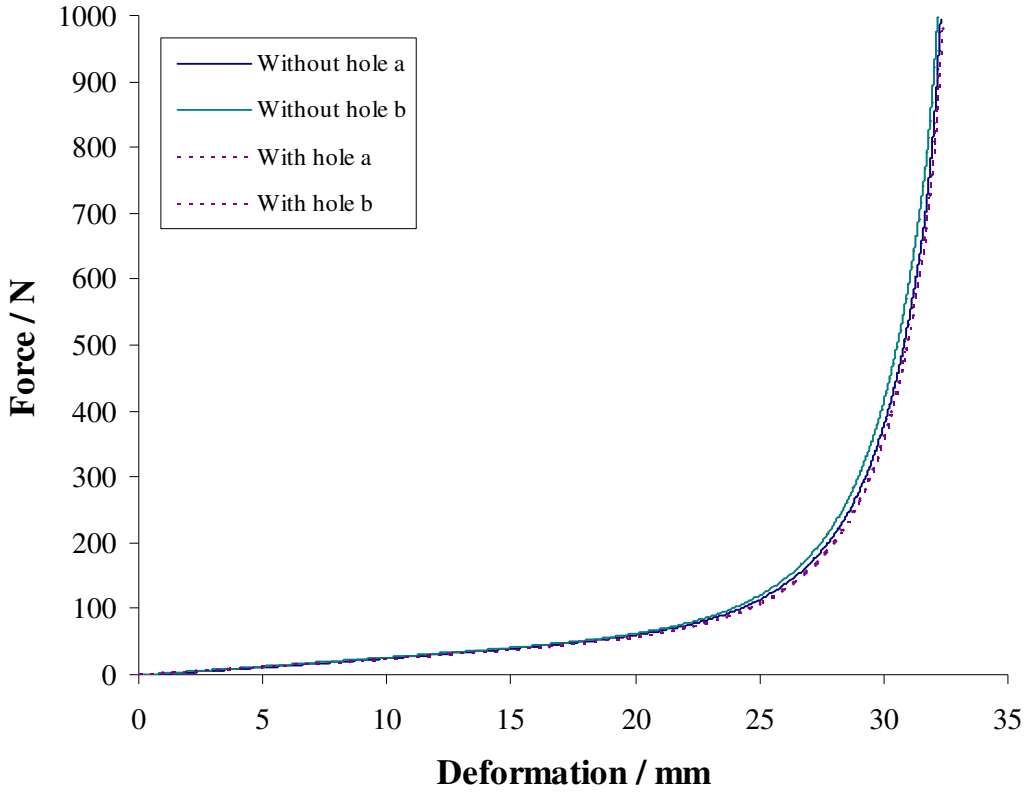

Figure 5.11: A sample of squash ball compression tests, with and without holes in the walls.

The curves produced for the squash balls are very different to that for the table tennis balls, they are much smoother with no obvious kinks due to flattening of the top and bottom surfaces and subsequent snap-through buckling. The maximum compression by approximately 32 mm meant that the squash balls were almost completely compressed flat, during each test. There were no obvious buckling phenomena from the measured stiffness with the squash balls expected to remain symmetrical around a polar

axis. The squash balls were elastic and so returned to their original shape when the crosshead was raised and the compressive load removed.

5.2.6.2 The ball-pool ball

Compression tests were conducted, using ball-pool balls manufactured from polyethylene, in a similar manner to the previous tests, again using a 1 kN load cell. However, in this case a flat clear 5 mm thick Perspex plate was used as the top rigid surface, this enable a video camera to be placed above, with a view through the test machine crosshead, to observe the flattening of the top surface and the buckling and folding that followed.

The ball-pool balls had a larger diameter of about 65 mm compared to the table tennis or squash balls tested previously so they were compressed to a maximum displacement of 55 mm.

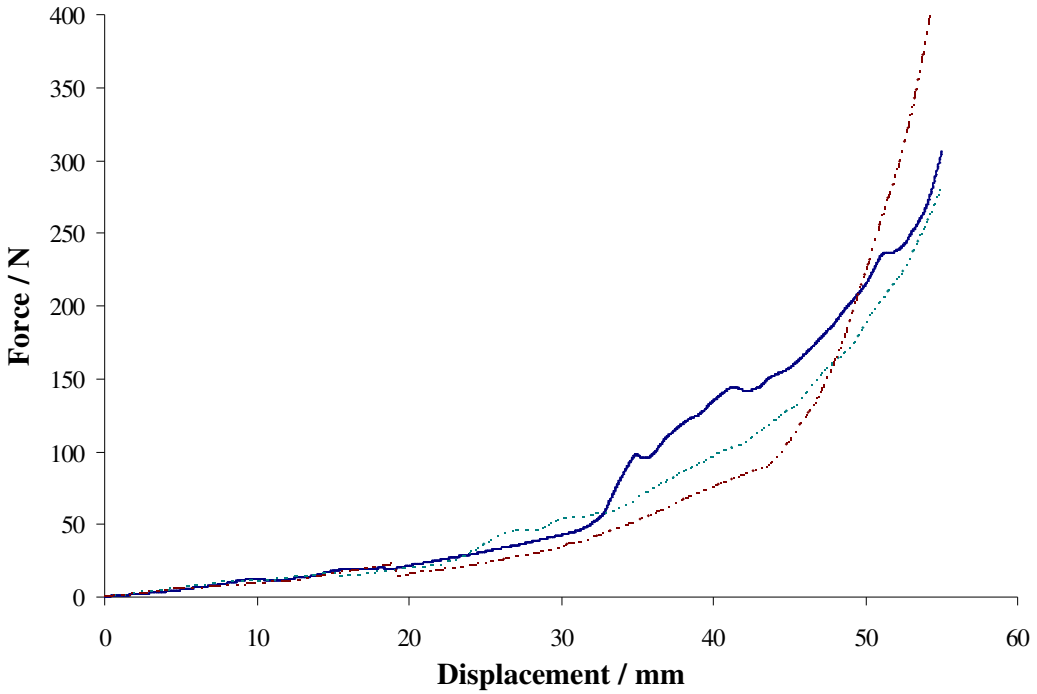

Figure 5.12: A comparison of the three ball-pool ball compression tests.

The ball-pool balls were made from a soft plastic. The balls were slightly over 65 mm in diameter and had a wall thickness that varied slightly in different locations, but which ranged between 0.5 mm and 0.7 mm. The balls were easily compressed by hand and a certain resistance was felt due to the air trapped within the balls, so all of the

balls had a pin hole made at the bottom pole to allow the air inside to escape during compression.

Three balls were tested, the results from the three tests are shown in Figure 5.12. Clearly there is a much broader range of behaviours, probably resulting from the wide range in wall thickness, at larger deflections due to the different buckling phenomena exhibited by the balls.

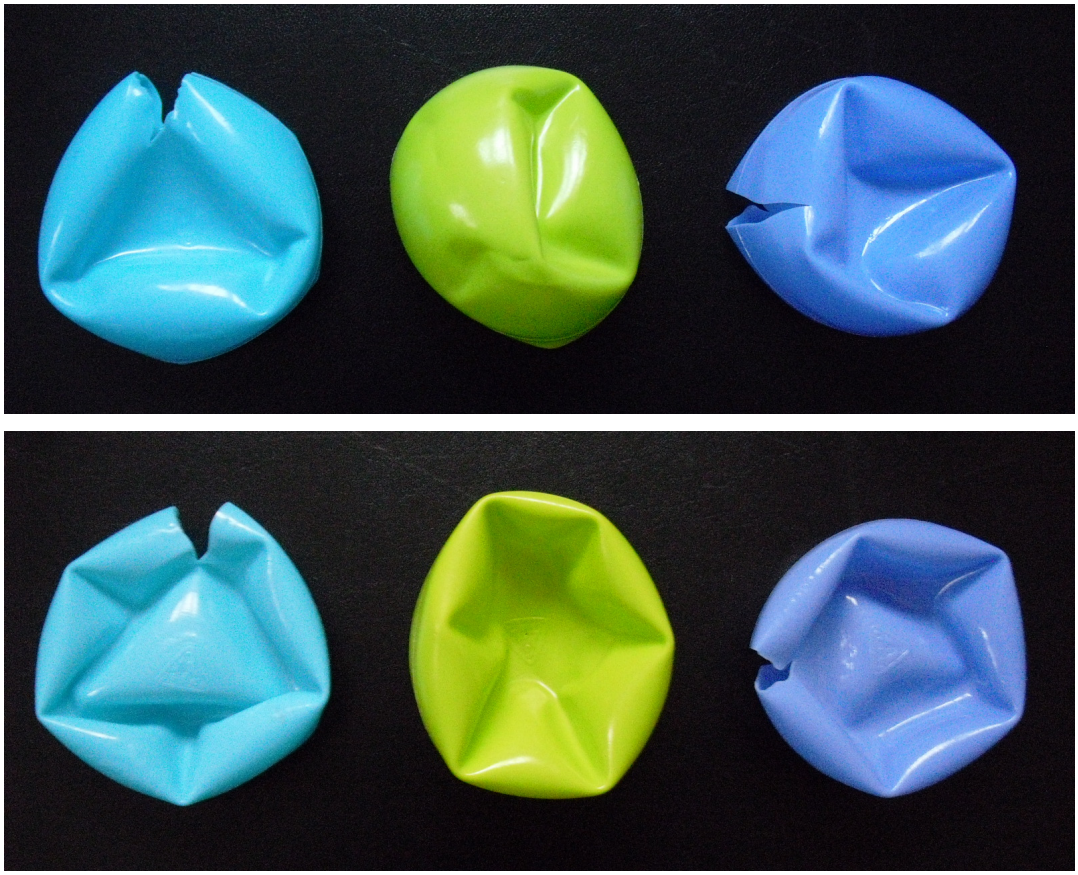

Figure 5.13: A comparison of the top and bottom surface of each ball-pool ball after the compression tests.

There was a much wider range of buckling and folding patterns, when compared to the more carefully manufactured table tennis balls. The ball-pool balls formed patterns with three, four, five and six folds.

During the tests one ball produced a pattern of three fold patterns which transformed into a pattern of four folds as the compression increased. A comparison of the folding patterns is shown in Figure 5.13, the buckling and folding process of two of the balls is shown in Figure 5.14.

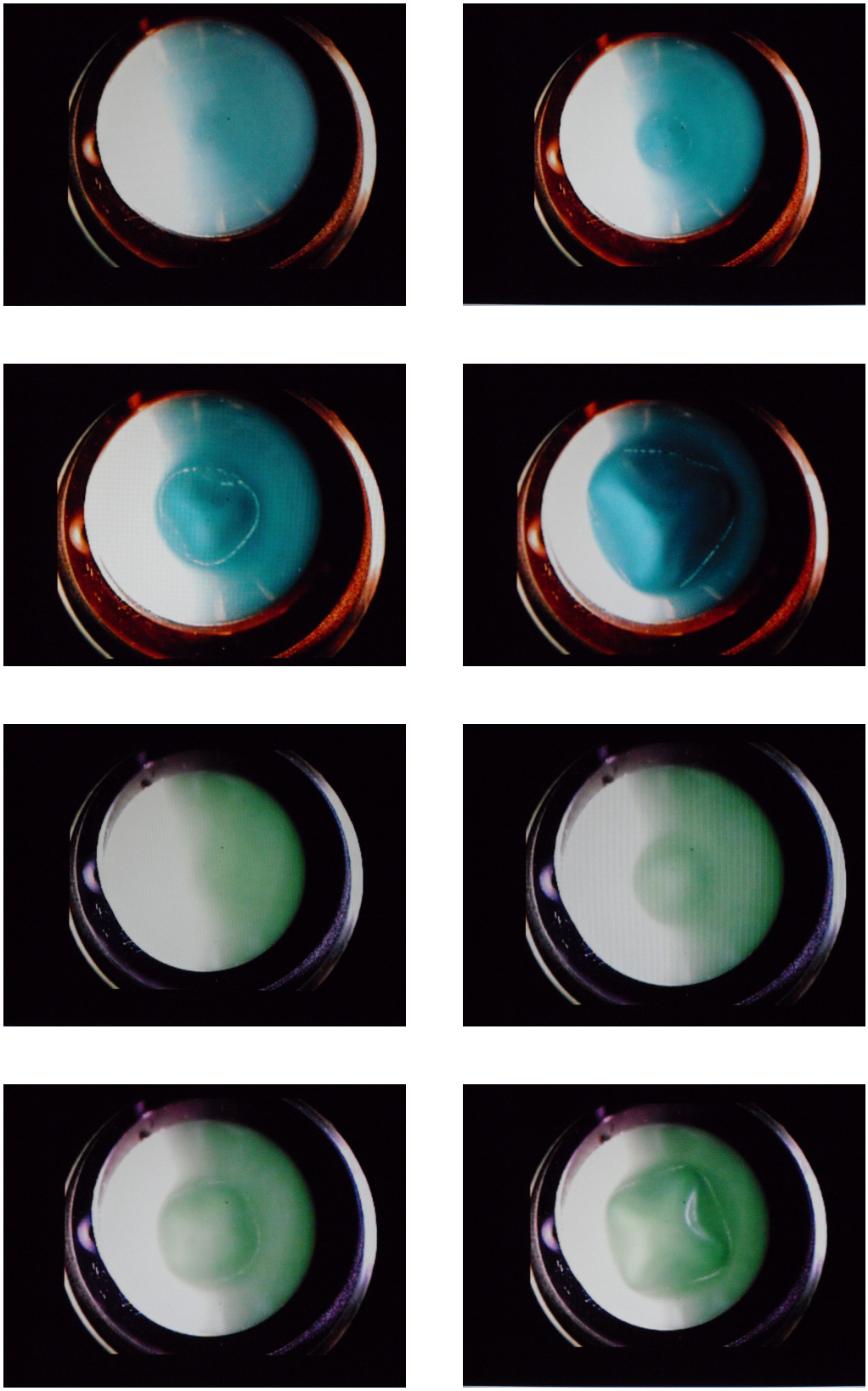

Figure 5.14: A series of images of two of the ball-pool balls during the compression process.

5.2.6.3 The cooling chamber ball

Compression tests of the cooling chamber balls were conducted in an identical manner to the previous tests, with a crosshead speed of 5 mm/min and a 1 kN load cell fitted to the crosshead of the Instron machine. Five balls were tested, these varied in diameter between 19.1 mm and 19.3 mm, the wall thickness of the balls varied between 1.1 mm and 1.3 mm.

The construction of the balls was similar to that of the table tennis balls, where each ball was made from two halves with a thick seam at the join. The diameter at the seam was also approximately 0.2 mm larger. To examine any effect that the seam may have had on the stiffness of the ball under compression three were tested with the seam positioned horizontally and two with the seam oriented vertically.

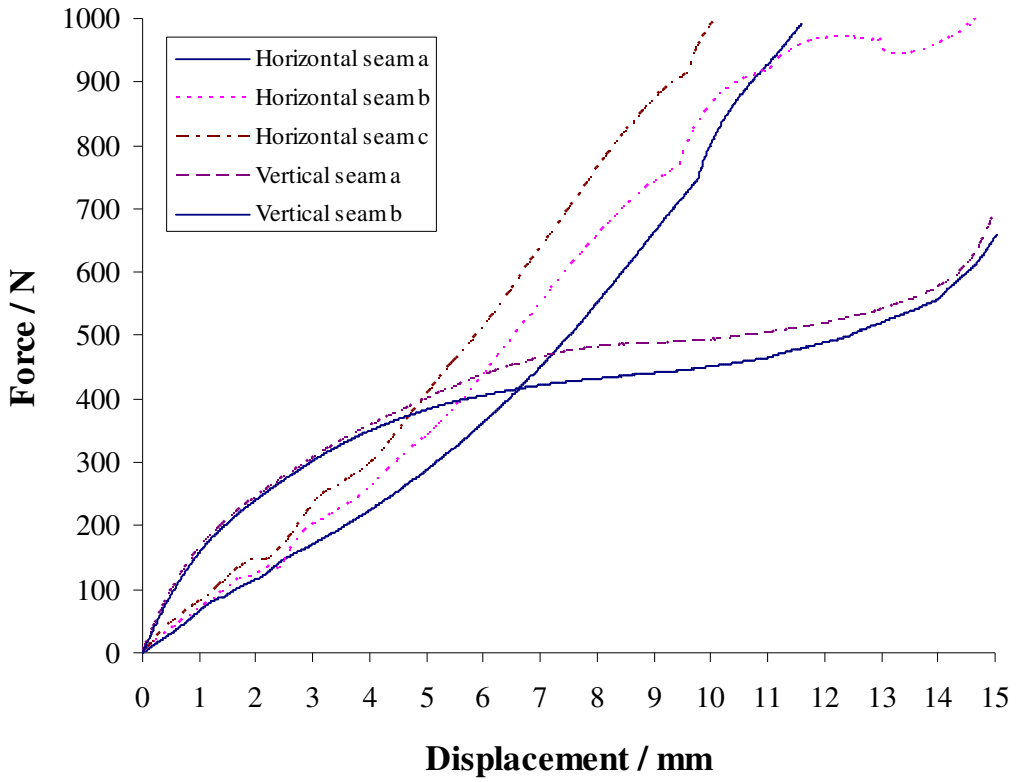

Figure 5.15: Comparison of the cooling chamber ball compression tests, with the seam vertical and horizontal.

The results of the five tests can be seen in Figure 5.15, the first three tests where conducted with the seam horizontal, the final two were conducted with the seam

vertical. The curves produced are very different; the vertical seam produced an initial doubling in stiffness compared to the tests where the seam was horizontal.

The initial displacement of the first test is shown in Figure 5.16, the curve shows the same characteristics as the initial curve for the table tennis balls, including a kink, which indicates a similar snap-through buckling to that seen for the table tennis balls.

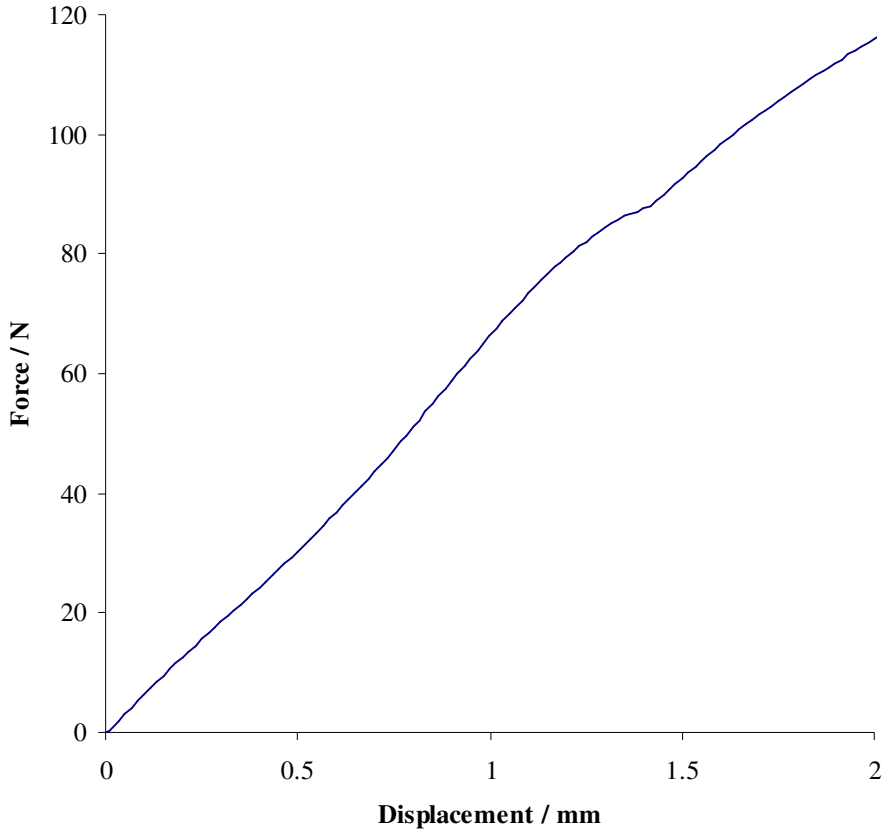

Figure 5.16: The initial displacement of the first cooling ball compression test.

The balls with the horizontal seam produced an annulus form when compressed, as can be seen in Figure 5.17, the two balls with the vertical seam folded along their equators and produced a rugby ball shape as can also be seen in Figure 5.17. This would explain the latter's greater initial stiffness and subsequently lower stiffness at higher displacement.

Figure 5.17: The cooling chamber balls after the compression tests (top views above, side views below).

5.2.7 A comparison of the various hollow spheres tested

The table tennis balls, the microspheres and the cooling chamber balls all behaved in a similar manner for deflections up to approximately 50 %. The initial deflection is very similar with a kink indicating a snap-through buckling at the same position in the curve at an approximate deflection of about 5 % of the diameter. This behaviour is compared in Figure 5.18 for a table tennis ball and a microsphere with a similar geometry.

The ball-pool balls were not manufactured in a sufficiently consistent manner to be compared to the other hollow spheres, but did produce a larger range of fold patterns.

The squash balls produced completely different results compared to the other hollow spheres tested as they were rubbery in nature and had a much larger wall thickness.

Both the table tennis balls and the cooling chamber balls were stiffer when the seam produced during manufacture was placed vertically, when compared to tests that were conducted with the seam positioned horizontally.

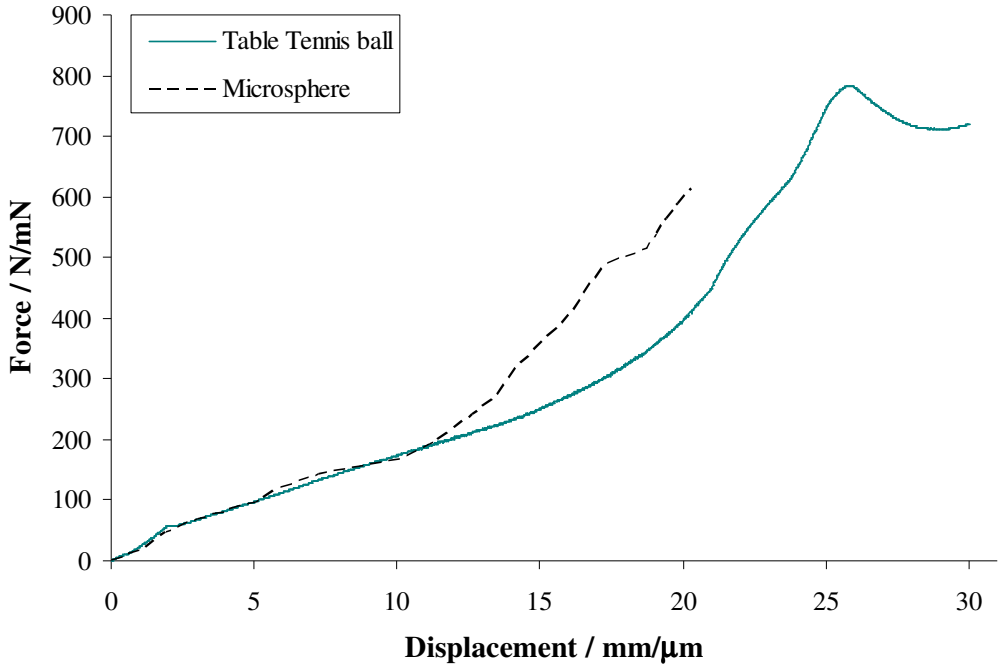

Figure 5.18: A comparison of the initial deformation of a table tennis ball and microsphere during compression tests.

5.2.8 The mechanical behaviour of hollow plastic spheres

The mechanical behaviour of hollow plastic spheres has been investigated, firstly by conducting physical tests of microspheres under uniaxial compression, then at a larger scale using table tennis balls as a model to better understand the behaviour.

By performing loading and unloading cycles on a microsphere it was seen that each loading cycle did not follow the previous loading cycle. This indicated that there was some yielding in the post buckled state which meant that the microspheres exhibit hysteresis and / or plastic yielding behaviour.

A typical force versus deflection curve for a compression test of a table tennis ball showed a small kink at an approximate displacement of 0.5 mm. This is the point where the top and bottom surfaces of the table tennis ball are forced flat by the downward movement of the top rigid plate. A second kink occurred at an approximate displacement of 2 mm due to the snap-through buckling, where the flat top and bottom surfaces inverted to produce a bowl profile, the snap-through buckling was anticipated by Updike and Kalnins (1972). There was then an increase in stiffness at a displacement of approximately 20 mm due to self contact of the inverted profiles meeting inside the table tennis ball. Beyond 25 mm displacement there were buckling and folding

phenomena as the table tennis ball was crushed further. The folding patterns produced were similar to those predicted by Pauchard and Rica (1998). Two types of folding pattern were produced during the table tennis ball tests, either four or five sided, with no obvious indication as to which pattern would develop during each test, some table tennis balls had two four sided patterns, some had two five sided patterns and others had one of each pattern.

The ball-pool balls were made from a soft plastic, they were larger than the table tennis balls with a diameter of slightly over 65 mm and their wall thickness varied between 0.5 mm and 0.7 mm. Results from uniaxial compression tests showed a much wider range of buckling and folding patterns compared to the more carefully manufactured table tennis balls, probably due to the variation in wall thickness. The ball-pool balls formed patterns with three, four, five and six folds. During the one test a ball-pool ball was seen to produce a pattern with three fold that transformed into a pattern of four folds as it was compressed further.

At the initial deflection of 5 % of the diameter the table tennis balls and microspheres both produced a very similar kink at the same position in the curve, which indicated a snap-through buckling, beyond this the deflections up to 50 % were also very similar.

The following Chapter describes the use of FEA software to simulate the behaviour of hollow spheres under uniaxial compression. The table tennis balls and microspheres are modelled, the latter with a range of ratios of wall thickness to diameter.

Chapter 6 Modelling the mechanical behaviour of the hollow plastic sphere

6.1 Finite Element Analysis (FEA) Modelling

6.1.1 Introduction

The aim of using Abaqus FEA software in this study was to model the behaviour of hollow plastic spheres in order to understand and predict the mechanical behaviour of micro spheres.

Table tennis balls were used as a physical model and these were also initially modelled in order to provide confidence in the FEA models of the microsphere, due to their similar ratio of diameter to wall thickness and material behaviour when compared to the microspheres. If the FEA models of the table tennis balls accurately replicates the behaviour seen in the physical tests it is reasonable to suspect that the microsphere behaviour should be accurately modelled as well. The mechanical properties of the table tennis ball and how they were measured is described in Chapter 3. The table tennis ball properties were more readily obtained and are therefore more accurate than those measured for the material in the microsphere shell. For this reason the table tennis ball is modelled extensively first. The finite element models require mechanical properties including the Young's modulus, Poisson's ratio as well as some measure of the yielding and plasticity behaviour.

A series of models were developed throughout this study, many to ensure that attributes of the actual models themselves did not affect the results obtained. Simple axisymmetric models were produced, as were 3-Dimensional models, a number of types of element have also been modelled including solid continuum elements, shell elements and membrane elements, implicit "standard" models and explicit models have also been produced. Models with purely elastic behaviour were modelled as were those with more complex plastic and elastic behaviour. Different modelling techniques were tried including using the Riks algorithm to try and model buckling instabilities using an implicit modelling approach and mass scaling to speed up modelling using explicit dynamics. Other effects that were modelled included an investigation on the rate of displacement and the effect of friction between the sphere and the flat compressing surfaces. Effects of various mesh densities and numbers of elements through the wall

thickness of the model were also been examined. Finally hollow spheres were also modelled with a range of wall thicknesses and a range of diameters as well as for a range of mechanical properties including materials with different values for Young's modulus, Poisson's ratio and yield strength. The significant table tennis ball and microsphere models developed throughout the study and the relevant results are described in the following sections.

6.1.2 Implicit models

The initial models were based upon the geometry of the table tennis ball, with an external diameter of 40 mm and a wall thickness of 0.4 mm. The initial models to predict the behaviour of a microsphere when compressed were "standard" or implicit axisymmetric models, these were produced as a two-dimensional half cross section of a table tennis ball wall which can then be revolved in the post processing to show a half dome geometry. An example of an axisymmetric model is shown in Figure 6.1.

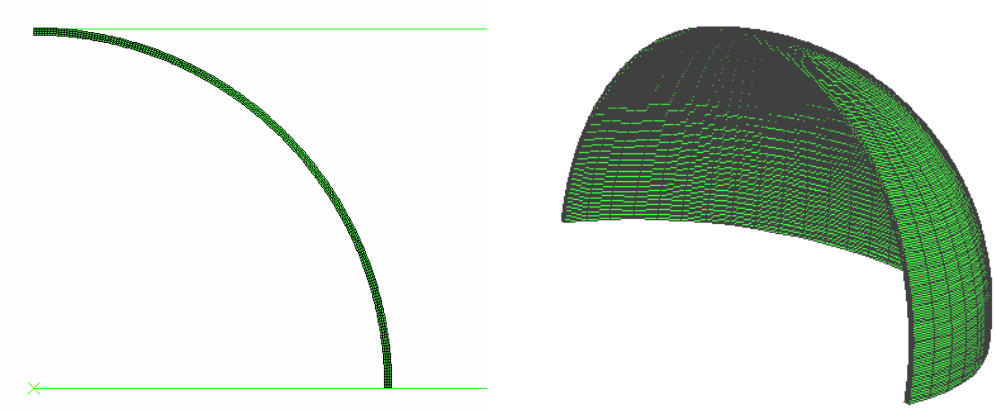

a. b.

Figure 6.1: Axisymmetrical model showing the two analytical rigid surfaces (a) and revolved in the post processing by 180 degrees to show a half dome geometry (b).

Initial "trial" models only had one or two elements through the wall thickness, later models were developed with more elements through the thickness. To replicate the rigid platens used in the experimental set up, the models also incorporated a rigid analytical surface to provide the correct form of contact during compression. A second rigid analytical body at the horizontal half symmetry line of the sphere was also used to represent the correct type of deformations that would arise if an internal self contact was created at large displacements.

Figure 6.2 shows the model from the previous figure under a large displacement and rotated through 180°, the coloured contours indicate principal stresses, with red denoting the highest stress through to dark blue denoting the lowest. The bottom analytical rigid surface is stationary, but the top analytical rigid surface has been made to move vertically downward in the –Y direction, this has caused the top surface of the sphere to buckle, as was observed during the compression tests of the table tennis balls. The initial models used an implicit modelling approach which allowed the model to progress to a point whereby large deformations could be seen, however it could not allow the sphere to be compressed sufficiently to produce the buckling and subsequent folded patterns observed experimentally on the table tennis balls.

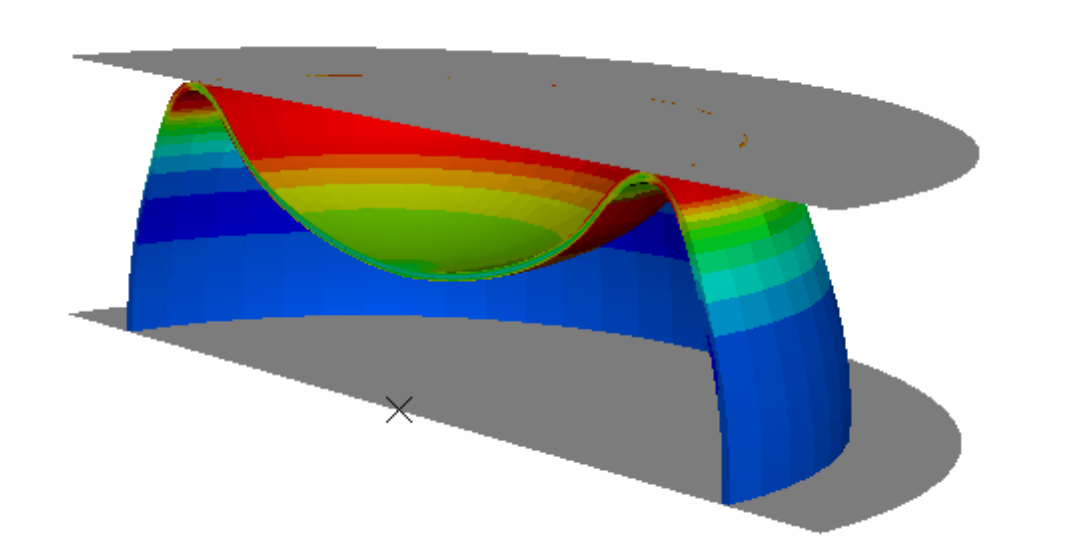

Figure 6.2: Image of an implicit model with rigid bodies applying contact, with deformation of the top surface, where the contours represent engineering stress.

Later models were developed using an explicit modelling approach which proved more effective at modelling the buckling of the table tennis balls at higher deformations. One clear point about using an axisymmetric model was that the resulting predicted deformation was artificially constrained to only deform in a symmetric manner. Clearly in the earlier experimental section it was seen that this was not actually the case at the largest deformations as complicated folding patterns are formed in the post buckled configurations.

Several further models were developed to examine the elastic, buckling and post buckling behaviour of the table tennis balls. These models are compared to the experimental behaviour, both from the point of view of the deformation patterns formed

as well as from a comparison between the force versus deflection results. The force versus displacement of the axisymmetric table tennis ball model, modelled using an implicit method and including a simple plastic yielding contribution is shown in Figure 6.3, which also shows the same model including the Riks algorithm.

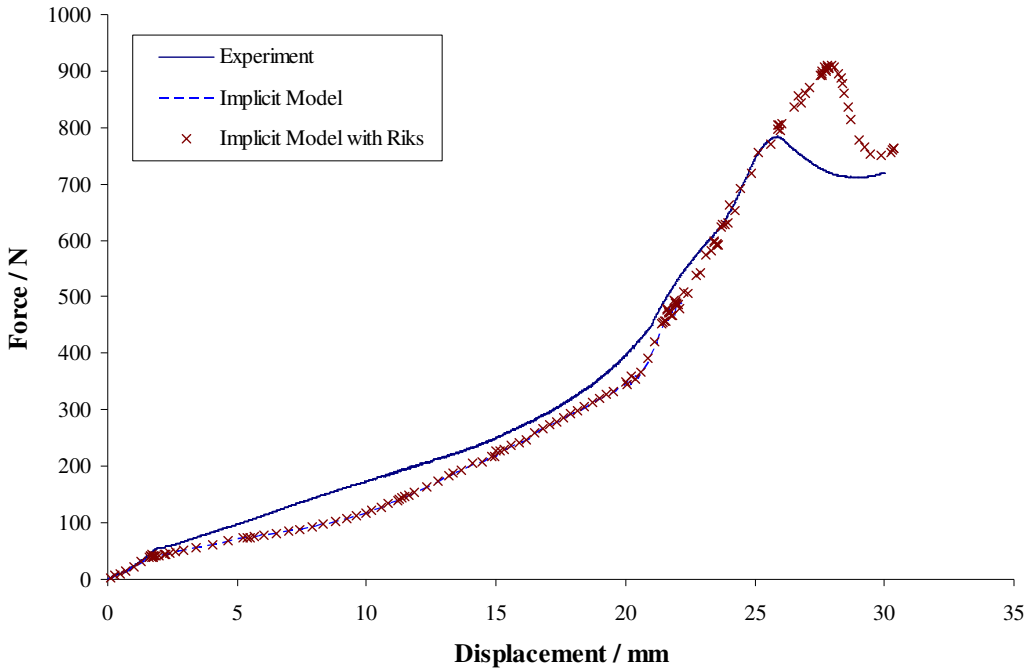

Figure 6.3: A comparison of an axisymmetric implicit table tennis ball model in compression that includes elastic and plastic yielding behaviour, the same model including the Riks algorithm and the experimental results taken from a measure of the force versus displacement behaviour.

The table tennis ball test shows a slight kink in the curve at approximately 0.5 mm, this is the point where the top and bottom surfaces of the ball are forced flat by the rigid plates, although the model does not show a significant deviation in the curve at this point. The second kink in the curve at approximately 2 mm is the snap through buckling, where the flattened surfaces are inverted into a concave curve that forms a bowl on the top and bottom surface of the table tennis ball, the slope of the graph changes slightly at this point where the stiffness decreases slightly. A large increase in stiffness is then shown on the graph above 20 mm displacement, this is due to the internal self-contact occurring when the top and bottom surfaces meet inside the table tennis ball, this is also predicted reasonably accurately by the model although the force up to and beyond this point is slightly under predicted. The peak and drop observed in

the experiment at approximately 25 mm deformation is due to the buckling and folding phenomenon that occurs as the table tennis ball becomes highly compressed. The implicit model that was used to initially represent this problem was unable to develop the significant buckling behaviour experienced in practice.

There is an improvement to the model with the introduction of the Riks algorithm (Riks, 1972) which allows solutions to be developed beyond a buckling instability using the implicit finite element modelling approach. At the higher deformations there is more realistic representation of the various buckling and folding modes. However, the model still under predicts the behaviour of the table tennis ball at lower deformations and conversely the forces required to perform the buckling and folding are over predicted.

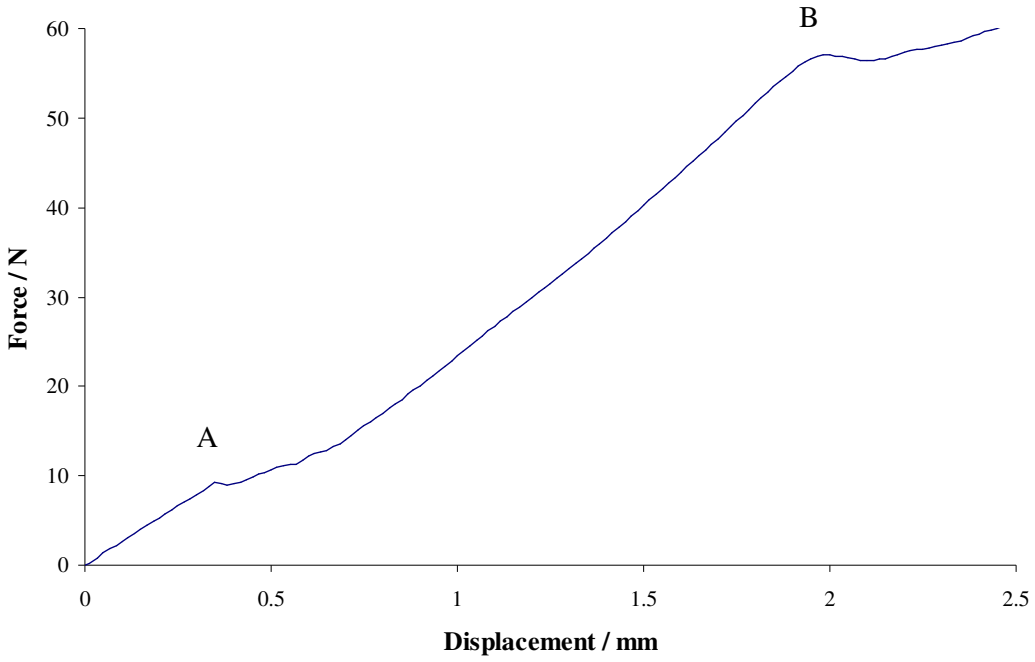

Figure 6.4: The two kinks in the curve from the implicit model of the table tennis ball, firstly the flattening of the top and bottom surfaces (A) and secondly the snap through buckling (B).

Figure 6.4 shows the initial slight kink at a displacement of approximately 0.5 mm from the table tennis ball test where the top and bottom surfaces of the ball are forced flat by the rigid plates.

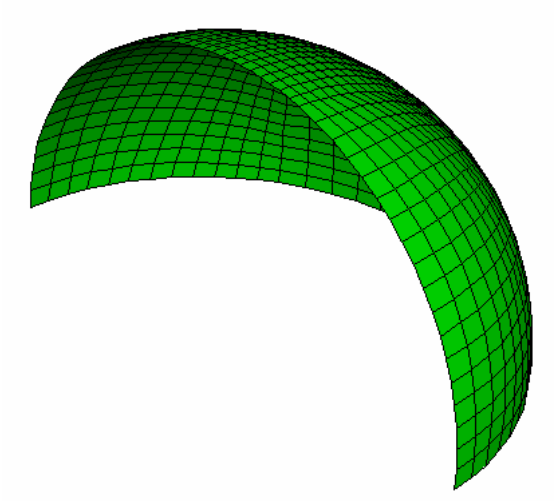

Figure 6.5: The initial geometry of the three dimensional half dome shell model.

After the initial implicit axisymmetric models appeared to show a reasonable fit between the model and the real measured data, it was thought that a series of three dimensional models might produce more accurate predictions as any out of plane deformations could be modelled. The artificial constraint of using an axisymmetric model forced any non-symmetric deformations not to arise and this might result in higher stiffness predictions from the models.

A half dome shell element implicit model was produced with a specified thickness of 0.4 mm. This model also under predicted the experimental behaviour of the table tennis ball and buckled in an unusual manner. The initial geometry of the three dimensional half dome shell model is shown in Figure 6.5.

Later three dimensional models were produced as a vertical half sphere with the axis of symmetry through the vertical axis. These models also included rigid analytical bodies to provide the compression in the same manner as the physical test. This type of model can also provide an accurate representation of the internal self contact and the buckling and folding phenomena. Implicit and then explicit models were produced.

A half sphere implicit solid model with 3 elements through the thickness and 800 elements in total was produced. This model greatly under predicted the stiffness and did not reach a deformation sufficient to achieve self contact. A more refined three dimensional implicit solid model with four elements through the thickness was developed; this had a total of 4800 elements.

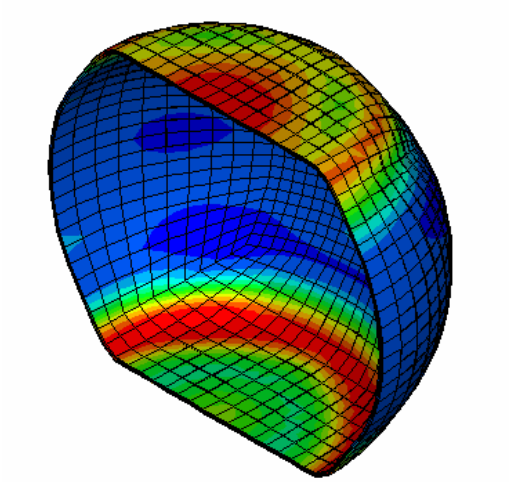

Figure 6.6: An initial low mesh density three dimensional half sphere model that failed to achieve a characteristic snap-through buckling.

However, as can be seen in Figure 6.6, the mesh was initially too coarse and the model did not perform a snap through buckling. An identical explicit model was produced, but with a finer mesh, as shown in Figure 6.7, this had 19,200 elements in total rather than the previous 4,800 elements and allowed the snap through buckling to occur, this is shown later in Figure 6.11.

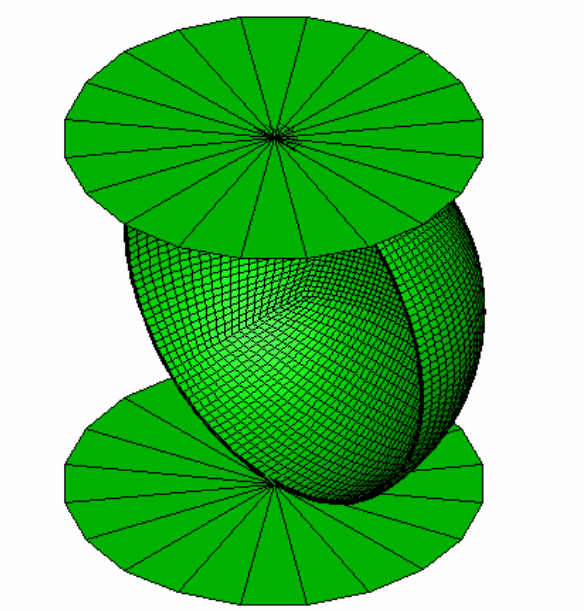

Figure 6.7: Three dimensional model of half a table tennis ball, with analytical rigid bodies for contact.

6.1.3 Explicit models

To see if the buckling behaviour could be more accurately modelled an explicit axisymmetric modelling approach using an identical geometric and materials model was solved and compared to the Riks implicit finite element model described earlier. Figure 6.8 compares the predictions of both models with the results from the physical test. Explicit models are ideally suited to high speed impacts and inertia problems and are also able to model buckling more readily than when using an implicit modelling approach; however, the results for the table tennis ball compression correlate with the measured behaviour less satisfactory when initially compared to the implicit model. The explicit model under predicts the stiffness to a greater extent than the implicit model and has extensive scatter in the data points that are possibly caused by additional inertia effects in the model which produce an irregularity to the curve, particularly at lower deformations. However, the buckling and folding phenomena at larger compressions beyond internal self contact are more accurately predicted, compared to the implicit model.

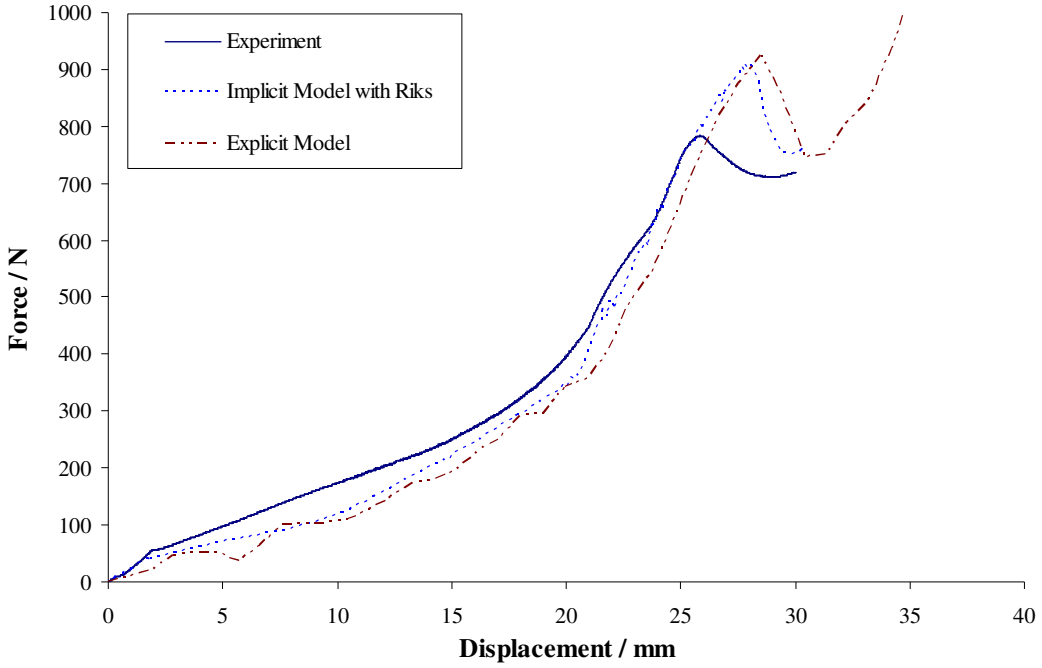

Figure 6.8: A comparison of the improved implicit model, an equivalent explicit model and a physical test result.

The next refinement was to make a half dome model using solid brick elements with a finer mesh and with at least four elements through the wall thickness. The model

was run as an explicit analysis, this allowed the model to deform more completely beyond any buckling instability. It was seen to fold into a pattern that very accurately reflected the pattern produced by the table tennis balls during the experiments. The model is show in Figure 6.9, where it is compared to the deformation of the table tennis ball after a compression test. The table tennis ball from the test appears slightly more rounded, this is due to spring back exhibited due to the elasticity of the material and possibly the small amount of air contained within the ball.

a.

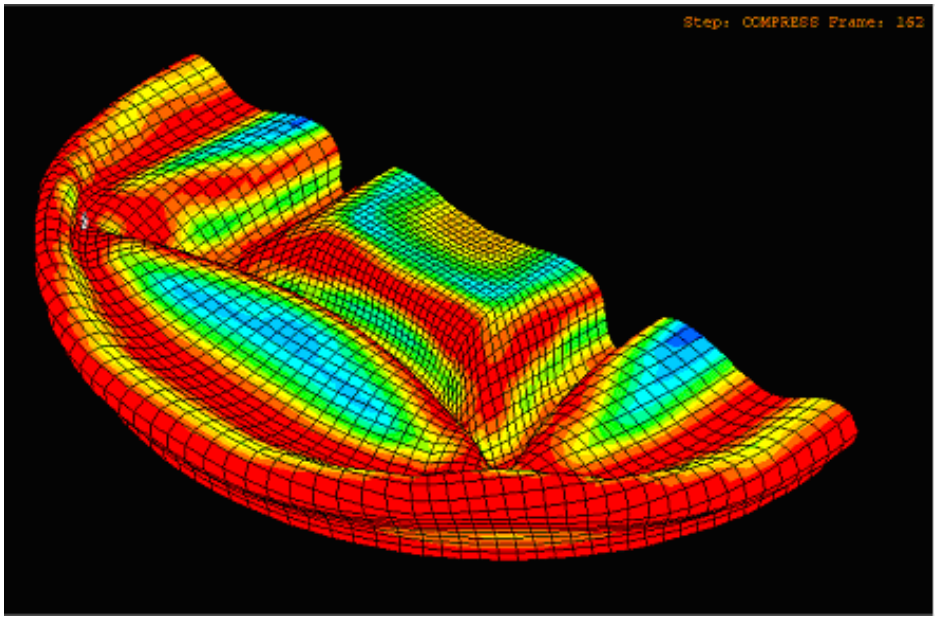

b.

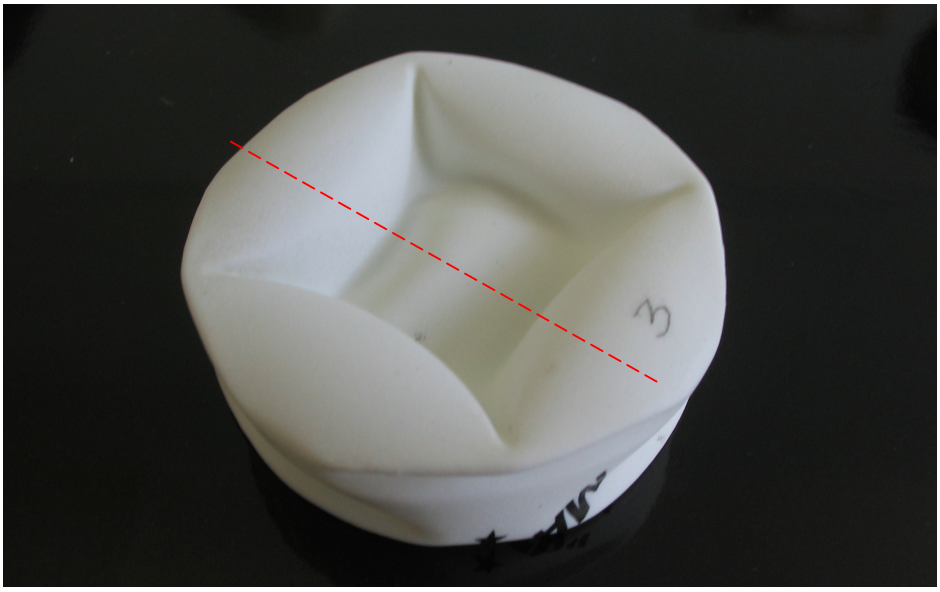

Figure 6.9: Explicit three dimensional half dome model of a table tennis ball (a), compared to a table tennis ball after a compression experiment (b).

Figure 6.10 demonstrates the inability of the initial three dimensional explicit model to accurately predict the full stiffness behaviour throughout the analysis.

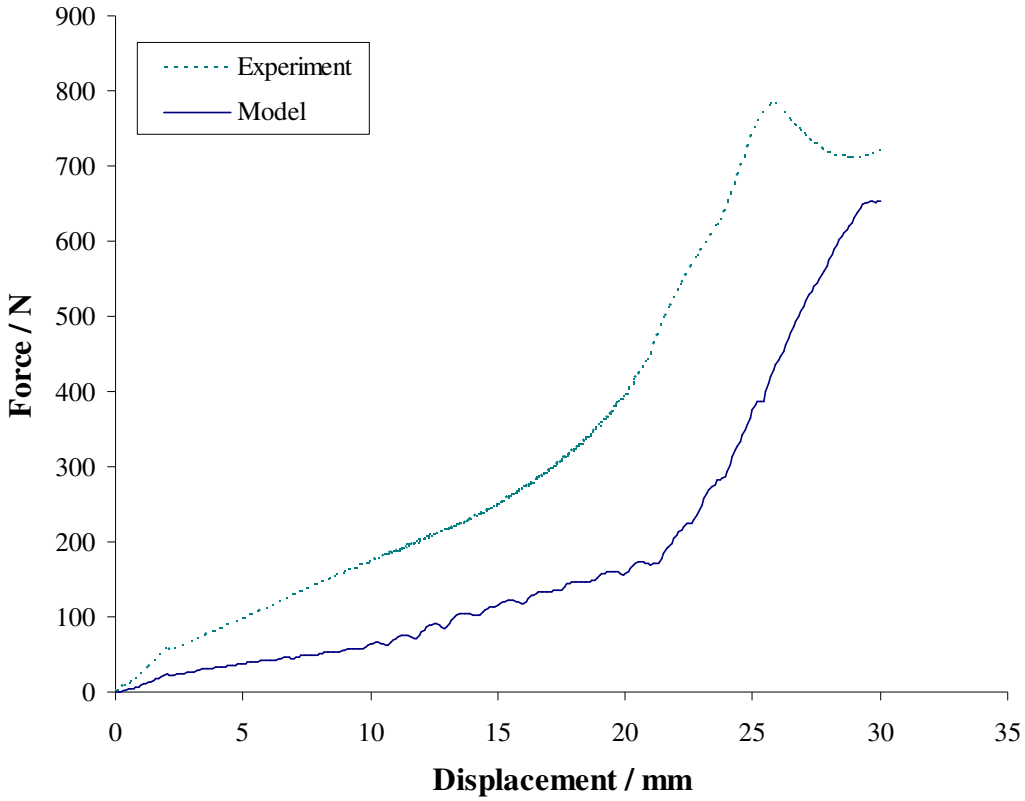

Figure 6.10: A comparison of the initial three dimensional solid brick element explicit model and the results from a compression test of a table tennis ball.

The more refined three dimensional model exhibited realistic behaviour and produced a much smoother initial curve than previous explicit models but, as can be seen in Figure 6.11, the predicted behaviour of this more complex model is very similar to the behaviour of the simpler revolved axisymmetric model, at lower deformations around the initial snap-through buckling region, which again fails to form a converged solution shortly beyond self contact at higher deformations. The explicit three dimensional model is shown for the four key stages of the hollow sphere deformation, firstly the flattening of the top and bottom surfaces, then the snap through buckling, followed by self contact and then the final folding and buckling of the sphere.

Because the axisymmetric models of the table tennis ball were simpler to develop and produced near identical behaviour at lower deformations compared to the

more complex three dimensional models, they were used to examine the effects of varying the model parameters including; mesh density, element geometry, material properties, run time, friction and plasticity.

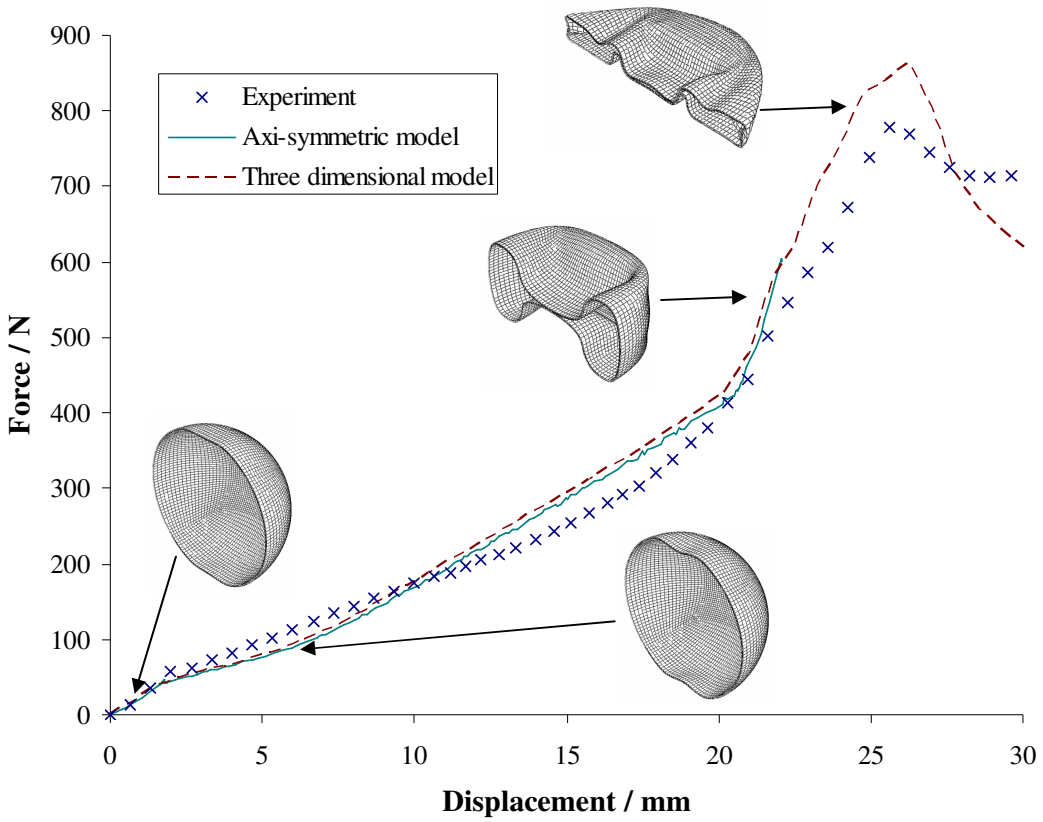

Figure 6.11: The final axisymmetric and three dimensional models compared to the experimental results for the compression of a table tennis ball, with images of the three dimensional model showing the four key stages of deformation.

6.1.4 An examination of the effect of mesh densities and element geometry used in the models

Axisymmetric models and three dimensional models were produced to examine the effect of the mesh density. This used the standard three dimensional half sphere model with four elements through the thickness as indicated in Figure 6.12. The figure also shows two other mesh densities, one with extra elements through the thickness of the sphere wall, eight instead of four, which creates elements that are further from the ideal cube shape. The lower diagram shows eight elements through the thickness, plus

extra elements around the circumference (c) of the sphere to ensure that the elements are of a better shape to produce more reliable results.

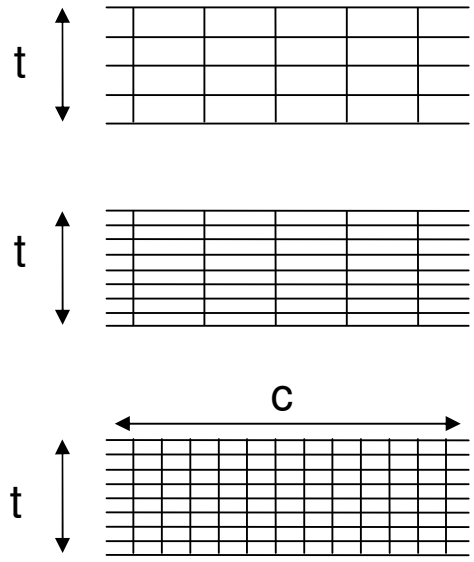

Figure 6.12: A comparison of mesh density and shape for a three dimensional half sphere model.

Figure 6.13, shows the results from the models with the different mesh densities. The doubling of the number of elements through the thickness increased the stiffness and the model no longer predicted the correct snap through when compared to experimental observations. It appears that the poor element geometry is over constraining the model. The model with extra elements both through the thickness and around the circumference was very similar up until the point of buckling, which was observed to occur at a slightly smaller displacement. This model however required a very significant solution time.

A range of mesh densities and element geometries were used for the axisymmetric model. These models were much less mesh sensitive than the full three dimensional model and four elements through the thickness was clearly sufficient together with reasonably square element geometries to ensure that at least up to and just beyond the point of the initial buckling that the models performed reliably.

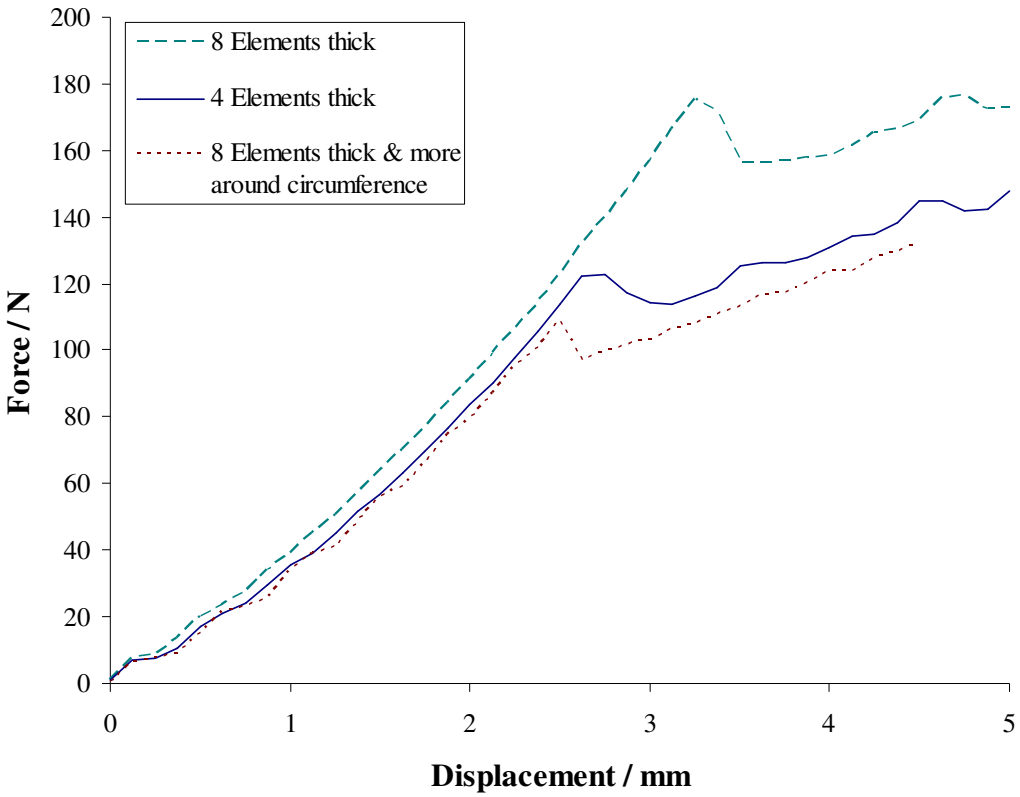

Figure 6.13: A comparison of results for three dimensional half sphere models with a range of mesh densities.

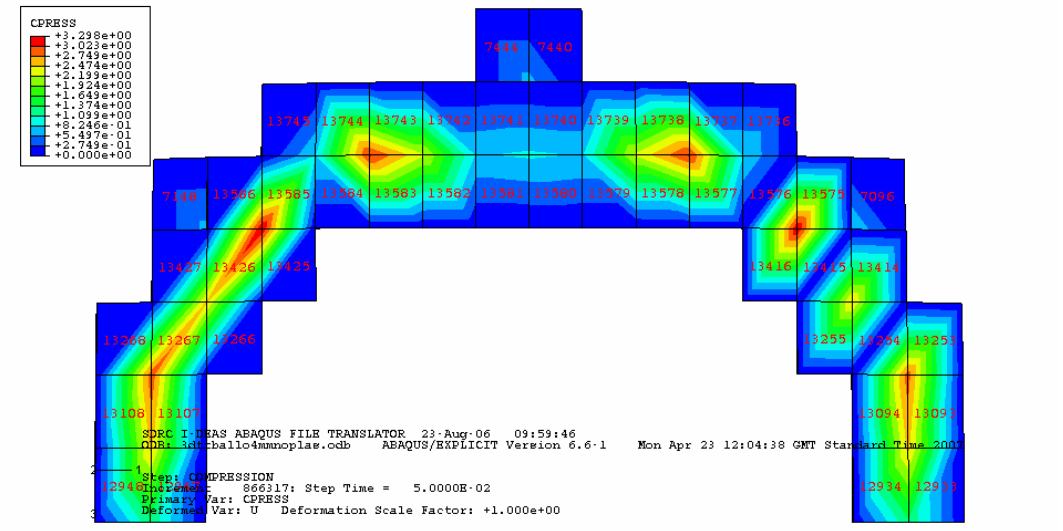

Figure 6.14: Nodes in contact with the top rigid compression surface for a 40 mm diameter hollow sphere after a 2.5 mm displacement.

Insight into why the full three dimensional models might be mesh sensitive can be considered by examining Figure 6.14 which shows the pressure profile of the top contact surface for this type of model. It is evident that the nodes at the element corners are able to come into contact with the rigid top surface (or bottom surface) and conversely they can also drop out of contact with the surface.

Clearly the number of elements in contact with the surface has to be above a minimum threshold to ensure that the observed behavior is continuous and not too discretised. If not then the model will not model the stiffness behaviour in a smooth manner and this is the most likely cause of non-smooth curves produced for force / displacement for the models.

Having completed a large number of axisymmetric models of the table tennis ball and microsphere, where only the actual values for force and dimension are different and so are scaleable, a model of this type was chosen for the analysis described later in this chapter. This was also due to its relative simplicity compared to three dimensional solid models and for its reliability at producing results that are most comparable to the experimental results.

6.1.5 An examination of methods for decreasing the run time for the models

Due to the relative complexity of these explicit dynamics models, including the relatively long time scales that are modeled using a relatively large numbers of elements in each model and the limited processing power available, two different techniques were examined to try and reduce the model solution times.

Firstly the time increment was altered for the same table tennis ball model to run ten times faster and a hundred times faster, this was then compared to the “normal” speed for the model. The time increment of 0.1 seconds was used for the “normal” models, this was altered to 0.01 and 0.001 seconds for the ten times and a hundred times faster models respectively.

The results of these three models are shown in Figure 6.15, the models were conducted to a displacement of 5 mm to capture the snap through buckling point and a section of the curve immediately after this point. The curves for each of the three models are identical. This shows that we are still solving an elastic problem without introducing any significant contributions from inertia.

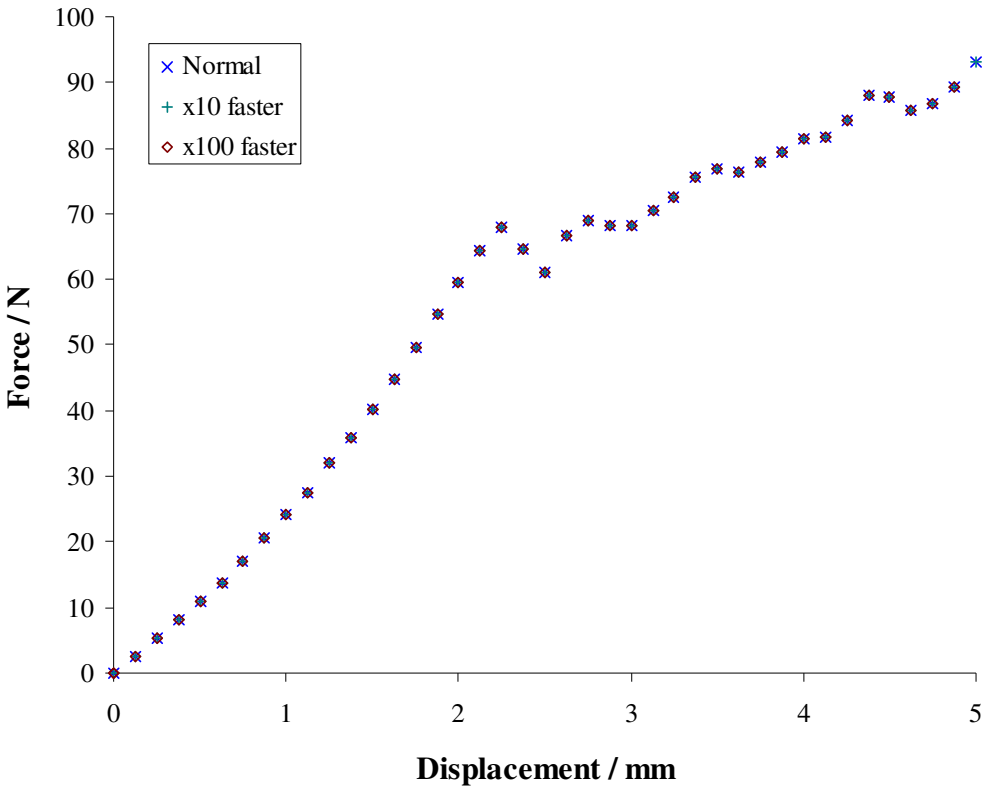

Figure 6.15: The table tennis ball model run at 10x and 100x the normal loading rate compared to the "normal" model.

A second set of table tennis ball models was run this time with mass scaling introduced to speed up the solution time by altering the wave speed in the model by altering the density of the sphere material. This was altered by a factor of 10 and a factor of 100. The predictions produced can be seen in Figure 6.16, they are initially similar, but the snap through buckling point varies. An increase in the scaling factor increases both the displacement and the force of the snap through buckling.

From these two sets of models it was deduced that for models with this geometry and similar material properties, running the models with a faster time increment was an option, but mass scaling was likely to have produced incorrect results. By using a faster time increment the solution time for the models was reduced from approximately eight hours to approximately two hours.

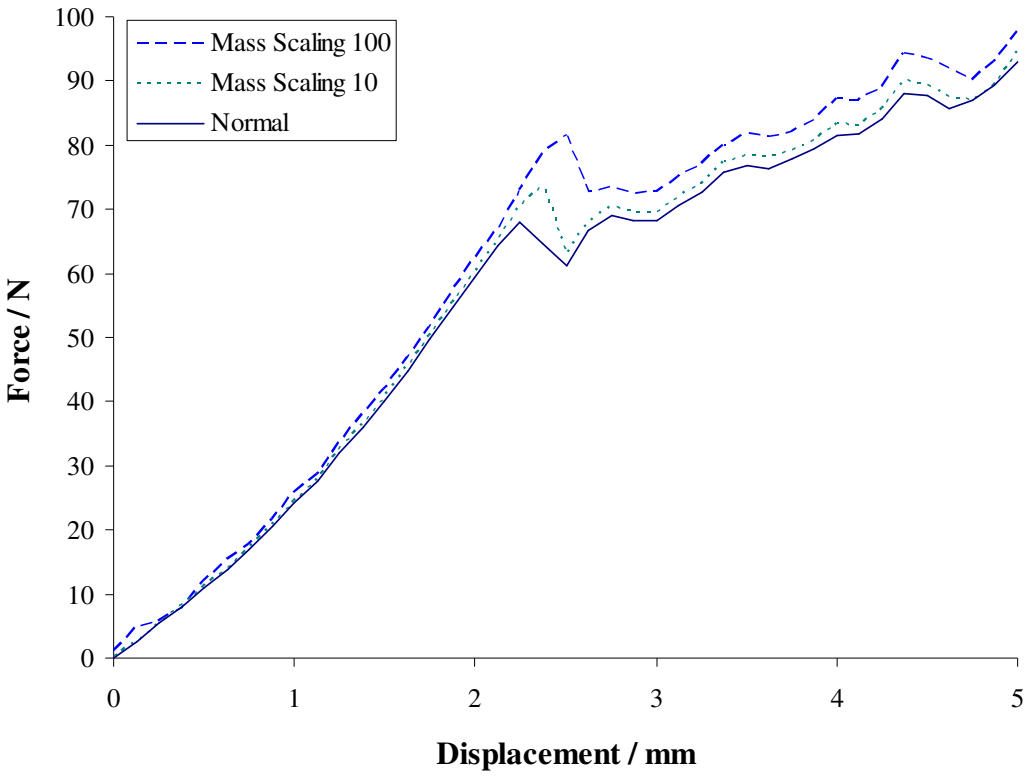

Figure 6.16: The table tennis ball model run at two increased mass scaling factors compared to the "normal" model.

6.1.6 An examination of varying material properties using axisymmetric models

The initial behaviour of the table tennis ball or microsphere was of particular interest for this study as the force at the point of the snap through buckling behaviour should provide an indication of the wall thickness of the hollow sphere. Therefore a series of axisymmetric models with a variety of materials properties were produced to examine how the initial snap through buckling behaviour at approximately 2 mm in the table tennis balls depends upon the material properties. These models and others were used to gain a good understanding of these particular instabilities and their development and general findings are described here.

A series of comparisons of various sphere properties were made, these were for Young's modulus, Yield Strength and Poisson's ratio, to see if the properties had an effect upon the stiffness and snap through buckling point. The results of these comparisons are shown in the following three graphs. The predicted benchmark value

for Young's modulus was 2.2 GPa for the table tennis ball material, the value for Poisson's ratio was 0.3 and the Yield strength was 50 MPa.

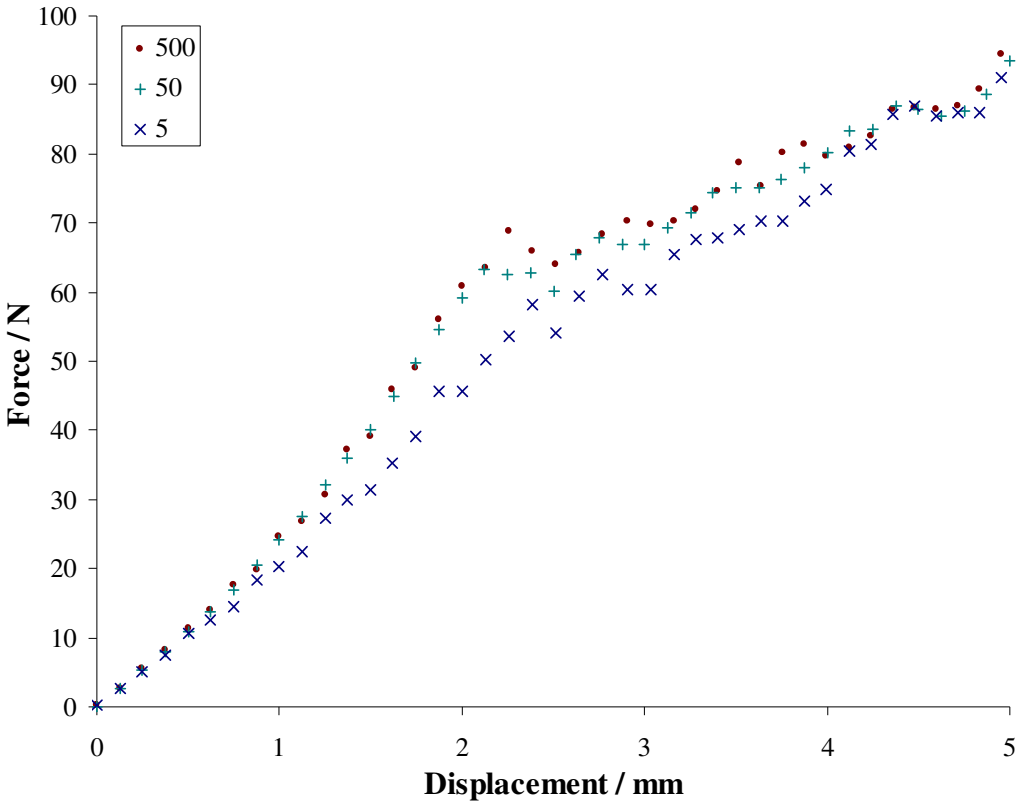

Figure 6.17: The axisymmetric explicit table tennis ball model with a range of Yield Strength as indicated in the legend in MPa.

Figure 6.17 compares the Yield strength, with the benchmark value of 50 MPa being altered by a factor of ten, both higher and lower. This has little effect upon the deformation at which the snap through buckling point occurs, but it does slightly affect the force at which the buckling point occurs, as would be expected. The 5 MPa model also appears slightly less stiff. An examination of the stress values in the model showed that they are always far below the Yield strength threshold of 50 MPa.

The modulus was altered over a range of moduli from 1 GPa to 20 GPa, as shown in Figure 6.18. The stiffness can be seen to increase with modulus, as expected. The snap through buckling point is indistinct, but it appears to occur at slightly higher deformations as the modulus increases, from approximately 2.1 mm when the modulus is 1 GPa to approximately 2.5 mm for a modulus of 20 GPa, as indicated by the solid line.

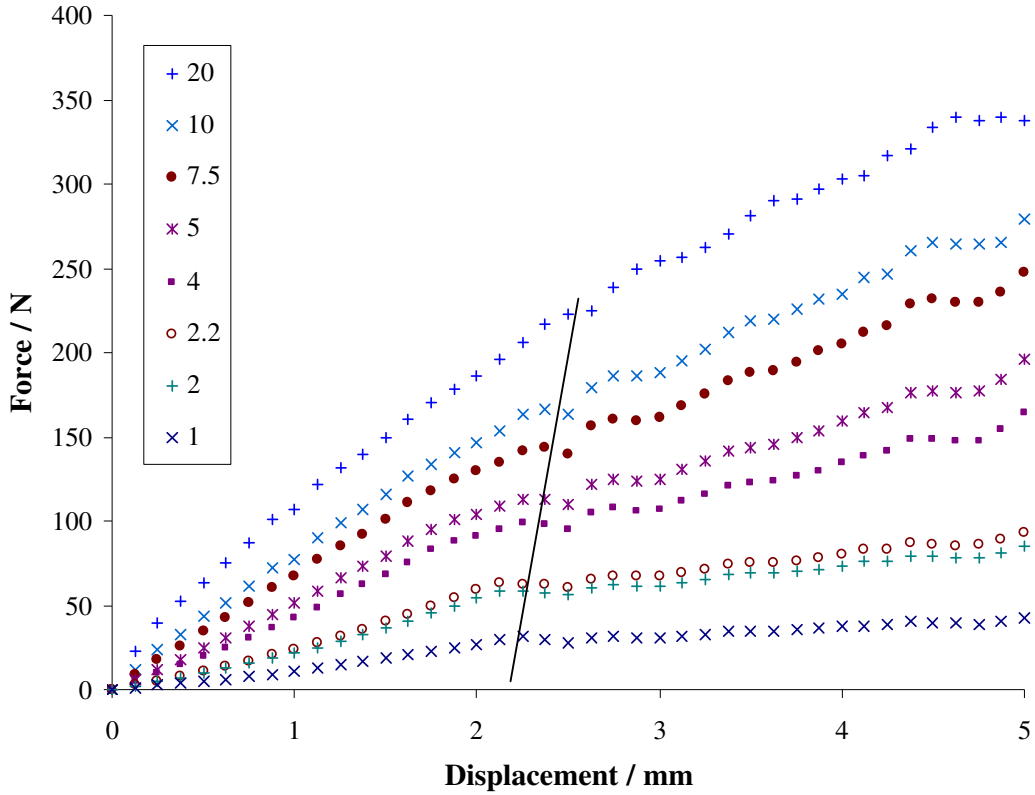

Figure 6.18: The axisymmetric explicit table tennis ball geometry with a range of Young's modulus values as indicated in the legend in GPa.

The final comparison figure, Figure 6.19, shows a range of Poisson's ratio, with 0.3 as the benchmark value, there is little difference between the curves up to the snap through buckling point, a very low Poisson's ratio of just 0.1 or even 0.0 increases the force at buckling slightly, the effect of Poisson's ratio on the snap through buckling appears very modest though as all the other curves are very similar pre-buckling and there is just limited scatter in the results beyond the snap through buckling.

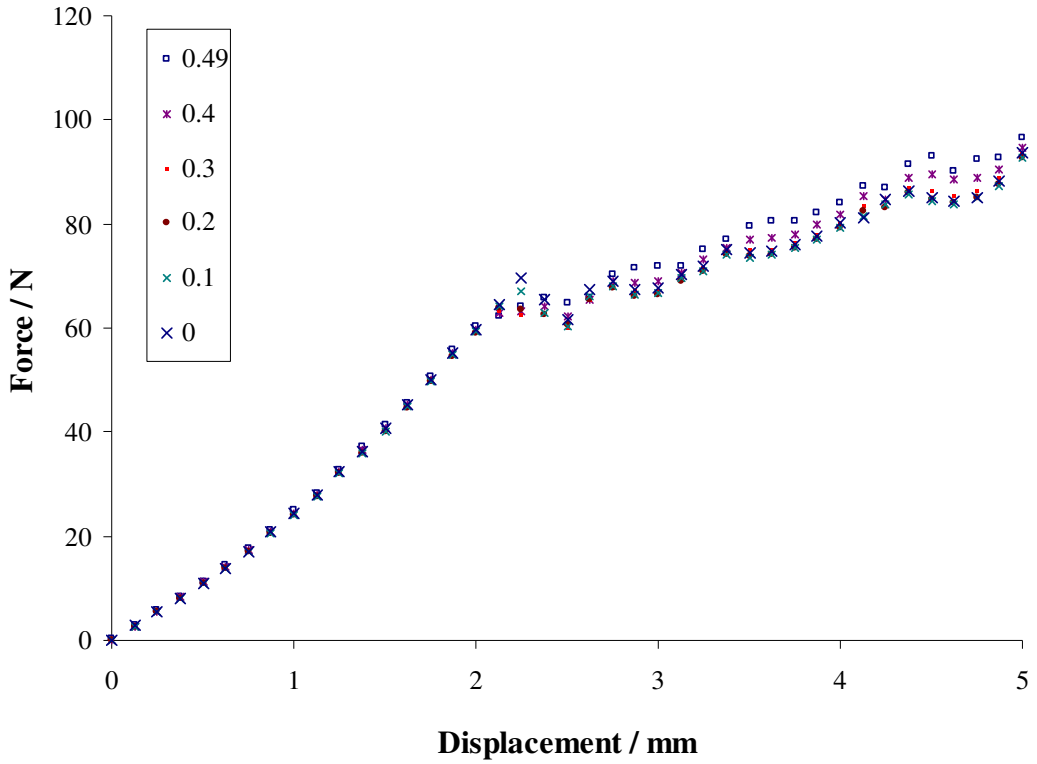

Figure 6.19: The axisymmetric explicit table tennis ball model with a range of Poisson's ratio.

6.1.7 An examination of varying the sphere geometry using axisymmetric and three dimensional models

A series of models was created for hollow spheres with varying wall thickness and with varying overall diameters in addition to the normal table tennis ball diameter of 40 mm. Some initial three dimensional solid element models were created for spheres with a greater wall thickness than table tennis balls of 4.0 mm rather than the true wall thickness of 0.4 mm. These explicit models were checked to ensure that mesh density considerations did not dominate the predicted stiffness behaviour with what is a relatively larger wall thickness and hence size of element compared to the previous models. Two different meshes are shown in Figure 6.20 for comparison, with the results of the two models shown in Figure 6.21.

The models were compressed by 10 mm, i.e. 25 % of the diameter to obtain the snap through buckling point. Both mesh densities produced near identical curves with only a slight difference developing toward the maximum compression, as can be seen in Figure 6.21. However no discernable snap through was obtained, with only a slight

change in the curve at around 2 mm compression, but what was observed graphically when compared to the visual deformation of the model was the initial flattening of the curved surface of the sphere in contact with the rigid body during compression.

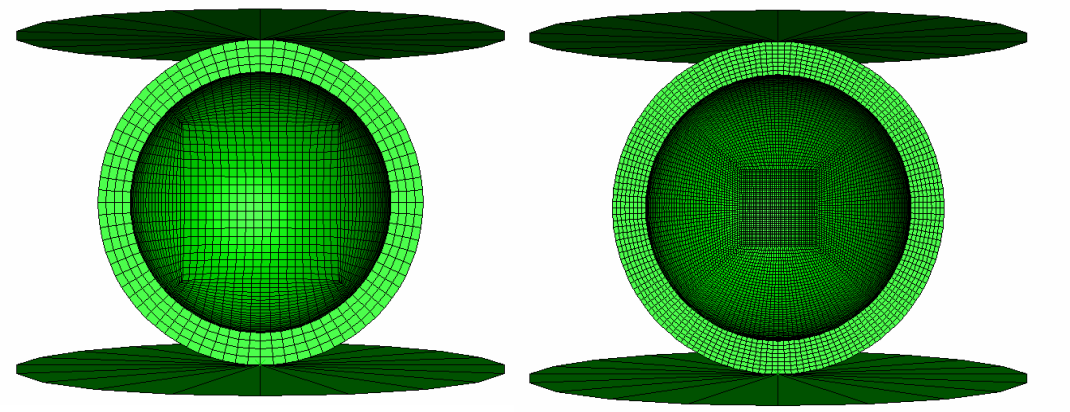

Figure 6.20: A comparison of the meshes used for the three dimensional solid element 40 mm outer diameter spheres with a wall thickness of 4 mm.

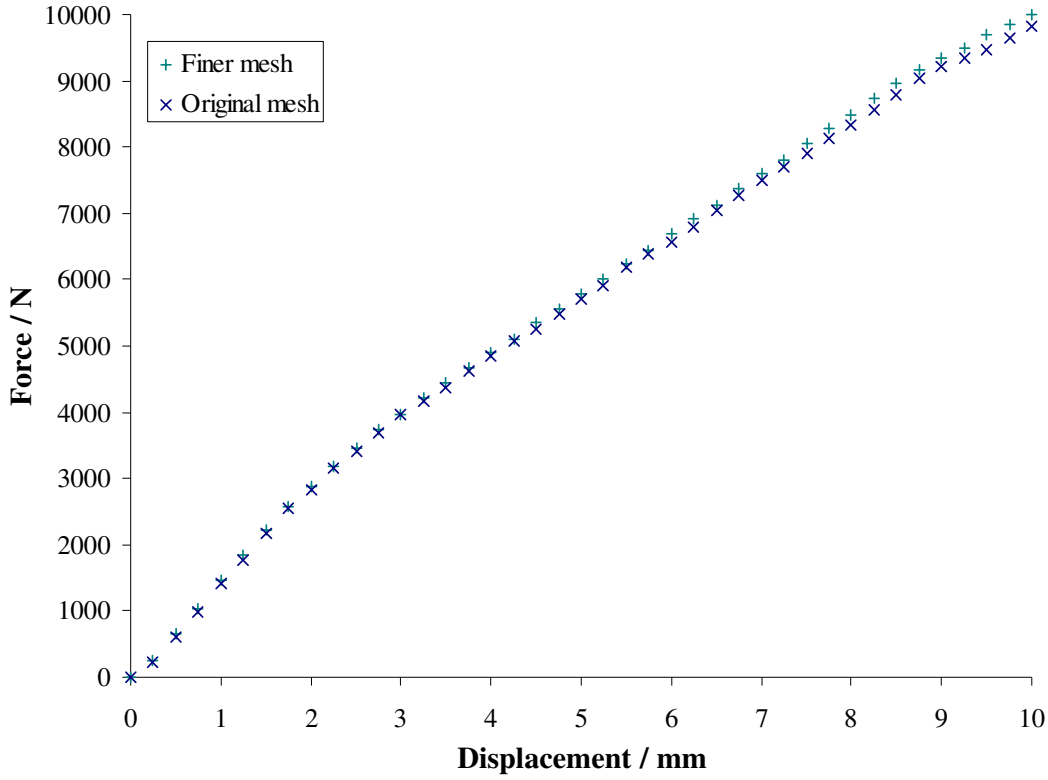

Figure 6.21: A comparison of the force / displacement results for the three dimensional solid element 40 mm outer diameter sphere with a wall thickness of 4 mm.

The explicit three dimensional model with the original mesh was analysed again to a larger displacement, to an approximately full compression of 32 mm. The results of this analysis are shown in Figure 6.22, where a definite snap through buckling can be a seen at approximately 12 mm deflection, as well as a subtle change in the curve at around 2 mm as noticed for the previous models, indicated by the two straight lines in the figure.

This model was later adapted and used to model the behaviour of squash balls, as the diameter of squash balls is 40 mm and the wall thickness is 4.0 mm, although the material and behaviour during compression is quite different and is described later in this chapter.

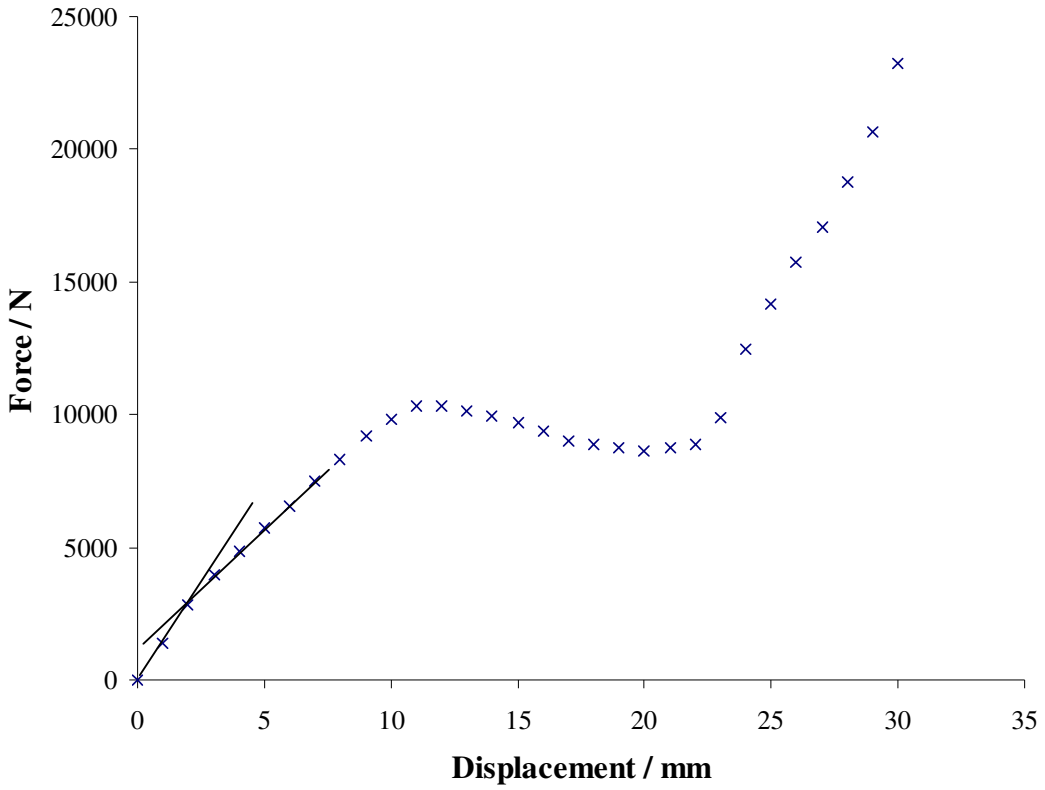

Figure 6.22: The force / displacement results for the three dimensional solid element 40 mm outer diameter sphere model with a wall thickness of 4 mm at a large compression.

Following these models with a wall thickness of 4.0 mm, further models were conducted for a range of other wall thickness values. The first few models had wall thickness that ranged between 0.2 mm and 1.0 mm (0.2 mm, 0.4 mm, 0.6 mm, 0.8 mm

and 1.0 mm). The results from these models are shown in Figure 6.23, where it can be seen that for an identical outer diameter of 40 mm, the initial snap through buckling point occurs at higher deformation, so it appears to be dependent upon the wall thickness and is indicated in the figure with a solid line. This behaviour is explored in more detail later in this chapter. The models were also repeated for larger wall thickness values of 1.5 mm and 2.0 mm.

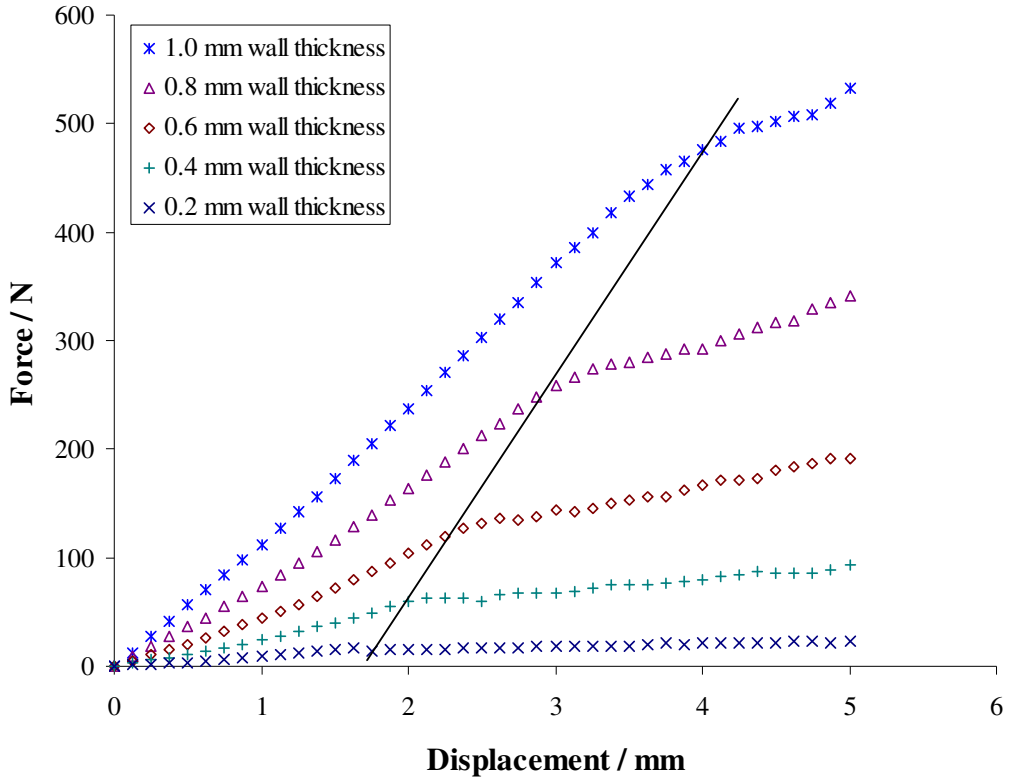

Figure 6.23: Comparison of a 40 mm diameter sphere with a range of different wall thickness.

Having explored the effect of varying the wall thickness for a fixed outer diameter of 40 mm a series of models were produced with an outer diameter five times larger (200 mm) and then one fifth of the size (8 mm). Three different 200 mm diameter sphere models had wall thickness values of 1 mm, 2 mm and 3 mm, with 2 mm giving an equivalent ratio of wall thickness to diameter (1:100) as the standard table tennis ball. Altering the ratio of the wall thickness to diameter clearly changes the initial stiffness of the sphere in compression as well as the point at which the snap through buckling starts. This is evident in Figure 6.24 where the kink in the curve occurs

between a displacement of approximately 8 mm and 12 mm, as indicated by the solid line in the figure.

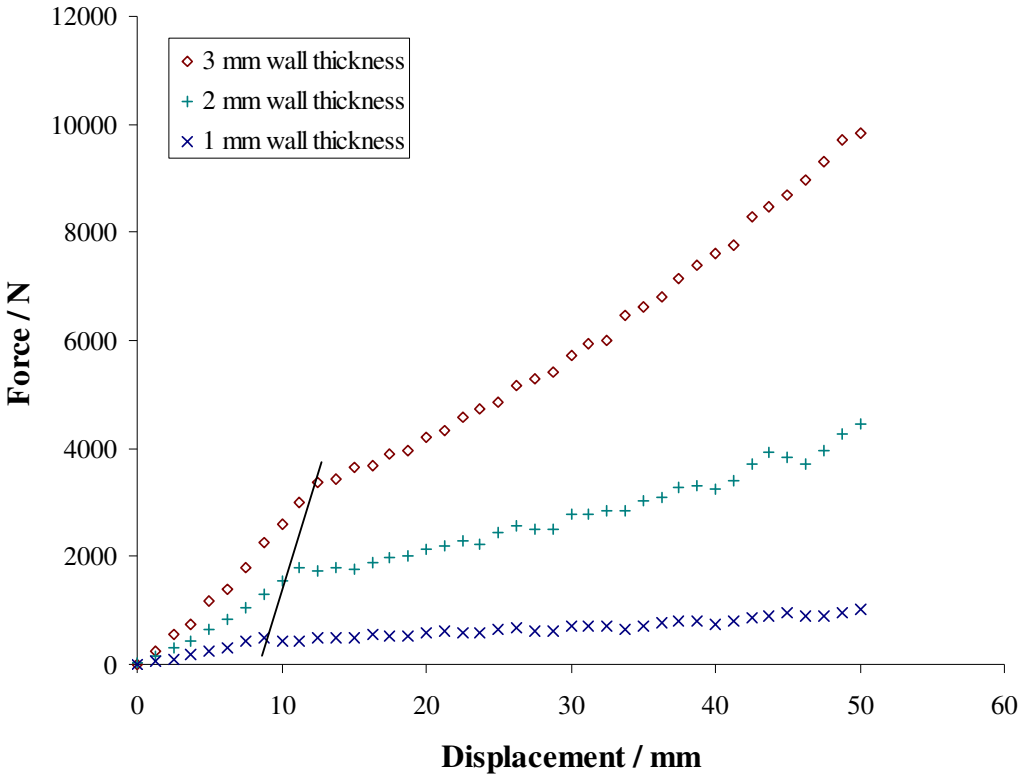

Figure 6.24: A comparison of how wall thickness alters the buckling behavior for a 200 mm diameter sphere.

Three models evaluated with similar ratios of wall thickness to diameter with a diameter of 8 mm and wall thickness values of 0.04 mm, 0.08 mm and 0.12 mm showed a similar family of curves, as can be seen in Figure 6.25. The snap through buckling point changes in sequence with wall thickness as had been observed in the previous models of the 200 mm diameter spheres, this is indicated in the figure by the solid line. One of the key points therefore for further investigation was what features can be seen to determine the point of onset for the snap through buckling behaviour in these models.

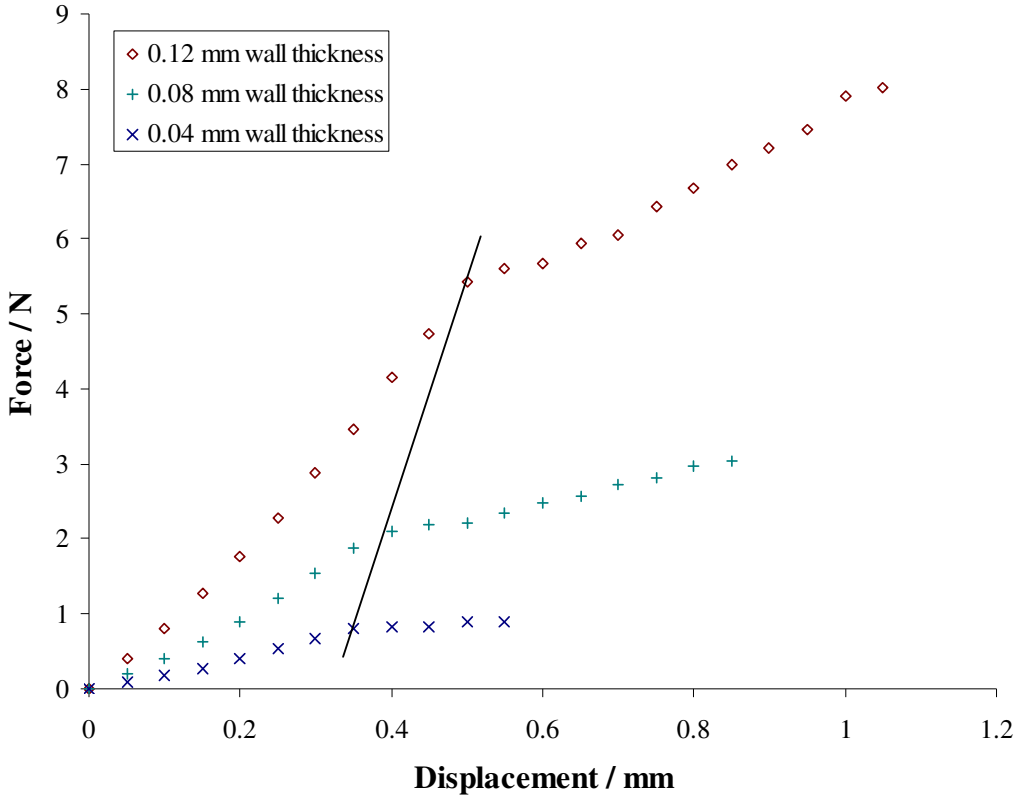

Figure 6.25: A comparison of how wall thickness alters the buckling behavior for an 8 mm diameter sphere.

6.1.8 An examination of the effect of friction in the models

The effect of friction on the deformation behaviour and the snap through was examined next, the initial approach being to see how an introduction of friction in the model of the table tennis ball might alter the results. For the model an estimated coefficient of friction of 0.5 was used, based upon the cellulose material of the table tennis ball and the steel surfaces used for compression during the experiments, the value was obtained from an engineering reference website (www.engineeringtoolbox.com). The model with friction is compared to the "normal" model in Figure 6.26. It can be seen from the figure that the model without friction is similar up until the snap through buckling point. Beyond the buckling point the introduction of friction both increases the force required for buckling to arise and also deflection at which the snap through takes place. The frictionless model was expected to behave in a slightly unrealistic manner and this was shown by the results, therefore friction was included in all subsequent models where relevant.

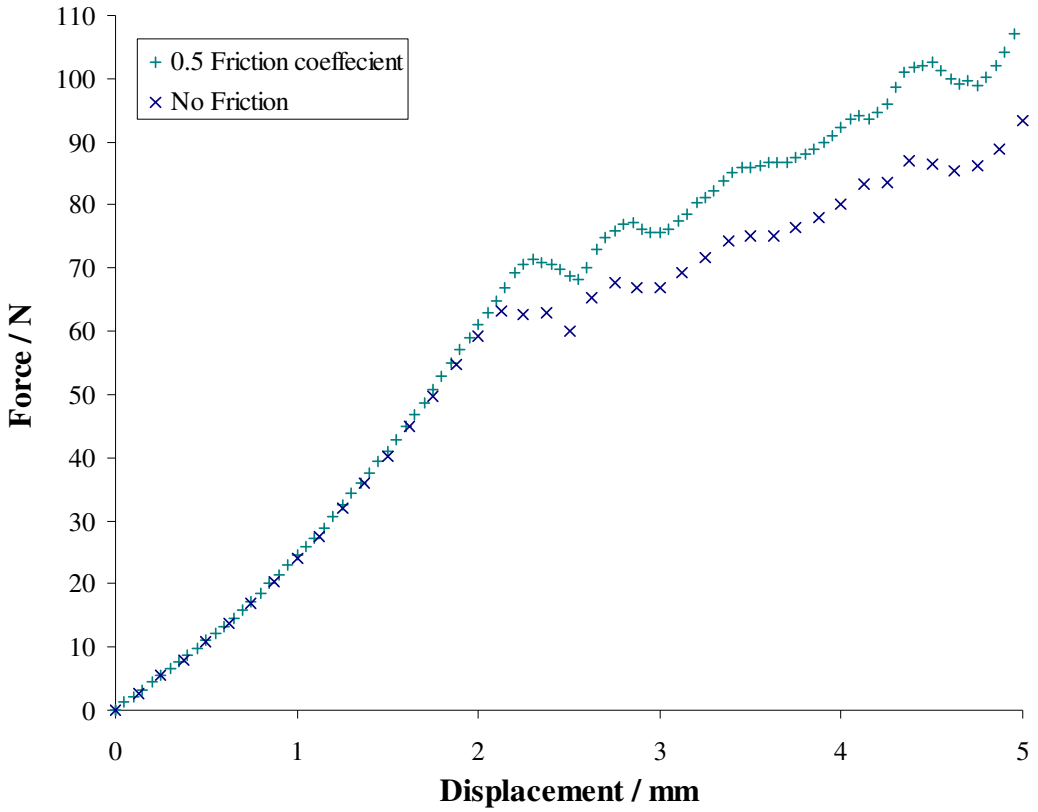

Figure 6.26: An evaluation of the effect of friction on the deformation of the table tennis ball model.

6.1.9 The effect of plasticity on the behaviour.

Up until this point all the models have incorporated yielding behaviour in the materials properties. It was wondered how significant this behaviour might be on predicted behaviour. Therefore a model without plastic properties was also examined and compared to a conventional model that includes both elastic and plastic properties. The values for the properties as used in the Abaqus input file for the "normal" model are shown here:

```
*SOLID SECTION,ELSET=PLASTIC,MATERIAL=PLASTIC
*MATERIAL,NAME=PLASTIC
*ELASTIC
 2200,0.30
*PLASTIC
 50,0
 60,0.012
*DENSITY
 1.3E-9
```

The plastic properties used in the model where obtained by mechanical testing as described previously. The initial yield stress was given as 50 MPa and some modest work hardening was included up until a plastic strain of 0.012 at a stress of 60 MPa, above which it was ascribed to be perfectly plastic. The elastic values include the Young's modulus of 2200 MPa and the Poisson's ratio of 0.3. The results for the model without plastic properties are shown in Figure 6.27, compared to the model that includes yielding behavior. The introduction of a yield mechanism has only a very limited effect on the behavior although the entirely elastic model has a snap through buckling taking place at a slightly higher displacement with a slightly higher force.

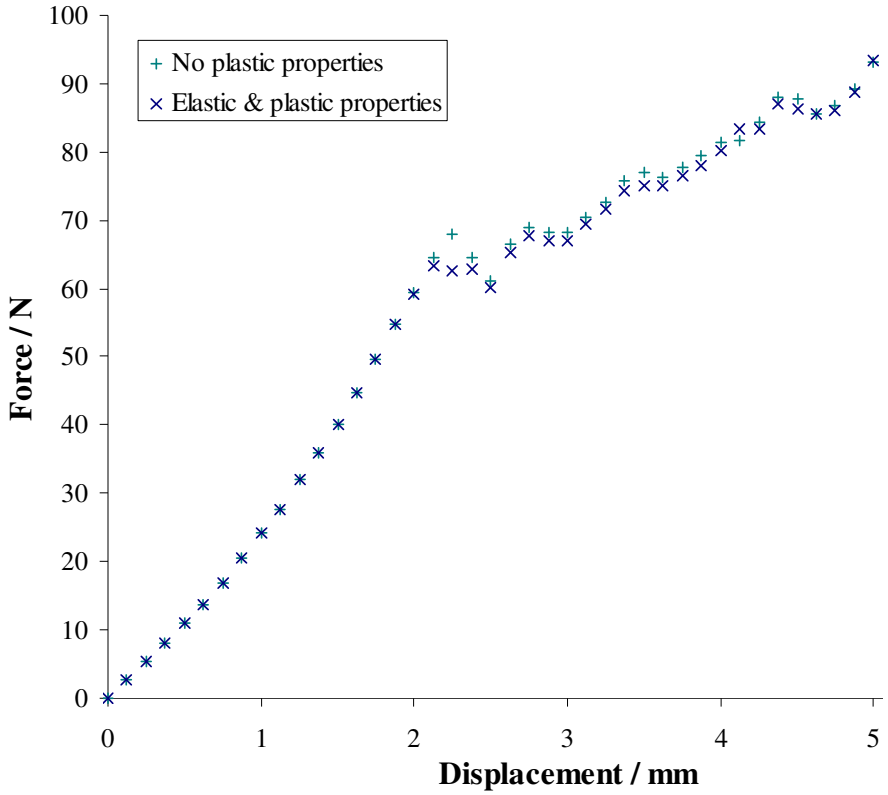

Figure 6.27: A model with realistic yielding behavior compared with an entirely elastic model.

The previous table tennis ball models for Poisson's ratio were rerun without any yield behavior to see if the difference between the models increased for the case of an entirely elastic solution for each value of Poisson's ratio. The results from these models are shown in Figure 6.28, where it can be seen that there is very little difference

between the curves for each value of Poisson's ratio, the snap through buckling point occurs at broadly the same displacement, but the force varies slightly.

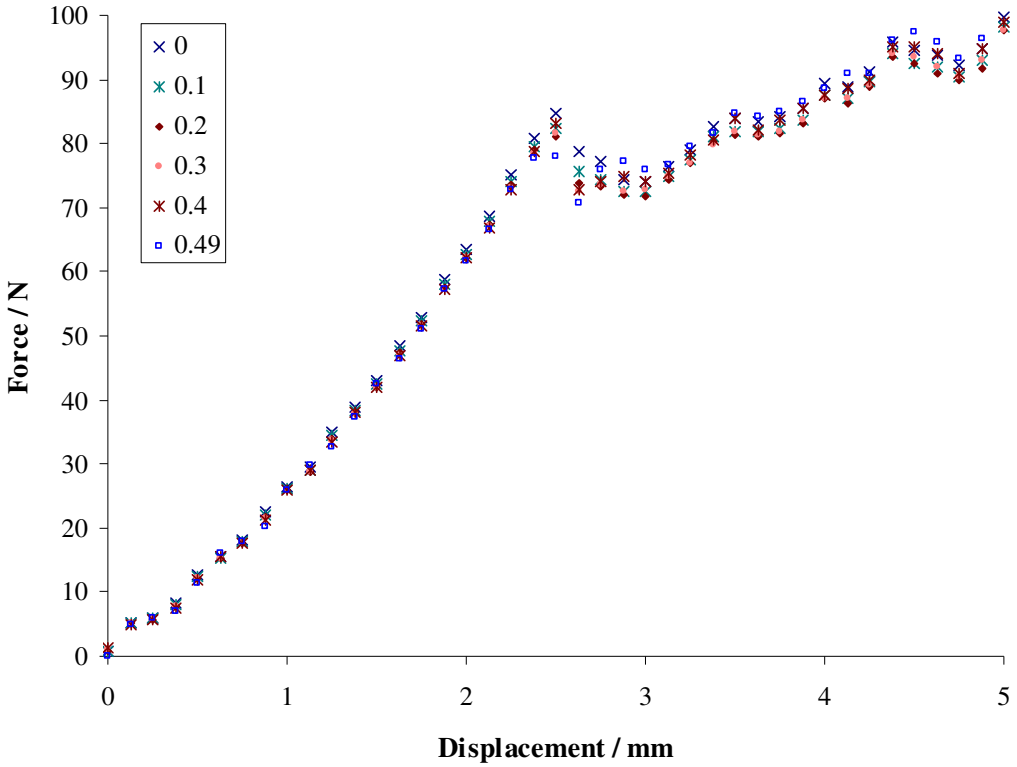

Figure 6.28: The table tennis ball model without plastic properties for a range of different Poisson's ratio.

6.1.10 Squash ball models

The axisymmetric and three dimensional models that had been developed to examine a range of wall thicknesses for the table tennis balls and microspheres were also used with a wall thickness of 4.0 mm to model the behaviour of squash balls. Some of the geometries for the models were the same as that shown in Figure 6.20 previously, however the material properties were clearly quite different between the cellulose table tennis ball and the rubber squash ball. The rubber material model used a Neo-Hookean model with the C_{10} value set to an initial estimate of the 0.5 MPa as the real material properties of the squash ball were unknown.

An example of the axisymmetric squash ball model revolved to produce a half dome is shown in Figure 6.29. The model had a diameter of 40 mm, a wall thickness of

4.0 mm and had four elements through the wall thickness and forty along its quarter circumference.

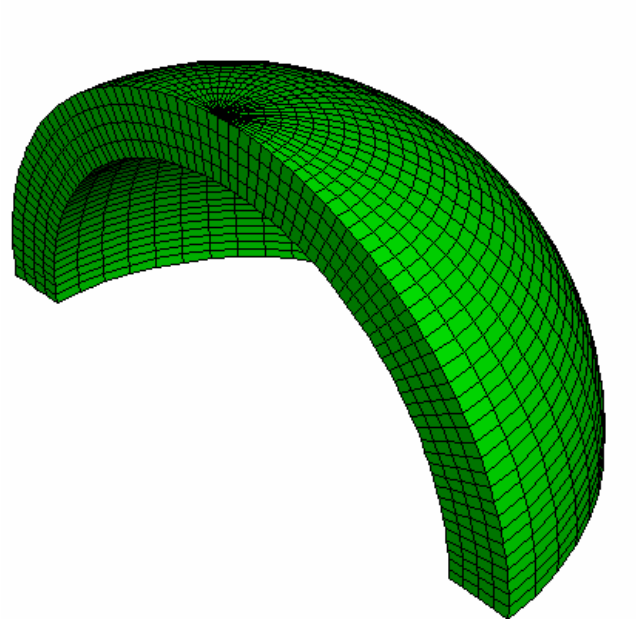

Figure 6.29: An example of the revolved axisymmetric squash ball model.

Images of the model during compression are shown in Figure 6.30, the images include the top and bottom analytical rigid bodies. The bottom rigid body does not move, but the top rigid body moves vertically downwards, this surface is “tied” to a reference node which is clearly visible as an “x” in the latter images.

The reference node provides the output for force and displacement. Due to the ratio of wall thickness to diameter of the rubber material, there is a flattening of the sphere against the top rigid compressive surface as can be seen in image "b”, but there is no obvious snap through buckling as is observed for the thinner walled plastic spheres.

The results from the axisymmetric squash ball model are shown in Figure 6.31. The graph includes the experimental results for a squash ball compression test compared to the model. The experiment produced a smooth curve with a gentle upsweep beyond a deflection of 22 mm, but the model continues to approximately 32 mm where it exhibits a more abrupt and steeper curve, indicating a greater more sudden increase in stiffness compared to the experiment.

a.

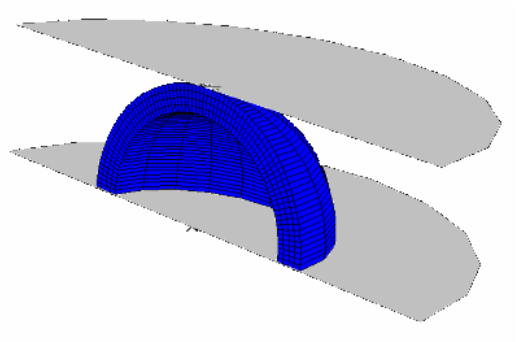

b.

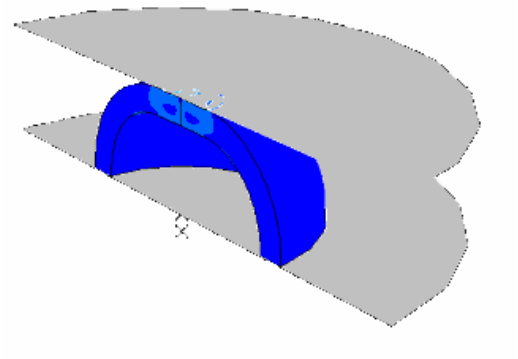

c.

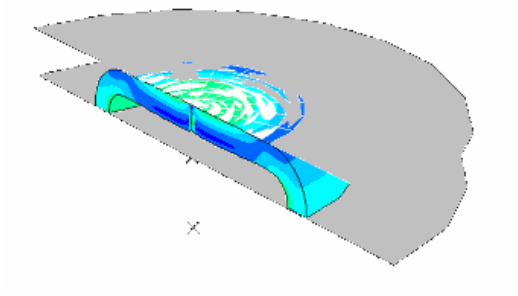

d.

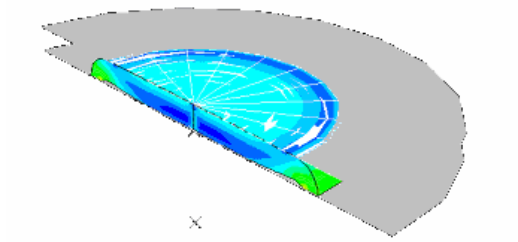

Figure 6.30: Images of the squash ball model during compression.

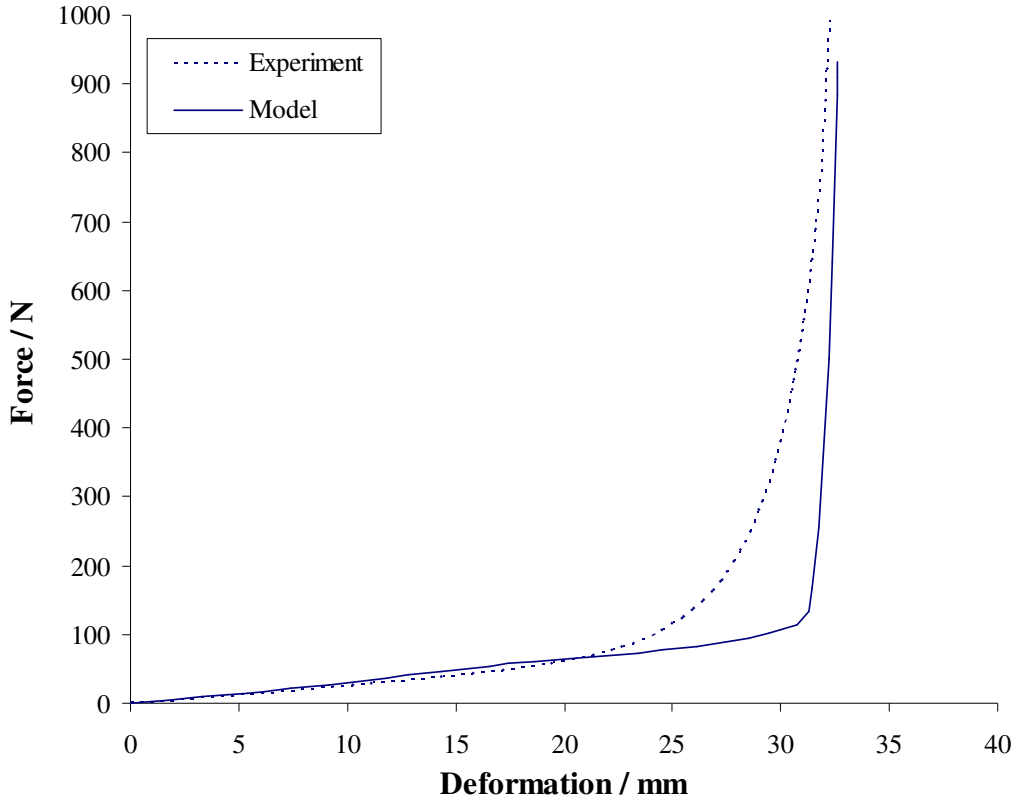

Figure 6.31: The results from the axisymmetric squash ball model compared to the experimental results.

The difference between the two curves is most likely due to an inappropriate material model and perhaps the lack of friction in the model. The Neo-Hookean materials model used being linear over the entire strain range in simple shear which clearly does not reflect the real non-linear behaviour of the rubber, where marked nonlinearities are seen particularly at large strains above 50 %. Additionally, the rubber sliding against steel plates will exhibit some friction, but this was not introduced into the model.

6.2 Development of a method to determine the wall thickness and modulus of a hollow sphere by using a simple axial compression test

6.2.1 Introduction

Microscopic fillers such as the microspheres used in this study or others such as those used in ultrasonic contrast agents are too small for their physical or material properties to be easily obtained once they have been manufactured and incorporated into

a matrix material. Often it would also be useful to know the properties of larger hollow thin-walled spheres but this is not easy without damaging the sphere. The FEA models mentioned in this chapter were developed in part to enable a numerical investigation to be conducted in order to produce a method of obtaining the wall thickness and modulus of a hollow sphere; this was validated by the experimental axial compression test results also mentioned.

The work of Updike and Kalnins (1970 and 1972) has been discussed in the literature review of this thesis, they proposed the flattening of the sphere surface during the initial compression of a hollow sphere, this was later discovered experimentally by Pauchard and Rica (1998). Pauchard and Rica also discovered that as the applied force was increased the shell exhibited a snap-through buckling at a deformation that was almost twice the thickness of the shell. They then deduced the form of the energy of the deformed shell, but this had unknown parameters that were thought to depend only upon the Poisson's ratio of the shell material. The work here uses the FEA modelling to show the dependence of the buckling transition and its associated force-deflection curve on the material and geometric properties.

The ratio of the displacement at buckling to the wall thickness depends upon the wall thickness and not just Poisson's ratio, additionally the initial force-deflection curve is dependant upon the sphere geometry and the modulus as well as Poisson's ratio. Therefore for a given Poisson's ratio a set of curves of the buckling force and displacement can be derived to enable the Young's modulus and thickness of the sphere shell to be determined, simply from a measurement of the force at a given displacement and the point of buckling instability.

6.2.2 Development of the models and a method to determine the point of instability

The models used initially for this part of the study were three dimensional models with eight node solid continuum elements with a reduced integration analysis, C3D8R elements, as shown in Figure 6.32.

However, the mesh sensitivity studies discussed previously showed that a minimum of four elements were required through the thickness and these elements were most reliable when they were approximately cube shaped. Therefore for very thin walled spheres it required a very large number of solid elements which required unrealistically long solution times.

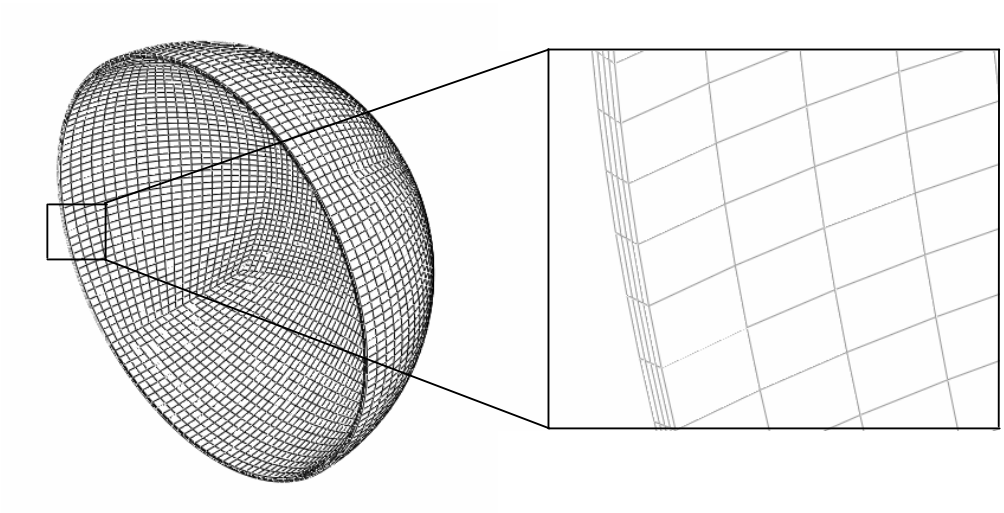

Figure 6.32: The three dimensional model showing mesh and boundary conditions.

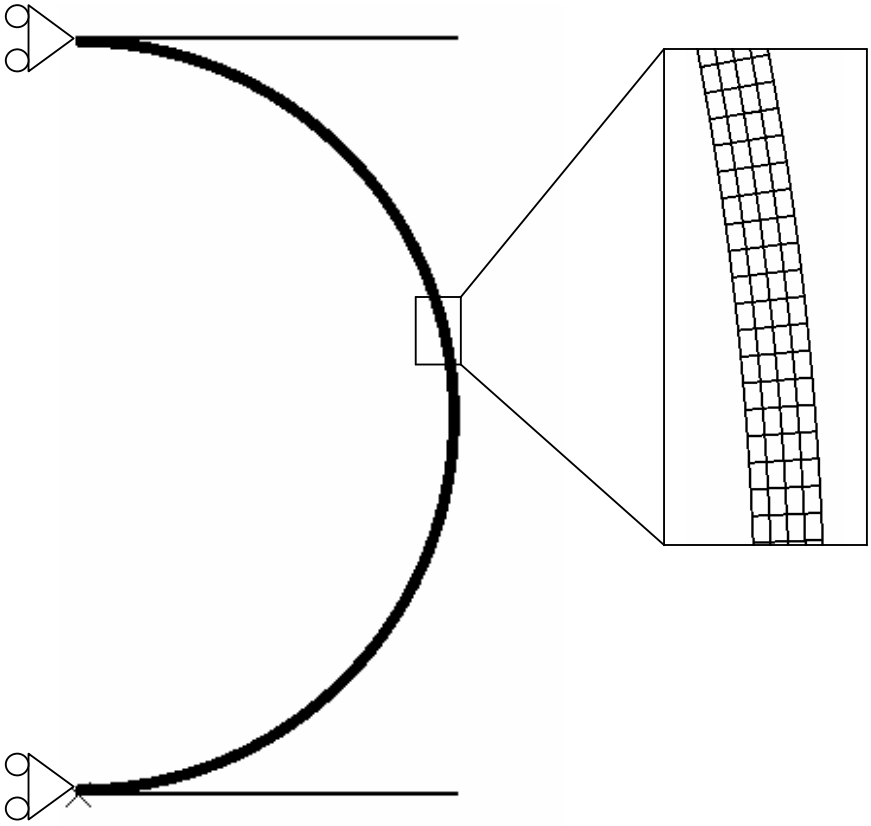

Figure 6.33: The axisymmetric model showing mesh and boundary conditions.

It is possible to increase the mesh density for models in sections of the model that are of particular interest, but in this case the area of interest is the contact regions

which move during the analysis, so it was easier to use a uniform mesh. A simple shell model was also produced but this was unable to sufficiently represent the contact.

The models that were chosen to produce the results for the majority of this part of the study were the less computationally demanding two dimensional continuum axisymmetric elements each with four nodes, CAX4 elements. These models cannot reliably model any out of plane buckling that might for example arise at very large compressions but have been shown to reproduce the initial snap through behaviour reliably, in the previous section. An example of this model is shown in Figure 6.33, where the element geometry and boundary conditions can be seen.

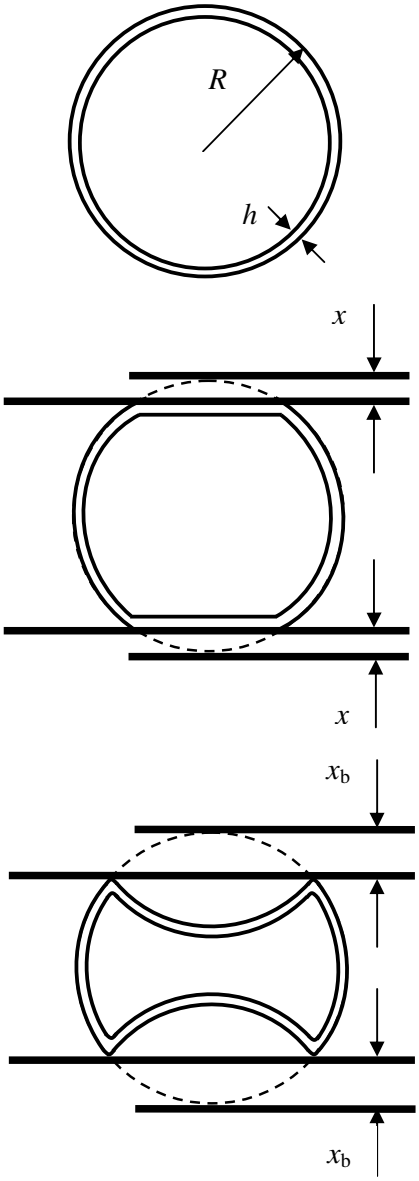

Figure 6.34: The nomenclature for the hollow sphere, pre and post buckling.

To develop the family of curves mentioned in the introduction the displacements and force must be presented in dimensionless terms as proposed by Pauchard and Rica (1998). The displacement is represented as the ratio of the deflection to the wall thickness ratio of the shell, where $\varepsilon = x / h$, where x is the displacement and h is the wall thickness. This is shown if Figure 6.34 where the displacement of buckling is also shown as x_b. The force was also expressed in normalised dimensions based upon those proposed by Pauchard and Rica as, RF / Eh^3.

For this analysis a more precise point of buckling was required than has been described so far, as the snap through buckling point was not always clearly defined by the FEA models due to the contact between the nodes of the model and the rigid surface varying during the compression process. This was particularly evident with the three dimensional models as mentioned previously, but was also evident for the axisymmetric models. Therefore a more accurate method of determining the true force and deflection was explored. This method is shown in Figures 6.35, 6.36 and 6.37.

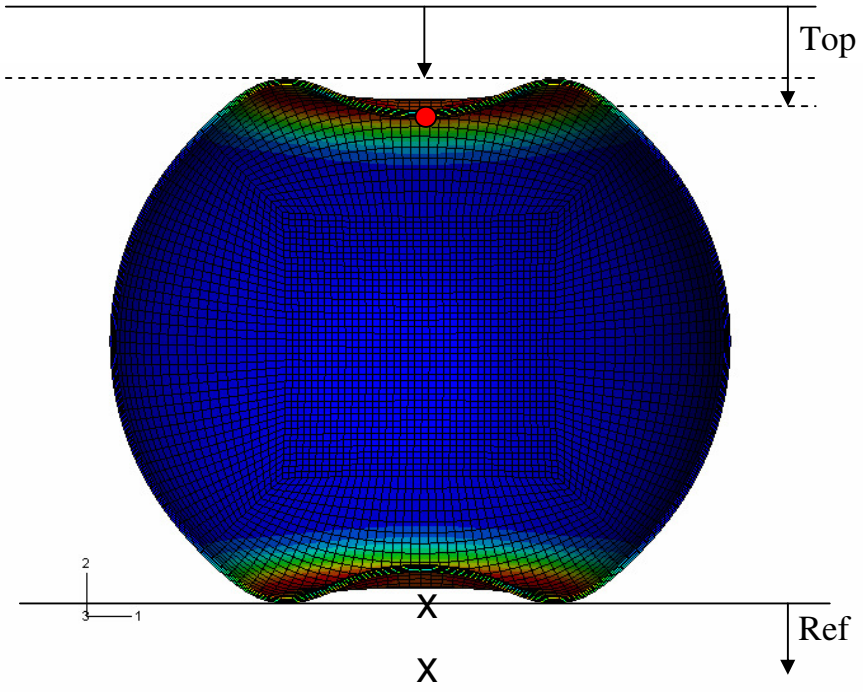

Figure 6.35: Deformation of model showing movement of Reference node (X) and the top rigid surface.

Figure 6.35 shows a model during deformation, it can be seen that the reference node will move the same amount as the top rigid surface until the point of buckling.

Beyond the point of buckling there is a difference between the displacements of the two nodes, this is shown graphically in Figure 6.36.

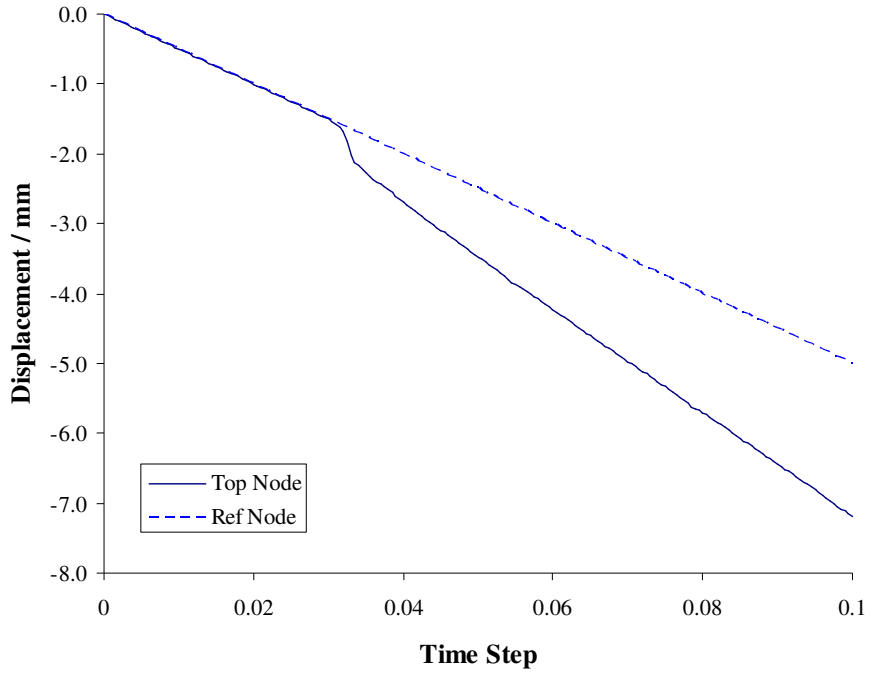

Figure 6.36: Graphical representation of the difference between the reference node and the top rigid surface.

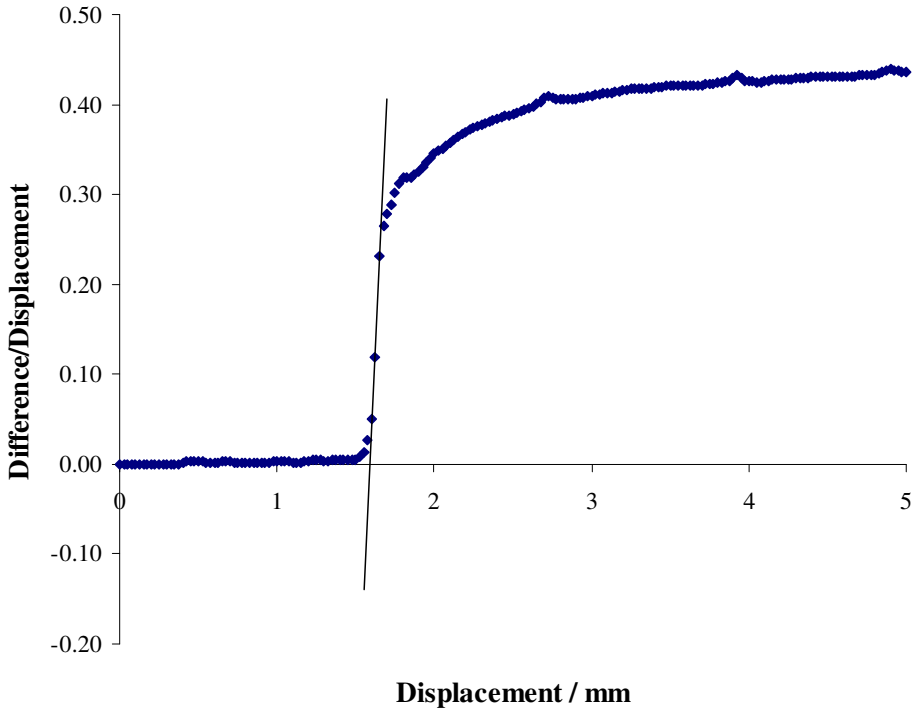

Figure 6.37: Determination of the point of buckling from the difference between the reference node and the top rigid surface.

The difference between the two displacements can then be plotted as shown in Figure 6.37, this method was used to accurately determine the point of buckling, but the possibility of a small error remained, depending upon the determination of the slope of the line drawn to find the corresponding displacement. For a more accurate solution the displacement half way to the buckling point displacement was chosen, this method was used when developing the family of curves to determine the material modulus.

A check was made by comparing the full three dimensional models against the two dimensional axisymmetric models, this was a simple comparison of the buckling points as a function of the ratio of the wall thickness to the radius of the sphere. The two dimensional models were deemed to be sufficiently similar for use to produce the families of curves. It also showed that the initial elastic buckling of the sphere was symmetrical and that no out of plane buckling occurred that would require the full three dimensional model. The comparison is shown in Figure 6.38.

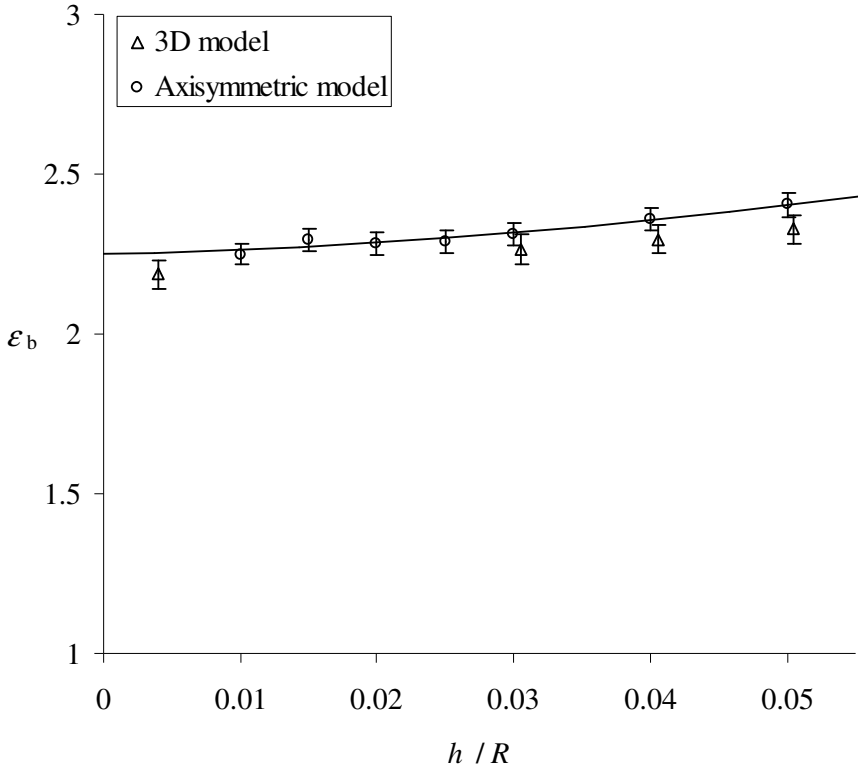

Figure 6.38: Snap through deflection of the three dimensional model compared to the two dimensional model as a function of sphere radius for a Poisson's ratio (ν) of 0.3.

6.2.3 Development of the models to determine effect of plastic properties

A check was also made of the material properties to determine if the buckling was purely elastic, to remove any possibility that the use of plastic properties may introduce errors. This was achieved by analysing a number of models with elastic properties only. The models had previously been produced with elastic and plastic properties, the results for this type of model for a range of Young's modulus is shown in Figure 6.39. The models are plotted without dimensions as force against displacement as F / Eh^2 against x / h.

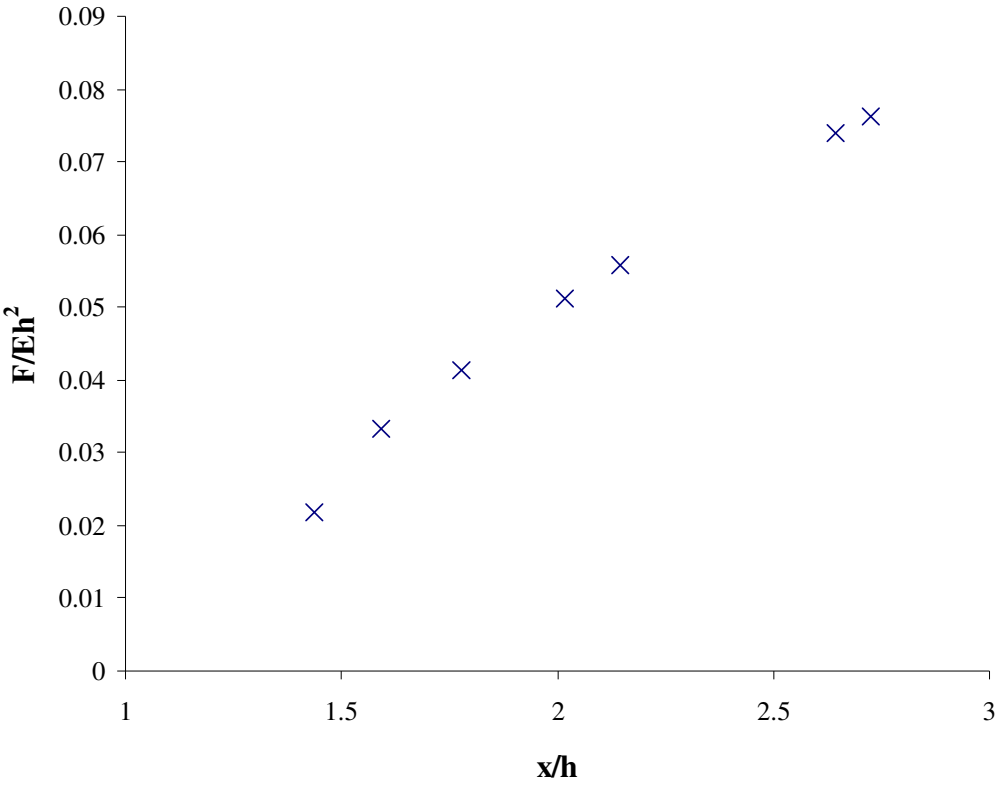

Figure 6.39: A curve for a sphere with a wall thickness of 0.4 mm and a radius of 20 mm, for range of Young's Modulus of 20, 10, 7.5, 5, 4, 2 and 1 GPa respectively (left to right).

If the models were of identical dimensions and Poisson's ratio, but with a range of Young's modulus and were only dependant upon the elastic properties, then when plotted as F / Eh^2 against x / h the results for the buckling point of each model should appear as a single point on a graph. This was found to be true and is shown in Figure 6.40.

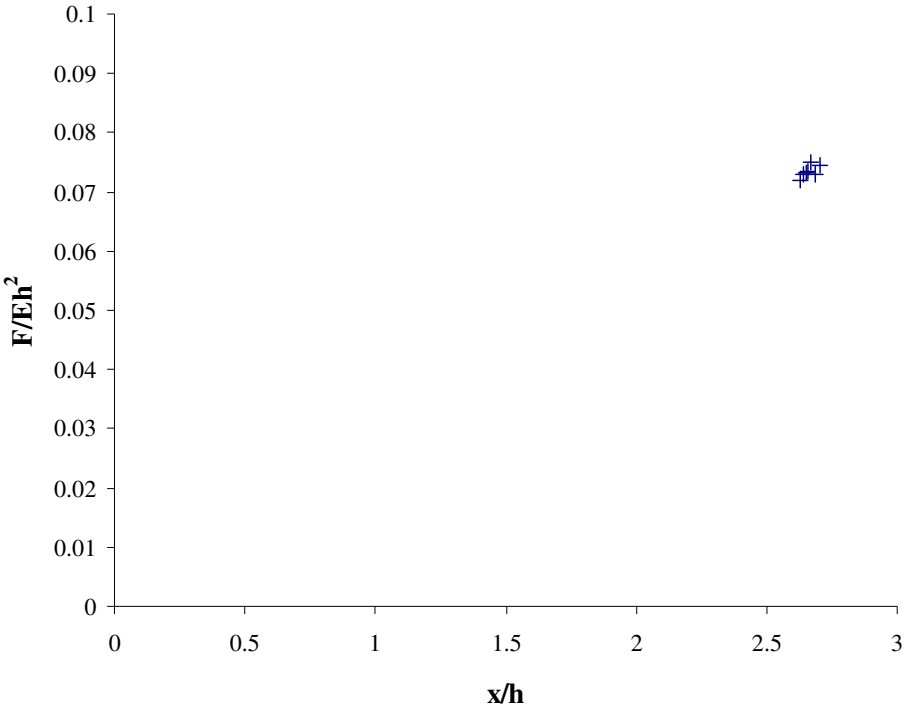

Figure 6.40: The two dimensional sphere models, with no plastic properties, plotted for a range of Young's modulus.

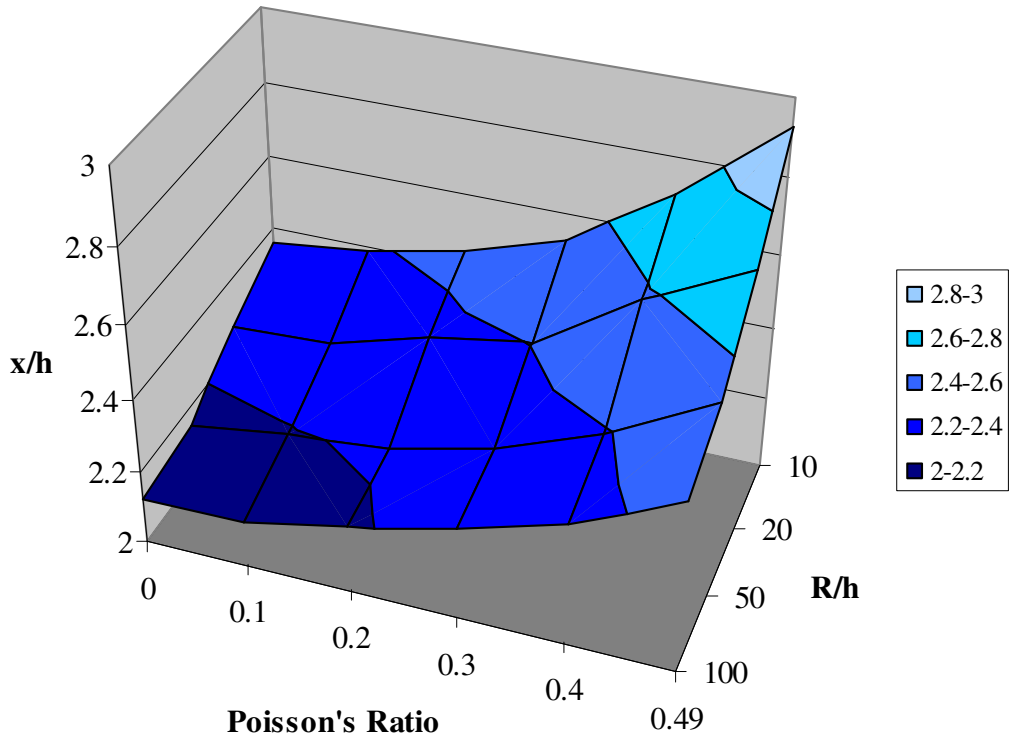

Figure 6.41: A three dimensional chart showing the expected behaviour for a range of sphere models with varying Poisson's ratio, wall thickness, radius and displacement at the buckling point.

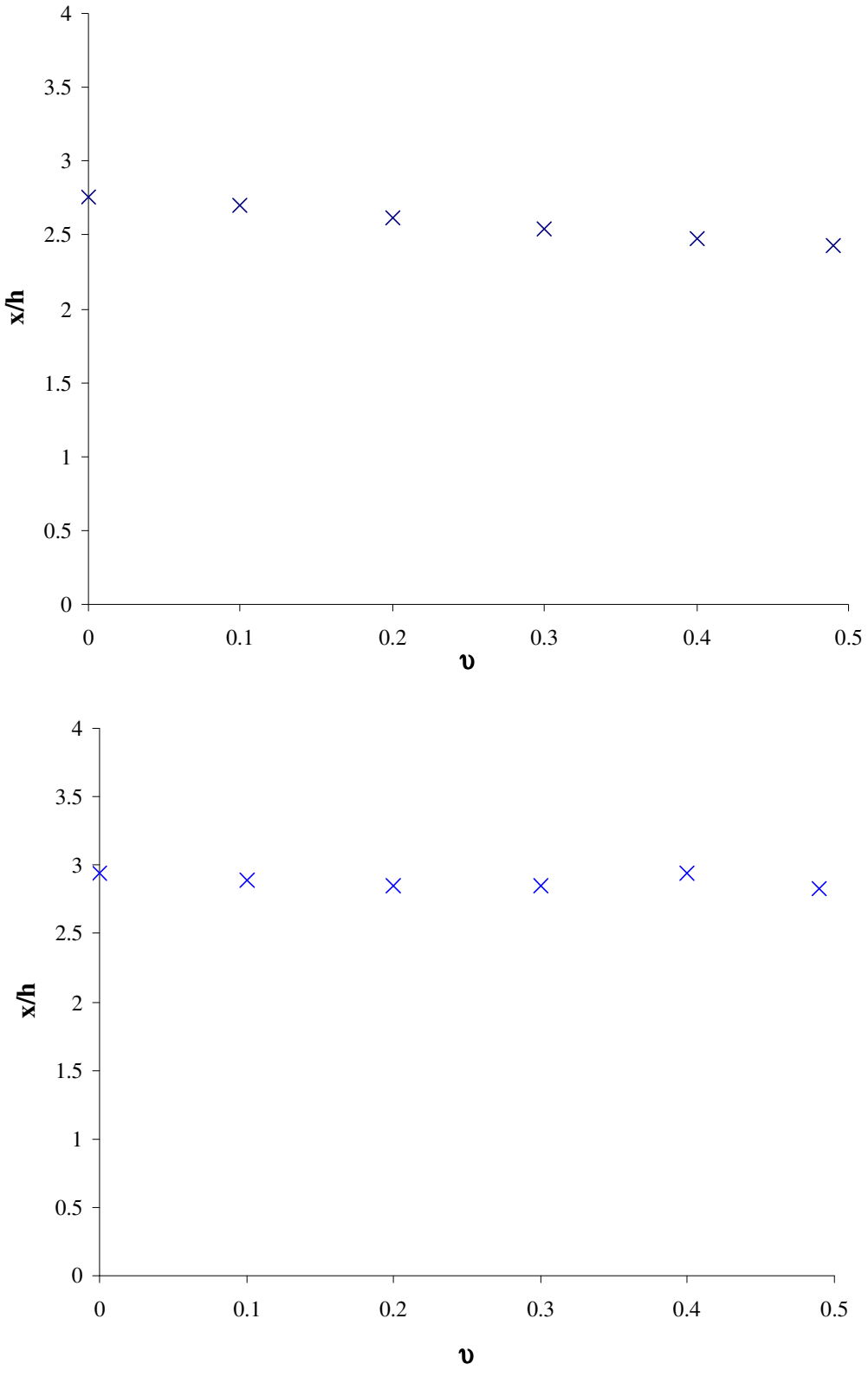

Figure 6.42: The effect of models plastic properties, with (top) and without (bottom) plastic properties for a range of Poisson's ratio.

Prior to producing families of curves from the range of models a chart was produced to examine the behaviour that could be expected from the models. The chart was produced as a three dimensional graph and is shown in Figure 6.41. The displacement is represented as before where it is the ratio of the deflection to the wall thickness ratio of the shell, x / h. The radius was kept constant at 20 mm, but the wall thickness for each model was 0.2 mm, 0.4 mm, 1.0 mm and 2.0 mm. For each of these wall thicknesses the Poisson's ratio was altered to give the range of 0, 0.1, 0.2, 0.3, 0.4 and 0.49.

The effect of plastic properties was also examined for a range of Poisson's ratio, this is shown in the two graphs in Figure 6.42. There is little difference between the two sets of results, so for the initial snap-through buckling it was confirmed that there was a negligible effect on the model when including or excluding plastic properties.

6.2.4 The family of curves to obtain the wall thickness and modulus

A number of variables were altered to produce the families of curves; these are shown in table 6.1, the "standard" table tennis ball properties are shown in bold, all other combinations of all of the variables were modelled.

Property	Unit	Value									
Wall Thickness	mm	0.2	**0.4**	0.6	0.8	1.0	1.5	2.0	3.0	4.0	5.0
Young's Modulus	MPa	1000	2000	**2200**	4000	5000	7500	10000	20000		
Yield Strength	MPa	5	**50**	500							
Poisson's ratio	n/a	0	0.1	0.2	**0.3**	0.4	0.499				

Table 6.1: The variables used to produce the families of curves.

The dependence of the displacement of buckling instability on the Poisson's ratio of the material and for a range of ratios of the wall thickness of the sphere to its radius is shown in Figures 6.43 and 6.44. These graphs allow the unknown wall thickness of a sphere to be measured by simply obtaining the value of the buckling displacement, providing that the Poisson's ratio of the material is known.

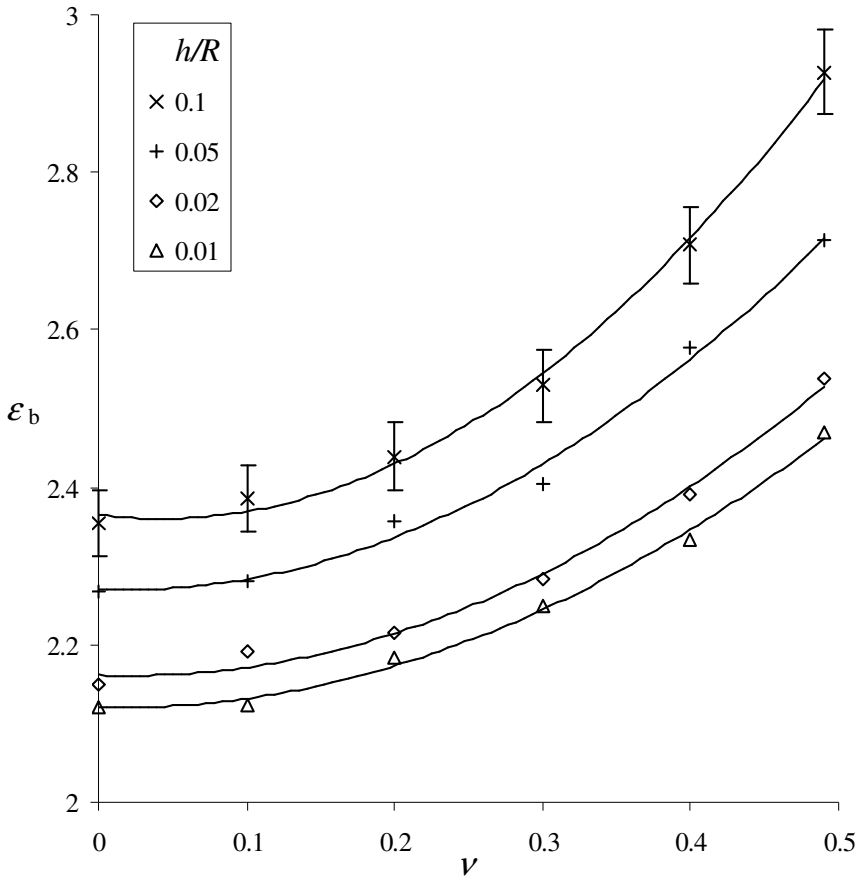

Figure 6.43: Snap through buckling point (ε_b) versus Poisson's ratio (ν) at a range of values for wall thickness / radius (h/R).

The work of Pauchard and Rica (1998) suggested that each of the various geometries would superimpose as a single master curve if the buckling point was plotted against Poisson's ratio. This has been proven not be true as there is a small dependence upon the geometry as shown in the graphs. Pauchard and Rica also suggested that the value at the buckling point would be 2, which is comparable to the thinner walled spheres represented in the graphs, but is probably only true for spheres with very thin walls.

The shape of the elements used in the models had an effect on the resulting buckling displacement, although the errors produced were less than 3 %. However for the maximum force, F_b, at the same buckling displacement, the discretisation details of the model produced errors of approximately 15 %. Therefore to reduce the effect of the error inherent in the models the force, f, at the half point to buckling, $\varepsilon_b/2$, was used. This point is sufficiently far from the buckling instability for the effects of the small

change in mesh density or the effects of the discretisation of the models time step to adversely affect the results.

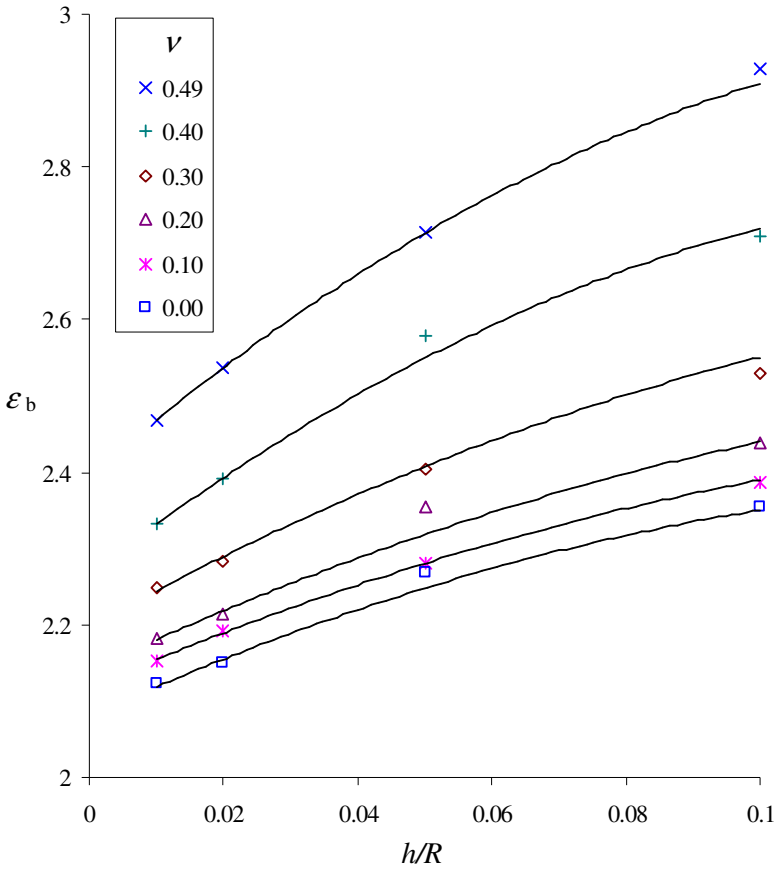

Figure 6.44: Snap through buckling point (ε_b) versus wall thickness / radius (h/R) at a range of values for Poisson's ratio (ν).

Figure 6.45, shows a family of curves that allow the buckling force to be used to obtain the modulus of the material of the sphere. The graph shows the range of geometric variations as used in the previous two graphs, but in Figure 6.45 it can be seen that the normalized force at the half displacement to the buckling point varies for a range of Poisson's ratio for different values of the normalized wall thickness. As for the previous graphs there is a geometric dependence that has not previously been predicted. The geometric dependence allows the modulus of the sphere material to be established simply by knowing the force, f, at the half way point to the snap through buckling, ε_b.

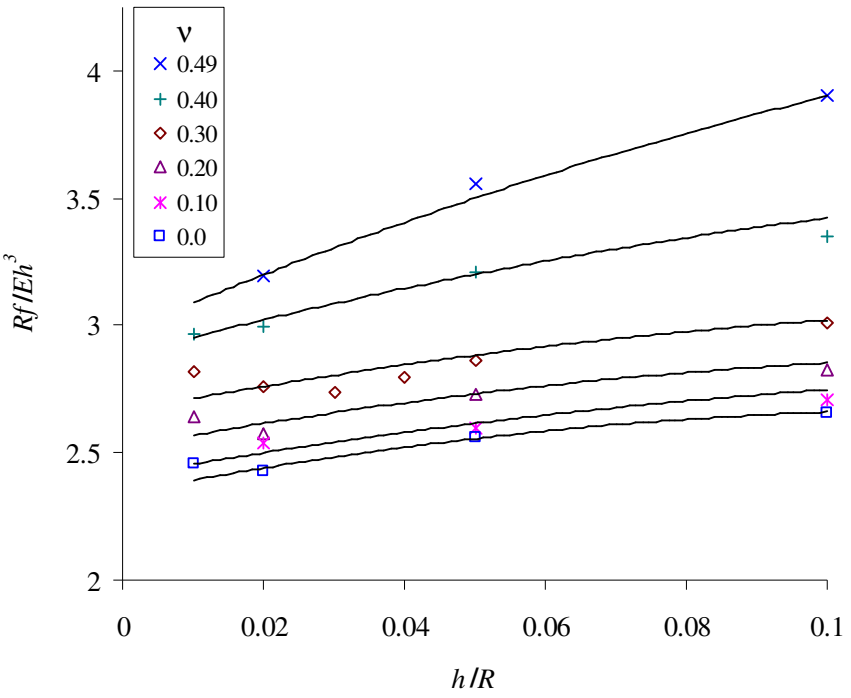

Figure 6.45: The normalised force versus radius where the value given is for the force at half of the buckling point, *f*.

6.2.5 The modelling of the mechanical behaviour of the hollow plastic sphere

To understand the behaviour of the elastomer material when filled with hollow microspheres, the mechanical behaviour of the single hollow plastic microsphere needed to be understood. This was achieved by physically testing the table tennis ball and using Abaqus FEA software to model their behaviour, in order to then provide confidence in the prediction of the mechanical behaviour of microsphere FEA models.

A number of types of model were developed, explicit models were found to model the buckling behaviour of the hollow spheres more accurately than implicit models. The three dimensional explicit models were better suited to higher deformations and accurately represented the buckling and folding that occurred at the higher displacements. The simpler axisymmetric explicit models were shown to accurately model the snap through buckling that occurred at smaller deformations, the Riks algorithm could be included to enable the buckling and folding phenomena to occur in an implicit model.

When the behaviour of the table tennis ball and microsphere in isolation was understood and could be modelled confidently, their behaviour when embedded in an elastomer could be modelled. In addition a method was developed where the wall thickness and modulus of a hollow sphere could be determined by using a simple uniaxial compression test.

The physical behaviour of a hollow plastic sphere embedded in an elastomer is explored in the following chapters, firstly using physical test pieces and then by FEA modelling to understand the single embedded microsphere and the microsphere filled elastomer.

Chapter 7 The mechanical behaviour of a hollow plastic sphere embedded in an elastomer

7.1 Introduction

The behaviour of a single hollow plastic sphere embedded in an elastomer is examined in this chapter. The previous chapters have examined the mechanical behaviour of hollow plastic spheres of different length scales, namely a microsphere and a table tennis ball, both experimentally under uniaxial compression tests and also by FEA modelling of the same behaviour.

To examine how these hollow spheres might behave when incorporated into rubber matrix, simple single hollow plastic spheres were embedded in translucent elastomer cylinders to create a simple unit cell. These were manufactured by embedding a single table tennis ball into a silicone rubber cylinder. The mechanical response of this test piece was measured carefully during uniaxial compression and uniaxial tension tests. The results of these measurements are contrasted in the following chapter, Chapter 8, with results from simple FEA models of unit cell elastomer cylinders containing a hollow plastic sphere.

7.2 Elastomer and Test Piece Manufacture

7.2.1 Introduction

The elastomer used to manufacture the cylindrical test pieces was the same translucent silicone elastomer as used for the other test pieces used throughout this study. As the volume of rubber used in each cylinder was quite large it was necessary to prepare sufficient rubber to produce at least one test piece at a time.

The various aspects of the test piece manufacture are described here including the technique to remove air bubbles entrapped during the elastomer mixing and preparation as well as the method used to ensure that the table tennis ball was centred within the elastomer cylinder.

7.2.2 Preparation of Elastomer material

The manufacture of the elastomer material is described in Chapter 3. The same silicone elastomer was used for the cylinder test pieces for a number of reasons; the

translucent nature of the material allowed the table tennis ball to be observed during the experiments, the mixing process was familiar and the use of a single elastomer type added continuity to the study.

The two part elastomer system was again mixed with a ratio of 95 % of the high viscosity component with 5 % of the corresponding lower viscosity catalyst component. The two liquids were stirred thoroughly to ensure that the resulting elastomer was homogenous, but the stirring process inevitably introduced air bubbles entrapped in the mixture. Bubbles introduced into the mixture were not a problem for the batches made for the previous test pieces, as for example, the dumbbell test pieces, which are relatively thin and allow any air bubbles to easily rise to the surface and escape. However due to the large volume of these unit cell cylinders, initial prototype moulding suggested this was no longer possible as the initial trial indicated that a large number of air bubbles remained after curing, therefore a novel preparation method had to be developed.

7.2.3 Manufacture of the Elastomer Cylinders with and without a table tennis ball

The two part silicone elastomer was mixed in an identical way, as for the manufacture of sheets from which the dumbbell test pieces were cut to characterise the material, but in larger quantities to fill the larger mould. The plastic pot was used for the moulding of the cylindrical test pieces which allowed cylinders to be produced that were 80 mm in diameter and approximately 80 mm in height, these dimensions would allow a table tennis ball with a diameter of 40 mm to be embedded centrally in the moulded test pieces with a volume fraction of approximately 8.5 %.

The silicone elastomer had a typical pot life of an hour but once poured into the much larger mould this was found to be too short, probably due to the larger volume of the test pieces produced. Therefore it was presumed that a full cure would be achieved after about two days. After an initial 24 hours, it was easy for the test pieces to be removed from their moulds, they were they were then left for at least another twenty four hours prior to testing to ensure that the material had cured fully.

Figure 7.1 shows the pot with a cut down one side. This facilitated the removal of the test piece from the mould after the initial 24 hour curing period, once the test piece was removed the pot was taped tightly to close the cut for the next test piece to be moulded.

a.  b. 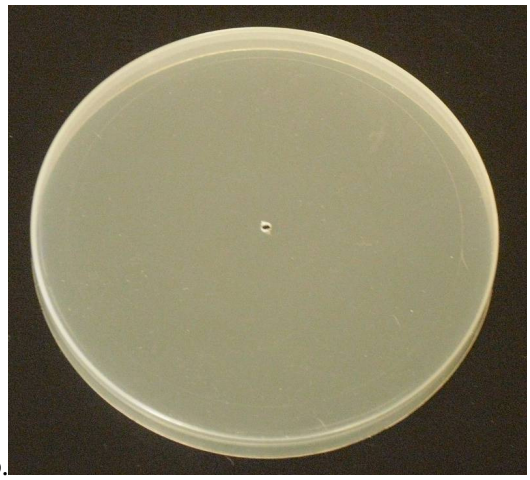

Figure 7.1: A photograph of the cut side of plastic pot used as a mould for the silicone elastomer test pieces (a) and the hole in the lid (b).

During the curing process the mould was kept level by using a spirit level with small pieces of paper placed under the mould to act as shims. The lid was kept on the pot but slightly ajar, this was to keep dust off, but allowed the material to "breathe". The entire curing process was conducted at a room temperature that was always in the range of 21 ℃ to 25 ℃.

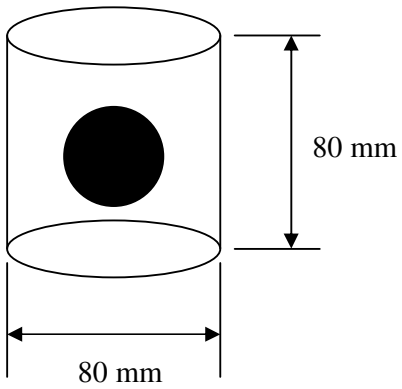

Figure 7.2: A schematic of the table tennis ball embedded in the elastomer cylinder.

Figure 7.2 shows the dimensions of the mould in relation to the table tennis ball, the diameter of 40 mm for the table tennis ball allowed it to be positioned centrally within the test piece.

The cylinder test pieces were all produced with a "Stiga Master" table tennis ball, the same type that had been used previously during the compression tests of the single table tennis balls. The initial test pieces were produced with a completely

unmodified table tennis ball, this created two significant problems. Firstly, the hollow table tennis ball floated upwards significantly in the viscous mixture, until the mixture had cured sufficiently for the matrix elastomer viscosity to increase to a point where it becomes locked in place. This in turn meant that the mould had to be repeatedly turned upside down and then upright to attempt to keep the table tennis ball central, both horizontally and vertically, in the mould. The second problem resulted from the entrapped air which was also not allowed to escape from the elastomer matrix. An initial test piece that had a table tennis ball in it is shown in Figure 7.3, the air bubbles can clearly be seen, as can an enlarged air cavity where the table tennis ball was positioned.

Figure 7.3: A photograph of an initial test piece with a table tennis ball embedded in the elastomer cylinder (cut open to show the trapped air and to remove the buckled table tennis ball after compression testing).

After the initial test piece had been produced the method was altered slightly for subsequent test pieces. Prior to pouring the mixed silicone elastomer into the mould it was first poured into an empty plastic dish, approximately 200 mm in length, by 150 mm in width. The plastic dish was then placed in a vacuum machine where the air was removed, this caused the air bubbles to evacuate from the mixture. The process usually ensured that most of the air bubbles were removed. The elastomer was then very

carefully poured into the mould to minimise the amount of air bubbles entrapped during the pouring phase. The mixed elastomer had a pot life of approximately one hour, this allowed sufficient time to fill the mould and work the elastomer before it began to cure and stiffen.

This method was a significant improvement but there were still a small number of air bubble present in all of the tests. The top of one of the better test pieces is shown in Figure 7.4, there are a few dimples evident on the top surface of the cylinder which are produced by a small number of air bubbles breaking the surface of the elastomer before it had cured.

Figure 7.4: A photograph of the top surface of a silicone elastomer cylinder test piece.

Unfilled elastomer cylinders that did not contain a single sphere were relatively straightforward to produce compared to the cylinders containing a table tennis ball, despite the difficulty in eliminating trapped air bubbles.

It was also noticed that the white table tennis ball appeared to be somewhat indistinct when embedded into the elastomer material. The more advanced test samples were produced using table tennis balls that had been painted black to give them a better contrast in the translucent elastomer. The table tennis balls were painted with black enamel paint used for plastic model kits and they were allowed to dry for twenty-four hours prior to being embedded into the rubber matrix, as shown in Figure 7.5.

Also to prevent the balls from floating in the elastomer mixture as it cured the table tennis balls were pierced on the top and bottom and a piece of cotton was passed through them, with a knot to prevent the table tennis ball from floating up the cotton when placed in the mould. The mould also had a hole pierced in the centre of the bottom

surface and in the centre of the lid for the cotton to pass through, to ensure that the table tennis ball was located centrally as the rubber cured.

The cotton was tightened to reduce any slack, the bottom piece of the cotton was taped to the bottom of the mould in such a position that the table tennis ball was approximately central in the mould vertically. The mixed silicone was then poured into the mould to a height of approximately 80 mm and by pulling the cotton tight and taping the top piece of the cotton to the top of the mould ensured that the table tennis ball was also held in the centre of the horizontal plane.

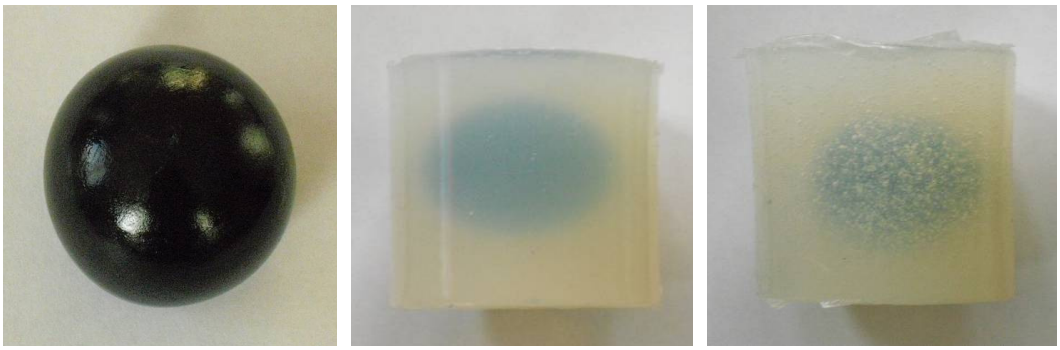

Figure 7.5: A photograph of a table tennis ball painted black and within two cylinder test pieces (one almost totally devoid of air bubbles and one with a significant number of entrapped air bubbles).

Once the elastomer mixture had cured enough to be sufficiently viscous to prevent the table tennis ball from floating, the cotton was pulled fully out of the mould through the hole in the top of the lid. The lid remained on the mould to keep dust off, but the hole in the lid also allowed air in and so the material was able to "breathe"

The test piece was then allowed to cure for twenty four hours before being removed from the mould and was left at room temperature for at least another twenty four hours prior to testing. A similar process was adopted for all of the elastomer cylinders containing a table tennis ball described in this thesis.

7.3 Physical Testing of Test Pieces

7.3.1 Introduction

Uniaxial compression and tensile tests were conducted for unfilled and filled silicone elastomer cylinders. The main aim was to test cylinders with a table tennis ball

embedded in them as the table tennis balls had been shown to be a suitable physical model for the microsphere in isolation and to manufacture and then observe a single microsphere embedded in an elastomer would be much more difficult. The size of the table tennis ball should allow any initial dewetting of the elastomer from the table tennis ball and later buckling of the table tennis ball to be observed. Cylinders without a table tennis ball were also tested to enable a comparison to be made between a hollow sphere filled and an unfilled elastomer material.

7.3.2 Compression Testing of the Elastomer Cylinders

A series of compression tests were conducted on solid unfilled silicone elastomer cylinders, without a table tennis ball embedded in them. The tests were conducted using a screw driven Instron 5584 mechanical testing machine.

The Instron machine crosshead was fitted with a 5 kN load cell, the machine had a flat steel plate placed directly below the axis of the load cell to provide a flat stable surface on which the test piece was placed. The steel plate was also of sufficient mass to not move during testing. A smaller flat plate was positioned on the top surface of the test piece to create a sandwich testing configuration, with the test piece between two flat rigid steel plates.

The crosshead of the Instron machine was fitted with a ball and socket adapter with a flat base. This flat base was easily aligned against the upper surface of the top steel plate due to the presence of the ball and socket joint. This ensured that the system was not significantly altered by any small misalignment and the force applied by the descending crosshead would be more reliable than if a completely rigid system was used. The downward rate of the crosshead was 5 mm/min.

The first cylinder was compressed until the maximum load of approximately 4950 N was reached, which equated to a compression of approximately 40 mm, or about half of the height of the cylinder. The results of the tests can be seen in Figure 7.6 where the compression of three different unfilled silicone cylinders is compared, the latter two test pieces were compressed by a displacement of 30 mm and 25 mm.

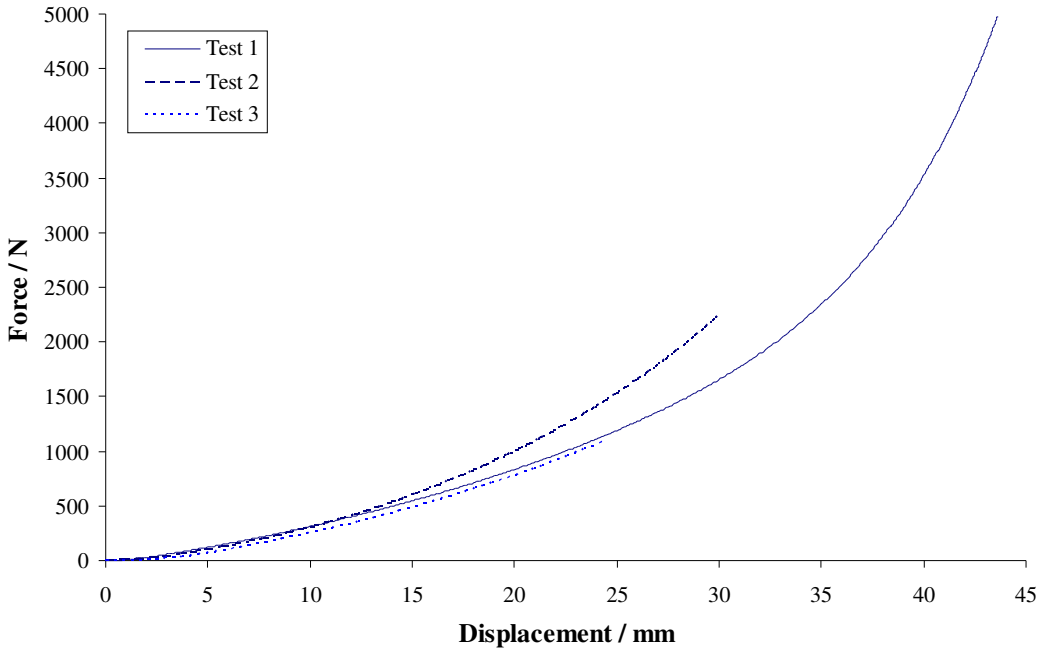

Figure 7.6: Compression tests of unfilled elastomer cylinders.

A subsequent test evaluated the amount of cyclic stress softening that was encountered in these test pieces. A similar process was conducted where the crosshead was again lowered manually with any slack being removed from the system and until a nominal force was indicated on the test machine.

This time the cylinder was compressed by 40 mm which corresponds to about 50 % of the test piece height. A dwell time of 30 seconds was introduced at this maximum displacement after which the load was then removed at a rate of 5 mm/min until the displacement returned to zero. After a 30 second unloaded dwell time the loading pattern was repeated cyclically.

Figure 7.7 shows the first three complete force versus displacement loading cycles. Here stress softening of the elastomer material can be seen with the subsequent loading cycles being slightly less stiff than the first. But the highly elastic nature of the materials is shown in that all three unloading curves follow an almost identical path. This is an example of the Mullins effect.

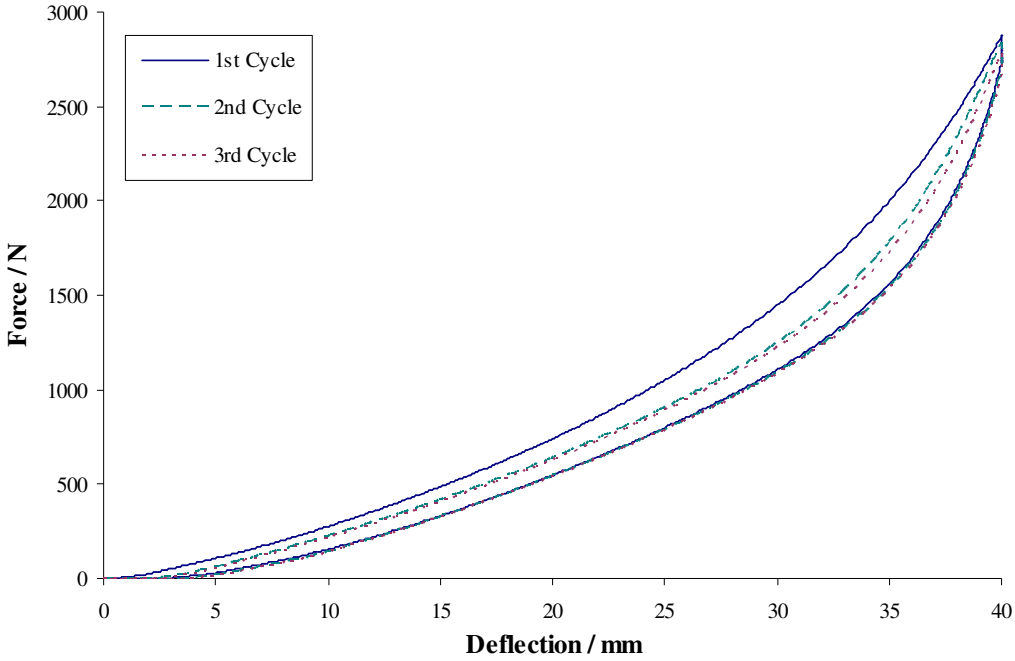

Figure 7.7: Compression test of an elastomer cylinder, repeated loading and unloading.

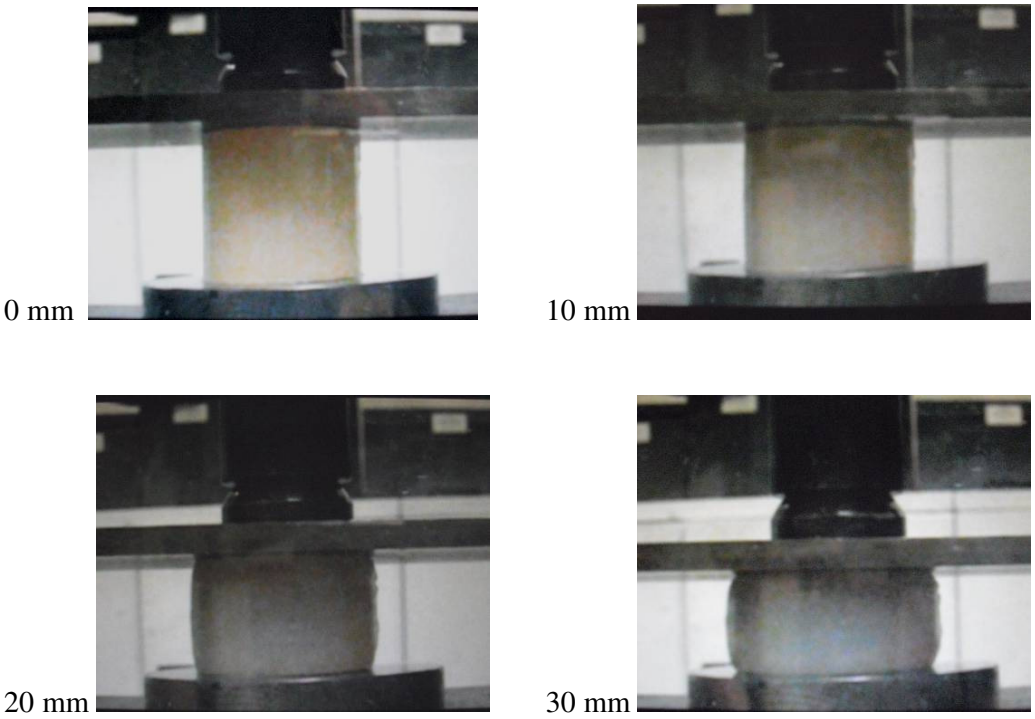

Figure 7.8: Compression test of unfilled elastomer cylinder.

Figure 7.8 shows a series of photographs taken from a video that was recorded during a compression test of an unfilled elastomer cylinder. The cylinder can be seen to

barrel at the larger deformations. Slippage at the top and bottom surfaces remained relatively modest throughout the tests. The displacement is shown in mm.

7.3.3 Compression Testing of the Elastomer Cylinders containing a table tennis ball

A series of compression tests were conducted on elastomer cylinders containing a single table tennis ball. The tests were all conducted using the same screw driven Instron 5584 mechanical testing machine as for the unfilled cylinder test pieces. Initial tests were conducted on less than ideal samples that contained both unpainted table tennis balls and which also had a large number of air bubbles entrapped as well as large air voids inadvertently incorporated during manufacture.

The crosshead test speed was programmed to descend at a rate of 5 mm/min. The maximum permitted force was set to 4980 N to protect the 5000 N rated load cell from being overloaded, the steel plate and ball and socket adapter were used as before. Prior to the start of the test the crosshead was lowered manually until it just touched the top steel plate and any slack caused by the ball and socket adapter was taken out of the system, at this point the force measured on the test machine was only of the order of a few Newtons.

The initial cylinders were tested twice. For the first test it was compressed to the maximum permitted force, this resulted in the cylinder being compressed by approximately 63 mm, compared to a cylinder height of about 80 mm. Once the maximum force had been reached the test stopped automatically.

For the second test the crosshead was then raised and the test repeated using the same test method and the same test piece, here the maximum compression was approximately 55 mm. In all of these compression tests reported here the maximum force reached was approximately 4950 N. The force and deflection data was collected for all tests using a PC attached to the Instron machine. The data was later analysed using Microsoft Excel.

The results of the first and second tests are shown in Figure 7.9, during the first test the curve produced shows that the cylinder is initially stiffer. The buckling of the table tennis ball as a hollow sphere can also be seen where the force drops a number of times. The curve of the second test is much lower, indicating that the test piece is behaving more like a cylinder containing a hollow void rather than like a cylinder reinforced using a hollow plastic spherical shell.

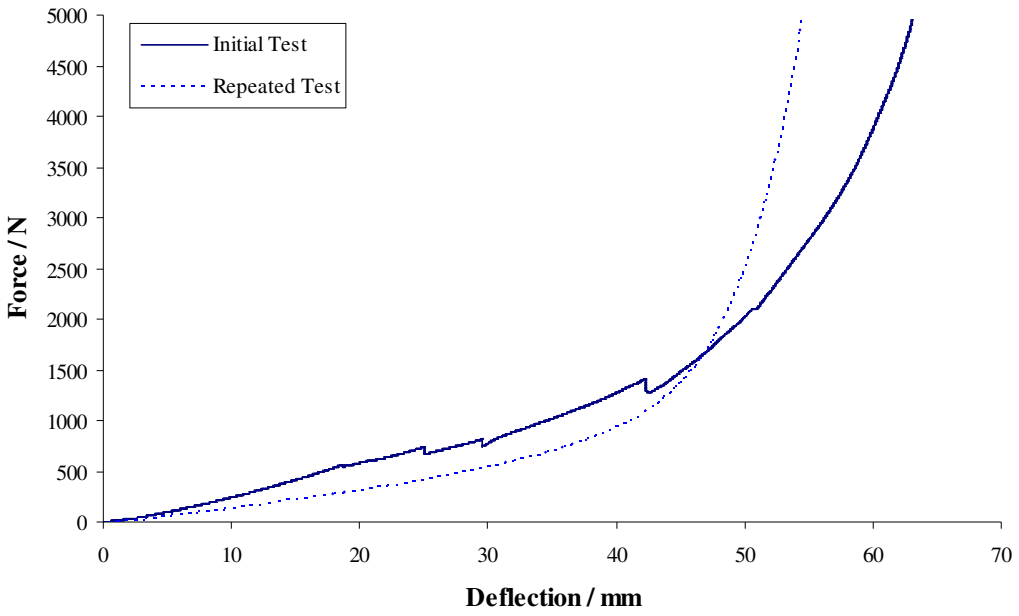

Figure 7.9: The first compression test of an elastomer cylinder containing a table tennis ball, repeated for the same test piece.

However the force does rise sharply beyond a deformation of 45 mm, this could be due to the now compressed table tennis ball moving within the sample, perhaps to align more into a vertical position and providing an increased stiffening effect to the cylinder.

a. b.

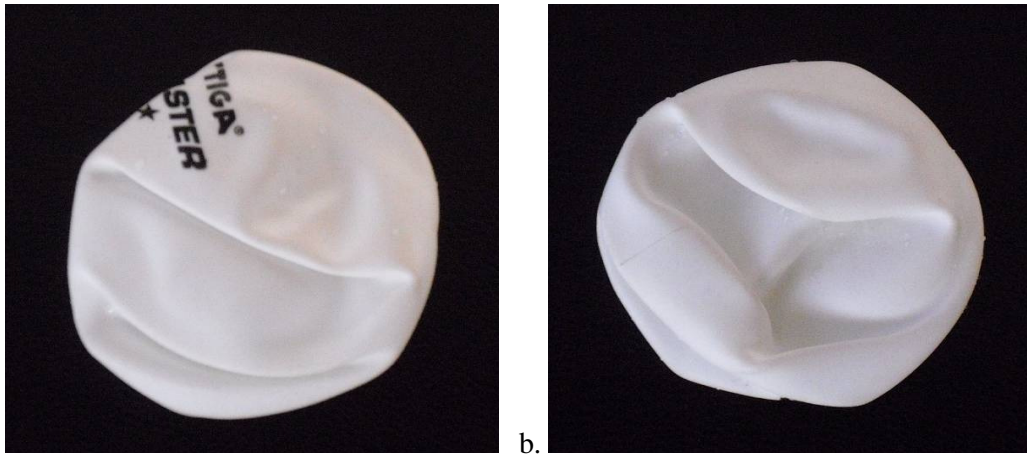

Figure 7.10: The table tennis ball removed from the first elastomer cylinder.

The table tennis ball was cut out after testing from the elastomer cylinder test piece as shown in Figure 7.10. The table tennis ball was plastically deformed into a permanent squashed shape, but not to the same extent as the table tennis balls compressed in isolation. The lower surface, image "b", shows an almost triangle shaped folding pattern. The buckling was also severe enough to cause the table tennis ball to split, a phenomena that was not observed for the table tennis balls compressed in isolation.

The experimental method was repeated for a number of cylinders containing a table tennis ball. These experiments used a table tennis ball that was painted black and used the method described previously to ensure that the table tennis ball was central in the moulded elastomer and did not contain significant entrapped air voids.

The results from two of these subsequent tests are shown in the Figure 7.11, the buckling of both table tennis balls is clear in each graph at 18.5 mm and 20 mm.

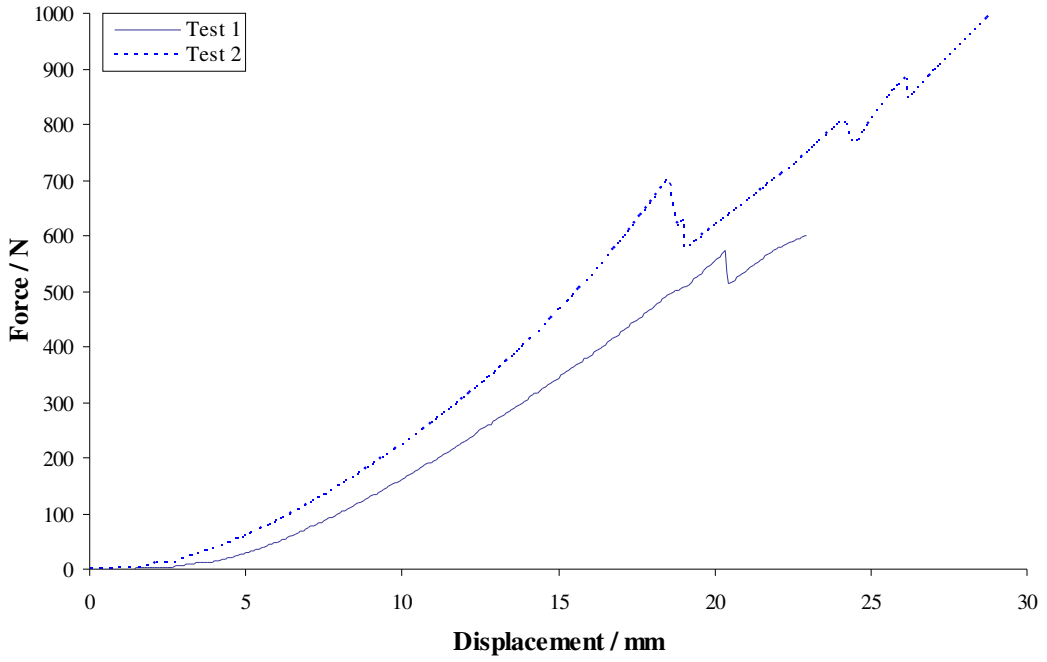

Figure 7.11: Reproducibility of compression tests of a table tennis ball filled elastomer cylinder.

Figure 7.12 shows a series of still images taken from a video that was recorded during a compression test of an elastomer cylinder containing a table tennis ball, the crosshead displacement is indicated in mm. The cylinder can be seen to barrel,

particularly at the larger deformation but the central section of the cylinder also flexes inwards due to the constraints provided by the table tennis ball and a double barrelling occurs. The top and bottom surface remained fairly static throughout the tests, with minimal slippage in the horizontal plane at the interface.

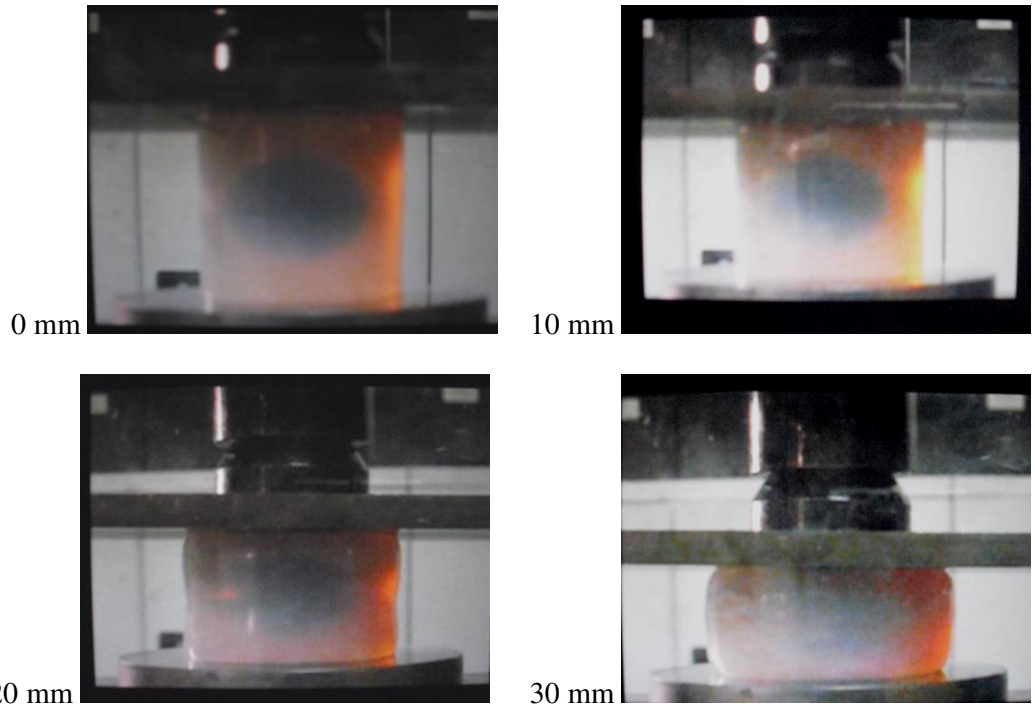

Figure 7.12: Compression test of elastomer cylinder containing a table tennis ball.

Figure 7.13 shows two painted table tennis balls after a compression tests. The upper two images are of a table tennis ball from a silicone cylinder that was compressed to a displacement of 23 mm. The top half of the table tennis ball was unchanged, but clearly the bottom half had buckled to form a triangular pattern. The lower two images are of a table tennis ball from a silicone cylinder that was compressed to a displacement of 30 mm, the table tennis ball itself is compressed almost flat. The top and bottom poles of the ball were relatively undeformed, it is interesting that the shape of the moulded elastomer surface clearly alters the deformation pattern in compression, the most significant region of deformation therefore being a buckled and folded zone around the central horizontal plane.

Figure 7.13: A photograph of two buckled table tennis balls removed from the elastomer after compression testing.

7.3.4 Tensile Testing of the Elastomer Cylinders

A single test was conducted in tension to observe the behaviour of a silicone elastomer cylinder without a table tennis ball embedded in it. However, to test the test cylinder in tension on the Instron test machine, end plates were required. These end plates were manufactured from circular mild steel plates. The steel end plates were larger than the cylinders being tested and were approximately 10 mm in thickness. The end plates had a blind hole tapped to accept an 8 mm thread in order for them to be fitted to the adapter on the Instron 5584 test machine.

The silicone elastomer cylinders were then bonded to the steel plates. Various different adhesives were evaluated under peeling condition using a 20 mm by 20 mm by 1.5 mm test silicone sample bonded to a steel substrate to see which would be the most suitable and effective. A two part epoxy type adhesive and a contact adhesive both proved to be unsuitable and the best bond was achieved using a Superglue Gel. Further testing showed that the use of a Polyolefin Primer on the surfaces of the silicone cylinder prior to bonding improved the interaction. The surfaces of the elastomer

cylinder, in particular the top surface, were not always perfectly flat so bonding to the steel plates was difficult. This arose from both the samples not being kept perfectly horizontal during pouring and curing as well as air bubbles that reached the top surface of the material during cure. For these tensile tests the same Instron machine was used as before but it was now fitted with a 1 kN load cell. The test method was set up so that the crosshead was raised at a speed of 5 mm/min, the test was programmed to stop when the force dropped to zero, as would be the case if either the test piece tore or the test piece peeled or debonded from one or other of the steel end plates.

Figure 7.14 shows the results from a tensile test of an unfilled elastomer cylinder up to approximately 10 mm displacement, when the cylinder debonded from the bottom steel plate, this is shown in the figure by the force dropping rapidly.

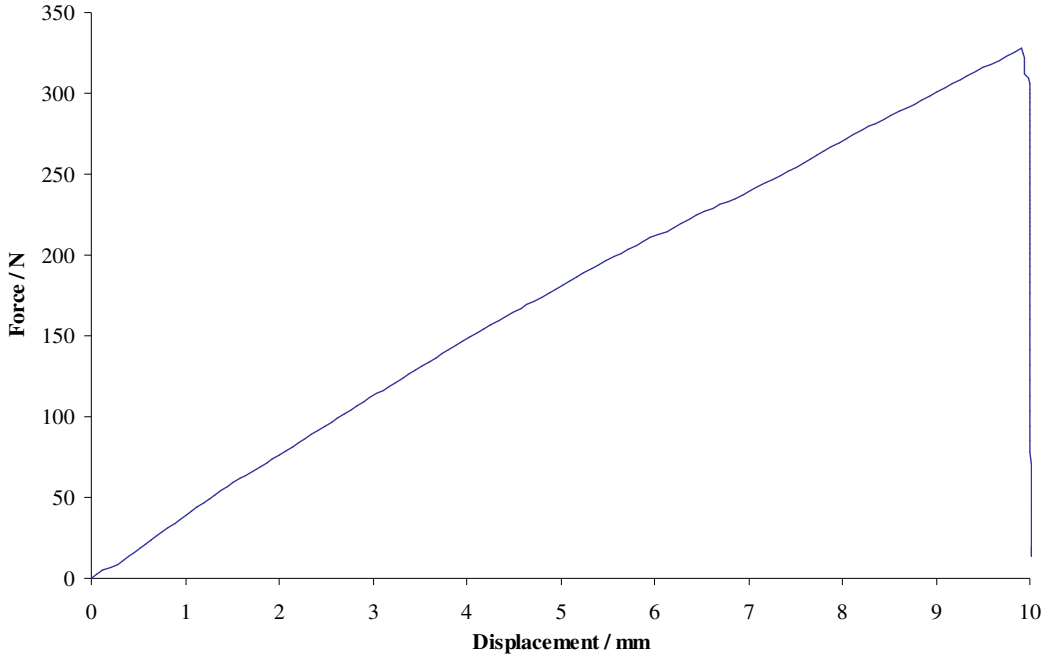

Figure 7.14: The results from a tensile test of an unfilled elastomer cylinder.

Figure 7.15 shows a series of photographs taken from a video that was recorded during the tensile test of the unfilled elastomer cylinder shown in Figure 7.14. The cylinder can be seen to neck slightly at higher displacements, but the diameter remains constant where it is bonded to the steel end plates. The peeling can be seen to start at approximately 7.5 mm deflection, the peeling then increased gradually up to 10 mm displacement when it accelerated rapidly and the test piece debonded completely from the bottom test piece.

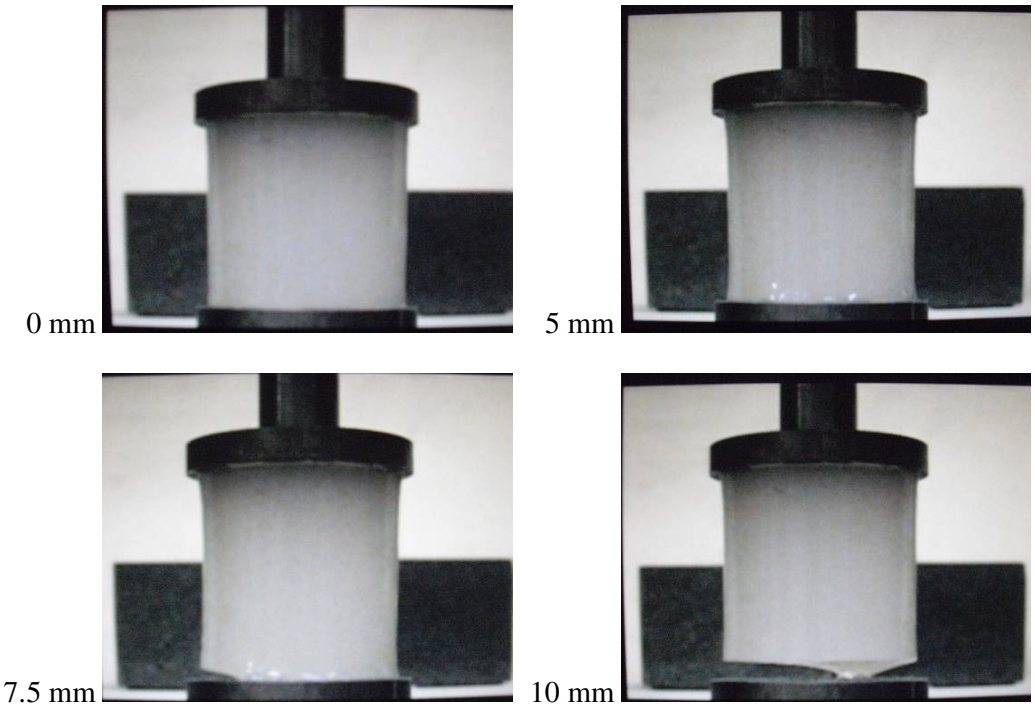

Figure 7.15: Tensile test of unfilled elastomer cylinder.

7.3.5 Tensile Testing of the Elastomer Cylinders containing a table tennis ball

Several different tensile tests were conducted using silicone elastomer cylinders that contained a table tennis ball. All of the test pieces contained a table tennis ball that had been painted black and an identical manufacturing method was used as for the previous test pieces.

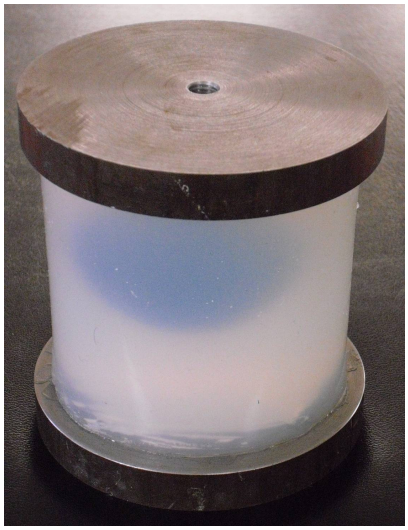

Figure 7.16: An example of one of the test pieces with a steel plate bonded to both ends.

The steel plates were again bonded to each end to enable the test piece to be attached to the Instron test machine, an example of the test piece with steel plates bonded to each end is shown in Figure 7.16.

The results of the tensile tests are shown in the Figure 7.17. Only small displacements, were achieved before the silicone cylinder started to peel from the steel end plate. Clearly testing in tension to large displacements was not possible without a stronger interfacial interaction between the cylinder and the end plates.

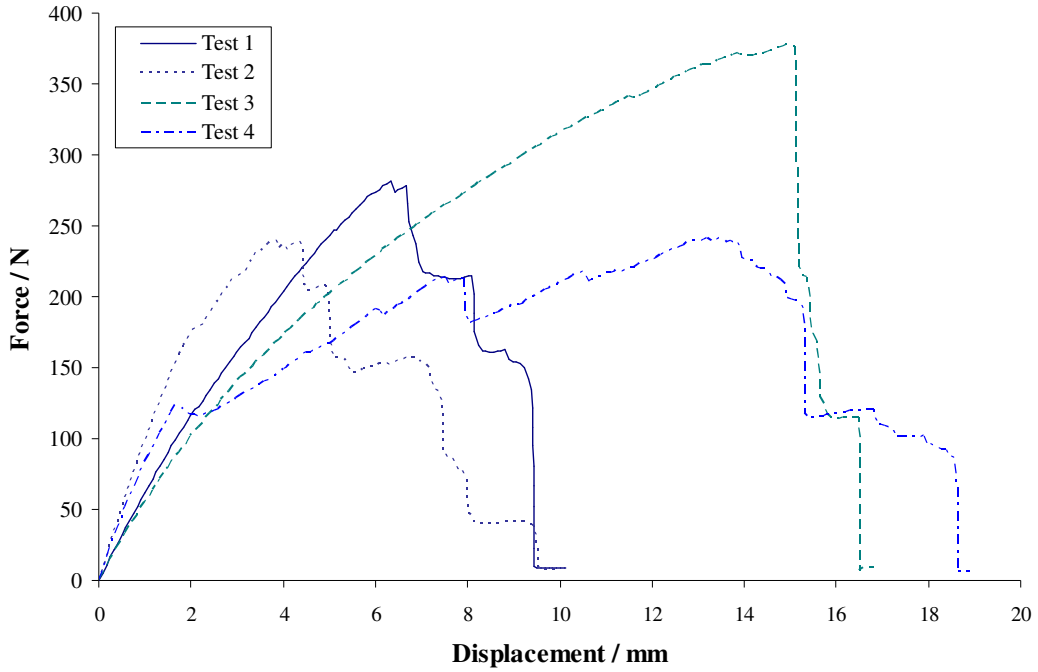

Figure 7.17: Four tensile tests of elastomer cylinders containing a table tennis ball.

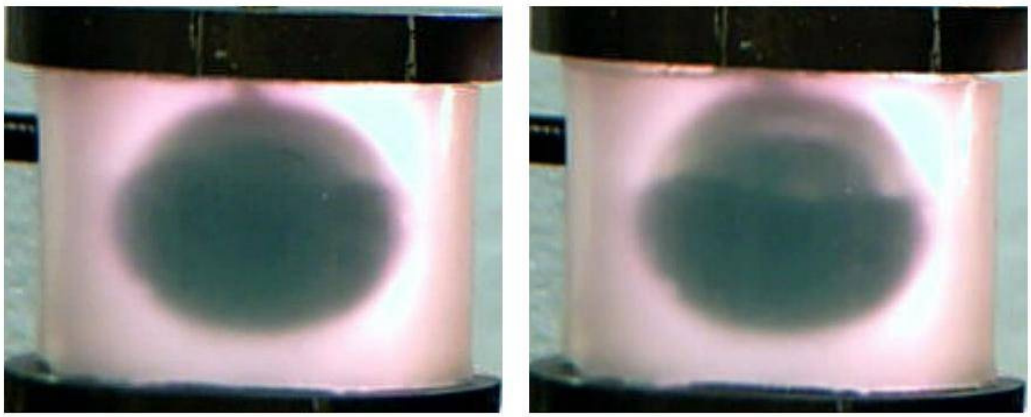

Figure 7.18: Photographs of a silicone elastomer cylinder test piece containing a table tennis ball during a tensile test.

The pair of photographs shown in Figure 7.18 were taken during one of the tensile tests. Dewetting between the table tennis ball and the elastomer material can be seen. However, the displacements are again relatively small and the cylinder can already be seen to have started to debond or peel from the steel plate.

In all of these tests the initial section of the Force / Displacement curve for each test is broadly similar, there is a slight difference in the apparent stiffness between each test piece, this could be due to the slight difference in height of each test piece. But it can be seen that the cylinders all started to peel from the steel end plates at small displacements, the best being at approximately 15 mm, the worst peeled slightly after only 2 mm.

Figure 7.19 shows a series of photographs taken from a tensile test of an elastomer cylinder containing a table tennis ball. The cylinder can be seen to neck slightly at higher deflections, but this is counteracted due to the stiffness provided by the table tennis ball. The elastomer cylinder started to peel from the steel end plate at displacement of approximately 10 mm.

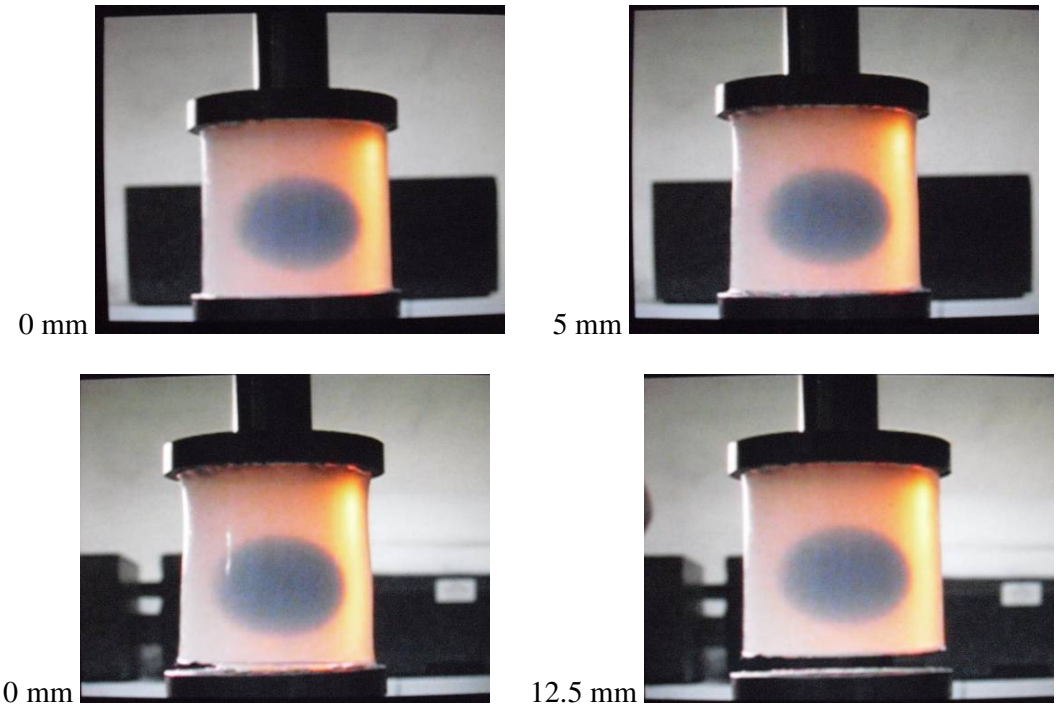

Figure 7.19: Tensile test of elastomer cylinder containing a table tennis ball.

Figure 7.20 shows the steel end plate after it had been peeled away from the silicone cylinder. Remnants of the bonding agent and some elastomer material can be

seen on the steel plate. Despite attempts at cleaning the steel surface and the elastomer surface meticulously and applying a suitable primer to the elastomer, it was clearly still difficult to affect a successful bond. The application of polyolefin primer did improve the bond, as initial tests without a primer fully debonded at less than 10 mm displacement, but subsequent tests with a primer applied debonded at nearer to 20 mm displacement.

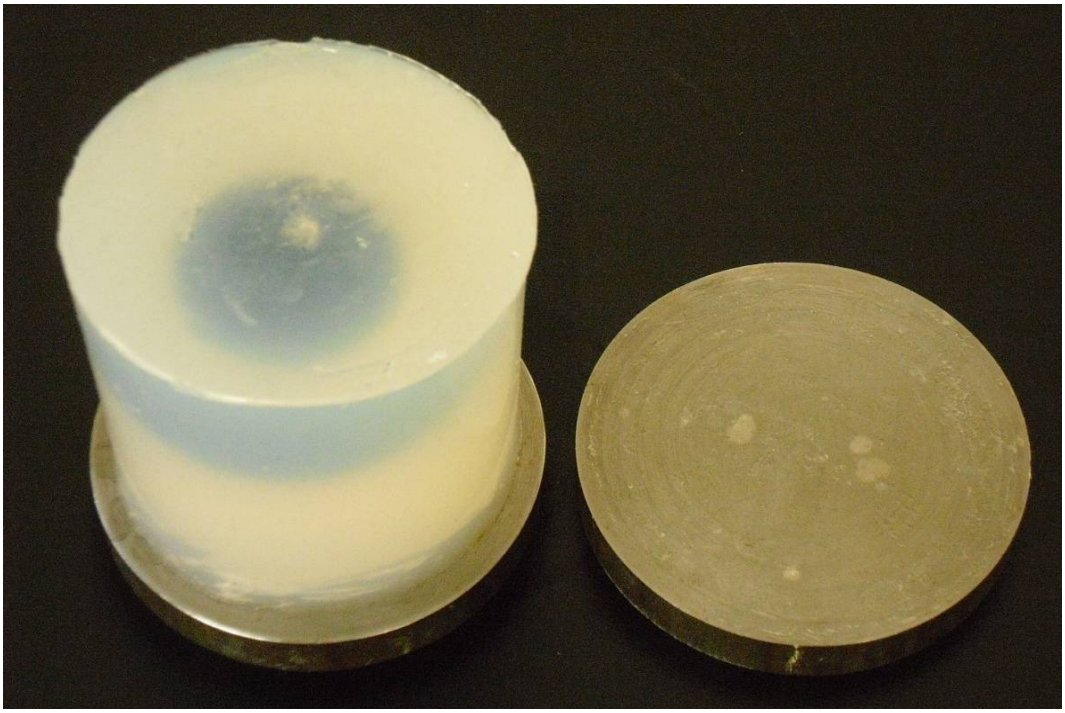

Figure 7.20: A silicone cylinder after the steel end plate had been peeled off.

Figure 7.21 shows three views of a cylinder having been tested in tension to a crosshead displacement of 10 mm. A vacuole is observed within the cylinder where the elastomer has dewetted from the table tennis ball. Dewetting was observed during the test at either end of the cylinder, three areas of dewetting at the top and two at the bottom. The side view also shows the significant dewetting at the top and the bottom of the ball.

Figure 7.22 shows the relationship between the table tennis ball that buckled to form a triangular pattern during a compression test and the dewetting produced between the table tennis ball and the elastomer surface within the elastomer cylinder during a test in tension. Red circles highlight that three points produced on the buckled table tennis ball correlate to the dewetted pattern.

Top 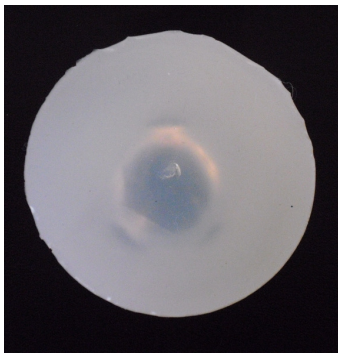 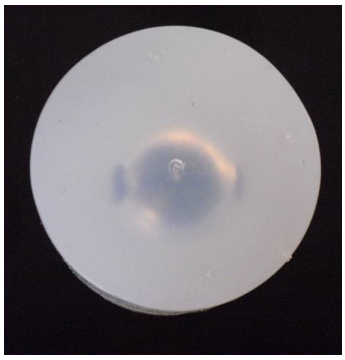 Bottom

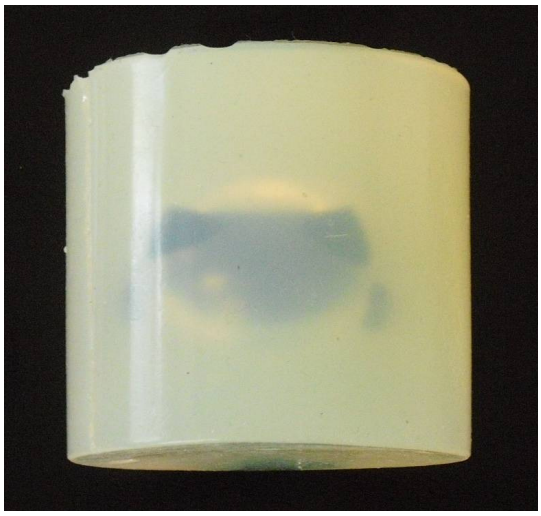

Figure 7.21: The top, bottom and side view of a cylinder showing dewetting of the elastomer from the table tennis ball.

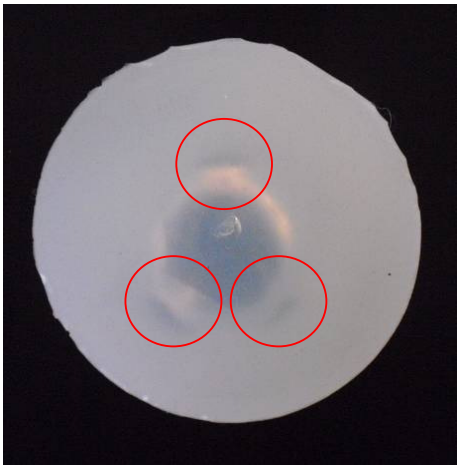 

Figure 7.22: A comparison of dewetting of the elastomer from the table tennis ball in compression and the buckled pattern seen on the table tennis ball after removal.

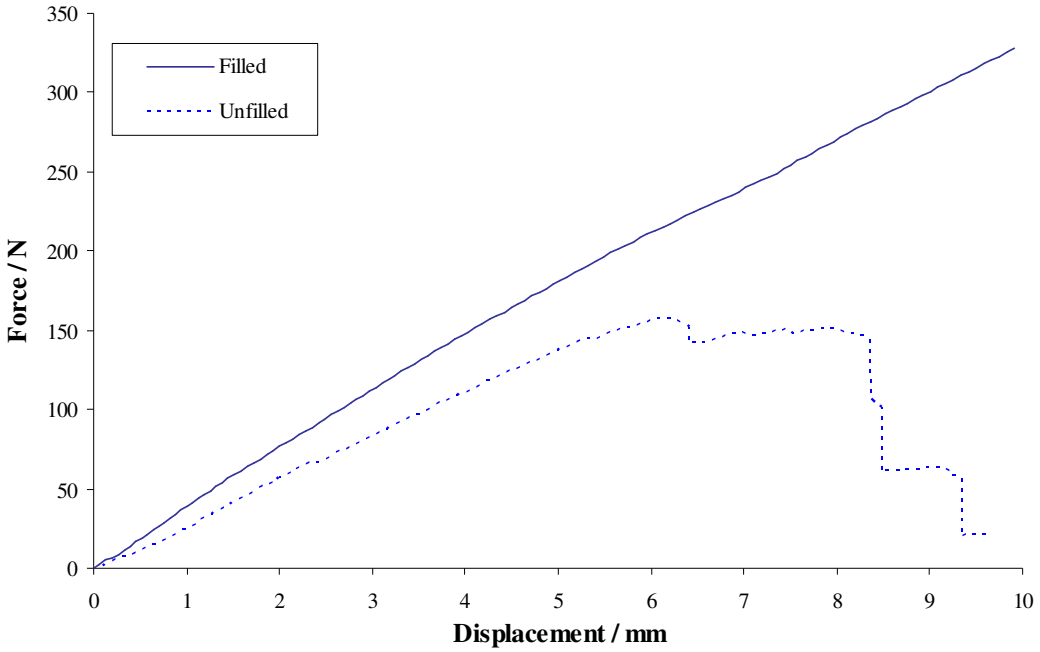

Figure 7.23: The results from tensile tests of an unfilled elastomer cylinder and one containing a table tennis ball.

The results of the unfilled test piece are compared to that of a filled test piece in Figure 7.23, where the unfilled cylinder started to peel at approximately 6 mm displacement. The initial Force v Displacement curve produced is less stiff for the unfilled test piece than those for the cylinders containing a table tennis ball, indicating that the table tennis ball as expected produced a stiffening effect on the material.

The physical behaviour of the elastomer cylinders both unfilled and containing a table tennis ball have been examined. The compression tests provided useful information as to the buckling behaviour of the hollow sphere when embedded in the elastomer material. The tensile tests showed that the individual hollow sphere had a stiffening effect at low strains, which had been previously observed for the elastomer material filled with hollow microspheres. The tensile tests were not able to show the behaviour beyond the initial small displacements. FEA would therefore be required to show the behaviour at small displacements as well as predicting the behaviour at much larger displacements.

Chapter 8 Modelling the mechanical behaviour of a hollow plastic sphere embedded in an elastomer

8.1 Introduction

This chapter examines the behaviour of hollow sphere filled elastomer materials using a finite element modelling behaviour. The approach adopted is to develop suitable representative volume elements that can effectively model the behaviour of both the bodies that contain large single spheres as well as the behaviour of systems that contain a dispersion of microspheres.

The models were developed to examine different phenomena in compression and in tension and are compared to the physical behaviour of the elastomer matrix and hollow sphere at small and wherever possible at larger displacements. A range of filler volume fractions was modelled. The approach is validated in compression deformation modes at small strains and at larger displacements and in tension the model is validated at small strains and then extrapolated to predict the behaviour at larger displacements.

8.2 Finite Element Analysis Modelling

8.2.1 Introduction

Both three dimensional representative volume elements as well as axisymmetric representative models were used to model and to understand the behaviour of how a single hollow sphere embedded in an elastomer matrix would deform and this was compared to both the model experiments on single spheres as well as for the bulk elastomer filled with a range of different volume fractions of the hollow microspheres.

8.2.2 Three dimensional models

Initial representative volume element models were created to represent a $1/8^{th}$ symmetric model of a sphere within an elastomer matrix. The geometry embedded the $1/8^{th}$ model of the hollow sphere into a cubic shape for the elastomer matrix. This type of model required an accurate representation of the symmetry constraints in all three symmetry planes that were present through the centre of the sphere. The model was

again created using Ideas. A typical final meshed geometric model can be seen in Figure 8.1. None of the three dimensional models developed contained a separate geometry to represent a filler particle, but used the curved inner surface to represent the outer surface of a spherical filler particle.

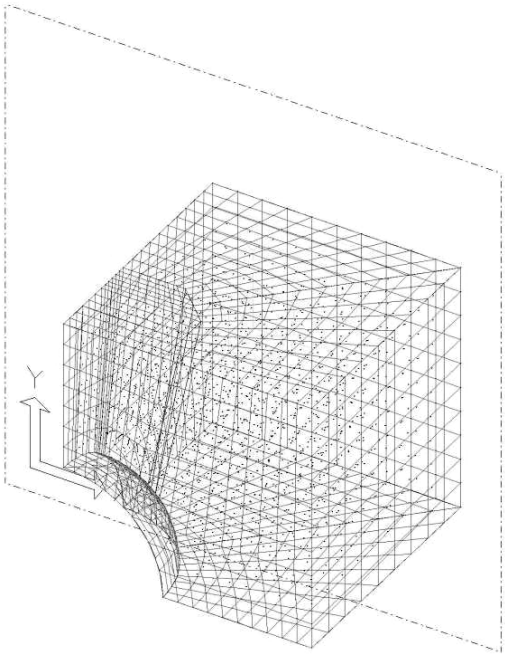

Figure 8.1: A three dimensional wireframe representation of the elastomer geometry created using in Ideas software.

a. b.

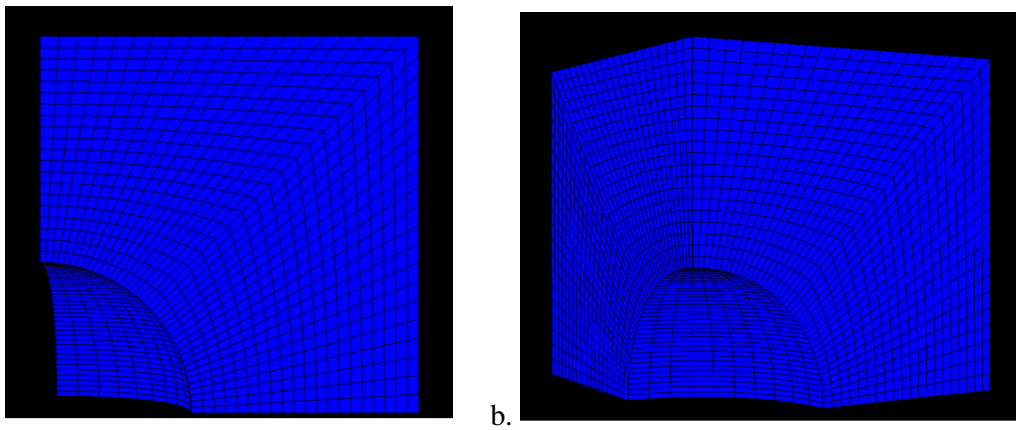

Figure 8.2: The three dimensional solid model in Abaqus software, side view (a) and edge view (b) showing the mesh.

Figure 8.2 shows the geometry imported into Abaqus. Image “a” shows a side profile with a spherical portion that represents the outer surface of the sphere within the elastomer matrix material. This can be seen more clearly in the angled view in image “b”.

Models can easily be deformed in both tension and compression. To do this the entire set of nodes on the top surface were moved either up or down in the vertical direction. The nodes on the bottom surface were free to only move in the horizontal plane. The nodes on the innermost vertical edge were only allowed to move vertically. The nodes around the equator of the spherical filler were not allowed to move in any direction. Finally the nodes on the vertical surfaces of the model were not constrained.

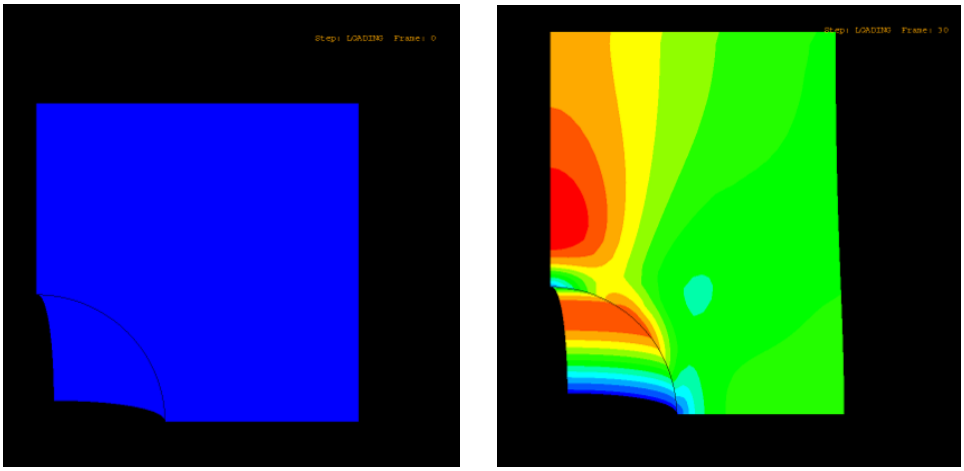

Figure 8.3: Side view of the three dimensional model with a bonded solid rigid spherical filler in tension.

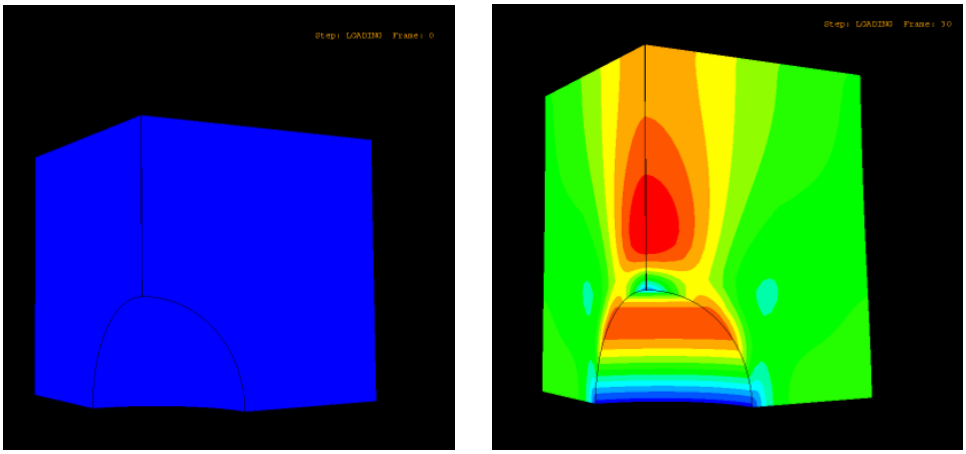

Figure 8.4: Angled view of the three dimensional model with a bonded rigid filler in tension.

The model was initially run as if the spherical filler were perfectly rigid. The model was firstly run to simulate what would happen if this rigid sphere were perfectly bonded to the matrix material; the second case was for a rigid sphere where the matrix material was unbonded.

Figure 8.3 and Figure 8.4 show the model with a bonded spherical filler in tension, for each figure the unstrained state is shown as are the corresponding stages of deformation. It can be seen that the highest principal stresses, represented by the contours, occur at a region above the filler particle, this is particularly evident in the angled view.

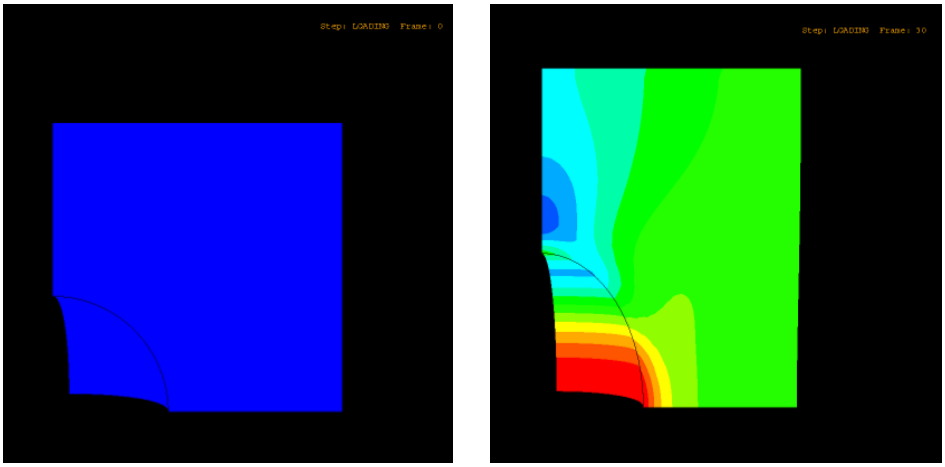

Figure 8.5: Side view of the three dimensional tensile model with an unbonded rigid filler in tension.

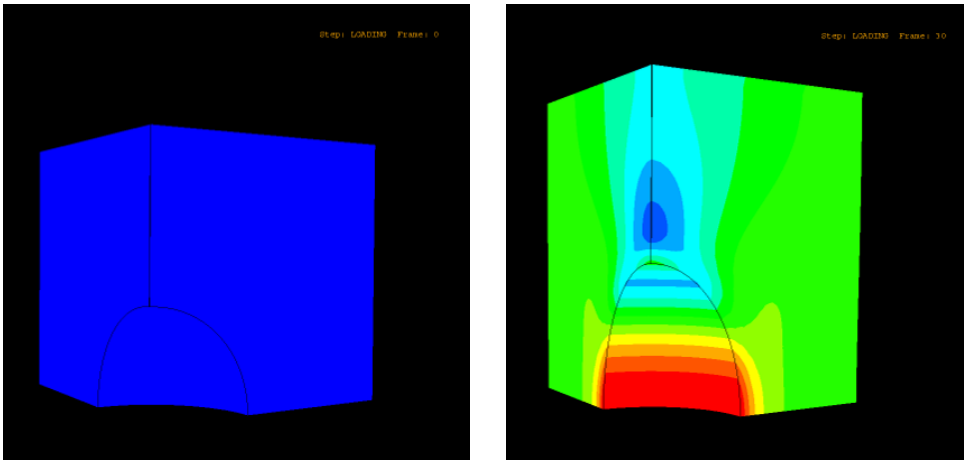

Figure 8.6: Angled view of the three dimensional model with an unbonded rigid filler in tension.

Figures 8.5 and Figure 8.6 show the model with a spherical cavity to represent an unbonded spherical filler in tension, again for each figure the unstrained state is shown as are the corresponding stages of deformation. It can be seen that the highest principal stresses occur at a region around the equator of the filler particle.

The three dimensional models showed that where a rigid spherical filler particle is perfectly bonded to the elastomer matrix material, the highest principal stresses in the elastomer matrix material occur at a region above the particle. This would suggest that in tension when the filler particle is bonded to the elastomer material, cavitation and debonding could occur above and below the filler particle. High stresses were also indicated around, but not quite at, the pole of the filler particle, this would indicate that debonding would occur at this region, as was seen in Chapter 7. The unbonded models indicated that the highest principal stresses occurred at the equator of the rigid particle, which would suggest that some debonding could occur in this region, although in tension the matrix material would tend to be compressed against the filler particle.

The three dimensional models were computationally too complex with the limited computing power available at the time to model a debonding between the rubber and the fillers, or for that matter any contact with associated sliding that might arise in the case of a real filled material. However they proved useful for visualising where the stresses occur over the surface of the filler for the two limiting cases. In this case the presence of the spherical filler was achieved only by constraining specific nodes. As the axisymmetric models had been a useful approach for modelling the hollow spheres in isolation in Chapter 6 they were therefore used for the rest of the modelling in this chapter of the modelling of the behaviour of an elastomer filled with a compliant soft hollow filler.

8.2.3 Two dimensional models

The development of the axisymmetric models for a single hollow sphere had produced reliable results in Chapter 6. The simplification of the geometry in such a manner had a dramatic impact on solution times and meant that much more complex behaviour could be examined. The following axisymmetric models were developed to replicate a hollow plastic sphere embedded in an elastomer matrix material. These models were viewed in two dimensions and also revolved to help generate a reasonable three dimensional visualisation. The model is symmetric both around the axis of

revolution as well as in the horizontal plane about the equator of the hollow sphere. The volume fractions and the other dimensions used were similar in scale to the dimensions of the cylinders that had been used during the physical experiments of a table tennis ball embedded in the silicone elastomer cylinder. The axisymmetric models were conducted as an explicit analysis, which had proved more capable of replicating the buckling of the hollow plastic sphere particularly at larger strains.

8.2.4 FEA modelling of an Elastomer Cylinder containing a table tennis ball in Compression

The axisymmetric models were conducted in compression, to replicate the behaviour of the silicone elastomer cylinders and the table tennis balls in compression. This was achieved by producing a model with an elastomer matrix with elastomer materials properties including the Yeoh values described in Chapter 3 and containing a separate geometry of the hollow sphere with plastic properties as obtained in Chapter 3. The models had the two components in contact but not bonded, friction between the outer surface of the hollow sphere and the elastomer matrix was ignored.

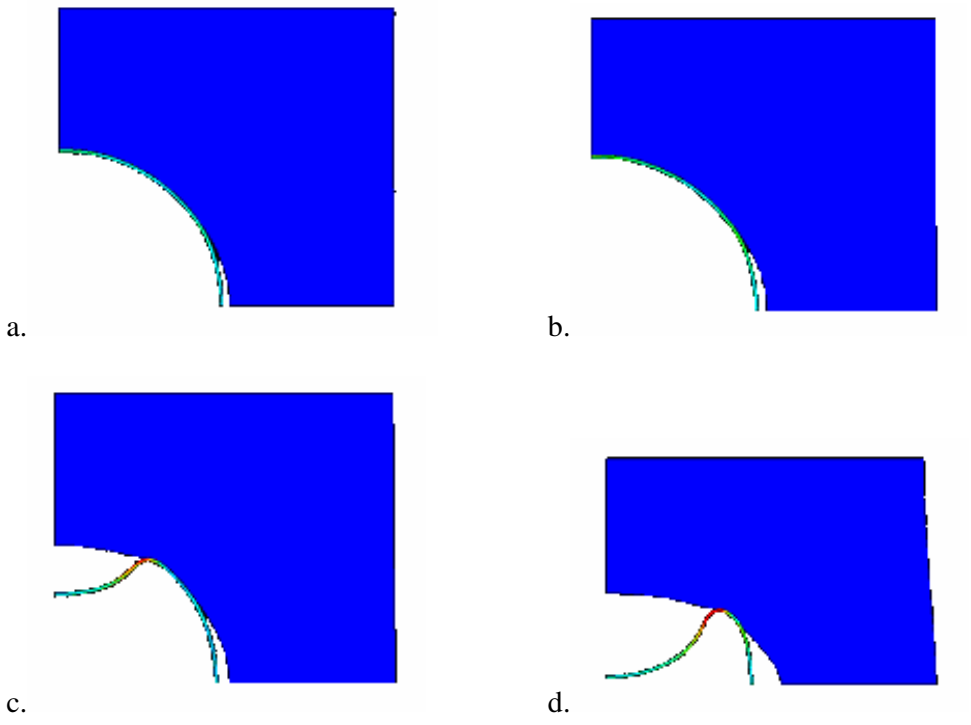

Figure 8.7: Images showing stages of compression of axisymmetric model of table tennis ball embedded in elastomer cylinder.

Figure 8.7 shows a model with a compressive force being applied to the top surface of the elastomer. The initial deformation is shown in image "a" where the lower portion of the elastomer has moved away from the hollow sphere, this movement is continued in image "b", where the top surface of the hollow sphere has also become flattened. Image "c" shows the sphere post snap-through buckling and image "d" shows the cylinder barrelling and the hollow sphere buckled to the point where self contact occurs. The hollow sphere, in this case a table tennis ball, has buckled in an identical manner to the axisymmetric models of the table tennis ball as a single component shown in Chapter 6.

The following figure, Figure 8.8, shows the fourth image from Figure 8.7, revolved through 180 degrees to generate a three dimensional visualisation at the point where the internal surfaces of the hollow plastic sphere have contacted each other.

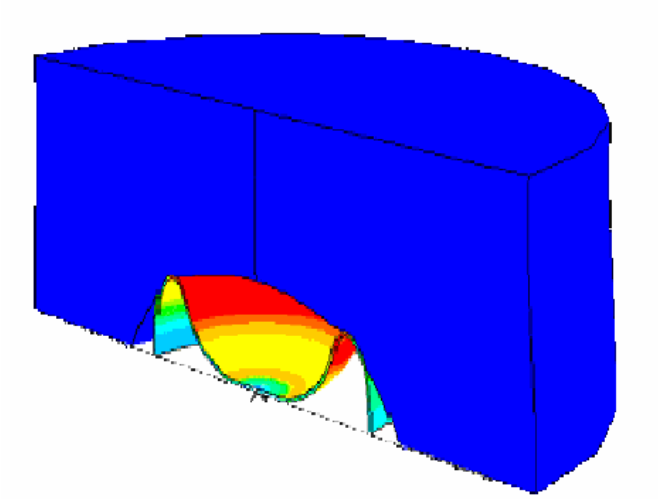

Figure 8.8: Image showing final compression of the axisymmetric model of table tennis ball embedded in elastomer. This half symmetry model is revolved through 180 degrees to enhance visualisation.

The model was reproduced for the same hollow plastic sphere size but where the elastomer matrix size was varied to represent different filler volume fractions. Further models were also produced without a hollow plastic sphere to represent a foamed elastomer model containing a void of the same size as the hollow plastic sphere. Further models were developed for the situation where the hollow plastic sphere was perfectly bonded to the elastomer matrix.

8.2.5 FEA modelling of an Elastomer Cylinder containing a table tennis ball in Tension

The model shown in the previous figures was repeated, but instead of compression a tensile force was applied to the top surface of the elastomer. Further axisymmetric models were conducted, to replicate the behaviour of the silicone elastomer cylinders and the table tennis balls in tension.

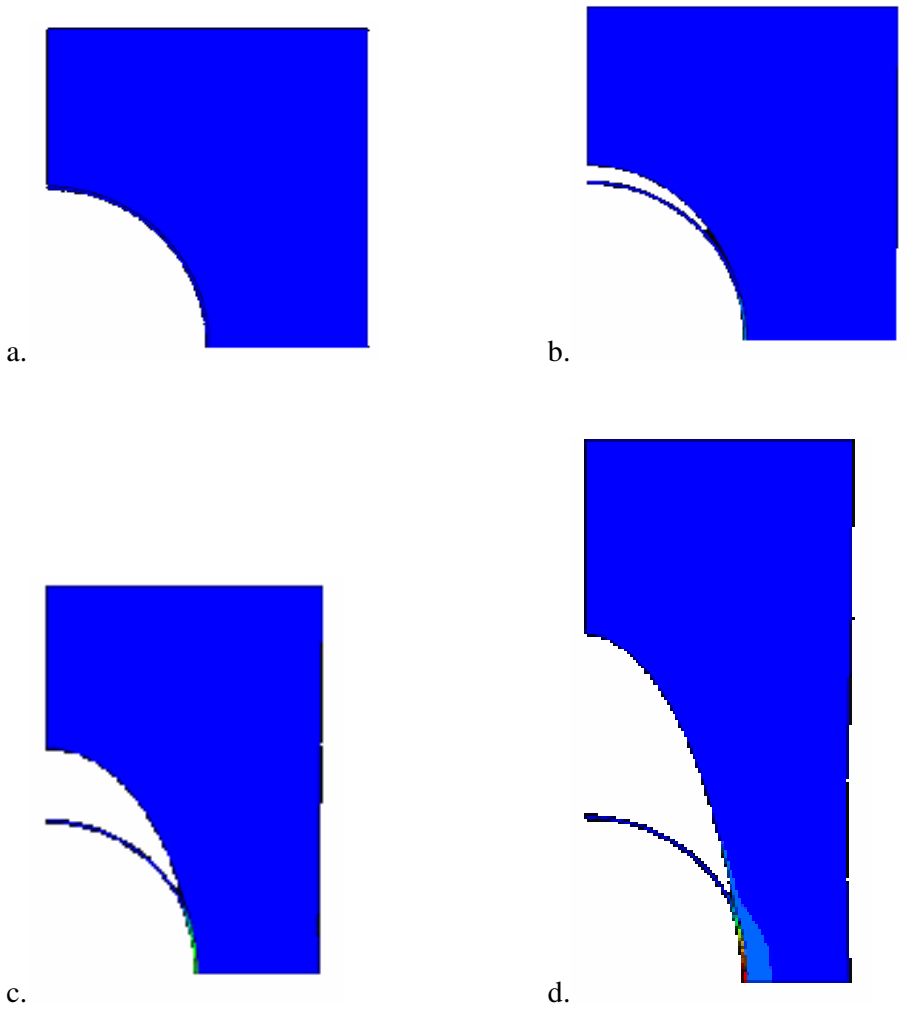

Figure 8.9: Images showing stages of tension of axisymmetric model of table tennis ball embedded in elastomer.

Here the elastomer can be seen to pull away from the hollow sphere immediately in image “a”, as there was no bonding between the two surfaces and this is even more obvious in image 2b”. Image “b” also begins to show a necking effect, opposite to the

barrelling effect observed in the compression model. Image "c" continues to show this and higher engineering stresses can also be observed at the equator of the hollow plastic sphere as this portion of the sphere is being compressed in an inwards direction.

The final image shows a large deformation for this model where a large amount of necking is evident. Although the two components are not bonded the model replicates a debonding or dewetting effect that is very similar to that observed during the physical experiments of the elastomer cylinders containing a table tennis ball.

The model was adapted to replicate a cylindrical unit model of a microsphere embedded in the silicone elastomer, in this case the right side was kept parallel to the left side. Again the hollow sphere did not buckle, but some debonding occurred.

8.2.6 FEA modelling results of an Elastomer Cylinder containing a table tennis ball

The results of the axisymmetric models from the previous section are examined here in the lower strain region.

Figure 8.10 and 8.11 are modelled in compression. Both figures clearly show the buckling points where the hollow plastic sphere buckles and there is a rapid drop in stress and a corresponding decrease in stiffness. Figure 8.10 shows results for a range of filler volume fractions (0.1, 0.2 and 0.3) and an unfilled cylinder. An anticipated increase in stiffness is seen as the filler volume fraction is increased. The snap through buckling is also large and beyond this point the behaviour becomes unstable as the hollow sphere continues to buckle.

The second figure, Figure 8.11, shows that, where there is no bonding between the hollow sphere and the elastomer material, as the filler volume fraction is increased there is a small increase in stiffness prior to the buckling point which is less pronounced than in the bonded models.

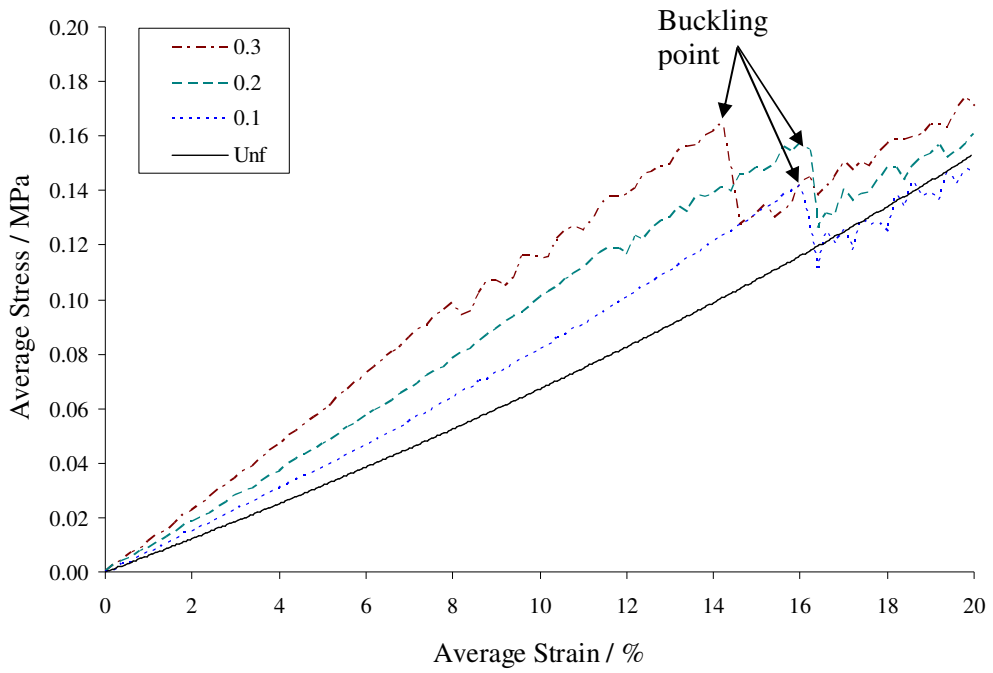

Figure 8.10: Models of an elastomer cylinder in compression, with the sphere perfectly bonded to the elastomer.

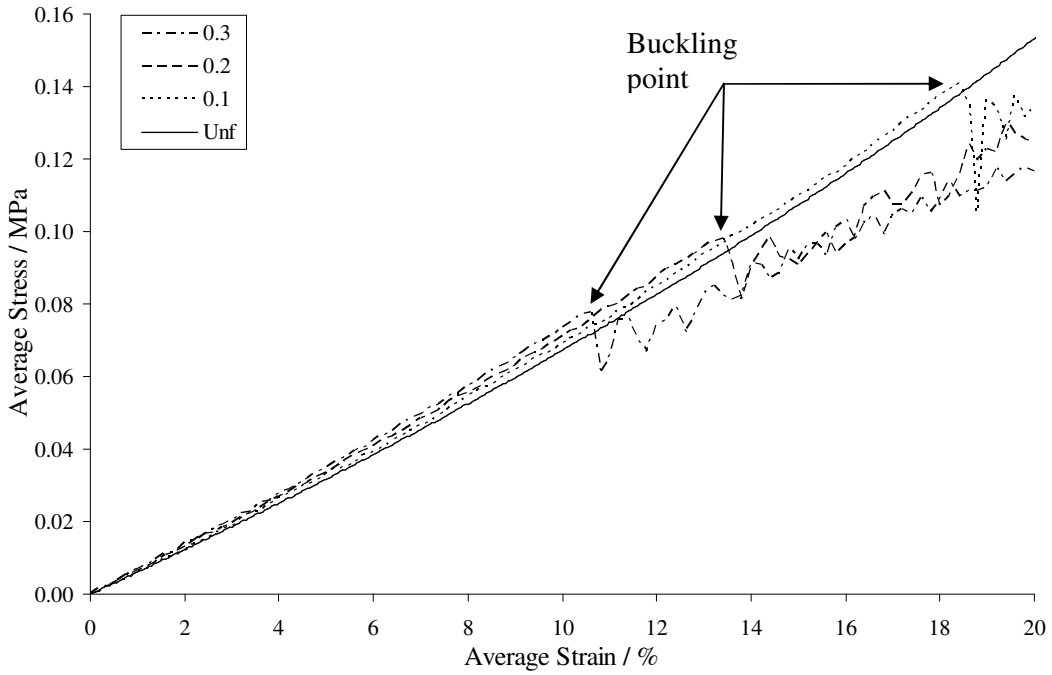

Figure 8.11: Models of an elastomer cylinder in compression, with no bonding between the sphere and the elastomer.

Figure 8.12 shows the results for the two limiting cases of perfect adhesion and zero friction at the filler-elastomer interface in tension. The filler volume fraction of the models is 10 %, this is broadly equivalent to the table tennis ball embedded in the silicone cylinder.

The model results compare well to the experimental result, where in reality although there is no deliberate attempt to bond the table tennis ball to the silicone elastomer some small amount of adhesion will arise naturally. The experimental result sits between the two model results, but more closely to the bonded model, this would indicate that there was significant bonding at least initially at these small strains.

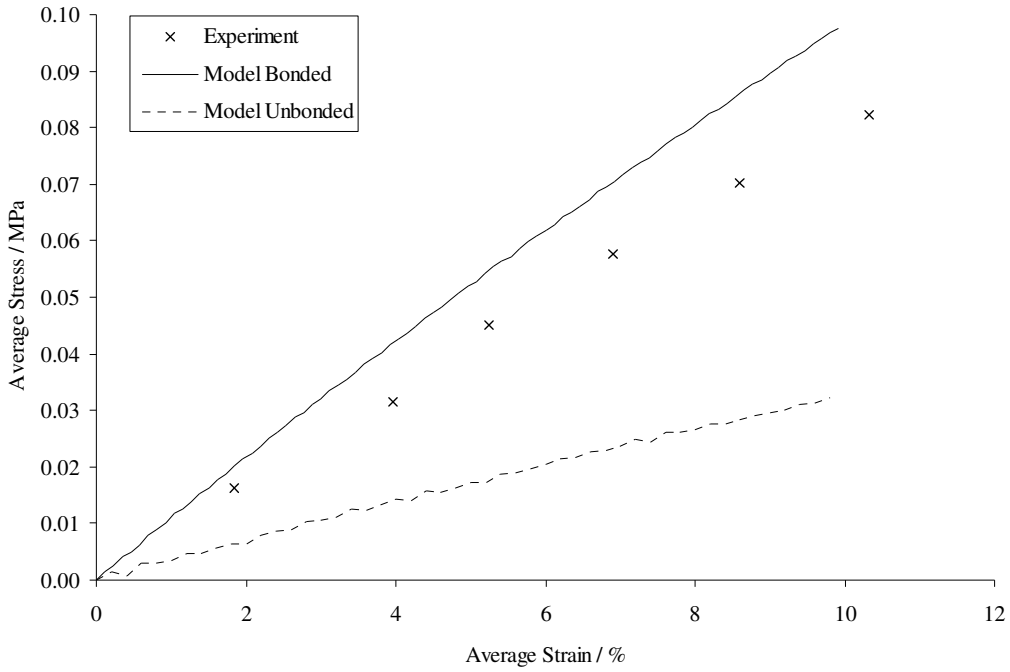

Figure 8.12: A comparison of the bonded and unbonded models in tension with experimental results, for a filler volume fraction of 10 %.

Figures 8.13 and 8.14 show results for the tensile models for a variety of filler volume fractions and unfilled. Figure 8.13 shows results where the hollow plastic sphere is bonded to the elastomer matrix and Figure 8.14, has no bonding between the two components.

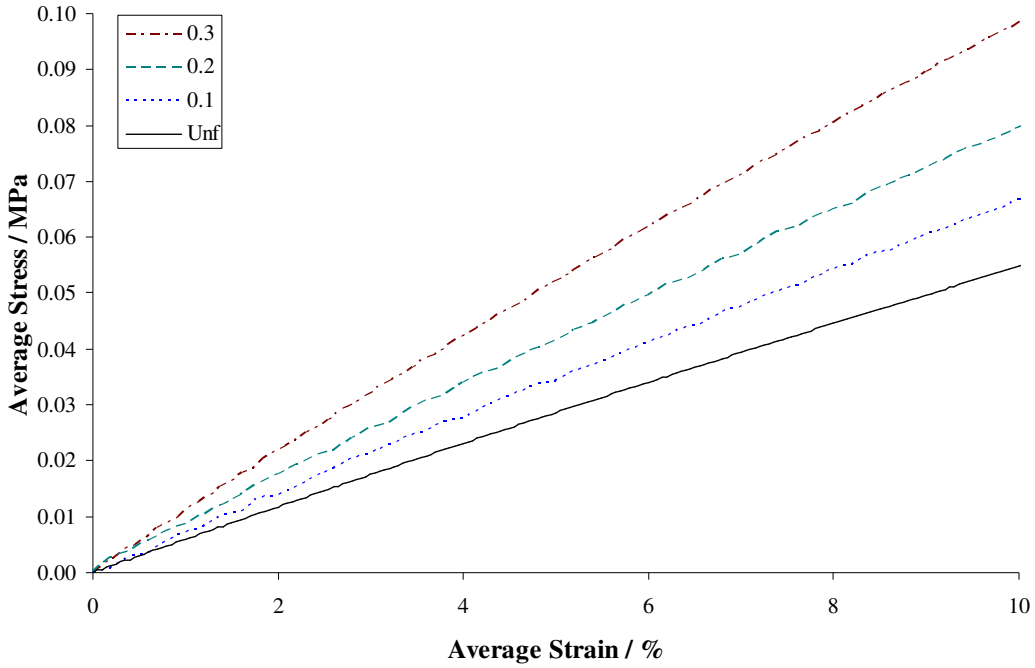

Figure 8.13: Models of different filler volume fraction of an elastomer cylinder in tension, with the sphere perfectly bonded to the elastomer.

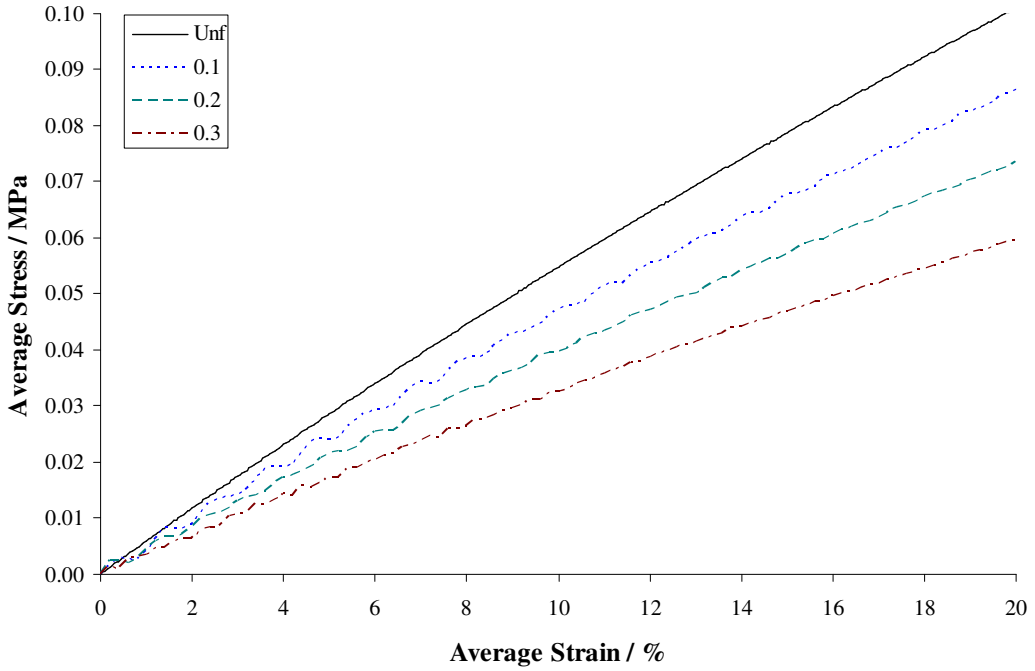

Figure 8.14: Models of an elastomer cylinder in tension, with no bonding between the sphere and the elastomer.

Figure 8.13, where the elastomer matrix is bonded to the hollow plastic sphere, shows that as the filler volume fraction is increased, so too the stiffness of the overall system increases. Figure 8.14 shows the opposite effect, where there is no bonding or friction between the elastomer matrix and the hollow plastic sphere, the stiffness of the overall system decreases with an increase in the filler volume fraction.

The results from these models provide help with the understanding of the physical behaviour that occurred during the various experiments. To fit the experimentally observed behaviour it appears to suggest that there is some initial bonding between the hollow plastic sphere and the elastomer matrix material for both the microspheres in an elastomer matrix as well as for the table tennis ball tests. Then as the strain increases there is some debonding resulting in a reduction in stiffness.

8.3 Analysis of the behaviour of the filled elastomer at low and high strains

8.3.1 Guth-Gold analysis of behaviour at low strains

The Guth-Gold theory has been described in Chapter 2, where at low strains the averaged Young's modulus of a filled composite can be related to the modulus of an unfilled elastomer. The theory can also be used to compare different geometries and for materials in compression or tension.

Figure 8.15 compares results in tension from the uniaxial tensile tests using dumbbell test pieces for the unfilled material and for a range of microsphere filler volume fractions, as well as the tensile tests of the large elastomer cylinder containing a table tennis ball and the axisymmetric FEA models of the hollow spheres in an elastomer matrix for a range of filler volume fractions.

The data was consistently measured at a strain of 5 % and the results agree well with the Guth-Gold theory, which is shown as a solid line in Figures 8.15 and 8.16. The uniaxial dumbbell test results are all slightly lower than the theoretical curve, probably because there is some small but hard to measure nonlinearity at small strains. The FEA model shown is the perfectly bonded model and again the results as expected also agree well with the Guth-Gold theory. This good correlation suggests that at these low strains the fillers act like rigid solid spheres and that no dewetting or buckling developed.

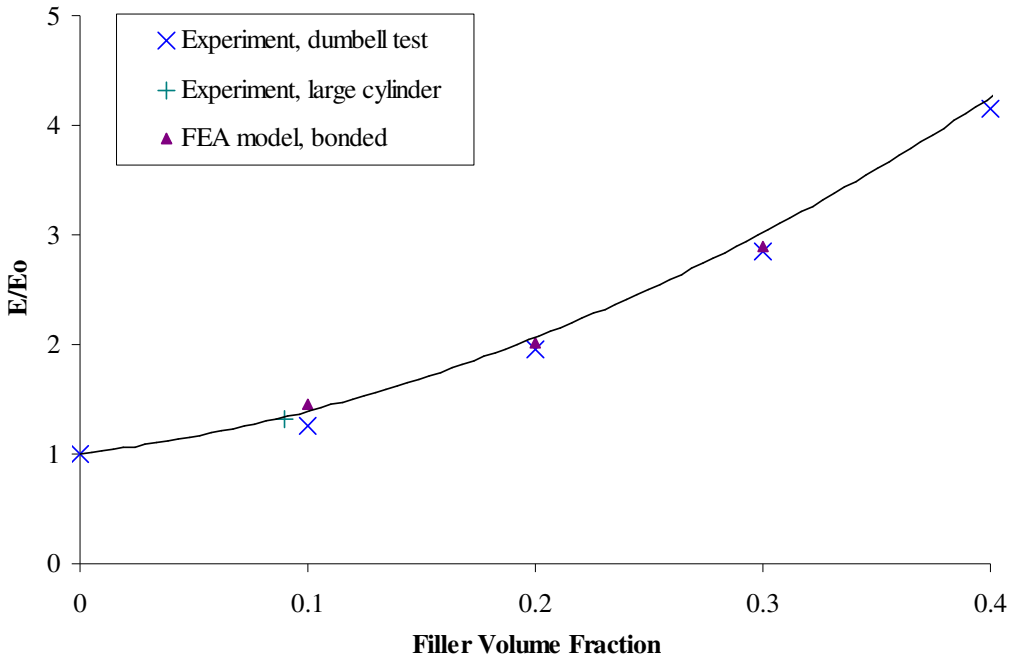

Figure 8.15: Guth-Gold graph of experimental and FEA results in Tension.

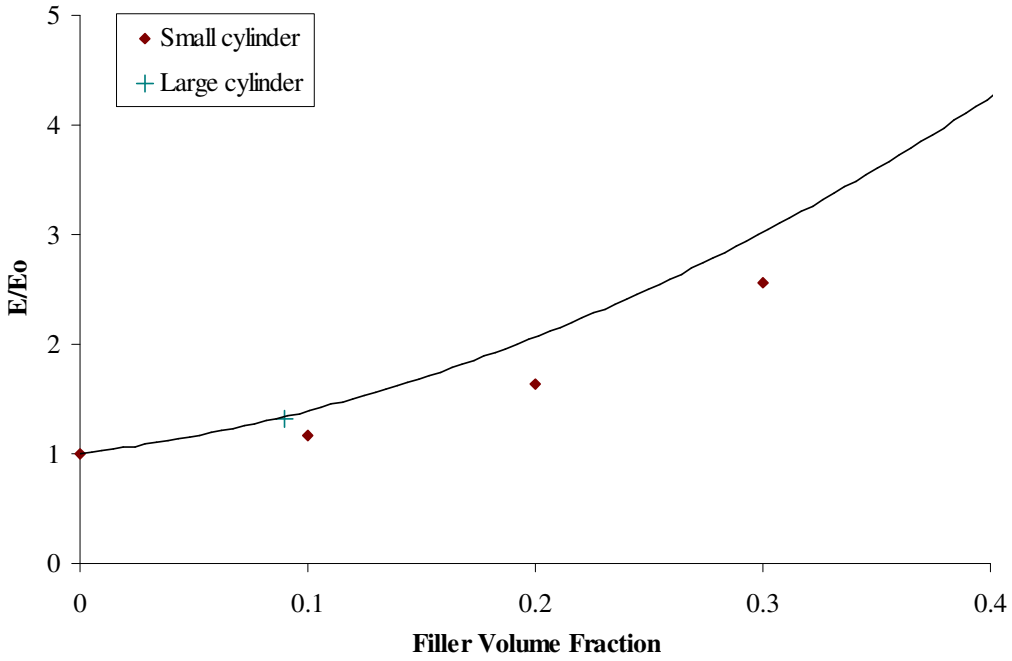

Figure 8.16: Guth-Gold graph of experimental results in Compression.

Figure 8.16 compares results measured in compression for the small cylindrical test pieces of both the unfilled material as well as for a range of microsphere filler volume fractions and for the large elastomer cylinder containing a table tennis ball.

The small cylinders sit below the theoretical Guth-Gold curve, this is probably due to some inclusions within the material resulting from entrapped air bubbles in the material as it cured. This effect was not evident for the dumbbell test pieces tested earlier in tension as these were manufactured from thin sheets of material which allowed any air bubbles to rise to the surface and escape from the material.

8.3.2 Analysis of behaviour at high strains

The initial behaviour of the single sphere embedded in the elastomer at small strains is helpful in explaining the behaviour of a silicone elastomer that is filled with Expancel microspheres, but to fully understand the behaviour larger strains must be examined.

To asses the behaviour at high strains both the previous bonded and unbonded axisymmetric models were modelled to greater extensions in tension, with the same Yeoh values as used previously.

The models shown in the Figure 8.17 can be seen to extend further in tension than the models shown previously in this chapter. It can also be seen that there is no buckling of the hollow plastic sphere under these large deformations. This may in part be due to the additional constraint that is imposed as a result of the axial symmetry in the model where the hollow sphere cannot buckle in a non-symmetric manner, as was the case with the more complex three dimensional compression models examined in Chapter 6, with buckling only possible symmetrically about the axis.

Alternatively the lack of buckling could just reflect that the stresses developed in the horizontal direction are too small to cause the sphere to buckle, even at the highest strains.

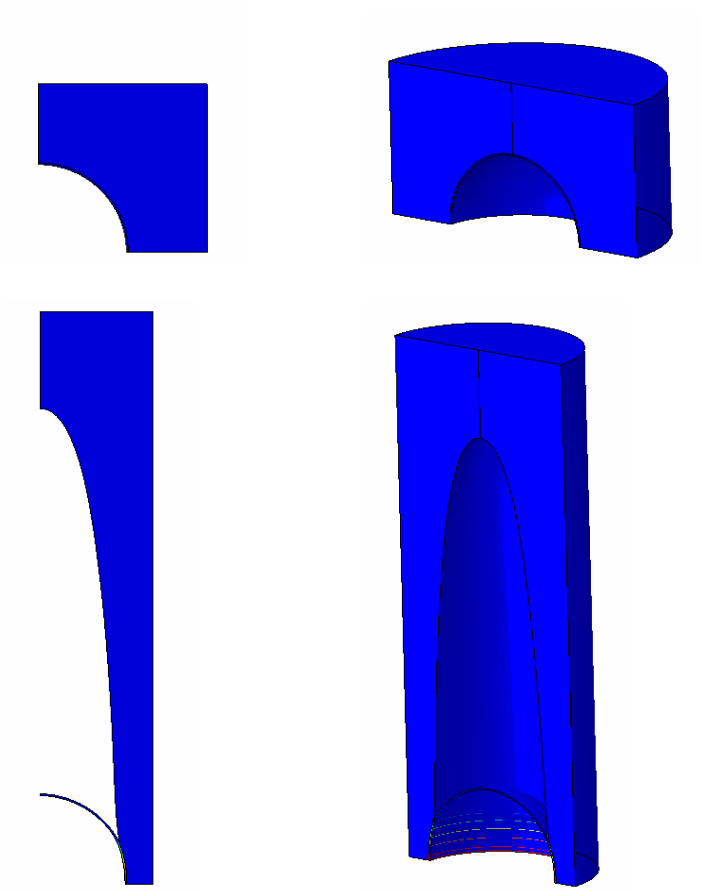

Figure 8.17: Images showing the large strain axisymmetric model of the unbonded table tennis ball embedded in the elastomer for a filler volume of 10 %.

The following three graphs in Figure 8.18, Figure 8.19 and Figure 8.20 show how the models of a single microsphere perfectly bonded and completely unbonded to the elastomer, compare with the tensile experiments using dumbbell test pieces of the silicone elastomer filled with microspheres.

The first two graphs for a filler volume of 10 % and 20 % were extended to a strain of 250 %, the third graph for a filler volume of 30 % was extended to a strain of 300 %. This was due to the limits of the models being reached as a result of the finite element mesh becoming too highly distorted.

All three graphs show that the experimental curve matches well the bonded model at initial strains, but as debonding occurs it then matches that of the unbonded model at higher strains. This, along with the images provided by the FEA, would indicate that in tension the softening behaviour observed is not caused by buckling but is a dewetting phenomenon.

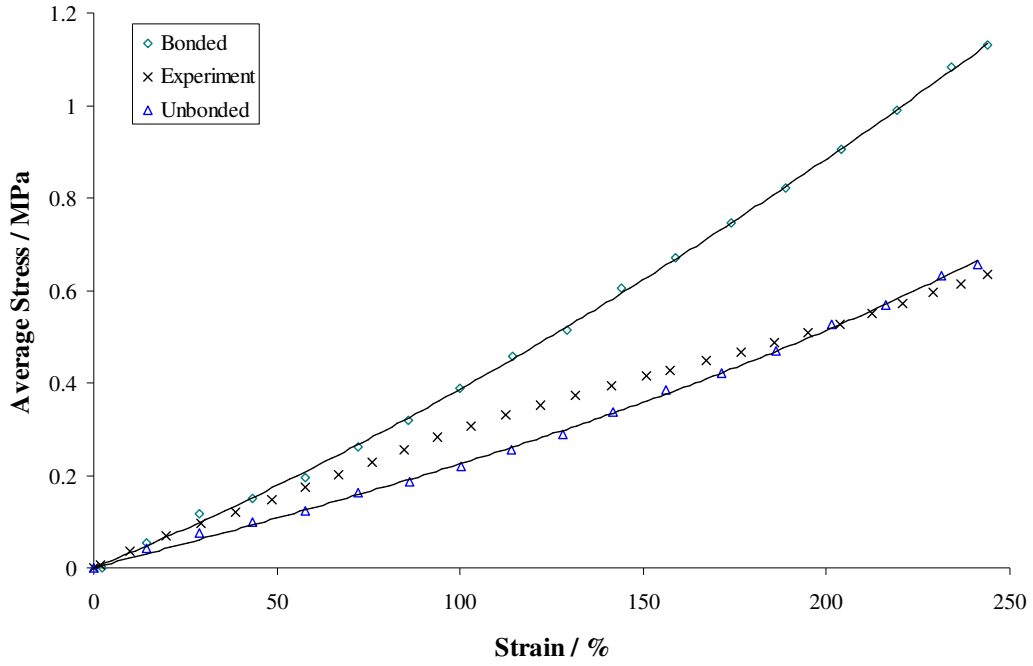

Figure 8.18: Tensile experiments of elastomer with 10 % filler volume compared to a bonded and an unbonded model.

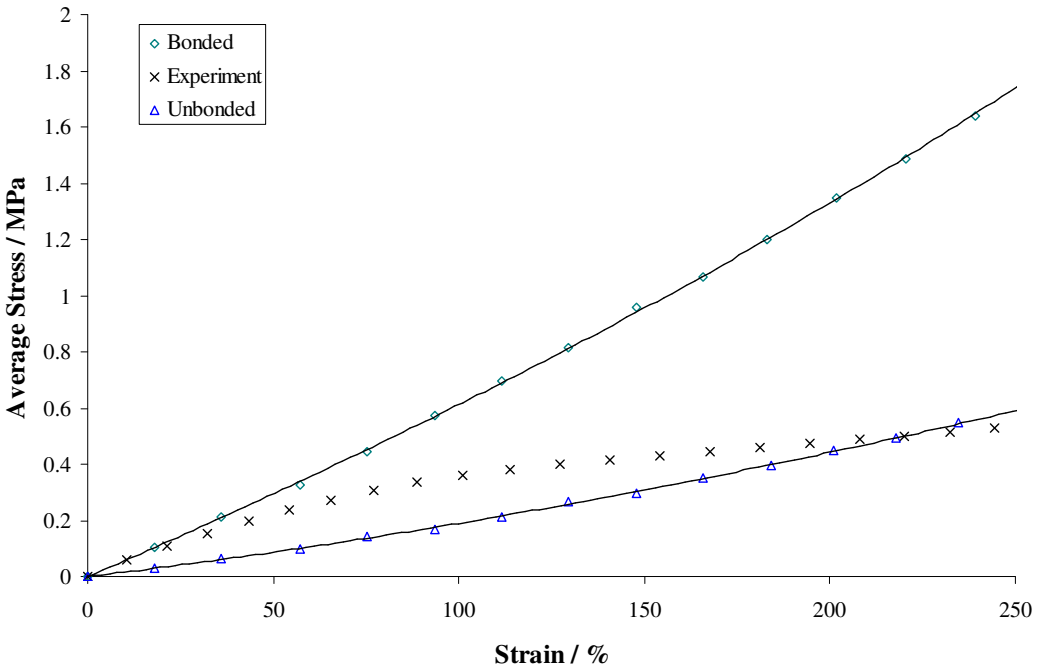

Figure 8.19: Tensile experiments of elastomer with 20 % filler volume compared to a bonded and an unbonded model.

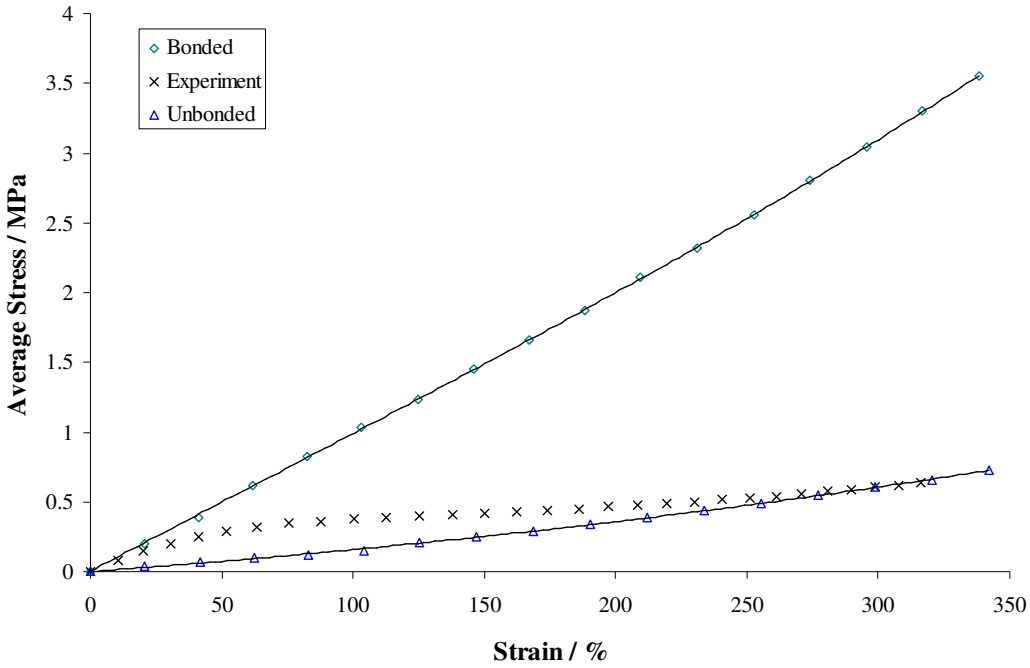

Figure 8.20: Tensile experiments of elastomer with 30 % filler volume compared to a bonded and an unbonded model.

8.3.3 Summary of behaviour

By using the Guth-Gold theory and comparing the experimental and modelling results at low strains along with the models for higher strains the behaviour of the filled material can be understood. The Guth-Gold theory follows very well for both the experimental and the modelling results in both tension and compression and therefore this suggests that there is no dewetting taking place at low strains.

In tension the model suggests that the spheres do not buckle. The filler reinforcing effect of increasing the material stiffness at lower strains but softening at higher strains is a dewetting phenomenon, where the experimental results initially match those of the perfectly bonded model, but at higher strains they almost exactly match the unbonded model. In compression the spheres do buckle at low strains which results in a more pronounced decrease in stiffness.

Chapter 9 Conclusions and Suggestions for Future Work

9.1 Conclusions

The work in this thesis has focused on investigating the behaviour of elastomers when hollow plastic microspheres are used as a particulate filler, as well as the behaviour of the individual hollow plastic sphere.

To understand the behaviour of the filled elastomer material it was essential to understand the mechanical behaviour of the individual hollow plastic sphere. This was achieved by physically testing a single microsphere in uniaxial compression and replicating the tests at a larger scale using a table tennis ball. The behaviour followed the expected pathway of initial elastic bending followed by various different types of snap through buckling. After this a variety of hollow spheres were tested and their behaviour observed and compared to that of the table tennis ball.

FEA software was used to model the behaviour of the table tennis ball under uniaxial compression. After validating the model against the experimental behaviour it was used to model the behaviour of the microsphere, which was also compared to its experimental behaviour.

The experimental results for the uniaxial table tennis ball tests were used to analyse the work of Pauchard and Rica (1998) who had observed during their experiments that as the applied force was increased the shell exhibited a snap-through buckling and when plotted for a ratio of the wall thickness to the radius of the table tennis ball, the value of this ratio at the buckling point was approximately 2. This value is comparable to the thinner walled spheres modeled in this thesis, but is probably only true for spheres with very thin walls. This work has shown that the buckling instability displacement varies for a range of different ratios of wall thickness to sphere radius and is similar to the value of 2.2 proposed by Updike and Kalnins (1970).

Pauchard and Rica (1998) also deduced the form of the energy of the deformed shell, where the unknown parameters were thought to depend only upon the Poisson's ratio of the shell material. However this work has shown that there is also a dependence upon the ratio of the wall thickness to the sphere radius which has not previously been recognised. Models were developed to predict the behaviour of microspheres with a range of ratios of wall thickness to diameter. These models were also used to develop a

method where analysis of the behaviour during a uniaxial compression test could be used to determine the wall thickness and the modulus of the shell material, this is otherwise impossible for very small hollow spheres. The wall thickness can be determined simply by obtaining the buckling displacement, providing that the Poisson's ratio is known. The modulus can be determined simply by knowing the force at the half way point to the snap through buckling. This approach can then be used to fully characterise individual microspheres of known outer diameter.

Uniaxial tensile tests were conducted with dumbbell test pieces manufactured from an unfilled elastomer and a filled elastomer with a range of filler volumes. Uniaxial compression tests were also conducted on small cylinders, again both unfilled and filled with a range of filler volumes. In both configurations the addition of microspheres to the elastomer increased the stiffness at low strains and made the material softer at higher strains.

Experiments were conducted using elastomer cylinders with a table tennis ball embedded in them to represent a single hollow plastic sphere and allow the mechanical behaviour to be observed and analysed. The tests were conducted in compression and tension to observe the debonding and subsequent buckling of the sphere, this configuration was also modelled using the FEA software and the behaviour at larger displacements was predicted.

The adhesion between the hollow sphere and the elastomer material affects the mechanical behaviour, also the buckling phenomena depends upon the extent of the debonding between the sphere and the elastomer in compression. This behaviour was successfully replicated in the FEA models of a single hollow sphere in an elastomer cylinder. There is initially a large amount of contact between the hollow sphere and the elastomer, but in compression this is greatly reduced as the hollow sphere buckles.

The Guth-Gold theory showed that for the experimental and modelling results in tension there was no apparent dewetting at low strains in tension. It was also thought that at high strains the hollow spheres did not buckle, therefore in tension the softening at higher strains is primarily a dewetting phenomenon.

9.2 Suggestions for future work

The work described here has investigated the behaviour of a single hollow plastic sphere, it has confirmed previous observations and made some new discoveries

that will have numerous applications. The behaviour of a novel elastomer where hollow plastic spheres are used as a particulate filler has also been discovered.

Further experiments could be conducted using other types of elastomer as the stiffness and other properties of the elastomer will affect the induced behaviour of the microspheres. Conversely, the microspheres are also available in other sizes, the behaviour of these as single spheres and as a filler material within an elastomer could also be examined as the size and thickness of the shell will affect the overall behaviour of the elastomer material. Also, rather than the translucent silicone elastomer used here, a clear elastomer could be used, where the behaviour of the embedded table tennis ball or microspheres could more easily be observed.

Further FEA models could be developed to examine the effects of friction between the hollow sphere and the elastomer matrix material and the peel energy at the interface between the sphere and the elastomer, this could then be used to predict when the dewetting will occur. Then the subsequent time dependent re-adhesion process should be examined to see how long it takes for the material to recover its initial virgin rubber behaviour. Models to accurately predict further compression and the numerous self contact occurrences within the buckled hollow sphere could also be examined. In this work only a very simple representative unit cell has been used, clearly to develop the model further it is necessary to consider how the various fillers interact when they are not perfectly spaced apart from each other. This could be done by developing models with multiple hollow filler particles to examine the interaction between them. Finally as these materials are often used in practice under quite large hydrostatic pressures the effect of pressure on the mechanical behaviour should also be examined.

References

Abaqus Inc., 2004, Manual set for version 6.4, 6.5 and 6.6, including "Getting Started with ABAQUS", Version 6.5, 2004.

Akzo Nobel, 2004, "Expancel® Microspheres, An Introduction", 2004 Brochure.

Akzo Nobel, 2010, "Product Specification for Expancel® Microspheres".

Ambersil, 2003, Technical Data sheet for "Ambersil 2-Part RV 282", Ambersil Silicone Division.

Baker, A.D., 1990, "The Naval Institute Guide to Combat Fleets of the World", Chapter 6, "Silence Makes Perfect".

Blatz, P. J. and Ko, W. J., 1962, "Application of Finite Elastic Theory to the Deformation of Rubbery Materials", Transactions of the Society of Rheology, VI, pp 223-251.

Busfield, J. J. C., 2003, "Rubber Materials", B.Eng/M.Eng Course notes, Department of Materials, Queen Mary, University of London.

CES Selector, Materials Selection, Cambridge Engineering Selector Software, 2013, Granta Design.

Canada Colors and Chemicals Limited (CCC), 1992, "Safety data sheet - EXPANCEL® Microspheres: 551 DE 40 d42".

Carlisle, K.B., Lewis, M., Chawla, K.K., Koopman, M., and Gladysz, G.M., 2007, "Finite Element Modeling of Carbon Microballoons", Acta Materialia, Vol. 55, pp 2301-2318.

Christensen, R.M., 1986, "Mechanics of Low Density Materials", Journal of Mechanics and Physics of Solids, Vol. 34, No. 6, pp 563-578.

Cordingley, L.P, Mitchell, S.R. and Jones, R., 2004, "Measurement and Modelling of Hollow Rubber Spheres: Surface-Normal Impacts", Plastics, Rubber and Composites, Vol. 33, No.2/3, pp 99-106.

Dow Plastics, 2000, "Vinylidene Chloride Monomer and Polymers, A Technical Report on VDC and PVDC", The Dow Chemical Company.

Einstein, A., 1906, "Eine neue Bestimmung der Moleküldimensionen", Ann. d. Physik 19, pp 289.

Einstein, A., 1911, "Berechtigung zu meiner Arbeit: Eine neue Bestimmung der Moleküldimensionen", Ann. d. Physik 34, pp 591.

Engineering Toolbox, 2013, http://www.engineeringtoolbox.com/friction-coefficients-d_778.html.

Fok, S-L. and Allwright, D.J., 2001, "Buckling of a Spherical Shell Embedded in an Elastic Medium Loaded by a Far-field Hydrostatic Pressure", Journal of Strain Analysis, Vol. 36, No. 6, pp 535-544. IMechE.

Gent, A.N. and Thomas, A.G., 1959a, "The Deformation of Foamed Elastic Materials", Journal of Applied Polymer Science, Vol. 1, No. 1, pp 107-113.

Gent, A.N. and Thomas, A.G., 1959b, "Failure of Foamed Elastic Materials", Journal of Applied Polymer Science, Vol. 2, No. 6, pp 354-357.

Gent, A.N. and Thomas, A.G., 1963, "Mechanics of Foamed Elastic Materials", Rubber Chemistry and Technology, Vol. 36, No. 3, pp 596-610.

Gibson, L.J. and Ashby, M.F., 1982, "The Mechanics of Two-Dimensional Cellular Materials", Proceedings of the Royal Society, London, A.382, pp 25-42.

Gibson, L.J. and Ashby, M.F., 1982, "The mechanics of Three-Dimensional Cellular Materials", Proceedings of the Royal Society, London, A.382, pp 43-59.

Gibson, L.J. and Ashby, M.F., 1988, "Cellular Solids: Structure and Properties", 1st Ed, Cambridge University Press, (2nd Ed, Cambridge University Press, 1997).

Gregory, D.R., Milac, T.I. and Wan, F.Y.M., 1999, "A Thick Hollow Sphere Compressed by Equal and Opposite Concentrated Axial Loads: An Asymptotic Solution", SIAM Journal of Applied Mathematics, Vol. 59, No. 3, pp 1080-1097.

Gumbrell, S.M., Mullins, L. and Rivlin, R.S., 1953, "Departures of the elastic behaviour of rubbers in simple extension from the kinetic theory", Trans Faraday Soc, Vol. 49, pp 1495-1505.

Gupta, N.K., Easwara Prasad, G.L. and Gupta, S.K., 1999, "Axial Compression of Metallic Spherical Shells Between Rigid Plates", Thin-Walled Structures, Vol. 34, pp 21-41.

Gupta, N.K., Sheriff, M.N. and Velmurugan, R., 2007, "Experimental and Numerical Investigations into Collapse Behaviour of Thin Spherical Shells Under Drop Hammer Impact", International Journal of Solids and Structures, Vol. 44, pp 3136-3155.

Guth, E., 1945, "Theory of Filler Reinforcement", Journal of Applied Physics, Vol. 16, pp 20-25.

Guth, E. and Gold, O., 1938, "On the hydrodynamical theory of the viscosity of suspensions", American Physical Society, Vol.53, pp 322.

Hales, T.C., 2000, "Cannonballs and Honeycombs", Notice of the American Mathematical Society (AMS), Vol. 47, No.4, pp 440-449.

Hall, I.H., 1968, "Deformation of Solids", Universities Press Ltd., Northern Ireland.

He, M.Y., Wu, B. and Zok, F.W., 1995, "On the Mechanics of Microballoon-reinforced Metal Matrix Composites", Mechanics of Materials, Vol. 20, pp 315-328.

Hearn, E.J., 1996, "Mechanics of Materials", 2nd Ed., Vols. 1 and 2, Butterworth-Heinemann.

Higgins, R.A., 1987, "Materials for the Engineering Technician", 2nd Ed., Hodder and Stoughton.

Hon, A.A., Busfield, J.J.C. and Thomas, A.G., 2003, "Filler reinforcement in rubber carbon-black systems". Constitutive Models for Rubber III. Edited by J.J.C. Busfield and A. Muhr, pp. 301-308.

Kalpakjian, S., 1995, "Manufacturing Engineering and Technology", 3rd Ed., Third Edition, Addison-Wesley Publishing Company.

Kiser, M., He, M.Y. and Zok, F.W., 1999, "The Mechanical Response of Ceramic Microballoon Reinforced Aluminium Matrix Composites Under Compressive Loading", Acta Materialia, Vol. 47, No. 9, pp 2685-2694.

Lakes, R.S., Rosakis, P. and Ruina, A., 1993, "Microbuckling Instability in Elastomeric Cellular Solids", Journal of Materials Science, Vol. 28, pp. 4667-4672.

Lim, T.J., Smith, B. and McDowell, D.L., 2002, "Behaviour of Random Hollow Sphere Metal Foam", Acta Materialia, Vol. 50, pp 2867-2879.

Maccarini, R.R., Saetta, A. and Vitaliani, R., 2001, "A Non-linear Element Formulation for Shells of Arbitrary Geometry", Computer Methods in Applied Mechanics and Engineering, Vol. 190, pp 4967-4986.

MARC Analysis Research Corporation, 1996, "Nonlinear Finite Element Analysis of Elastomers", 1996 White paper.

Mark, J.E., 1975, "The Constants $2C_1$ and $2C_2$ in Phenomeno-logical Elasticity Theory and Their Dependence on Experimental Variables", Rubber Chemistry and Technology, Vol. 48, Iss. 3, pp 495-512.

Mooney, M., 1940, Journal of Applied Physics, Vol. 11, pp 582-592.

Nakamura, K., Wada, M., Kuga, S. and Okano, T., 2004, "Poisson's Ratio of Cellulose Ib and Cellulose II", Journal of Polymer Science, Vol. 42, pp 1206-1211.

Ogden, R.W., 1972, "Large Deformation Isotropic Elasticity - On the Correlation of Theory and Experiment for Incompressible Rubberlike Solids", Proceedings of the Royal Society, London, A.326, pp 565-584.

Ogden, R.W., 1982, "Elastic Deformations of Rubberlike Solids", Department of Mathematics, Brunel University.

Oliveira, de, J.G. and Wierzbicki, T., 1982, "Crushing analysis of rotationally symmetric plastic shells", Journal of Strain Analysis for Engineering Design, Vol. 17, No. 4, pp 229-236.

Pauchard, L., Pomeau, Y. and Rica, S., 1997, "Deformation des coques elastiques: Deformation of elastic shells", Mechanique des solides et des structures: Mechanics of solids and structures, pp 411-418.

Pauchard, L. and Rica, S., 1998, "Contact and Compression of Elastic Spherical Shells: The Physics of a "Ping-Pong" Ball", Philosophical Magazine B, Vol. 78, No. 2, pp 225-233.

Powell, Peter C., 1983, "Engineering with Polymers", Chapman and Hall, Ltd. London.

Rachik, M., Barthes-Biesel, D., Carin, M. and Edwards-Levy, F., 2006, "Identification of the Elastic Properties of an Artificial Capsule Membrane with the Compression Test: Effect of Thickness", Journal of Colloid and Interface Science, Vol. 301, pp 217-226.

Riks, E., 1972, "The Application of Newton's Method to the Problem of Elastic Stability", Journal of Applied Mechanics, Vol. 39, Issue 4, pp1060-1065.

Rivlin, R.S., 1992, "The Elasticity of Rubber", Rubber Chemistry and Technology, Vol. 65, pp G51-66.

Rivlin, R.S., 1948, Philosophical Transactions of the Royal Society London, A241, pp 379-397.

Rivlin, R.S. and Thomas, A.G., 1953, "Rupture of Rubber 1: Characteristic energy for tearing", Journal of Polymer Science, Vol. 10, Issue 3, pp 291-318.

Roland, C.M., 2004, "Naval Applications of Elastomers", Rubber Chemistry and Technology, Vol. 77, No. 3, pp 542-551.

Ruan, H.H., Gao, Z.Y. and Yu, T.X., 2006, "Crushing of Thin-walled Spheres and Sphere Arrays", International Journal of Mechanical Science, Vol. 48, pp 117-133.

Shorter, R., 1998, "Determining Material Models for Rubber Automotive Components", MSc by Research in Engineering Dissertation, Coventry University.

Taber, L.A., 1983, "Compression of Fluid-Filled Spherical Shells by Rigid Indenters", Journal of Applied Mechanics, Vol. 50, pp 717-722.

Tamura, K., Komura, S. and Kato, T., 2004, "Adhesion Buckling of Spherical Shells", Institute of Physics Publishing, Journal of Physics: Condensed Matter, Vol. 16, L421-L428.

Timoshenko, S., 1968, "Elements of Strength of Materials", Chapter 3 "Biaxial Tension and Compression", 5th Ed.

Timoshenko, S. and Goodier, J.N., 1951, "Theory of Elasticity", 2nd Ed., McGraw-Hill, New York.

Treloar, L.R.G., 1975, "The Physics of rubber elasticity", 3rd Ed., Clarendon Press, Oxford.

Treloar, L.R.G., 1976, "The Mechanics of Rubber Elasticity", (Dept. of Polymer and Fibre Science, U.M.I.S.T.), Proceedings of the Royal Society, London, A.351, pp 301-330.

Tschoegl, N.W., 1971, "Constitutive equations for elastomers," Journal of Polymer Science Part A-1: Polymer Chemistry, Vol. 9, pp 1959-1970.

Updike, D.P. and Kalnins, A., 1970, "Axisymmetric Behavior of an Elastic Spherical Shell Compressed Between Rigid Plates", Journal of Applied Mechanics, Vol. XX, pp 635-640.

Updike, D.P. and Kalnins, A., 1972, "Axisymmetric Postbuckling and Nonsymmetric Buckling of a Spherical Shell Compressed Between Rigid Plates", Journal of Applied Mechanics, Vol. XX, pp 172-178.

Yeoh, O.H., 1990, "Characterisation of Elastic Properties of Carbon Black Filled Rubber Vulcanizates", Rubber Chemistry and Technology, Vol. 63. No.5. pp 792-805.

Young, W.C., 1989, "Roark's Formulas for Stress and Strains", 6th Ed., McGraw-Hill Book Company.

Zhu, E., Mandal, P. and Calladine, C.R., 2002, "Buckling of Thin Cylindrical Shells: An Attempt to Resolve a Paradox", International Journal of Mechanical Sciences, Vol. 44, pp 1583-1601.

Appendix

Refereed journal papers and conference papers submitted by the author as part of this research

Title: Axial Compression of Hollow Elastic Spheres
Authors: Robert Shorter, John D. Smith, Vincent A. Coveney and James J. C. Busfield.

Journal: Journal of Mechanics of Materials and Structures, Vol. 5, No. 5, 2010.

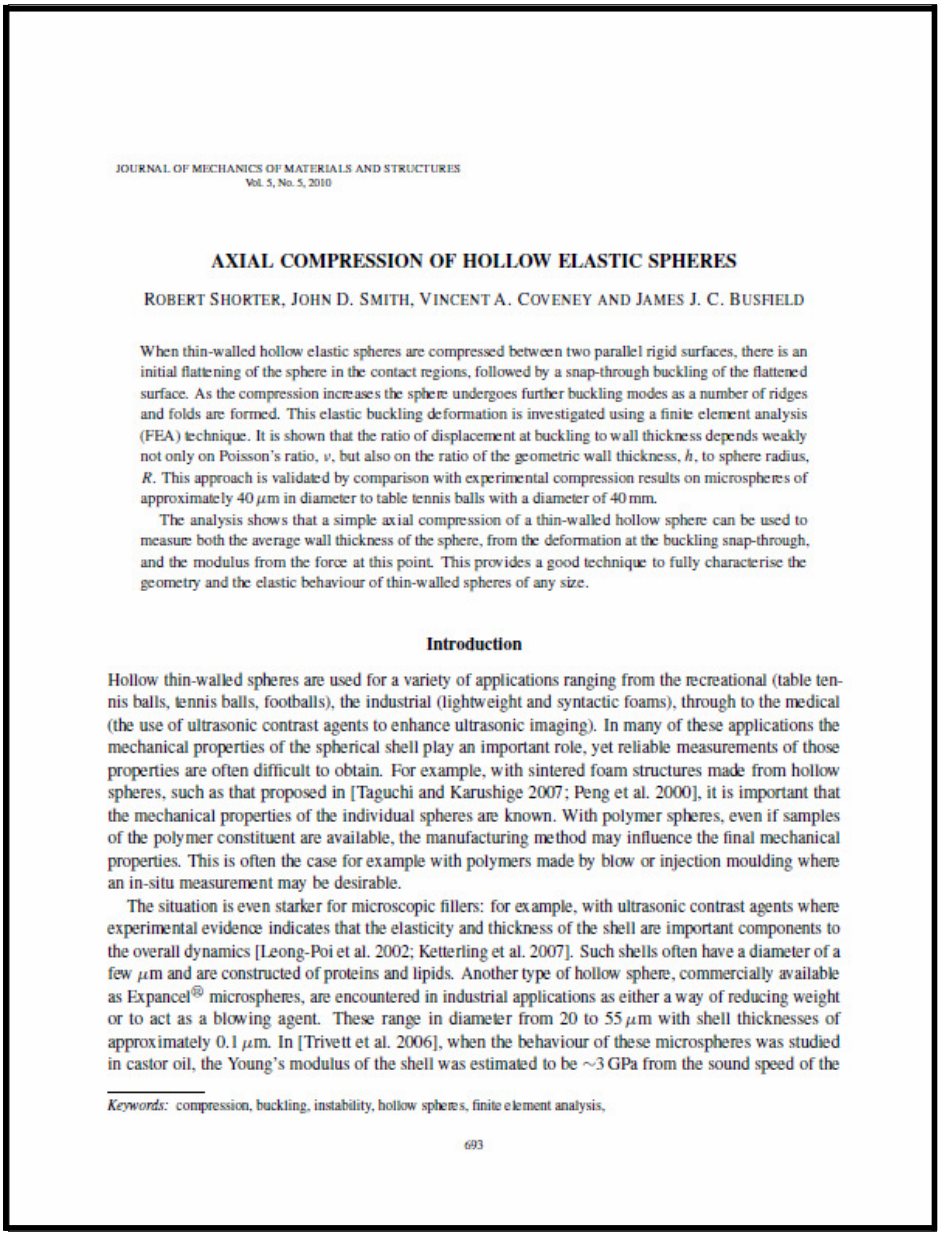

JOURNAL OF MECHANICS OF MATERIALS AND STRUCTURES
Vol. 5, No. 5, 2010

AXIAL COMPRESSION OF HOLLOW ELASTIC SPHERES

ROBERT SHORTER, JOHN D. SMITH, VINCENT A. COVENEY AND JAMES J. C. BUSFIELD

When thin-walled hollow elastic spheres are compressed between two parallel rigid surfaces, there is an initial flattening of the sphere in the contact regions, followed by a snap-through buckling of the flattened surface. As the compression increases the sphere undergoes further buckling modes as a number of ridges and folds are formed. This elastic buckling deformation is investigated using a finite element analysis (FEA) technique. It is shown that the ratio of displacement at buckling to wall thickness depends weakly not only on Poisson's ratio, ν, but also on the ratio of the geometric wall thickness, h, to sphere radius, R. This approach is validated by comparison with experimental compression results on microspheres of approximately 40 μm in diameter to table tennis balls with a diameter of 40 mm.

The analysis shows that a simple axial compression of a thin-walled hollow sphere can be used to measure both the average wall thickness of the sphere, from the deformation at the buckling snap-through, and the modulus from the force at this point. This provides a good technique to fully characterise the geometry and the elastic behaviour of thin-walled spheres of any size.

Introduction

Hollow thin-walled spheres are used for a variety of applications ranging from the recreational (table tennis balls, tennis balls, footballs), the industrial (lightweight and syntactic foams), through to the medical (the use of ultrasonic contrast agents to enhance ultrasonic imaging). In many of these applications the mechanical properties of the spherical shell play an important role, yet reliable measurements of those properties are often difficult to obtain. For example, with sintered foam structures made from hollow spheres, such as that proposed in [Taguchi and Karushige 2007; Peng et al. 2000], it is important that the mechanical properties of the individual spheres are known. With polymer spheres, even if samples of the polymer constituent are available, the manufacturing method may influence the final mechanical properties. This is often the case for example with polymers made by blow or injection moulding where an in-situ measurement may be desirable.

The situation is even starker for microscopic fillers: for example, with ultrasonic contrast agents where experimental evidence indicates that the elasticity and thickness of the shell are important components to the overall dynamics [Leong-Poi et al. 2002; Ketterling et al. 2007]. Such shells often have a diameter of a few μm and are constructed of proteins and lipids. Another type of hollow sphere, commercially available as Expancel® microspheres, are encountered in industrial applications as either a way of reducing weight or to act as a blowing agent. These range in diameter from 20 to 55 μm with shell thicknesses of approximately 0.1 μm. In [Trivett et al. 2006], when the behaviour of these microspheres was studied in castor oil, the Young's modulus of the shell was estimated to be ~3 GPa from the sound speed of the

Keywords: compression, buckling, instability, hollow spheres, finite element analysis,

Title: The Physical Behaviour of Elastomers Containing Hollow Spherical Fillers

Authors: R. Shorter, A.G. Thomas & J.J.C Busfield - *Department of Materials, Queen Mary, University of London, Mile End Road, London, E1 4NS, UK.*
J.D. Smith - *DSTL, Defence Science and Technology Laboratory, Porton Down, UK.*

Conference: 5th European Conference on Constitutive Models for Rubber (ECCMR), Paris, France (Presented plus Poster, 4-7 Sep 07,).

ABSTRACT

Elastomer materials frequently incorporate fillers. The mechanical behaviour is fairly well understood for elastomers filled with rigid particles, where the stiffness increases as the amount of filler material is increased, or for elastomer foams with either closed or open cells that become softer as the volume of the voids is increased. This research explores the relatively unknown mechanical behaviour of a third type, a novel elastomer where hollow plastic microspheres are used as a filler material. For this analysis a foam is produced by adding hollow plastic microspheres of about 40μm in diameter to the elastomer. The mechanical behaviour of the filled elastomer material is compared to a model of the microsphere in an elastomer matrix using FEA. A physical model was also used where a table tennis ball was embedded in a transparent elastomer material to observe the bending, buckling and dewetting under strain. There is an observed increase in the stiffness of the filled material at small strains and a reduction in the stiffness at large strains. Micro-structural finite element analysis models of the embedded microspheres in the elastomer show that the interfacial adhesion is a key parameter in determining the exact mechanical response. This work therefore indicates that the physical behaviour of the filled material is strongly determined by the polymer filler interaction.

Title: The physical behaviour of elastomers filled with hollow spherical fillers

Authors: R Shorter, JJC Busfield, AG Thomas - *Department of Materials, Queen Mary, University of London, Mile End Road, London, E1 4NS, UK.*
JD Smith - *DSTL, the Defence Science and Technology Laboratory.*

Conference: Elastomers for Engineering: Future Trends, Rubber in Engineering Group, Institute of Materials, Minerals and Mining, London (Presented plus Poster, 23 Nov 06).

ABSTRACT

Little is currently known about a type of closed cell foam elastomer that is produced when hollow plastic microspheres are used as a filler material. The mechanical behaviour is understood for elastomers filled with either rigid particles, such as carbon black, or produced as an open cell foam. Elastomers filled with rigid materials like carbon black become stiffer as the amount of carbon black added is increased, conversely foamed elastomers become softer as the volume occupied by the voids increases.

Hollow plastic micro-spheres of about 0.04 mm in diameter have been added to an elastomer. There is an observed increase in the stiffness at small strains and a reduction in the stiffness at large strains.

Micro-structural finite element analysis models of single micro-spheres as well as embedded micro-spheres in the elastomer have been made to compare the predicted deformation behaviour with experimental observations of the deformation.